Investigations into electrocatalytic reduction of protons to hydrogen by complexes inspired by the FeFe hydrogenase enzyme active site

David Gwilym Unwin

A thesis submitted in partial fulfilment for the degree of Doctor of Philosophy

University College London

March 2012

I, David Gwilym Unwin confirm that the work presented in this thesis is my own. Where information has been derived from other sources, I confirm that this has been indicated in the thesis.

Abstract

FeFe hydrogenase enzymes efficiently catalyse the reduction of protons to dihydrogen. The active site (H-cluster) of the enzyme is $Fe_2(\mu\text{-}SCH_2XCH_2S)(CO)_3(CN)_2(H_2O)(S(cys)(Fe_2S_2))$ (X = CH_2, NH or O). Although the enzyme is highly catalytic and consists of abundant elements, it has several drawbacks; for example, sensitivity to oxygen. Thus it has been proposed that complexes with similar structure to the H-cluster could be strategically designed in order to alleviate these drawbacks, and generate cheap catalysts for hydrogen generation.

This dissertation reports on eleven mimics of the H-cluster, each expanding on the simplest model in the literature: $Fe_2(\mu\text{-}SCH_2CH_2CH_2S)(CO)_6$. The aim of the research was to assess the electrocatalytic ability of these complexes, and interpret these results to assist in developing more efficient catalysts in the future.

The first two complexes investigated ($Fe_2(\mu\text{-}SC_6F_5)_2(CO)_6$ and $Fe_2(\mu\text{-}SC_6F_5)_2(CO)_4(Ph_2P\text{-}CH_2PPh_2)$) had a highly electron withdrawing dithiolate bridge to decrease the electron density on the Fe centres. The influence of the bridge was found to have a significant benefit to the overpotential required for catalysis.

The next four complexes analysed ($Fe_2(\mu\text{-X})(CO)_3(\mu,\eta^2\text{-}Ph_2PCH_2CHP(Ph)CH_2CH_2PPh_2)$; X = $SCH_2CH_2CH_2S$, $SCH_2N(CH_2C_6H_5)CH_2S$, $(SCH_3)_2$ or SCH_2CH_2S) used a triphos ligand to exert steric and electronic influence on the complexes. Although the complexes were found to be catalytic, the overpotential required for catalysis was large. As a sub-investigation, a range of electrolyte solutions were used, and found to have a significant influence on the electrocatalytic behaviour of the complexes.

Three tri-iron complexes have been investigated ($Fe_3(\mu\text{-}SCH_2CH_2S)_2(CO)_{7-x}(PPh_3)_x$; x = 0, 1, 2). It was found that moving from a di- to a tri-iron system significantly improved the catalytic overpotential.

Finally, two isomeric complexes exhibiting a ligand bound to the di-iron centres in both a bridging or chelating orientation ($Fe_2(\mu\text{-}SCH_2CH_2CH_2S)(CO)_4(Ph_2PN(CH_2CH\text{-}CH_2)PPh_2)$) were analysed. The orientation of the ligand played a role in the susceptibility to protonation of the complexes, and therefore their catalytic activities.

Acknowledgements

There are several people I would like to thank for their valuable contributions to this Ph.D. research.

Firstly, my supervisor Katherine Holt for providing her expert knowledge in the field, and for her guidance and motivational leadership throughout the Ph.D. process.

Graeme Hogarth for providing his expert knowledge in the field and for providing such interesting complexes for us to investigate.

Jean Talarmin for hosting me for three weeks early on in this research project; his assistance really got me up to speed with the electrochemistry of these complexes. Also for his rugby insights.

Our collaborators Shariff Kabir, Shishir Ghosh and Ahibur Rahaman in Jahangirnagar University, Bangladesh, and Michael Richmond in the University of North Texas.

University College London for providing me with a studentship.

Also everyone I have had the pleasure of working with in the electrochemistry lab at UCL, particularly Daren Caruana, who has always been there as an inspirational electrochemist providing ideas and motivation, and Mohammed Haque for his assistance and ideas.

Finally, I would like to thank my wife, family and friends for their continued support throughout my studies.

Contents

List of Figures

1 Introduction

This dissertation reports on the electrocatalytic activity towards proton reduction of a selection of mimics of the FeFe hydrogenase enzyme active site. The complexes investigated are $Fe_2(SC_6F_5)_2(CO)_6$, $Fe_2(SC_6F_5)_2(\mu\text{-}Ph_2PCH_2PPh_2)(CO)_4$, $Fe_2(\mu\text{-X})(CO)_3(\mu,\eta^2\text{-}Ph_2PCH_2CH_2P(Ph)CH_2CH_2PPh_2)$ (X = $SCH_2CH_2C\text{-}H_2S$; $SCH_2N(CH_2C_6H_5)CH_2S$; $(SCH_3)_2$; SCH_2CH_2S), $Fe_3(\mu\text{-edt})_2(CO)_{7-x}(PPh_3)_x$ (x = 0, 1, 2), $Fe_2(\mu\text{-pdt})(CO)_4(\mu\text{-}(Ph_2PN(CH_2CHCH_2)PPh_2))$, and $Fe_2(\mu\text{-pdt})(CO)_4(\kappa\text{-}(Ph_2P\text{-}N(CH_2CHCH_2)PPh_2))$ (the structures of these complexes are shown in Section 1.6). The molecular structure, susceptibility to protonation, electrochemical behaviour and electrocatalytic activity of these complexes are investigated, using relevant experimental techniques such as cyclic voltammetry, infrared spectroscopy and x-ray diffraction. A range of organic solvents (dichloromethane and acetonitrile), electrolyte salts ($[NBu_4][PF_6]$, $[NBu_4][ClO_4]$ and $[NBu_4][BF_4]$) and proton sources ($HBF_4.Et_2O$, toluenesulfonic acid and acetic acid) have been used.

The research presented in Chapter 5 on the tri-iron complexes $Fe_3(\mu\text{-edt})_2(CO)_{7-x}\text{-}(PPh_3)_x$ (x = 0, 1, 2) has recently been reported in Chemical Communications[1]. A more extensive paper on the tri-iron research has been submitted for publication in the Journal of the American Chemical Society. Three more papers on the research presented in Chapters 3, 4 and 6 are in preparation.

The motivation for this research and a review of the relevant literature is presented first. Familiarity with techniques such as cyclic voltammetry and spectroscopy is assumed. Readers unfamiliar with these topics are recommended to read Chapter 2, which gives an introduction to the techniques.

1.1 Motivation

1.1.1 The energy challenge

There are two energy challenges that human civilisation must solve for its continued development. Firstly, fossil fuel energy resources, upon which human civilisation is now dependent, are becoming depleted. Secondly, it is proposed that rising greenhouse gas levels due to combustion of fossil fuels is causing a significant warming in the climate due to an enhanced greenhouse effect; this warming would have severe impacts such as rising sea levels making presently inhabitable land uninhabitable. Viable energy resources are required, which are inexhaustible and do not lead to net gains in greenhouse gas levels in the atmosphere.

1.1.2 Renewable energy

Renewable energy sources harness natural and sustainable flows of energy across the Earth, and do not lead to a net increase in greenhouse gases, so have been proposed as a solution to the energy challenge described above. Renewable energy resources are generally derived from energy received from the sun, such as direct solar radiation and wind flows. As the sun's energy is likely to be available for many millions of years into the future, it is a solution to the energy challenge faced.

One of the major drawbacks of renewable energy resources is their intermittency. For example, although there may be enough wind energy available to provide power on certain days, on other days there may be no wind and thus no power from this source. Therefore, before a transition from fossil fuels to renewable energy resources is possible, a method for renewable energy storage is required.

1.1.3 Hydrogen

One such energy storage solution is splitting water (H_2O) into hydrogen (H_2) and oxygen (O_2). While renewable energy resources are available H_2 could be generated. This H_2 could be stored and used as a fuel at times when sufficient renewable energy is not available.

Electrochemical hydrogen generation may be considered as two reactions occurring simultaneously, one reaction at each electrode:

Anode: $H_2O \longrightarrow 2H^+ + 2e^- + \frac{1}{2}O_2$

Cathode: $2H^+ + 2e^- \longrightarrow H_2$

As with every electrochemical process, these reactions exhibit an activation barrier, seen as a greater potential difference required across the electrodes than predicted from the thermodynamic standard potentials. This greater potential difference, referred to as overpotential, is achieved at the expense of greater amounts of energy. In real terms, a higher overpotential means more renewable energy is used to generate a mole of hydrogen than would be used if a lower overpotential was required.

A method for decreasing the overpotential is to introduce a catalyst to the process. A catalyst offers an alternative reaction pathway with a lower overall activation barrier. Both the anode and cathode reactions require catalysts. This thesis shall be concerned exclusively with catalysing the proton reduction reaction.

The predominant catalysts used today for the proton reduction reaction are platinum (Pt) based. Unfortunately Pt is a scarce metal, used in many catalytic processes, driving its price up. Although minute quantities of Pt are required on the electrode for substantial catalytic improvements, the price of Pt will inevitably rise as demand increases (even at today's prices the Pt required for a fuel cell powered car costs in the region of $ 3000). Therefore, sustainable electrochemical generation of hydrogen requires a cheap and abundant alternative to Pt.

1.1.4 Hydrogenase enzymes and the H-cluster

Hydrogenase enzymes are naturally occurring and reversibly reduce protons to hydrogen. The turnover frequency at which this is accomplished is high, and the overpotential required is low, thus hydrogenase enzymes are proposed as alternatives to Pt as catalysts for the proton reduction reaction. There are three known forms of hydrogenase, each classified by their metal centres: FeFe, NiFe and Fe. This thesis focuses exclusively on the FeFe hydrogenase active site, known as the H-cluster, which generates hydrogen as a sink for excess electrons, and uses hydrogen as a source of

energy.

The FeFe hydrogenase enzymes consist of a large protein framework that encloses the H-cluster. Although FeFe hydrogenase enzymes were known since the 1930s the structure of the H-cluster, shown in Figure 1, was only elucidated in the late 1990s[2;3;4]. At the centre of the structure are two Fe centres, which are bridged by a three membered dithiolate bridge, with an unidentified central atom (X) proposed to be CH_2, NH or O. The active site is bound to the enzyme via the cystine ligand, which is bound to an Fe_4S_4 cluster. The apical distal ligand (L) is proposed to be H_2O. The remaining ligands are CO and CN, one of the CO ligands is in a semi-bridging position.

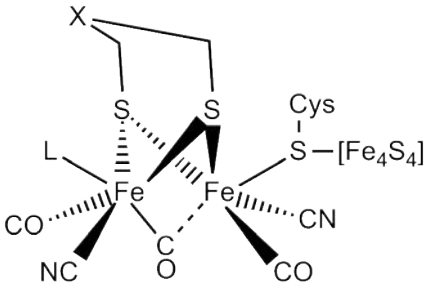

Figure 1: Hydrogenase active site

The catalytic mechanism for the hydrogenase enzyme is not known definitively, however several viable mechanisms have been proposed. One of the key assumptions that must be made in any catalytic mechanism is the identity of the central atom of the dithiolate bridge. Assuming the central atom to be N, an example of a proposed catalytic mechanism from the literature is given in Figure 2[5]. The first step is a reduction followed by loss of the labile H_2O ligand, which opens a coordination site for protons to bind. A second reduction follows, together with protonation at the N. The proton is transferred to the vacant coordination site and reduced to a hydride, which concurrently oxidises the Fe centres to Fe(II)Fe(II). A second proton binds at the N, and the Fe centres are reduced again to Fe(I)Fe(II). The proton combines with the hydride to form dihydrogen, which is liberated to close the catalytic cycle. In the enzyme this process is very reversible, with the release and pick up of the hydrogen ligand being dependent upon the concentration of hydrogen at the active site.

Although the FeFe hydrogenase enzyme does exhibit excellent catalytic ability, and groups such as that of Armstrong have had success using it as a catalyst[6], it does have several drawbacks. For example, the enzyme has a limited lifespan, is sensitive to O_2, and also is bulky in comparison to the catalytic active site, thus on an electrode surface much of the area is taken up by the non-catalytic part of the enzyme rather than the active site, decreasing the current produced per unit area of electrode. These issues, together with the reasonably simple structure of the hydrogenase enzyme active site, led researchers to synthesise mimics of the active site. This dissertation shall look at the work done to date on these mimics, and present new contributions to the research field.

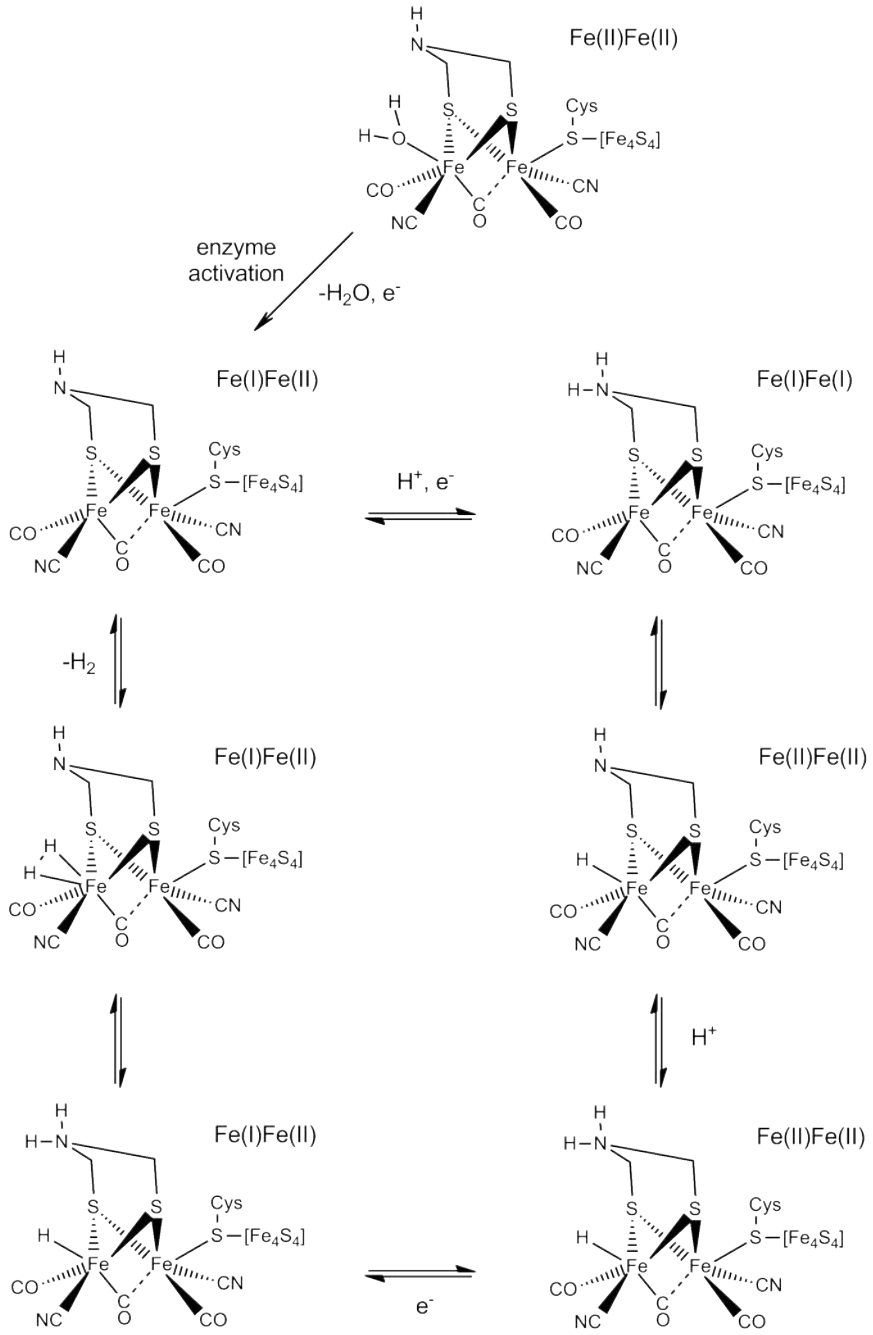

Figure 2: Proposed catalytic mechanism of the H-cluster assuming N as the central atom of the dithiolate bridge

1.2 A first mimic of the hydrogenase enzyme: $Fe_2(\mu\text{-pdt})(CO)_6$

Once elucidated, it was clear that the structure of the H-cluster is similar to that of the di-iron complex $Fe_2(\mu\text{-pdt})(CO)_6$ (Figure 3; pdt = $SCH_2CH_2CH_2S$). It was therefore questioned whether this simple di-iron complex, consisting of abundant and cheap elements, could catalyse the reduction of protons to hydrogen at similar rates to the significantly more complicated hydrogenase enzyme.

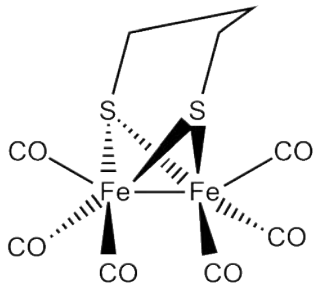

Figure 3: $Fe_2(\mu\text{-pdt})(CO)_6$

The complex $Fe_2(\mu\text{-pdt})(CO)_6$ was indeed found to be catalytic towards proton reduction[7]. The catalytic response is shown in Figure 4, which shows the cyclic voltammograms of the complex in the absence of protons (black line) and in the presence of 10 molar equivalents of HOAc (red line) (see Section 2 for an introduction to cyclic voltammograms). In the presence of protons a catalytic cycle at -1.88 V increases the current observed. Best, Pickett and co-workers have carried out a thorough investigation into the catalytic behaviour of the complex[8]. They found that the catalytic process is initiated after the complex undergoes a 1 electron reduction at -1.88 V. This species was then characterised by IR, UV-vis and EPR spectroscopy. A second reduction process at -2.03 V, which was not present under a CO atmosphere, was attributed to the reduction of a dimeric product of the first reduction process. Dimer formation was prevented under a CO atmosphere as CO ligand loss from the reduced complex was suppressed, preventing the generation of reactive species that could dimerise. This dimeric species was also found to be catalytic. The catalytic mechanism the complex undergoes is clearly different to the H-cluster. The H-cluster cycles through oxidation states Fe(I)Fe(II) and Fe(I)Fe(I), whereas the oxidation states of this complex are Fe(I)Fe(I) and Fe(0)Fe(I).

Although the catalysis exhibited by the complex was at a significantly greater overpotential than that of the H-cluster, and the catalytic mechanism was so different, the fact that the complex was indeed catalytic prompted a rapid expansion of the research into mimics of the H-cluster. To date, many different mimics have been synthesised with the hope of making a catalyst of similar activity to the enzyme. All of the complexes synthesised are analogous to the simple $Fe_2(\mu\text{-pdt})(CO)_6$ complex, and the variations in the structure can be classified as: varying the dithiolate bridge, varying the ligand set, and varying the iron centres (Figure 5). Each of these design considerations shall be discussed below.

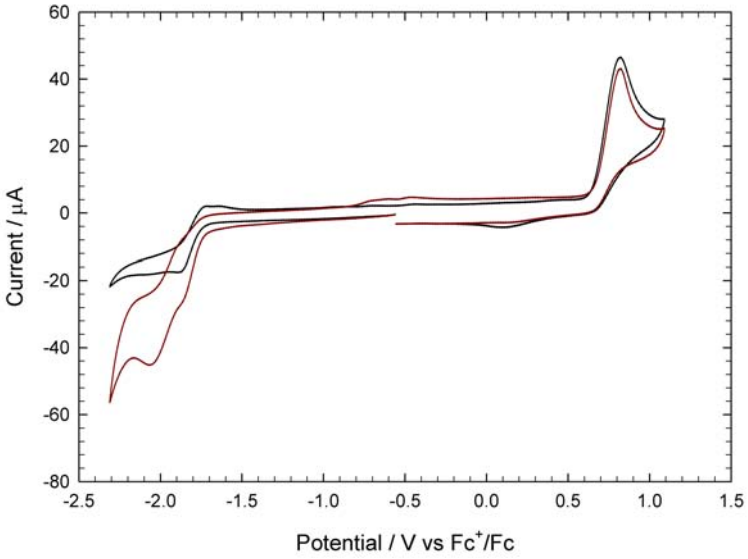

Figure 4: Cyclic voltammetry of $Fe_2(\mu\text{-pdt})(CO)_6$ (0.5 mM) in DCM-$[NBu_4][PF_6]$ in the absence of acid (black line) and in the presence of 10 molar equivalents HOAc (red line) (v=0.1 Vs^{-1}, glassy carbon electrode; V vs Fc^+/Fc)

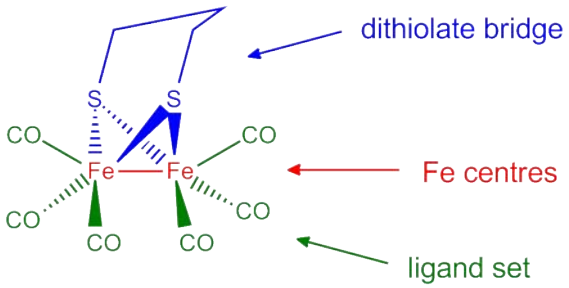

Figure 5: The components that make up a standard mimic of the H-cluster

1.3 Varying the dithiolate bridge

Variations in the dithiolate bridge of synthetic mimics of the H-cluster have been used primarily to: (i) tune the electron density on the Fe centres; (ii) provide a basic site for protonation in the bridge; and (iii) exert steric influences on the complex.

1.3.1 Tuning the electron density on the Fe centres

The electrocatalytic mechanism for the reduction of protons by H-cluster mimics follows one of two initial steps. One possibility is a protonation of the neutral complex, which could be followed by a reduction, a protonation, a further reduction and liberation of H_2. The possibility is an initial reduction of the complex, potentially making the Fe centres sufficiently basic to protonate, followed by a second reduction, a protonation and liberation of H_2. These two generic pathways are shown in Figure 6 (note, the steps following the initial step may be different to those shown, the key step here is the initial step).

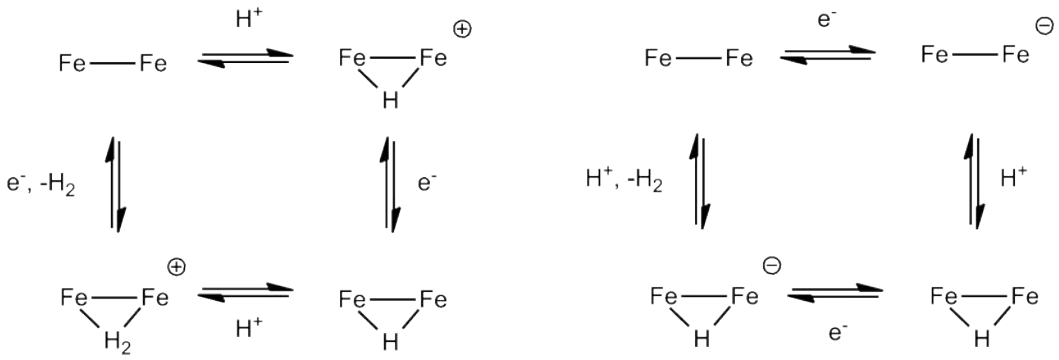

Figure 6: Two generic catalytic mechanisms initiated by either a protonation (left) or a reduction (right) of the complex (the dithiolate bridge and ligand set have been removed for clarity)

Assuming the second of the mechanisms, i.e. a reduction of the complex initiating catalysis, the reduction potential of the Fe centres is key in the determining the overpotential at which catalysis will occur. The reduction potential of the complex is determined by the electron density on the Fe centres - less electron density will mean reduction happens at less negative potentials, and thus a lower overpotential is required for catalysis. The dithiolate bridge has therefore been used to tune the electron density on the Fe centres, and thus the overpotential of catalysis.

An early example of using the dithiolate bridge to tune the electron density on the Fe centres was the addition of a benzene dithiolate bridge by Capon et al[9]. The electron withdrawing nature of the bridge resulted in the Fe centres being reduced at a more mild potential than the pdt analogue in a two-electron process. The complex was found to be catalytic towards proton reduction. Further studies have been carried out to tune the electron density on the Fe centres using the dithiolate bridge. For example, Charreteur et al[10] showed that dithiolate bridges with strong electron withdrawing groups (CO_2Me, tetrachloro-biphenyl) could be reduced at potentials 0.7 V less negative than the pdt bridge.

The effect of even subtle changes in the bridge can be significant. For example, in 2004 Åkermark, Sun and coworkers[11] reported their investigations into the two very similar complexes shown in Figure 7. Their intention was to later attach redox active species where the NO_2 or NH_2 are positioned. Using IR spectroscopy it was found that including NH_2, rather than NO_2, resulted in a shift in the CO stretching bands of 4-6 cm^{-1} to lower wavenumbers, showing that the electron releasing effect of the NH_2 was having a subtle effect on the CO ligands via the electron density on the Fe centres. This effect carried through to the electrochemistry where, whereas both complexes were easier to reduce than the analogous pdt-bridged complex, the complex with NO_2 was easier to reduce than the complex with NH_2, implying that even this minor change in the bridge was altering the electrochemistry of the complex.

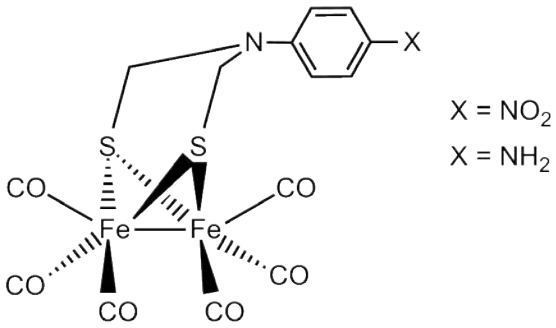

Figure 7: Two complexes investigated by Åkermark, Sun and coworkers

There is however a balance to be made. If the electron density on the Fe centres is too low, the complex can not undergo a protonation even after it is reduced, and will need to undergo a further reduction to make the Fe centres basic enough to protonate. For example, Schwartz et al[12;13] looked at many different electron withdrawing bridges, and found that the complex with reduction at the most mild potential was unable to catalyse the reduction of protons.

From the generic catalytic mechanism shown in Figure 6, it is clear that a second strategy is to use the bridge to increase the electron density on the Fe centres, making them more basic and thus more likely to protonate. To our knowledge this has not yet been achieved.

1.3.2 Basic site in the bridge

As was discussed earlier, the central atom in the bridge of the H-cluster has not yet been identified. One possibility is a N atom, which would provide a basic site for protonation, and shuttling of a proton to the Fe centres, as shown in Figure 2. In such a mechanism the N is the kinetic site for protonation, whilst the Fe centres are the thermodynamic site, therefore, the proton moves down to the Fe to form a hydride. This hydride is then protonated to form a dihydrogen ligand, which is released to give the neutral complex.

It has been found that when N is used in the bridge of mimics of the H-cluster it does indeed protonate[14]. In an interesting study, Eilers et al[15] were able to observe three different protonation

states for their complex $Fe_2(\mu\text{-adt})(CO)_4(PMe_3)_2$ (adt = N-benzyl-azadithiolate). These were protonation at the N, protonation at the Fe centres, and protonation at both the N and the Fe centres (Figure 8[15]). Specific conditions were required to achieve these protonation states, as detailed in their paper. The peak reduction potentials for the neutral complex, the complex protonated at N, the complex protonated at the Fe centres, and the complex protonated at both the N and the Fe centres, were -2.2, -1.6, -1.1, -1.0 V, respectively. The trend was as expected, with more mild reduction potentials seen as the electron density on the FeFe bond was decreased through protonation / hydride formation. The N protonated complex was catalytic, however, the doubly protonated complex was not able to catalyse proton reduction on the experimental timescale; this was put down to either the slow intramolecular reaction between the proton and the hydride, or a slow release of molecular hydrogen.

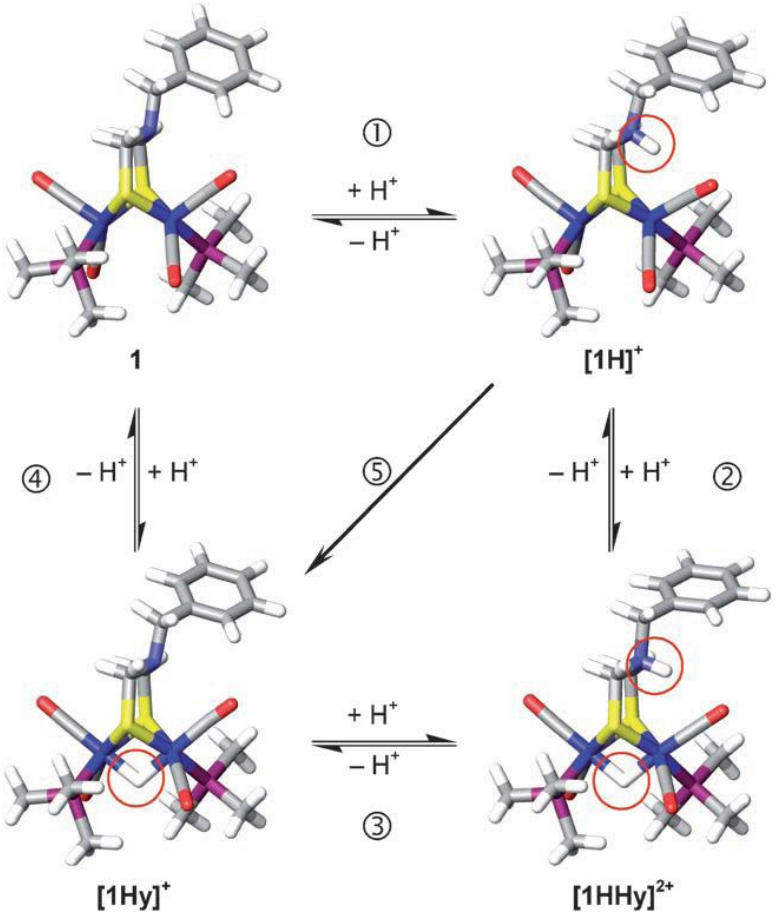

Figure 8: The protonation states of $Fe_2(\mu\text{-adt})(CO)_4(PMe_3)_2$ (adt = N-benzyl-azadithiolate)

1.3.3 Steric variations in the bridge

In the hydrogenase enzyme there are substantial steric influences at play, with the protein structure contorting the complex into configurations favourable for catalysis. Although an exact mimic of the enzyme configuration is not possible, dithiolate bridges have been investigated for their ability to impose a steric influence on the complexes.

The simplest variation away from the pdt bridge is an ethane-dithiolate (edt) bridge, giving

$Fe_2(\mu\text{-edt})(CO)_6$ (edt = SCH_2CH_2S). Here the bridge has been shortened by one carbon atom, hence constraining the bridge and Fe centres. Best, Hall and co-workers undertook an in-depth study of this complex[16]. Figure 10[16] shows the complicated behaviour of the complex, that has been understood through the use of spectroelectrochemistry. It is seen that upon reduction the complex is able to form a dimeric species; this can be prevented by working under a CO atmosphere. Felton et al have observed that there was a potential inversion of the reduction process[17]. Using variable scan rates they were able to observe the reduction as a one-electron process (at fast scan rates) going to a two electron process (at slow scan rates). This is due to a structural rearrangement in the molecule when it is reduced, and this rearranged product having a less negative reduction potential than than the original complex. Thus, the small structural change in the dithiolate bridge, which could be anticipated to have have little electronic influence on the reactivity of the di-iron complex, results in quite significant changes in the electrochemistry and reactivity of the complex.

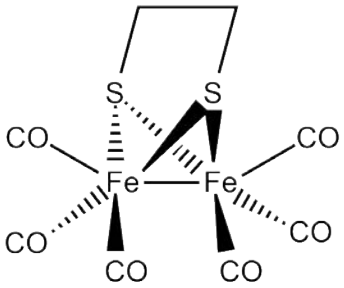

Figure 9: $Fe_2(\mu\text{-edt})(CO)_6$

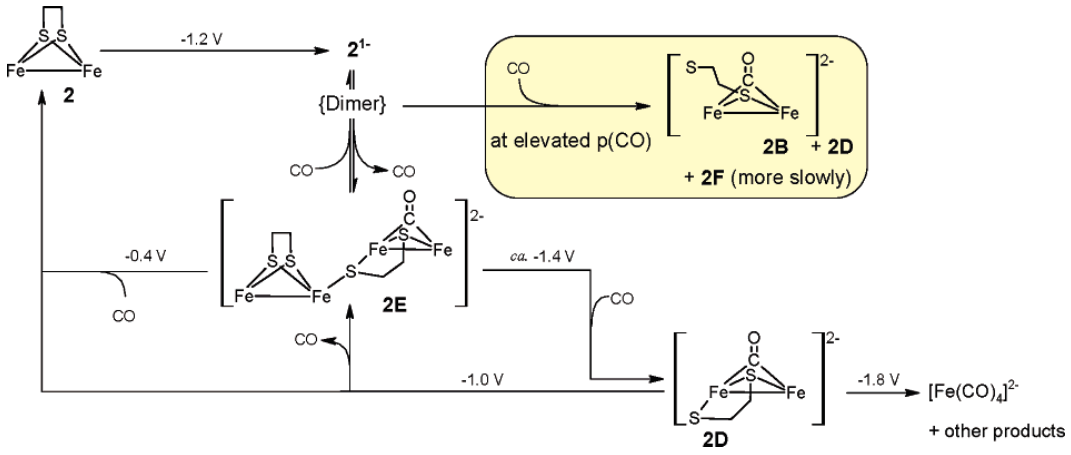

Figure 10: The behaviour of di-iron edt in MeCN

Rather than constraining the complex, the bridge may also be open, which will place less constraint upon the complex (Figure 11). Examples of such bridges are $(SMe)_2$ and $(PPh_2)_2$. A study by Darensbourg and co-workers found that an $(SEt)_2$ bridge had similar electrochemical response to the pdt bridge[7].

A further example is the use of bulky groups to impart a steric influence on the bridge. For example a large arene group will re-arrange more slowly than a small alkane group.

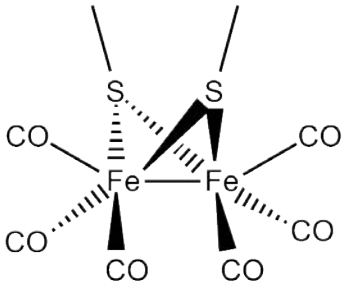

Figure 11: An open bridge

1.3.4 Further bridges

Other topics looked at by other groups include using an oxygen in the bridge (the final option for the identity of the central atom in the enzyme itself), photosensitisers, and linking to an electrode. These topics shall not be covered in this thesis.

1.4 Varying the ligand set

The ligand set of the first complex $Fe_2(\mu\text{-pdt})(CO)_6$ consists of six CO ligands, whereas the H-cluster has a more complicated set of ligands. In attempts to improve the catalytic performance, CO ligands have been replaced with alternative ligands. The main aims in varying the ligand set are to: (i) increase the basicity on the Fe centres; and (ii) induce electronic asymmetry within the complex.

1.4.1 Increase basicity on the Fe centres

As was discussed earlier, there are two options for the initial step of a catalytic mechanism: reduction or protonation of the complex (Figure 6). Hexacarbonyl complexes cannot be protonated at the Fe centres in the neutral form, and thus any catalytic mechanism must start with a reduction of the complex. In order to encourage protonation at the Fe centres, CO ligands have been exchanged with more electron donating groups to direct electron density towards the Fe centres, and make them more basic. The enzyme itself contains CN ligands which fulfill this role, and complexes were synthesised with CN ligands[18;19;20]. In more recent work, many phosphine based ligands have been used[21], as they impart the same basicity on to the Fe centres, without the complication of protonation at the CN lone pair.

Upon the first substitution of an electron donating ligand such as PPh_3, the complex is still unable to protonate at the Fe centres[21]. The substitution does however shift the reduction potential of the complex further negative, as greater electron density is on the Fe centres. This is not useful, as any catalytic mechanism will now require a greater overpotential, and thus more energy. Moving to a di-substituted complex shifts the reduction of the neutral complex even further negative. However, if the substitutions are made strategically, the complex can now protonate[21]. Upon protonation, electron density is removed from the Fe centres to form the hydride bond, and therefore the reduction potential of the protonated complex is shifted ca. 1 V less negative, which is an improved overpotential. This

trend continues with further substitutions - a neutral tri-substituted complex will have an even more negative reduction potential, however, it is likely to protonate, and therefore the reduction potential shifts in the positive direction.

In summary, it should be noted that the additional basicity on the Fe centres shifts the reduction potential of the complex more negative. This compromise is only worthwhile if the Fe centres do indeed protonate, which will shift the reduction potential back in the positive direction due to electron density being removed from the Fe centres to form the hydride bond.

1.4.2 Induce electronic asymmetry and rotated structure within the complex

It is believed that a terminal hydride is important for high catalytic activity - rather than a bridging hydride which is more stable, and therefore less likely to be removed from the Fe centres. Hall and co-workers carried out a computational investigation which suggested a terminal hydride would be favoured if there was an asymmetry of electron density between the two Fe centres, and the ligands sit in a rotated (non-eclipsed) position (Figure 12)[22].

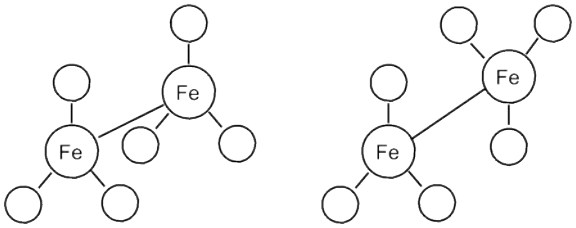

Figure 12: Illustration of eclipsed (left) and rotated (right) geometries

Since their study much work has been undertaken to analyse electronically asymmetric complexes. More and more sophistication has been integrated into the design of the complexes, using ligands such as PMe_3, PPh_3, $P(MeO)_3$, to direct electron density[23]. Single-, double-, triple- and quadruple-substitutions have been made in an attempt to achieve the right balance of electron density. The ligands used have also been chelating and bridging, such as dppm ($Ph_2PCH_2PPh_2$), dppe ($Ph_2PCH_2CH_2PPh_2$) and triphos ($Ph_2PCH_2CH_2P(Ph)CH_2CH_2PPh_2$). Both terminal hydrides[24;25;26;27;28;29] and rotated structures[30;31] have been achieved under specific conditions. Unfortunately, these have not yet matched the catalytic activity of the H-cluster.

1.5 Varying the Fe centres

The great majority of complexes reported as mimics of the H-cluster have contained two Fe centres, as is seen in the active site of the enzyme. However, the effect of increasing the number of Fe atoms has been investigated.

1.5.1 The most accurate structural model of the H-cluster

The di-iron centre of the H-cluster is linked to an Fe_4S_4 structure, which channels electrons towards the active site. To model this, and other components of the H-cluster, Pickett and co-workers synthesised the most accurate structural model of the H-cluster to date[32], as shown in Figure 13[32]. Unfortunately, the complex did not exhibit the same catalytic activity as the enzyme. Indeed, better *structural* models of the H-cluster, are not necessarily better *functional* models - likely due to the lack of the surrounding protein structure present in the hydrogenase enzymes.

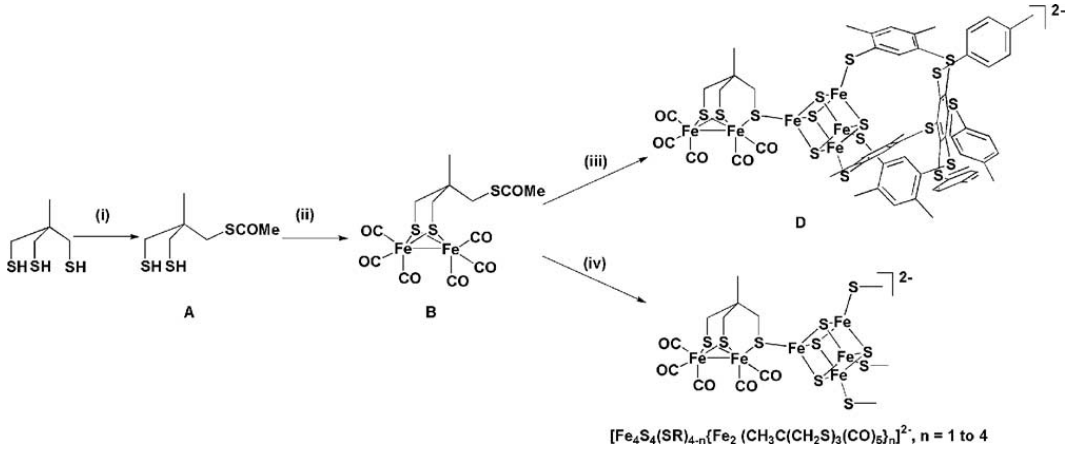

Figure 13: Synthetic procedure for Pickett and co-workers' accurate structural model of the H-cluster

1.5.2 Tetra-iron complexes

A further complex which varies the number of Fe centres is the tetra-iron complex $Fe_4(CO)_8\mu_3$-$(SCH_2)_3CMe_2$ synthesised by Pickett and co-workers in 2005 (Figure 14)[33]. The complex was found to be highly catalytic. In its neutral form this complex has mixed valent Fe(I)Fe(II)Fe(II)Fe(I) oxidation states. With respect to functional modeling of the hydrogenase active site, while the one-electron reduction product was shown to be only a moderate catalyst for proton reduction, addition of a second electron resulted in species in the Fe(I)Fe(I)Fe(I)Fe(I) state shown to be an excellent electrocatalyst. Interestingly, the H-cluster is also catalytic in the all Fe(I) state, as seen in Figure 2, as opposed to all previous H-cluster mimics which were catalytic in the Fe(I)Fe(0) state. Later detailed electrochemical and DFT studies shed some light onto the high activity of the doubly reduced species[34]. It is proposed that upon addition of two electrons the central iron-iron bond of the complex is cleaved, which in turn leads to rotation of the iron-tricarbonyl groups and formation of bridging carbonyls and vacant coordinations sites, the latter being able to bind protons efficiently and thus leading to high electrocatalytic ability. This research further emphasises the fact that models do not necessarily have to be accurate structural models of the H-cluster to be good electrocatalysts for proton reduction.

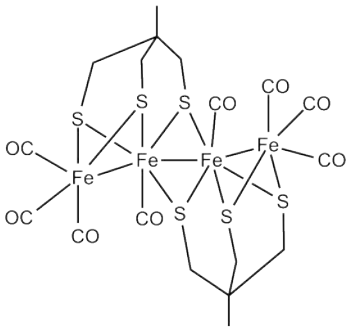

Figure 14: The tetra-iron structure of Pickett and co-workers

1.6 The research presented in this thesis

This thesis shall present four projects which contribute to the research of mimics of the FeFe hydrogenase active site introduced above.

1.6.1 $Fe_2(SC_6F_5)_2(CO)_6$: The influence of a highly electron withdrawing dithiolate bridge

As was discussed above, the bridge of a H-cluster mimic influences electron density on the Fe centres, and therefore the reduction potential of the mimic. The more electron withdrawing the bridge, the more mild the reduction potential. It was therefore of interest to investigate the $Fe_2(SC_6F_5)_2(CO)_6$ (Figure 15) complex, in which the highly electron withdrawing $(SC_6F_5)_2$ bridge removes electron density from the Fe centres. The findings of this research shall be presented in Chapter 3. As an extension to this work a small amount of $Fe_2(SC_6F_5)_2(\mu\text{-}Ph_2PCH_2PPh_2)(CO)_4$ has been synthesised and tested for electrocatalysis.

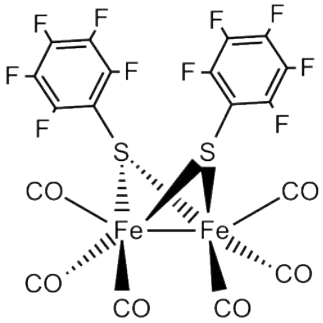

Figure 15: $Fe_2(SC_6F_5)_2(CO)_6$

1.6.2 $Fe_2(\mu\text{-}X)(CO)_3(\mu,\eta^2\text{-}Ph_2PCH_2CH_2P(Ph)CH_2CH_2PPh_2)$ (X: pdt = $SCH_2CH_2CH_2S$; adt = $SCH_2N(CH_2C_6H_5)CH_2S$; $(SCH_3)_2$): Imparting electronic asymmetry and steric twist through use of the triphos ligand

Hall and co-workers carried out computational studies which suggested that asymmetrical electron distribution and a rotated structure would favour formation of a terminal hydride on protonation, which would be beneficial to catalytic activity (see Section 1.4.2). This led Hogarth to synthesise a complex using the triphos ligand to provide both electronic asymmetry and steric twist in an attempt to achieve these objectives and thus improve catalytic activity [35].

The initial complex reported by Hogarth was pdt-bridged (Figure 16); its electrochemistry and electrocatalytic activity shall be reported in Chapter 4. The chapter shall also report on two analogous complexes that retain the triphos ligand, but vary the dithiolate bridge to $SCH_2N(CH_2C_6H_5)CH_2S$ and $(SCH_3)_2$. As discussed earlier, there has been much interest in having a N atom in the bridge of the complexes, and this is present in the $SCH_2N(CH_2C_6H_5)CH_2S$ bridged complex. Open bridges are of interest as they do not impart strain on the complex during a catalytic mechanism; the complex

with the $(SMe)_2$ bridge allows for further understanding of this topic.

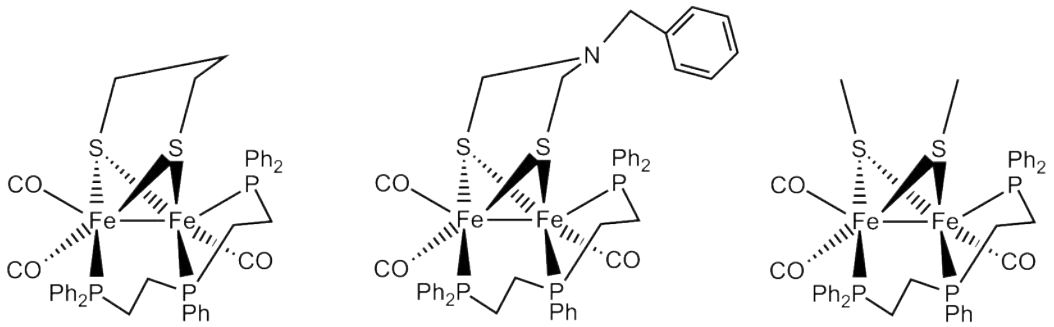

Figure 16: $Fe_2(\mu\text{-X})(CO)_3(\mu,\eta^2\text{-}Ph_2PCH_2CH_2P(Ph)CH_2CH_2PPh_2)$ (X: pdt = $SCH_2CH_2CH_2S$; adt = $SCH_2N(CH_2C_6H_5)CH_2S$; $(SCH_3)_2$)

As an extension to the analysis of the above complexes, a small quantity of edt-bridged complex has been synthesised and analysed for electrocatalytic activity. The edt bridge exerts more strain on the complex than the other three bridges, and thus was of interest to study.

To our knowledge a systematic analysis of the effect of the electrolyte solution on the electrochemical and electrocatalytic behaviours of mimics of the H-cluster has not been undertaken. The triphos-ligand complexes have been used to assess the influence of the electrolyte solution on both electrochemistry and electrocatalytic activity. The electrolyte solutions used were DCM-$[NBu_4][PF_6]$, DCM-$[NBu_4][ClO_4]$, DCM-$[NBu_4][BF_4]$ and MeCN-$[NBu_4][PF_6]$.

1.6.3 $Fe_3(\mu\text{-edt})_2(CO)_{7-x}(PPh_3)_x$ (x = 0, 1, 2): Using three iron centres instead of two

As was seen in Section 1.5.2, the investigations of Pickett, Best and co-workers of a mixed-valence tetra-iron complex proved fruitful, showing that the tetra-iron complex exhibited an excellent catalytic turnover frequency. In an early paper on the synthesis of di-iron dithiolate complexes, Huttner and co-workers reported that while reaction of $HS(CH_2)_nSH$ (n = 2, 3) with $[Fe_3(CO)_{12}]$ afforded predominantly the diiron complexes $[Fe_2(CO)_6\mu\text{-}S(CH_2)_nS]$, in both cases smaller amounts of trinuclear materials $[Fe_3(CO)_7\mu\text{-}S(CH_2)_nS_2]$ could also be isolated[36]. No later reports detail these mixed-valence complexes, or their electrocatalytic activity towards proton reduction. Thus, it was of interest to study them to see how they compared to the di-iron and tetra-iron complexes.

Three tri-iron complexes, $Fe_3(\mu\text{-edt})_2(CO)_{7-x}\text{-}(PPh_3)_x$ (x = 0, 1, 2), have been investigated each with a slightly different ligand set (Figure 17). The ligands of the simplest complex are all CO; the other two complexes have CO ligands replaced with either one or two PPh_3 ligands. All of the complexes exhibited an edt bridge, thus comparisons could be made with the analogous edt-bridged di-iron and tetra-iron complexes. The findings of this research shall be presented in Chapter 5.

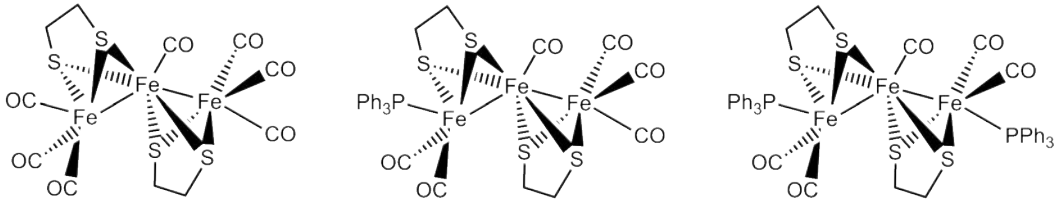

Figure 17: $Fe_3(\mu\text{-edt})_2(CO)_{7-x}(PPh_3)_x$ (x = 0, 1, 2)

1.6.4 $Fe_2(\mu\text{-pdt})(CO)_4(\mu\text{-}(Ph_2PN(CH_2CHCH_2)PPh_2))$ and $Fe_2(\mu\text{-pdt})(CO)_4(\kappa\text{-}(Ph_2P\text{-}N(CH_2CHCH_2)PPh_2))$: An investigation into a ligand with a basic site, in both bridging and chelating orientations

As discussed in Section 1.4, one of the key ways to vary the catalytic performance of H-cluster mimics is to vary the ligand set. Our research into two isomeric, di-substituted complexes with a basic site in the bridging / chelating ligand ($Fe_2(\mu\text{-pdt})(CO)_4(\mu\text{-}(Ph_2PN(CH_2CHCH_2)PPh_2))$ and $Fe_2(\mu\text{-pdt})(CO)_4(\kappa\text{-}(Ph_2PN(CH_2CHCH_2)P\text{-}Ph_2))$, Figure 18) shall be presented in Chapter 6.

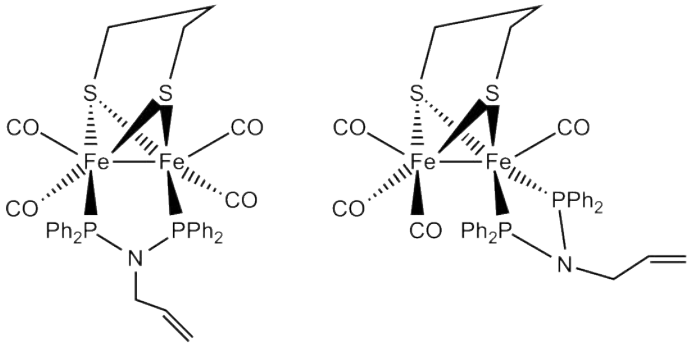

Figure 18: $Fe_2(\mu\text{-pdt})(CO)_4(\mu\text{-}(Ph_2PN(CH_2CHCH_2)PPh_2))$ and $Fe_2(\mu\text{-pdt})(CO)_4(\kappa\text{-}(Ph_2P\text{-}N(CH_2CHCH_2)P\text{-}Ph_2))$

As the complexes are di-substituted with electron donating ligands, it was of interest to test whether the electron density on the Fe centres would be sufficient to allow hydride formation. The complexes differ in that the ligand is either bridging or chelating, which allows for further understanding about the influence of asymmetrical electron density on catalytic activity. Additionally, there is a basic site in the ligand, which could allow protonation and perhaps shuttling of the proton to the Fe centres.

Talarmin and co-workers found that the chelating ligand of $Fe_2(\mu\text{-}SCH_2XCH_2S)(CO)_4(\kappa\text{-}(Ph_2(CH_2CH_2)PPh_2))$ rearranges to become a bridging ligand upon its first reduction via an electron transfer catalysis mechanism[37]. As an additional study, the chelating-ligand complex $Fe_2(\mu\text{-pdt})(CO)_4(\kappa\text{-}(Ph_2PN(CH_2CHCH_2)PPh_2))$ has been tested to see if it will rearrange to the bridging-ligand isomer in a similar way.

2 Experimental Theory and Techniques

This Chapter will describe the main techniques used in this dissertation. Particular emphasis is placed on the electrochemical and electrocatalytic analysis techniques, as these were the focus of this research. Other techniques include: the x-ray diffraction of the complexes to obtain their crystal structure; the assessment of the complexes' susceptibility to protonation using infrared spectroscopy; and the assessment of the complexes' susceptibility to oxidation using infrared spectroscopy. The synthesis of the complexes is described in an appendix.

2.1 Molecular structures of the complexes investigated, using single crystal x-ray diffraction

Single crystal X-ray diffraction (XRD) is the primary technique that has been used to determine the molecular structures of several of the complexes investigated.

In single crystal XRD a single crystal made solely of the molecule is mounted on a fibre. A beam of X-rays is directed at the crystal, creating a diffraction pattern. From the angles and intensities of this diffraction pattern, the density of electrons within the complex may be determined and thus the mean positions of the atoms in the crystal established. Thus a three dimensional picture of the molecule is obtained.

Single crystals of the complexes analysed were mounted on fibres and diffraction data collected at 150 K on a Bruker SMART APEX diffractometer using Mo-Kα radiation ($\lambda = 0.71073$ Å). Data collection, indexing and initial cell refinements were all done using SMART software (Version 5.628, Bruker AXS, Inc., Analytical X-ray Systems, 5465 East Cheryl Parkway, Madison WI 53711-5373, 2003). Data reduction was accomplished with SAINT software (Version 6.36A, Bruker AXS, Inc., Analytical X-ray Systems, 5465 East Cheryl Parkway, Madison WI 53711-5373, 2002) and SADABS programs (G. M. Sheldrick, SADABS Version 2.10, University of Gottingen, 2003) were used to apply empirical absorption corrections. The structures were solved by direct methods or Patterson methods and refined by full matrix least-squares (SHELXTL, V6.12). All non-hydrogen atoms were refined anisotropically and hydrogen atoms were included using a riding model. Scattering factors were taken from International Tables for X-ray Crystallography.

All XRD reported in this dissertation was performed by Graeme Hogarth in University College London.

2.2 Susceptibility to protonation of the complexes investigated

To understand any catalytic mechanism the complexes might exhibit, it was important to determine whether or not they protonate in the presence of a Brönsted acid. This was to aid understanding of whether the first step of a catalytic mechanism is a protonation or a reduction process. Infrared (IR) spectroscopy was used to probe if protonation was occurring.

IR spectroscopy uses the infrared region of the electromagnetic spectrum. Molecules absorb IR electromagnetic waves at specific frequencies and become vibrationally excited. Of key importance for the research presented in this dissertation is the frequencies at which the CO bonds absorb IR radiation. These frequencies are altered by the degree of Fe-CO backbonding into the CO π^* orbitals, an illustration of which is given in Figure 19. σ-bonding is present between the Fe and C atoms, where the CO ligand is donating electron density to the Fe atom. Additionally, the Fe donates electron density through a d-orbital to the π^* orbital of the C atom.

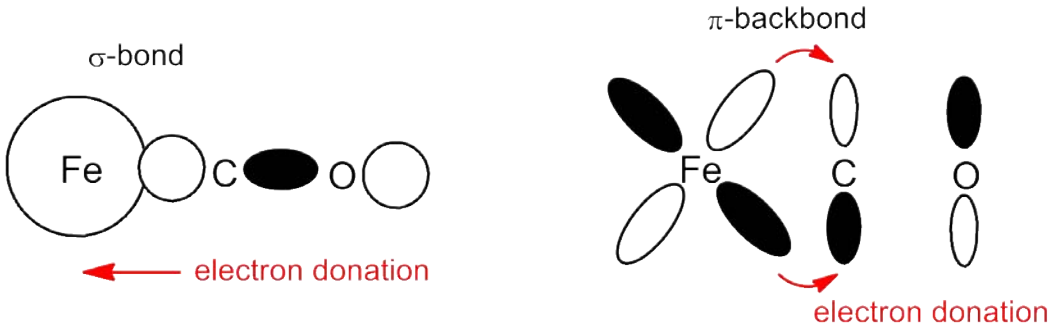

Figure 19: Illustration of backbonding from the Fe centre to the CO ligand

Protonation of the complexes is assessed by comparing the CO stretches region of the IR spectrum for the neutral complex and IR spectrum of the complex in the presence of protons. Upon protonation the electron density of the complex will be redistributed to allow for the proton binding, and the back-bonding into the CO ligands will be altered, thus changing the frequency of the CO stretches.

The complexes in this dissertation have up to two possible protonation sites - the Fe centres and a nitrogen atom (if present). A protonation could be detected by a shift in the CO-stretches to higher wavenumbers. This is due to the protonation resulting in less electron density on the Fe centres, which leads to decreased backbonding into the CO ligands, thus strengthening the CO bond and shifting the corresponding IR bands to higher wavenumbers. The location of the proton can be assumed by the magnitude of the shift in the bands - a shift in the wavenumbers of ca. 80-100 cm^{-1} is expected for protonation at the Fe centres, whereas a shift of ca. 10 cm^{-1} is expected for protonation at a N atom in the dithiolate bridge (if present).

The IR spectroscopy presented in this dissertation was performed using a Nicolet 205 FT-IR spectrometer in a solution cell fitted with calcium fluoride plates, subtraction of the solvent absorptions being achieved by computation. A 2 mM solution of the complex was made up in DCM. The CO-stretches region (2200 - 1800 cm^{-1}) of the IR-spectrum was recorded for this solution. The proton source was then added to the solution. The IR-spectrum was then taken for this solution. A protonation could be detected by a shift in the CO-stretches to higher wavenumbers, as described above.

2.3 Oxidation of the complexes investigated using ferrocenium

Several of the complexes have been assessed for chemical oxidation for one of two reasons. Firstly, complexes have been reported in the literature which upon oxidation form a bridging-CO ligand within the complex, and the bridging-CO ligand is thought to be an important feature of the H-cluster (see Chapter 1). Secondly, evidence has been found for some of the complexes reported in this dissertation undergoing oxidation in the presence of $HBF_4.Et_2O$ and O_2. Oxidation by ferrocenium was used to assess the band positions of the oxidised species, and thus test this hypothesis.

To perform the oxidation experiment, a ca. 2 mM solution of the complex was made up in DCM. The CO-stretches region (2200 - 1800 cm^{-1}) of the IR-spectrum of this solution was recorded. 1.25 molar equivalents of ferrocenium ($[Fe(C_5H_5)_2]^+[PF_6]^-$) were then added to the solution. The IR-spectrum of this solution was then taken. A chemical oxidation of the Fe centres could be detected by a shift in the CO-stretches to higher wavenumbers. This is due to the oxidation resulting in less electron density on the Fe centres, which leads to decreased backbonding into the CO ligands, thus strengthening the CO bond and shifting the corresponding IR bands to higher wavenumbers. If a bridging-CO ligand were present, it would be observed in the bridging-CO region of the IR spectrum (1800-1600 cm^{-1}).

2.4 Electrochemistry and electrocatalytic activity of the complexes investigated

Electrochemical analysis, in particular cyclic voltammetry, has been used extensively throughout this dissertation. A brief introduction to electrochemistry will be presented below, leading to an explanation of cyclic voltammetry. Following this the experimental setup used in this dissertation to investigate electrochemical behaviour and electrocatalytic activity shall be presented.

2.4.1 Introduction to dynamic electrochemistry

In general, electrochemistry is the study of redox reactions between an electrode and reactant molecules, usually in solution. Equilibrium electrochemistry is concerned with measurements taken under the conditions where no net current flows, enabling thermodynamic parameters such as reaction free energies to be obtained. A simple redox process at an electrode is shown in Equation 1. The Nernst equation can be used to determine the potential established at the electrode under equilibrium conditions, Equation 2, where the equilibrium potential (E^{eq}) results from the standard electrode potential (E^o) of the reaction and the concentrations of O and R at the electrode surface, under equilibrium conditions, which are the same as their values in bulk solution.

$$O_{(aq)} + ne^- \rightleftharpoons R_{(aq)} \tag{1}$$

$$E^{eq} = E^o + \frac{RT}{nF} \ln \frac{[O]}{[R]} \tag{2}$$

Dynamic electrochemistry, on the other hand, involves conditions where a net current does flow. If a potential more negative than E^{eq} is applied to the electrode, electron transfer occurs from the electrode to O in solution, resulting in the reduction of O to R, and consequently a current begins to flow. The magnitude of the current is given by Equation 3, where F is Faraday's constant (96485 Cmol^{-1}), A is the electrode area (cm^2), and j is the flux of O towards the electrode surface ($\mathrm{molcm}^{-2}\mathrm{s}^{-1}$)). The flux, j, can be described by a rate law (Equation 4) where k^o is the heterogeneous rate constant for the electron transfer reaction, and $[O]_0$ is the concentration of reactant at the electrode surface. Note that as current is now flowing, resulting in the conversion of O to R, it can no longer be assumed that the concentration of O at the electrode surface is the same as in bulk solution.

$$i = AFj \tag{3}$$

$$j = k^o[O]_0 \tag{4}$$

As A and F are fixed for a particular electrode, it is clear from Equations 3 and 4 that the observed current (equivalent to the reaction rate) is dependent upon two factors: firstly, the rate (k^o) of the heterogeneous electron transfer; and secondly, the rate of mass transport of fresh reactant to the electrode surface. The variables that influence these factors will be discussed in the following two sections, as they will enable understanding of the behaviours observed during cyclic voltammetry.

2.4.2 Rate of heterogeneous electron transfer

In this section two important models shall be discussed - the Butler-Volmer equation and Marcus theory - each of which illustrate the variables affecting the rate of heterogeneous electron transfer.

Equations 3 and 4 can be combined to give the current passed at the cathode for the simple electron transfer reaction given in Equation 1. In a similar way the anodic current can be obtained, and the two equations combined to give an expression for the net current (Equation 6).

$$i_c = FAk_{red}[O]_0 \tag{5}$$

$$i = FAk_{ox}[R]_0 - FAk_{red}[O]_0 \tag{6}$$

The Arrhenius equation gives an expression for the rate constant of a solution-phase reaction (Equation 7). The activation energy E_A represents the 'energy barrier' over which reactant molecules

must pass to become the products. X' is a frequency factor related to the frequency of attempts to pass the energy barrier. As electron transfer occurs in an analogous manner to chemical rate processes, the Arrhenius model can be used to give an expression for electron transfer rate constants. E_A can be designated as the Gibbs free energy of activation, $\Delta G^{\ddagger}$, and X is a frequency factor, which represents the rate of collision of the electroactive molecule with the electrode surface. ΔG is equal to $-nF\Delta E$ (in this case $n = 1$).

$$k = X' \exp\left(\frac{-\mathrm{E}_A}{RT}\right) \tag{7}$$

$$k = X \exp\left(\frac{-\Delta G^{\ddagger}}{RT}\right) \tag{8}$$

$\Delta G^{\ddagger}$ is sensitive to the change in electrical potential between the electrode and the solution, and hence the rates of oxidation and reduction will change with potential. When the applied potential (E) is equal to the equilibrium potential (E^{eq}) no current will flow through the cell. For electrolysis to occur a potential different in value to E^{eq} must be applied to the working electrode in order to drive the electrode reaction, this difference in potential is termed the overpotential $\eta = E - E^{eq}$. Equations 9 and 10 show how overpotential influences k_{red} and k_{ox}.

$$k_{red} = k^{o}_{red} \exp\left(\frac{-\alpha F\eta}{RT}\right) \tag{9}$$

$$k_{ox} = k^{o}_{ox} \exp\left(\frac{(1-\alpha)F\eta}{RT}\right) \tag{10}$$

α is the transfer coefficient and reflects the sensitivity of the transition state to the drop in electrical potential between the electrode and the solution. The value of α lies between 0 and 1. α is close to zero then the transition state resembles the reactants in its potential dependence, whereas when it approaches unity the transition state behaves in a product-like manner. The value of α is typically found to be close to 0.5 for many reactions.

Equations 9 and 10 can be substituted into Equation 6, to give an expression for the net current i flowing at the electrode as a function of the overpotential and transfer coefficient (Equation 11). This is the Butler-Volmer equation, which is fundamental to electrode kinetics.

$$i = i_0 \left[\exp\left(\frac{(1-\alpha)F\eta}{RT}\right) - \exp\left(\frac{-F\alpha\eta}{RT}\right)\right] \tag{11}$$

$$i_0 = FAk^{o}[R]^{\alpha}_{bulk}[O]^{1-\alpha}_{bulk} \tag{12}$$

The value i_0 is called the exchange current, which can essentially be considered as a scaling factor which is dependent on the experimental conditions and the value of the standard rate constant. If

i_0 is large, little applied overpotential is required to drive the reaction either in anodic or cathodic directions and the electrode reaction is said to be reversible. Because i_0 is large, the net current i will have considerable contributions from both i_a and i_c except at very large overpotentials. For processes with a very small value of i_0, a high overpotential is required to induce current flow and the process is said to be irreversible. At overpotentials that drive the anodic (oxidative) process, the cathodic (reductive) current is vanishingly small.

Marcus theory of electron transfer reactions provides a microscopic view of the origins of these two extreme classes of electrode processes - reversible (fast kinetics) and irreversible (slow kinetics). If we consider the simple one-electron reduction of O to R at a metal electrode, for the reduction of O to R to take place, an electron must be transferred from the metal electrode to the species O in solution. For this process to be viable thermodynamically, the electrons in the Fermi level of the metal (E_F) must have a higher energy then the lowest unoccupied molecular orbital (LUMO) of O. If the Fermi level of the electrode is gradually increased from low energy to high, the transfer of an electron from the metal to O will become thermodynamically favourable once the Fermi level of the electrode crosses the LUMO energy level of O, and reduction can take place. As the electrode potential becomes more negative, the free energy for electron transfer from metal to O will become smaller and the rate of reduction of O will increase. Thus, k_{red} increases as the overpotential becomes more negative.

Electron transfer occurs via quantum mechanical tunneling of the electrons from the metal to O, and is subject to two constraints. Firstly, the electron transfer must follow the Frank-Condon Principle. As electron transfer takes place on a time-scale of 10^{-15} - 10^{-16} s and nuclear motions (i.e. vibrations) occur on the significantly longer time-scale of 10^{-13} s, it is assumed that there is no change in geometry of O during the electron transfer. It follows that the product R, after electron transfer, must posses the same molecular shape and solvation shell as O did before reduction. The second constraint is that no loss or gain of energy accompanies the electron transfer. Therefore, R must be formed with an energy that exactly matches the sum of the energy of the electron in the Fermi level immediately preceding transfer and the energy of O immediately before reduction.

These constraints imply that for electron transfer to take place the O molecule must become thermally excited and the R molecule formed will also be energetically excited. This activated state of O is the transition state for the reaction, since it represents the structure for which O and R have the same geometry that is intermediate between the equilibrium geometries of unexcited O and R. The energy required for this activation will be greater in those cases where the molecular geometry of O and R are very different. For simple electron transfer reactions, fast (reversible) electrode processes will be observed when both species in the redox process have comparable shapes and solvation, and slow (irreversible) electrode kinetics will be observed when reactant and product have very different geometries.

2.4.3 Rate of mass transport of reactant to the electrode surface

In Section 2.4.1 it was seen that the rate of electron transfer at an electrode is controlled by the heterogeneous rate of reaction and the concentration of reactant at the electrode surface. The heterogeneous rate was discussed above, in this section the factors affecting the concentration of the reactant at the electrode surface shall be discussed.

Assume a dynamic electrochemical process is underway at an electrode, i.e. there is electron transfer between the electrode and reactants in solution. The reactant is being consumed and products are being generated. Without supply of fresh reactant the reaction would quickly stop. In a real system however, a fresh supply of reactant is being supplied to the electrode surface through three mass transport processes: convection, migration and diffusion. Convection occurs naturally in a solution due to thermal gradients and density differences in the solution; and can also be controlled mechanically, for example by pumping or stirring the solution. Migration occurs due to the electrostatic force exerted on charged particles due to the potential drop in solution near the electrode interface. Diffusion arises from concentration gradients within a solution.

In an electroanalytical cell, it is desirable to control these three mass transport mechanisms in order to achieve reproducible results which are easily compared to other results in the literature and can be analysed by established theory. Convection is controlled by ensuring the solution is stable before performing the electrochemical measurements, and there are minimal thermal and density gradients through the solution. An alternative method does not seek to prevent convection, but rather it ensures a reproducible convection rate by imparting a mechanical force on the solution, for example by rotating the electrode. Migration is limited by the addition of a relatively high concentration of an inert background electrolyte, which maintains near electrical neutrality in the interfacial region.

With convection and migration controlled, this leaves diffusion as the major source of fresh reactant to the electrode surface. Diffusion of a reactant, B, in solution can be described by Fick's first and second laws, given in Equations 13 and 14, respectively (D_B is the diffusion coefficient of B). The first law gives a formula for $J_B(x,t)$, the number of moles of B that pass a given location per second per cm^2. The second law provides a formula for calculating the rate of change of concentration over time. These laws enable the prediction of the concentration changes of electroactive material near an electrode surface.

$$J_B(x,t) = -D_B \frac{\partial [B]_{(x,t)}}{\partial x} \tag{13}$$

$$\frac{\partial [B]}{\partial t} = D_B \left(\frac{\partial^2 [B]}{\partial x^2} \right) \tag{14}$$

During the electrochemical process, B is transported to the electrode by diffusion to a point within 1-2 nm of the surface, where the drop in potential between the electrode and the solution

induces the transfer of the electron by tunneling, from B to the electrode. Any B at the electrode surface is therefore reduced, which causes a concentration gradient to be established between the surface (where the concentration of B is zero) and the bulk solution (where the concentration is unchanged). This forces more B from the bulk solution to the electrode surface and establishes a diffusion layer, whose thickness increases with time of electrolysis. At a real electrode the thickness of the diffusion layer is ultimately limited by mixing of the bulk solution by natural convection. A constant steady-state diffusion layer thickness is established soon after commencement of electrolysis, with a greater degree of convection in solution resulting in a thinner diffusion layer.

2.4.4 Cyclic voltammetry

It has been seen above that the rate of reaction at an electrode is governed by the heterogeneous rate of electron transfer and the mass transport of fresh reactant to the electrode surface, the variables affecting these two key factors were then discussed. In this section, the topics discussed above shall be related to a practical technique that has been used extensively throughout this research, namely cyclic voltammetry.

Cyclic voltammetry (CV) is one of the most common and popular electrochemical techniques used to assess parameters such as redox potentials, reversibility of redox reactions, and redox reaction kinetics. The method measures current as a function of voltage and so can give detailed mechanistic information about the electron transfer processes occurring at an electrode. A typical cyclic voltammogram is shown in Figure 20.

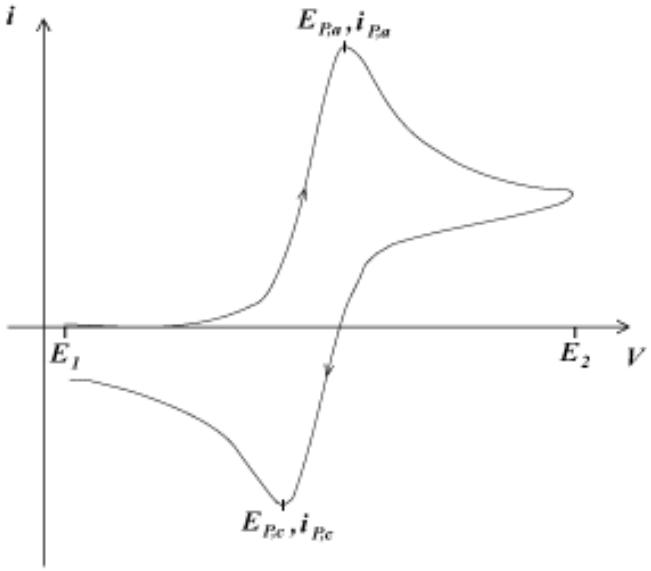

Figure 20: Example of a cyclic voltammogram

To explain the CV process, let's consider the simple one-electron electrode reaction given in Equation 15.

$$R_{(aq)} \rightarrow O_{(aq)} + e^- \tag{15}$$

The potential of the working electrode is first swept from E_1, at which R cannot undergo oxidation, to E_2, where the electron transfer is driven rapidly and R is converted to O. The current response shows an initial exponential rise in current with increasing voltage, which reaches a peak value i_P at voltage E_P and thereafter begins to fall away. The form of the current / voltage behaviour can be explained as follows: initially no current is passed since the applied potential is not great enough to induce electron transfer, but as the potential is swept to more positive values it reaches a value at which R can be oxidised to O, and current begins to flow. As described earlier the current is dependent on the heterogeneous rate constant for electron transfer k_{ox}, which in turn has an exponential dependence on the overpotential η. Therefore, initially the current rises almost exponentially with overpotential. However, it was also seen above that the current is also dependent on the concentration of reactant R at the electrode surface. As the potential is swept to more positive values, electrolysis consumes R, which is only partially replenished by diffusion of fresh R from the bulk solution. Therefore, as the concentration of R at the electrode surface becomes less, the thickness of the diffusion layer progressively increases and there is a resulting decrease in current. The current at potentials less than E_P is dependent on the rate of heterogeneous electron transfer and the current at potentials greater than E_P is dependent on rate of mass transport of the reactant R to the electrode surface.

The second step of the CV process is to sweep back from E_2 to E_1. On sweeping the potential back from E_2 to E_1, the species O formed at the electrode surface during the forward sweep is re-reduced back to R. Current flows in the reverse direction due to the reduction of O to R. In a similar way to the forward scan, the reduction current increases initially, as the concentration of O at the electrode surface is high and the increasing overpotential results in a faster rate of heterogeneous electron transfer. Gradually all of the O present in the diffusion layer is reconverted to R and the current drops to zero.

The shapes of the current peaks on a CV reveal the reversibility of the electrode kinetics for the redox couple. For a reversible couple (those with fast kinetics), significant currents flow at small overpotentials and the heights of the forward and reverse current peaks are equal in magnitude and for one electron transfers have a constant separation of 59 mV at all scan rates (Equation 16). Irreversible couples have a larger peak separation ΔE_P, as a bigger overpotential is required to drive the electron transfer. The size of the backward peak is smaller relative to the forward peak and depends on the voltage scan rate, as does the potential of the peaks E_P. The peak separation and dependence on the scan rate are therefore diagnostic of the nature of the electrode kinetics. 'Reversible' and 'irreversible' electrode kinetics refers to limiting cases of reaction but often electrode kinetics are intermediate in nature, and these are termed 'quasi-reversible'. Quasi-reversible reactions have a

forward and backward peak current ratio of close to unity, like reversible reactions, but the peak separation is dependent on scan rate.

$$\Delta E_p = \left|E_P^{ox} - E_P^{red}\right| = \frac{2.218RT}{nF} \tag{16}$$

The size of the peak current for a reversible reaction is given by Equation 17, where n is the number of electrons transferred, A is the area of the electrode (cm^2), D is the diffusion coefficient (cm^2s^{-1}), v is the scan rate (Vs^{-1}) and C is the bulk concentration ($molcm^{-3}$). It can be seen that i_P varies with $v^{1/2}$ for reversible reactions and plotting these experimental values can further aid identification of electrode kinetics. The explanation for the scan rate dependence of i_P is that i_P is dependent on the flux of reactant at the electrode surface, which is controlled by the rate of diffusion. This is dependent on the concentration gradient near the electrode surface, i.e. the diffusion layer thickness. If fast scan rates are used, less time is available for the electrolysis of reactant, so its depletion near the electrode is less. This results in a thinner diffusion layer and a steeper concentration gradient, which leads to increased flux of reactant and higher i_P.

$$i_P = (2.69) \times 10^5 n^{\frac{3}{2}} A D^{\frac{1}{2}} C v^{\frac{1}{2}} \tag{17}$$

2.4.5 Experimental procedure used in this research for investigating electrochemistry in the absence of protons

A glass cell has been used for all of the electrochemical experiments. The cell was large enough to hold 5 ml of the solution being investigated. A lid was used to prevent oxygen entering the cell during experiments. The lid had four tightly-fitting holes: one for the working electrode, another for the reference electrode, a third for the counter electrode and a final for a syringe to carry Ar gas for de-oxygenating the cell.

The working electrode was a glassy carbon disc of 3 mm diameter (Bioanalytical Systems). This was polished before every CV using 0.3 μm alumina suspended in de-ionised water on a Buehler Microcloth polishing pad, then rinsed thoroughly in de-ionised water to remove all alumina, and dried. A Ag wire quasi-reference electrode has been used. This was in a separate compartment containing background electrolyte, electrically connected to the electrochemical cell through a vicor frit. The counter electrode was Pt wire. An Autolab potentiostat (EcoChemie, Netherlands), controlled by GPES version 4.7, has been used.

The solvents used for the background electrolyte were DCM and MeCN (both laboratory reagent grade, Fisher Scientific). The electrolytes were $[NBu_4][PF_6]$, $[NBu_4][ClO_4]$ and $[NBu_4][BF_4]$ (all electrochemical grade, Sigma-Aldrich) at a concentration of 0.1 M. The solution was de-oxygenated using either Ar or CO (both BOC).

After all of the required experiments had been performed, ca. 5 mM ferrocene was added to the

solution and a CV was taken to obtain the potential of the first oxidation of ferrocene, Fc/Fc^+. The CVs taken for the test solution were then referenced to this Fc/Fc^+ potential.

2.4.6 Experimental procedure used in this research for testing electrocatalytic activity

The experimental setup described above was also used for testing the electrocatalytic activity of the complexes. After obtaining a CV of the complex in the absence of protons, a proton source was added to the solution in increments; after each addition of acid a CV was taken. The acids used were $HBF_4.Et_2O$, HOTs and HOAc (all from Sigma-Aldrich). The available protons in solution after addition of $HBF_4.Et_2O$ was found to decrease over time, thus when using this acid the experimental steps were performed in rapid succession to limit the losses (this is thought to be due to evaporation from the cell over time or hydrolysis).

2.5 Molecular orbitals of the tri-iron complexes investigated, using density functional theory (DFT) calculations

The DFT calculations were performed with the Gaussian09 package of programs. The calculations were carried out with the B3LYP function, which utilises the Becke three-parameter exchange function (B3) combined with the correlation functional of Lee, Yang and Parr (LYP). The Fe atoms were described by Stuttgart-Dresden effective core potentials and the SDD basis set, while the 6-31G(d') basis set, as implemented in the Gaussian09 program suite, was employed for the remaining atoms. The geometry-optimised structures reported here represent minima based on zero imaginary frequencies (positive eigenvalues), as established by frequency calculations using the analytical Hessian. The computed harmonic frequencies for the carbonyl stretching bands have been scaled using Radom's scaling factor of 0.9614. The charges associated with the non-hydrogen atoms in the compounds were determined by natural population analysis at the B3LYP level of theory. The geometry-optimised structures have been drawn with the JIMP2 molecular visualisation and manipulation program.

3 $Fe_2(SC_6F_5)_2(CO)_6$: The influence of a highly electron withdrawing dithiolate bridge

This chapter presents the susceptibility to protonation, electrochemical behaviour and electrocatalytic activity of $Fe_2(SC_6F_5)_2(CO)_6$ (Figure 21). As an extension, an initial investigation into the di-substituted analogue $Fe_2(SC_6F_5)_2(\mu\text{-}Ph_2PCH_2PPh_2)(CO)_4$ is also presented.

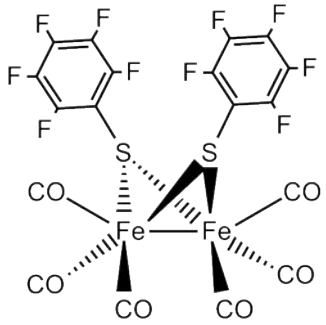

Figure 21: $Fe_2(SC_6F_5)_2(CO)_6$

As was discussed in Section 1.3, the bridge of the di-iron complexes influences electron density on the Fe centres, and therefore the reduction potential of the complexes. The more electron withdrawing the bridge, the more mild the reduction potential. It was therefore of interest to investigate the $Fe_2(SC_6F_5)_2(CO)_6$ complex, in which the highly electron withdrawing $(SC_6F_5)_2$ bridge removes electron density from the Fe centres.

3.1 Susceptibility of $Fe_2(SC_6F_5)_2(CO)_6$ to protonation

Understanding the susceptibility of $Fe_2(SC_6F_5)_2(CO)_6$ to protonation is vital in order to elucidate any catalytic mechanism the complex may exhibit. In particular, this indicates whether the first step of the catalytic mechanism is likely to be a protonation or an electrochemical reduction (see Section 1.3).

Infrared (IR) spectroscopy was used to investigate whether $Fe_2(SC_6F_5)_2(CO)_6$ would undergo protonation. Protonation at the Fe centres would result in electron density being withdrawn from the Fe centres to form the hydride bond, in turn decreasing backbonding into the CO ligands, thus strengthening the CO bond and shifting the corresponding IR bands to higher wavenumbers.

The IR spectrum of the complex in the absence of protons is shown in Figure 22. Bands are seen at 2089, 2059, 2023 and 2011 cm^{-1}. Upon addition of 1, and then 5, molar equivalents of the strong acid $HBF_4.Et_2O$ to the solution, there was no change in the band positions. Therefore $Fe_2(SC_6F_5)_2(CO)_6$ does not undergo protonation in the presence of $HBF_4.Et_2O$. After 24 hours the band positions still had not changed, indicating both that the complex would not protonate, and that it was stable, over this timescale.

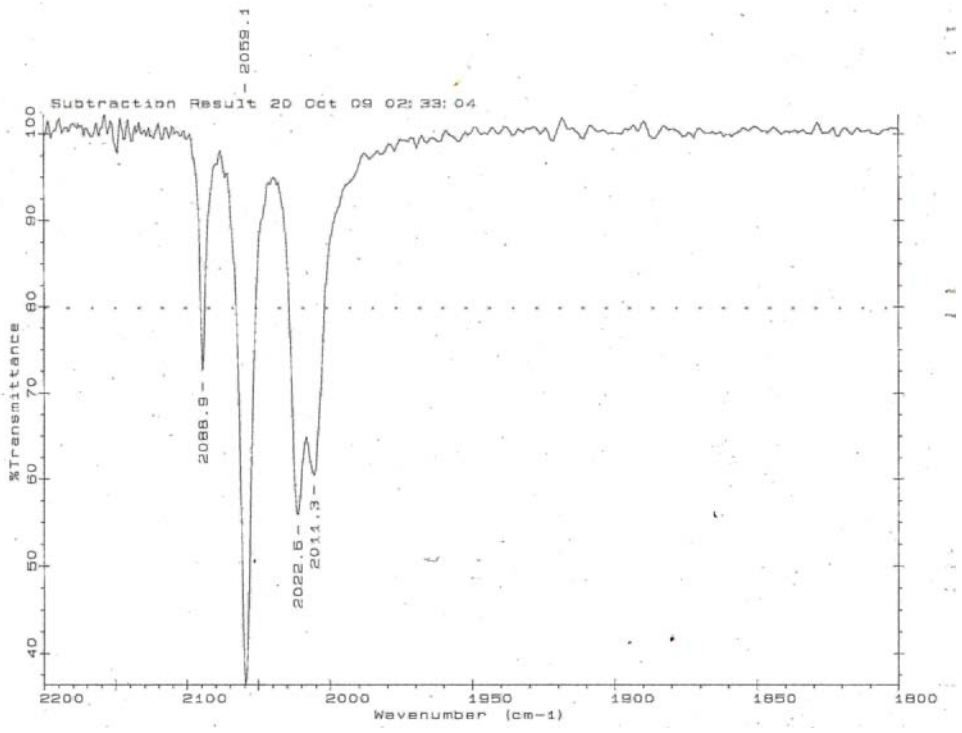

Figure 22: IR spectrum of $Fe_2(SC_6F_5)_2(CO)_6$ in DCM

The electron withdrawing nature of the $(SC_6F_5)_2$ bridge has caused the IR band positions of the complex to be at higher wavenumbers than complexes which have less electron withdrawing bridges - for example, for the analogous pdt-bridged complex the bands are at 2074, 2036 and 1995 cm^{-1} (in MeCN)[7]. The decreased electron density on the Fe centres has resulted in the complex not being susceptible to protonation. The decreased electron density is, however, expected to make the reduction potential of the complex less negative than complexes with less electron withdrawing

bridges, which is favourable for a lower overpotential for catalysis.

As there was no indication of protonation from the above IR study, no further protonation studies with other techniques such as NMR were undertaken.

3.2 Electrochemistry of $Fe_2(SC_6F_5)_2(CO)_6$ in the absence of protons

The electrochemical behaviour of $Fe_2(SC_6F_5)_2(CO)_6$ has been investigated in both DCM and MeCN. The first set of experiments were carried out without protons present to aid in understanding any catalytic mechanism the complex may exhibit.

3.2.1 Electrochemistry of $Fe_2(SC_6F_5)_2(CO)_6$ in the absence of protons, in DCM

The CV of $Fe_2(SC_6F_5)_2(CO)_6$ in DCM is shown in Figure 23. The complex is reduced at -1.37 V. A small reduction feature occurs at -1.71 V, with a larger reduction peak at -2.15 V. On the return scan, two peaks are observed at -0.65 V and -0.50 V, which are due to products formed during the reductive processes. At the positive limit of the potential window a large oxidation occurs. The product of this oxidation is reduced at 0.2 V.

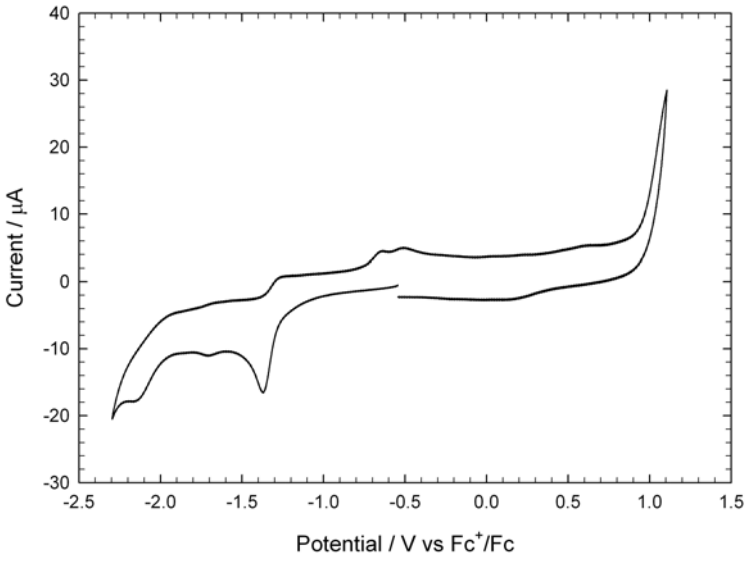

Figure 23: Cyclic voltammetry of $Fe_2(SC_6F_5)_2(CO)_6$ (0.5 mM) in DCM-$[NBu_4][PF_6]$ (v=0.1 Vs^{-1}, glassy carbon electrode; V vs Fc^+/Fc)

By comparison with similar complexes in the literature, the reduction process appears consistent with a transfer of one electron (see Chapter 1). The change in the formal oxidation states is therefore Fe(I)Fe(I) to Fe(I)Fe(0).

3.2.2 Electrochemistry of $Fe_2(SC_6F_5)_2(CO)_6$ in the absence of protons, in CO-saturated DCM

The reduction processes of many complexes in the literature have been studied under a CO atmosphere, as a common fate following reduction is CO ligand loss. It was seen above that the reduction of $Fe_2(SC_6F_5)_2(CO)_6$ is irreversible under an Ar atmosphere, suggesting a subsequent chemical process which alters the structure of the complex. The electrochemical response of $Fe_2(SC_6F_5)_2(CO)_6$ has therefore been analysed under CO, as shown in Figure 24. The CVs under CO and under Ar

are very similar. As the first reduction process is equally irreversible under a CO atmosphere, CO ligand loss is not the sole cause of its irreversibility. It is therefore likely that the complex undergoes a structural rearrangement following the first reduction process. There is a clear difference between the two CVs at ca. -1.7 V where a small reduction feature is present under Ar, but not under CO. This difference suggests that some CO ligand loss could indeed occur. Thus the steps under an Ar atmosphere are suggested to be:

1. First reduction of the neutral complex (-1.4 V)
2. Rearrangement of the singly reduced species and loss of a CO ligand
3. Reduction of the resulting species (-1.7 V)

The peak at -1.7 V shall be found to be significant in the catalysis studies later in this chapter, and will be discussed further there. It will be also be seen that it is possible that the complex forms a dimer after rearrangement and CO ligand loss step.

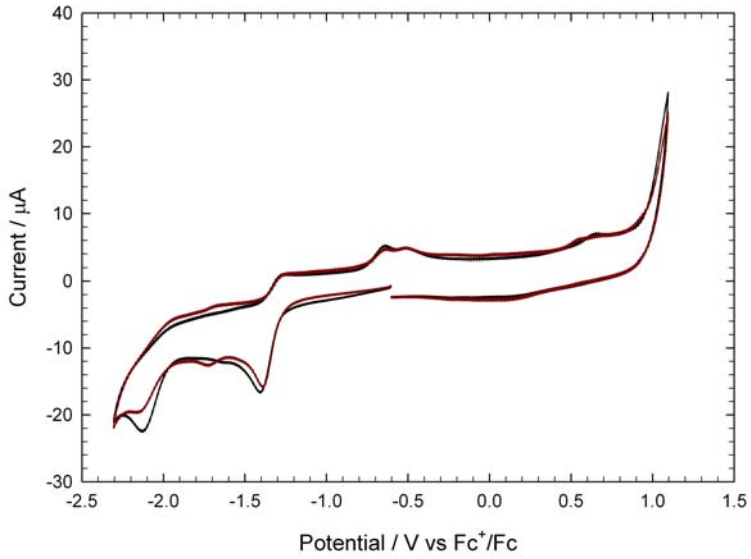

Figure 24: Cyclic voltammetry of $Fe_2(SC_6F_5)_2(CO)_6$ (0.5 mM) in DCM-$[NBu_4][PF_6]$ saturated with CO (black line) and Ar (red line) (v=0.1 Vs^{-1}, glassy carbon electrode; V vs Fc^+/Fc)

3.2.3 Electrochemistry of $Fe_2(SC_6F_5)_2(CO)_6$ in the absence of protons, in MeCN

The $Fe_2(SC_6F_5)_2(CO)_6$ complex has also been investigated in an MeCN solvent. MeCN is a co-ordinating solvent that has been used by several groups in the field. Thus, to make comparisons between $Fe_2(SC_6F_5)_2(CO)_6$ and other complexes in the literature, and to analyse the complex in a coordinating solvent, it was deemed important to replicate the investigations in MeCN.

The CV of the complex in MeCN is shown in Figure 25. The first reduction of the complex occurred at -1.15 V. A minor reduction feature is at -1.59 V, with a larger peak at -2.06 V. On the return scan a large oxidation peak occurs at -0.47 V, which is attributed to products formed during

the reduction process. Other minor oxidations of these products occur at -0.15 and 0.47 V. The first oxidation of the neutral complex is at 1.02 V, and is approximately twice the peak height of the first reduction.

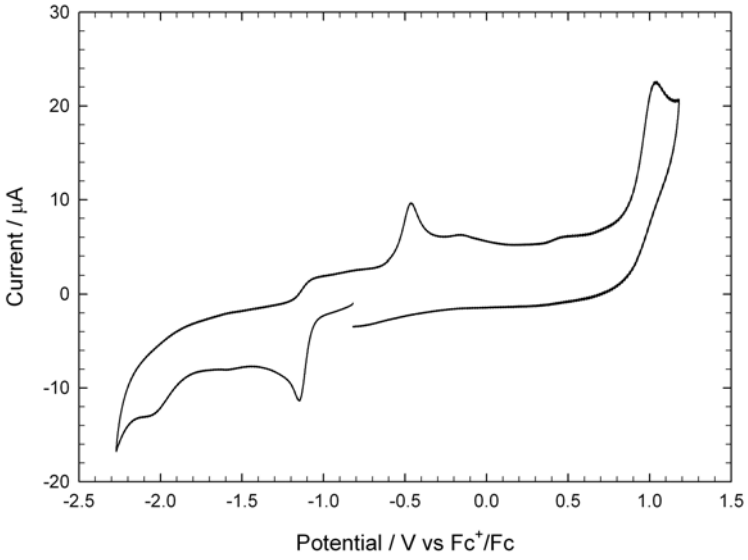

Figure 25: Cyclic voltammetry of $Fe_2(SC_6F_5)_2(CO)_6$ (0.5 mM) in MeCN-$[NBu_4][PF_6]$ (v=0.1 Vs^{-1}, glassy carbon electrode; V vs Fc^+/Fc)

To probe the behaviour of the reduction process further, the scan rate was varied (Figure 26). At scan rates above 5 Vs^{-1} the reduction remains irreversible, and an extra oxidation peak is seen at -0.72 (5 Vs^{-1}) or -0.69 V (10 Vs^{-1}). Normalising the current to scan rate, i.e. dividing current by square root of scan rate, indicated that the reduction remained a 1-electron process for all of the scan rates used.

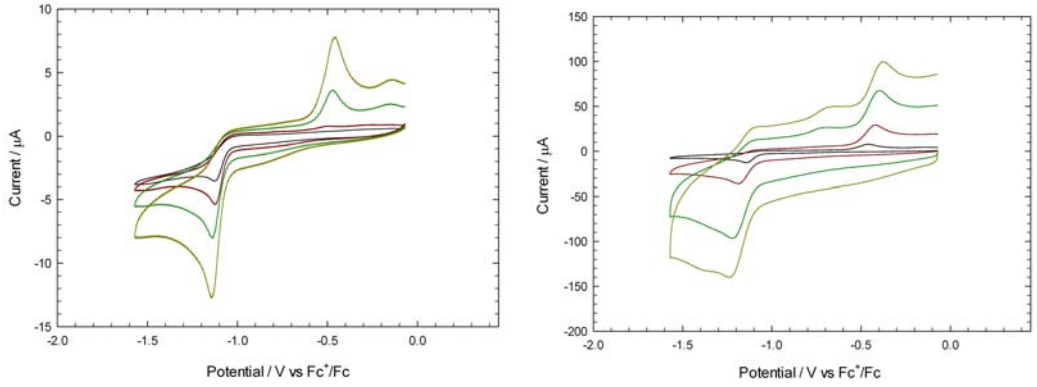

(a) v=0.01, 0.02, 0.05, 0.1 Vs^{-1} (b) v=0.1, 1.0, 5.0, 10.0 Vs^{-1}

Figure 26: Cyclic voltammetry of $Fe_2(SC_6F_5)_2(CO)_6$ (0.5 mM) in MeCN-$[NBu_4][PF_6]$ (glassy carbon electrode; V vs Fc^+/Fc)

3.2.4 Summary and discussion

A useful benchmark for the first reduction of the H-cluster mimics is the pdt-bridged hexacarbonyl complex $Fe_2(\mu\text{-pdt})(CO)_6$. A comparison between $Fe_2(SC_6F_5)_2(CO)_6$ and the analogous pdt-bridged complex in DCM is shown in Figure 27. As predicted by the IR spectrum, the substitution of the pdt bridge with the highly electron withdrawing $(SC_6F_5)_2$ bridge has resulted in a large positive shift in reduction potential of 0.49 V. Indeed, compared to other complexes in the literature, $Fe_2(SC_6F_5)_2(CO)_6$ has one of the mildest reduction potentials (-1.15 V in MeCN) observed. For example, $Fe_2(\mu\text{-benzenedithiolate})(CO)_6$ is reduced at -1.35 V (in MeCN)[38], and $Fe_2(SC_6H_4NHCOFC_6H_4)_2(CO)_6$ is reduced at -1.2 V (in MeCN)[39]. A complex with an even less negative reduction potential is the o-carborane bridged complex $Fe_2(\mu\text{-}SC_2(BH)_{10}S)(CO)_6$, which undergoes a one electron reduction at -0.94 V (in MeCN)[13].

A second feature of the $(SC_6F_5)_2$ bridge which may influence the lower reduction potential is its open structure. Unlike the pdt bridge, this bridge is more flexible and can sit in a more favourable position with greater bond overlap between the Fe centres and the bridging S atoms. As will be discussed in Section 4.6.5, this may make the reduction potential less negative.

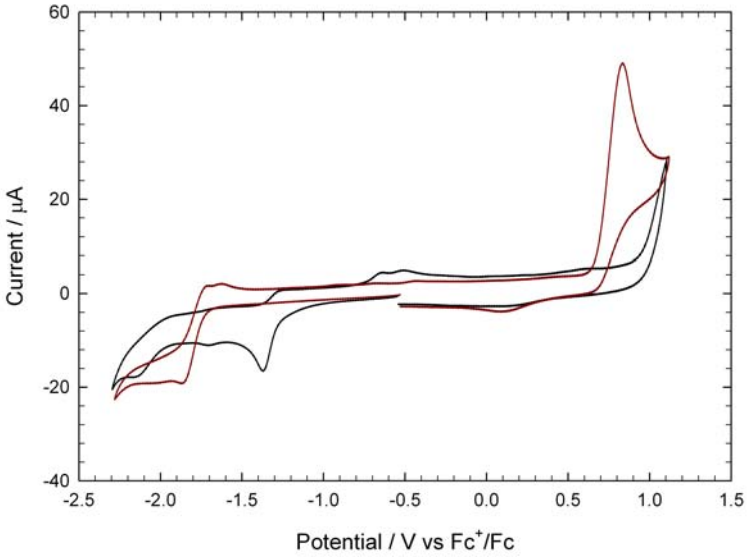

Figure 27: Cyclic voltammetry of $Fe_2(SC_6F_5)_2(CO)_6$ (black line, 0.5 mM) and $Fe_2(\mu\text{-pdt})(CO)_6$ (red line, 0.5 mM) in DCM-$[NBu_4][PF_6]$ (v=0.1 Vs^{-1}, glassy carbon electrode; V vs Fc^+/Fc)

The protonation study presented in Section 3.1 indicated that the complex would not protonate; therefore if catalysis is to occur it will be after the first reduction, when the Fe centres become more basic and may protonate. Based on the electrochemical results presented in this section, the reduction potential is very mild in comparison with other complexes in the literature, thus, if $Fe_2(SC_6F_5)_2(CO)_6$ is protonated after it has been reduced, and this protonation leads to a catalytic mechanism, the complex would be catalytic at one of the lowest overpotentials recorded in the literature. This would be a step forward in decreasing the overpotential for catalysis by H-cluster

mimics. The catalytic behaviour of the complex will be investigated in the next section.

As a side note, it is striking that the first reduction of the complex in MeCN occurred at a potential 0.22 V less negative than in DCM. Also the difference in potential between the first reduction and first oxidation of the neutral complex is smaller in MeCN than DCM. This shows that the solvent has a strong influence on the observed electrochemical behaviour of the complex, indicating that care must be taken in comparing and interpreting reported reduction / oxidation potentials in different solvents.

3.3 Testing for electrocatalytic reduction of protons by $Fe_2(SC_6F_5)_2(CO)_6$, using the strong acid $HBF_4.Et_2O$ as the proton source

As discussed in Chapter 2, the procedure for testing the catalytic activity of a complex is to provide a source of protons, and monitor whether this results in an enhanced reduction current due to the catalytic cycle taking up electrons. This section shall investigate whether, in the presence of protons, $Fe_2(SC_6F_5)_2(CO)_6$ is able to protonate once it has been reduced, and if so, does this lead to a catalytic mechanism for proton reduction.

The strong acid $HBF_4.Et_2O$ was used throughout this thesis as the proton source, as it is an acid commonly used in the literature, so useful comparisons can be made with other complexes.

3.3.1 Testing for electrocatalytic reduction of protons by $Fe_2(SC_6F_5)_2(CO)_6$, using the strong acid $HBF_4.Et_2O$ as the proton source, in DCM

The CV of the complex after the addition of 1 molar equivalent $HBF_4.Et_2O$ to $Fe_2(SC_6F_5)_2(CO)_6$ is shown in Figure 28. The limiting current of the first reduction is increased, and the peak potential is shifted 0.03 V positive to -1.34 V. The peak height of the small reduction feature at -1.71 V is significantly larger. A third reduction process is present at -2.06 V. The two re-oxidation processes that were present at -0.65 and -0.50 V, are now one peak at -0.58 V. The large oxidation at the edge of the potential window is still present at the same position.

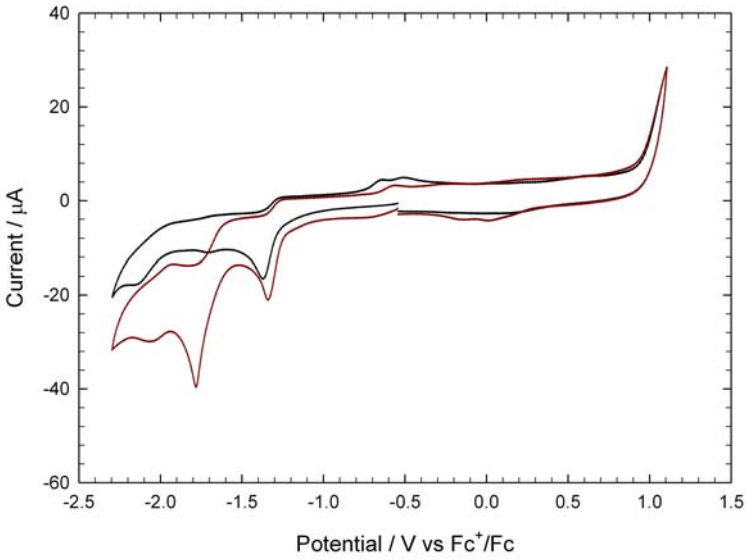

Figure 28: Cyclic voltammetry of $Fe_2(SC_6F_5)_2(CO)_6$ (0.5 mM) in DCM-$[NBu_4][PF_6]$ in the absence of acid and in the presence of 1 molar equivalent $HBF_4.Et_2O$ (v=0.1 Vs^{-1}, glassy carbon electrode; V vs Fc^+/Fc)

On further additions of $HBF_4.Et_2O$ (Figure 29) the current seen at the first reduction continues to grow. There is a slight shoulder to the peak at 2 and 3 equivalents, however this does not continue for higher concentrations of acid. The increase in current is less with each equivalent of acid added;

however, a limit has not been reached by 10 equivalents. The large second reduction at -1.8 V that was seen after 1 equivalent does not grow with further additions of acid. There is a third / fourth process which continues to grow evenly as further equivalents of acid are added. The return scan is similar to the CV obtained after the addition of 1 molar equivalent of acid, the only difference being the oxidation feature at 0.12 V, which gets larger in a more concentrated acid environment.

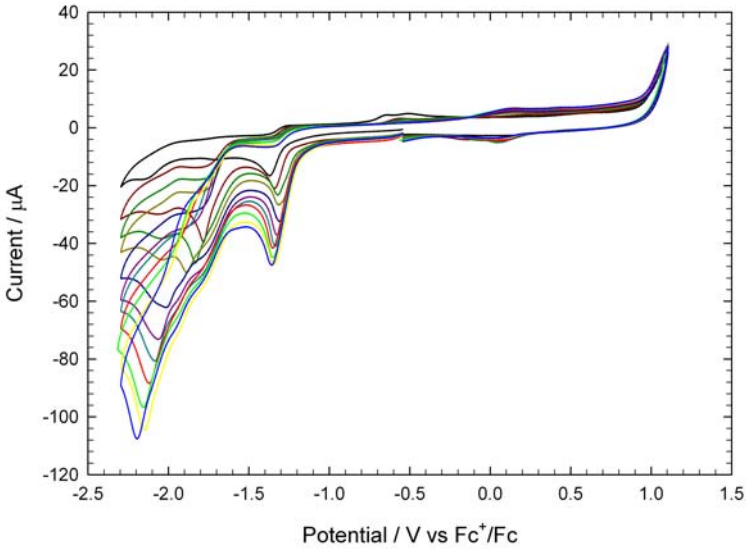

Figure 29: Cyclic voltammetry of $Fe_2(SC_6F_5)_2(CO)_6$ (0.5 mM) in DCM-$[NBu_4][PF_6]$ in the absence of acid and in the presence of up to 10 molar equivalents $HBF_4.Et_2O$ in steps of 1 molar equivalent (v=0.1 Vs^{-1}, glassy carbon electrode; V vs Fc^+/Fc)

These results indicate that the complex is catalytic towards proton reduction. The first reduction of the complex initiates a catalytic mechanism, the second step of which is likely to be a protonation, followed by a further reduction and protonation, i.e. an ECEC process. Additionally, the species responsible for the reduction peak at -1.71 V is highly catalytic based on its small concentration in solution. These results shall be discussed further below.

3.3.2 Testing for electrocatalytic reduction of protons by $Fe_2(SC_6F_5)_2(CO)_6$, using the strong acid $HBF_4.Et_2O$ as the proton source, in MeCN

CVs of $Fe_2(SC_6F_5)_2(CO)_6$ in increasing concentrations of $HBF_4.Et_2O$ have been taken in an MeCN solvent. On the addition of 1 molar equivalent $HBF_4.Et_2O$ (Figure 30) the first reduction peak height increases and is shifted less negative to -1.12 V, with a shoulder at -1.09 V. A small peak is also present due to reduction of the neutral complex. Two reduction peaks that were not present for the neutral complex, are now seen at -1.52 and -1.61 V. A further reduction process is present at -1.89 V. On the return scan, the oxidation process at -0.47 V has diminished, and is now two processes. The oxidation of the complex has shifted 0.02 V less positive to 1.00 V.

On further additions of $HBF_4.Et_2O$ (Figure 31) the peak current of the first reduction process rises to a limit of 30 μA. Once the limit is reached, a second reduction process appears at -1.4 V.

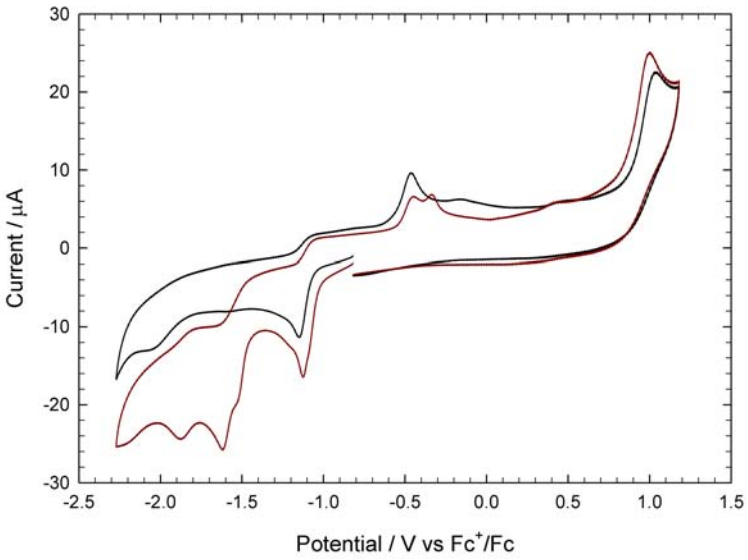

Figure 30: Cyclic voltammetry of $Fe_2(SC_6F_5)_2(CO)_6$ (0.5 mM) in MeCN-$[NBu_4][PF_6]$ in the absence of acid and in the presence of 1 molar equivalent $HBF_4.Et_2O$ (v=0.1 Vs^{-1}, glassy carbon electrode; V vs Fc^+/Fc)

The reduction processes that were observed for 1 molar equivalent at -1.52 and -1.61 V continue to grow, becoming more broad and merging into one peak. A further cathodic process that grows continuously with additions of acid is observed at a more negative potential. The return scan is similar to that seen for one molar equivalent, however a peak is present at 0.05 - 0.10 V, the shape of which suggests a stripping of species deposited onto the electrode surface when sweeping to reductive potentials.

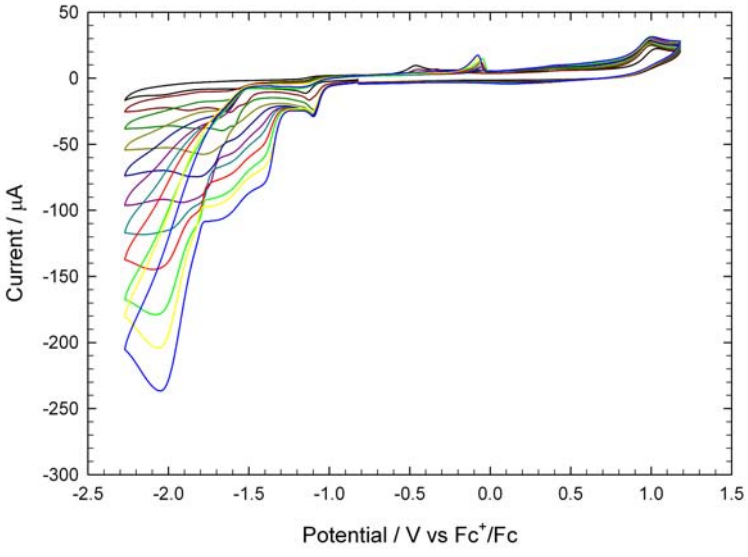

Figure 31: Cyclic voltammetry of $Fe_2(SC_6F_5)_2(CO)_6$ (0.5 mM) in MeCN-$[NBu_4][PF_6]$ in the absence of acid and in the presence of up to 10 molar equivalents $HBF_4.Et_2O$ in steps of 1 molar equivalent (v=0.1 Vs^{-1}, glassy carbon electrode; V vs Fc^+/Fc)

As with the DCM experiment above, this behaviour is indicative of the complex being catalytic.

Catalysis is initiated by the first reduction of the complex, once this catalytic mechanism reaches its limiting rate, a secondary mechanism is available at -1.4 V. One of the steps in the first catalytic mechanism limits the current.

3.3.3 Summary and discussion

A comparison between $Fe_2(SC_6F_5)_2(CO)_6$ and the analogous pdt-bridged complex after the addition of 10 molar equivalents $HBF_4.Et_2O$ is shown in Figure 32. Whereas the fluorinated benzene bridged complex is catalytic towards proton reduction at -1.34 V, the pdt-bridged complex is not catalytic until -1.65 V. This implies that the $(SC_6F_5)_2$ bridge has resulted in a improvement in reduction potential of 0.31 V. As was discussed earlier, compared to complexes with other bridges used in the literature, this complex exhibits one the mildest reduction potentials, and catalysis is therefore at one of the lowest overpotentials recorded.

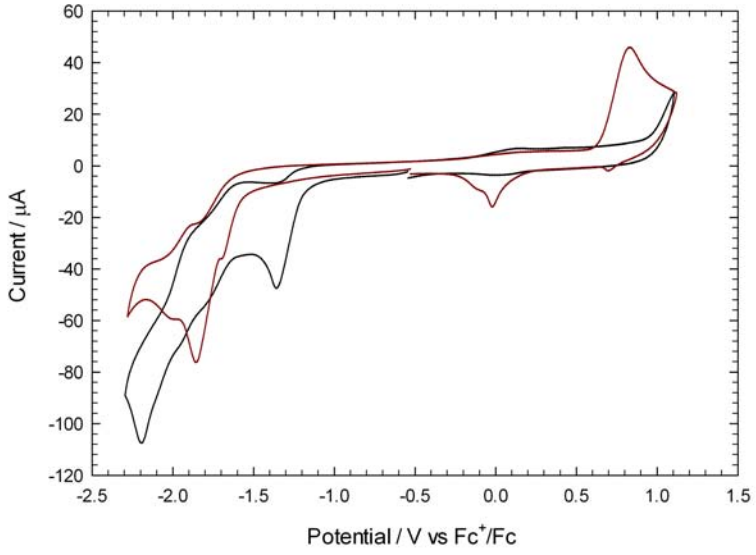

Figure 32: Cyclic voltammetry of $Fe_2(SC_6F_5)_2(CO)_6$ (black line, 0.5 mM) and $Fe_2(\mu\text{-pdt})(CO)_6$ (red line, 0.5 mM) in the presence of 10 molar equivalents $HBF_4.Et_2O$ in DCM-$[NBu_4][PF_6]$ (v=0.1 Vs^{-1}, glassy carbon electrode; V vs Fc^+/Fc)

Clear differences in the catalytic behaviour in DCM and MeCN have been observed. The catalysis begins at a lower overpotential in MeCN, due to the less negative reduction potential of the neutral complex in MeCN found earlier. However, the catalytic current at the first reduction peak is limited at 30 μA in MeCN, whereas in DCM a limit has not been reached after 10 molar equivalents $HBF_4.Et_2O$ have been added. Overall, however, taking into account additional catalytic processes at more negative potentials, the catalysis reaches a higher rate in MeCN than in DCM.

A key result evident in both DCM and MeCN is the highly catalytic species formed after the reduction of the neutral complex, which is reduced at -1.71 V in DCM (-1.59 V in MeCN). Given its small concentration in solution, this minor species results in a very large catalytic reduction current. The species has not yet been identified, however it was seen in Section 3.2.2 that this species is not

present when the solution is saturated with CO. One possible identity is a dimeric species formed after the loss of a CO ligand from the singly reduced, electron rich, complex. Pickett, Best and co-workers reported a similar dimer formation following reduction of the analogous edt- and pdt-bridged hexacarbonyl complexes; the dimers were also found to be highly catalytic[8;16]. In this case the steps presented in Section 3.2.2 would be updated to:

1. First reduction of the neutral complex (-1.4 V)
2. Rearrangement of the singly reduced species and loss of a CO ligand
3. **Dimer formation**
4. Reduction of the resulting species (-1.7 V)

An alternative explanation is that upon reduction the complex decomposes to a mono-Fe fragment, with a vacant coordination site making the complex highly catalytic. Under CO the coordination site is occupied by CO, thus limiting the catalytic activity of the complex.

Based on the observed results, a possible catalytic mechanism is proposed in Figure 33. The neutral complex (denoted A) is first reduced at -1.37 V (DCM). In the presence of the strong acid, the complex can either protonate (AH) or form the minor species (denoted B^-); when the concentration of the acid is high, the former process is favoured. The protonated species is reduced (AH^-), protonated again, and then releases H_2 to return the neutral complex, which re-enters the catalytic cycle. If instead, A^- goes on to form B^-, this minor species is reduced at -1.71 V (DCM) to form B^{2-}, which goes on to be protonated (BH^-), reduced (BH^{2-}), protonated again, and release H_2 to return B^-.

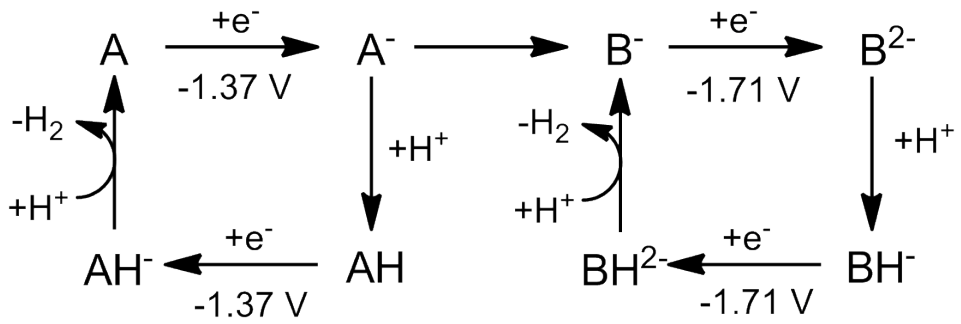

Figure 33: Possible catalytic mechanism of $Fe_2(SC_6F_5)_2(CO)_6$ (denoted A) in the presence of $HBF_4.Et_2O$; B^- denotes the highly catalytic species formed after reduction of the neutral complex; potentials are taken from the cyclic voltammograms obtained in DCM

3.4 Testing for electrocatalytic reduction of protons by $Fe_2(SC_6F_5)_2(CO)_6$, using the weak acid HOAc as the proton source

The $Fe_2(SC_6F_5)_2(CO)_6$ complex has also been investigated in the presence of the far weaker acetic acid. From above it was known that in the presence of a strong acid the complex is catalytic after a one electron reduction, therefore the next step was to find out if the complex is catalytic when the proton source is the weaker acid HOAc.

3.4.1 Testing for electrocatalytic reduction of protons by $Fe_2(SC_6F_5)_2(CO)_6$, using the weak acid HOAc as the proton source, in DCM

CVs of $Fe_2(SC_6F_5)_2(CO)_6$ in the presence of up to 10 molar equivalents HOAc are given in Figure 34. After the addition of 1 equivalent HOAc there is no change in the first reduction peak. The current of the small reduction process at -1.71 V increases. The third reduction process at ca. -2.2 V also increases slightly. The return scan is very similar to the complex with no protons, except for a change in the positions of re-oxidation peaks and a small reduction feature at 0.2 V.

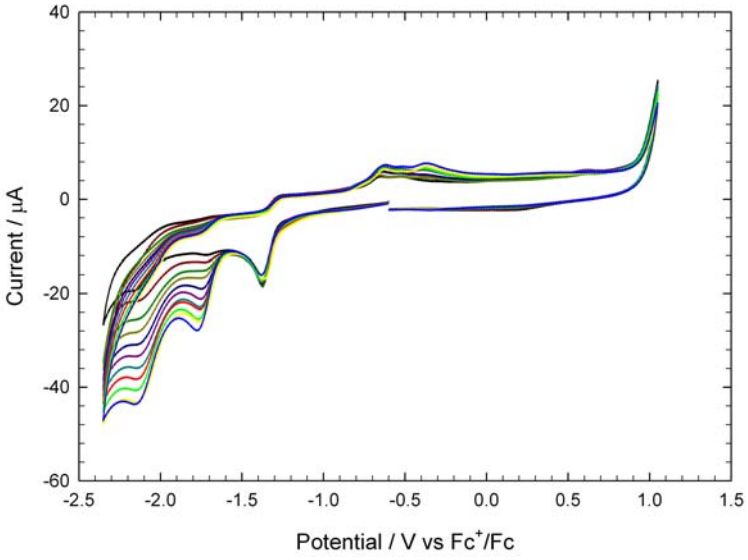

Figure 34: Cyclic voltammetry of $Fe_2(SC_6F_5)_2(CO)_6$ (0.5 mM) in DCM-$[NBu_4][PF_6]$ in the absence of acid and in the presence of up to 10 molar equivalents HOAc in steps of 1 molar equivalent (v=0.1 Vs^{-1}, glassy carbon electrode; V vs Fc^+/Fc)

On further additions of HOAc in steps of 1 molar equivalent, the first reduction peak remained unchanged. The second reduction peak grew uniformly, with no indication of reaching a limiting rate; as did the third reduction peak. The oxidation peaks at ca. -0.5 V grew. A new small oxidation peak was observed at 0.6 V, as well as a reduction peak of similar magnitude at 0.2 V.

On further additions of HOAc in steps of 10 molar equivalents (Figure 35) the second reduction peak reached a limiting current after adding 40 molar equivalents. The third reduction continued to increase in height. The first of the re-oxidation peaks decreased in height, while the other remained

unchanged. There was a large drop in the current of the oxidation of the complex.

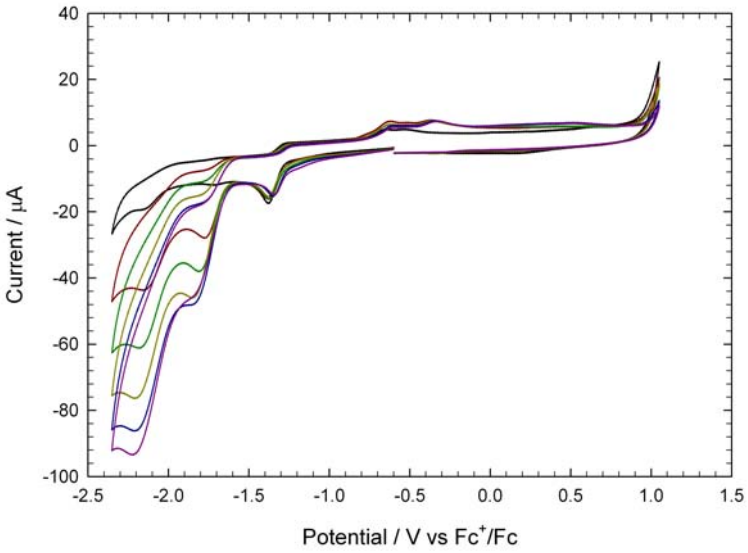

Figure 35: Cyclic voltammetry of $Fe_2(SC_6F_5)_2(CO)_6$ (0.5 mM) in DCM-$[NBu_4][PF_6]$ in the absence of acid and in the presence of up to 50 molar equivalents HOAc in steps of 10 molar equivalent (v=0.1 Vs^{-1}, glassy carbon electrode; V vs Fc^+/Fc)

These results indicate the presence of a species that is highly catalytic at -1.71 V. Interestingly, the reduction process which begins the catalytic mechanism is not the first reduction of the neutral complex, rather it is associated with the small peak at -1.71 V, which we have attributed previously to the decomposition product B^-. It is also intriguing that the concentration of this catalytic species is low (as the peak height is small in the absence of protons), however, in the presence of protons a large current is observed even for a very weak acid, implying that the species is highly catalytic.

3.4.2 Testing for electrocatalytic reduction of protons by $Fe_2(SC_6F_5)_2(CO)_6$, using the weak acid HOAc as the proton source, in CO-saturated DCM

It was seen above that the catalytic reduction of HOAc occurs at -1.71 V in DCM, which coincides with a minor reduction feature. In Figure 24 it was seen that this small reduction peak was not present when the CV was performed under a CO atmosphere, therefore the catalysis experiments were repeated in this environment.

CVs of $Fe_2(SC_6F_5)_2(CO)_6$ in the presence of up to 10 molar equivalents HOAc under a CO atmosphere are shown in Figure 36. Again, the peak height of the first reduction did not increase on addition of acid. Notably, the peak present at -1.71 V under an Ar atmosphere, was now absent. The reduction peak at -2.1 V increased on each addition of HOAc.

Further additions of HOAc were made, as shown in Figure 37. Again, no peak was observed at -1.71 V.

These results confirm that the small peak at -1.71 V due to the reduction of a species formed following the reduction of the neutral complex, is not present under a CO atmosphere. As the species

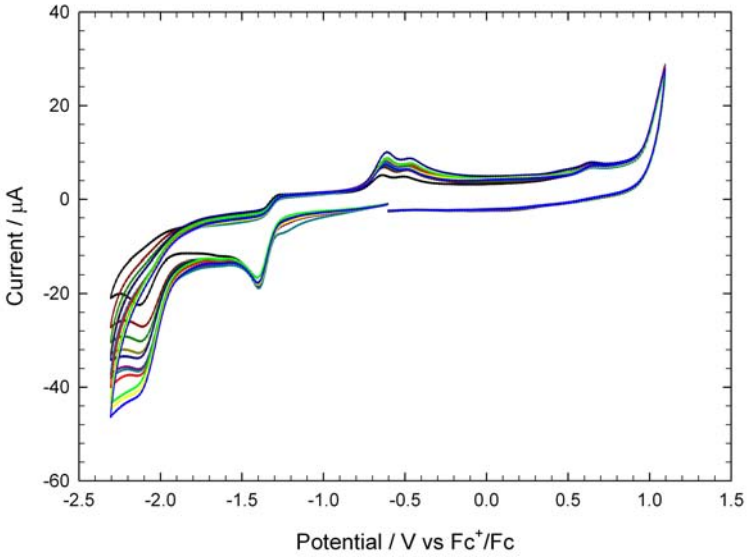

Figure 36: Cyclic voltammetry of $Fe_2(SC_6F_5)_2(CO)_6$ (0.5 mM) in DCM-$[NBu_4][PF_6]$ under CO in the absence of acid and in the presence of up to 10 molar equivalents HOAc in steps of 1 molar equivalent (v=0.1 Vs^{-1}, glassy carbon electrode; V vs Fc^+/Fc)

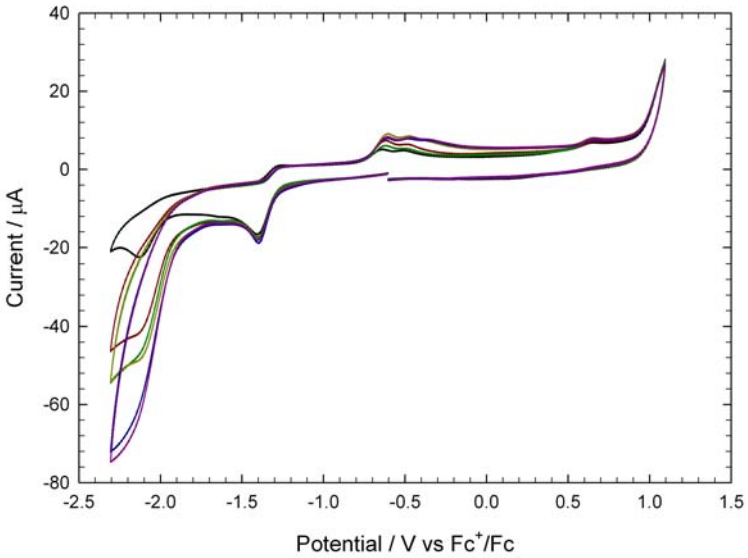

Figure 37: Cyclic voltammetry of $Fe_2(SC_6F_5)_2(CO)_6$ (0.5 mM) in DCM-$[NBu_4][PF_6]$ under CO in the absence of acid and in the presence of up to 50 molar equivalents HOAc in steps of 10 molar equivalent (v=0.1 Vs^{-1}, glassy carbon electrode; V vs Fc^+/Fc)

is not present, the catalytic mechanism that it exhibits does not occur.

3.4.3 Testing for electrocatalytic reduction of protons by $Fe_2(SC_6F_5)_2(CO)_6$, using the weak acid HOAc as the proton source, in MeCN

HOAc was also added to $Fe_2(SC_6F_5)_2(CO)_6$ in MeCN (not under a CO atmosphere), as shown in Figures 38 and 39. The first reduction peak remains unchanged on additions of HOAc. A second reduction process grows at -1.6 V, but reaches a limiting current after the addition of 3 molar equivalents HOAc. The third reduction process grows uniformly with each addition of acid.

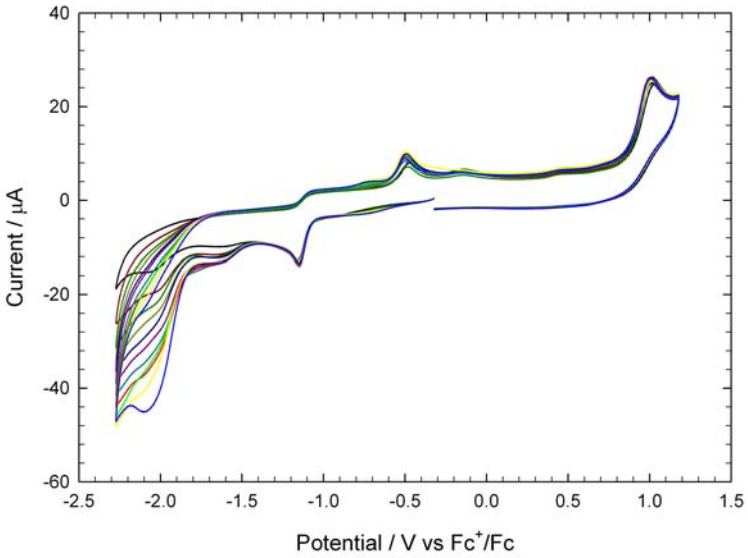

Figure 38: Cyclic voltammetry of $Fe_2(SC_6F_5)_2(CO)_6$ (0.5 mM) in MeCN-$[NBu_4][PF_6]$ in the absence of acid and in the presence of up to 10 molar equivalents HOAc in steps of 1 molar equivalent (v=0.1 Vs^{-1}, glassy carbon electrode; V vs Fc^+/Fc)

These results indicate that the minor species generated after the first reduction of the neutral complex is again catalytic. Unlike in the DCM electrolyte, this catalytic mechanism reaches a limiting rate in MeCN.

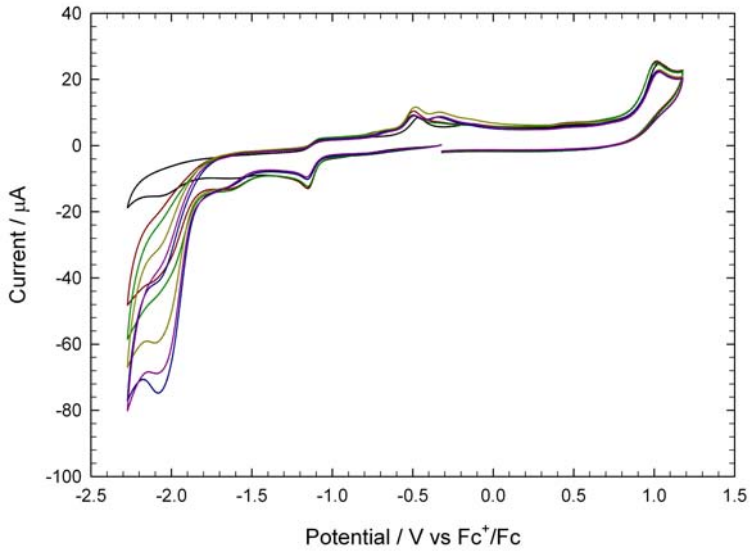

Figure 39: Cyclic voltammetry of $Fe_2(SC_6F_5)_2(CO)_6$ (0.5 mM) in MeCN-$[NBu_4][PF_6]$ in the absence of acid and in the presence of up to 50 molar equivalents HOAc in steps of 10 molar equivalent (v=0.1 Vs^{-1}, glassy carbon electrode; V vs Fc^+/Fc)

3.4.4 Summary and discussion

A comparison of $Fe_2(SC_6F_5)_2(CO)_6$ with the analogous pdt-bridged complex after the addition of 10 molar equivalents of HOAc is shown in Figure 40. Whereas the pdt-bridged complex is catalytic after its first reduction, only the decomposition product B^- of the $(SC_6F_5)_2$-bridged complex is catalytic under these conditions. This catalysis takes place at ca. 0.1 V less negative than the pdt-bridged complex.

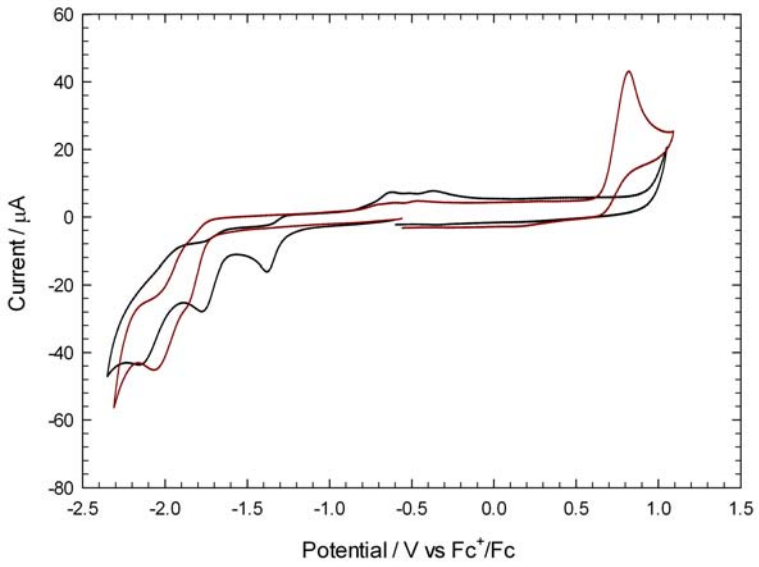

Figure 40: Cyclic voltammetry of $Fe_2(SC_6F_5)_2(CO)_6$ (black line, 0.5 mM) and $Fe_2(\mu\text{-pdt})(CO)_6$ (red line, 0.5 mM) in the presence of 10 molar equivalents HOAc in DCM-$[NBu_4][PF_6]$ (v=0.1 Vs^{-1}, glassy carbon electrode; V vs Fc^+/Fc)

Figure 41 shows the clear difference between the CVs performed under CO and under Ar. This figure emphasises the highly catalytic nature of the species reduced at -1.71 V.

A comparison of the catalytic behaviour in DCM and MeCN is given in Figure 42. Unlike in the experiments performed in DCM, the catalysis due to the minor species B^- is severely limited in MeCN. One possible reason for this is that after $Fe_2(SC_6F_5)_2(CO)_6$ undergoes CO ligand loss on reduction, the vacant coordination site generated is occupied by the coordinating MeCN solvent molecule. This limits formation of the catalytic (possibly dimeric or mono-Fe) species B^-.

A comparison of the catalytic performance of the complex in the presence of 10 molar equivalents $HBF_4.Et_2O$ and 10 molar equivalents HOAc is shown in Figure 43. As expected, the rate is faster in the presence of the stronger acid $HBF_4.Et_2O$. This comparison indicates that the catalytic mechanism presented in Figure 33 for $HBF_4.Et_2O$ is also valid for the catalytic mechanism exhibited in the presence of HOAc. However, in the weaker acid after the first reduction process, the complex is unable to proceed down the protonation pathway, and the catalytic mechanism occurs after the formation of B^-. This is indicated in the mechanism shown in Figure 44. Note that when the solution is saturated with CO, this catalytic cycle is also unavailable, and catalytic proton reduction

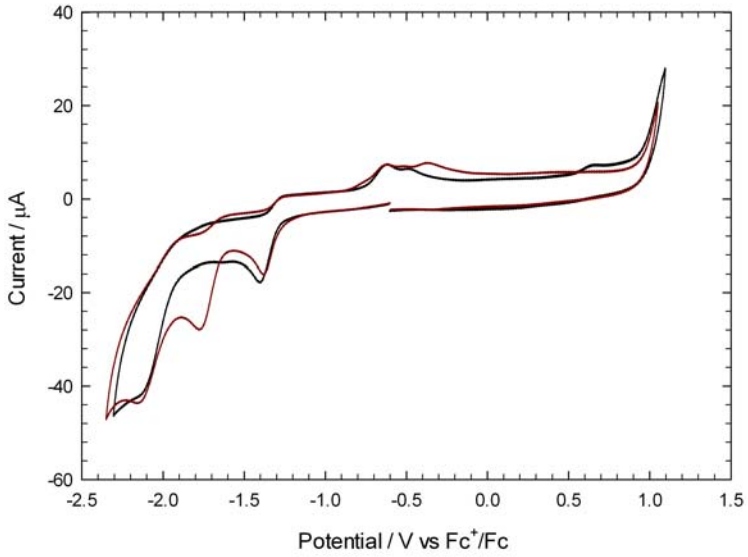

Figure 41: Cyclic voltammetry of $Fe_2(SC_6F_5)_2(CO)_6$ in DCM-$[NBu_4][PF_6]$ saturated with CO (black line) and Ar (red line) in the presence of 10 molar equivalents HOAc (v=0.1 Vs^{-1}, glassy carbon electrode; V vs Fc^+/Fc)

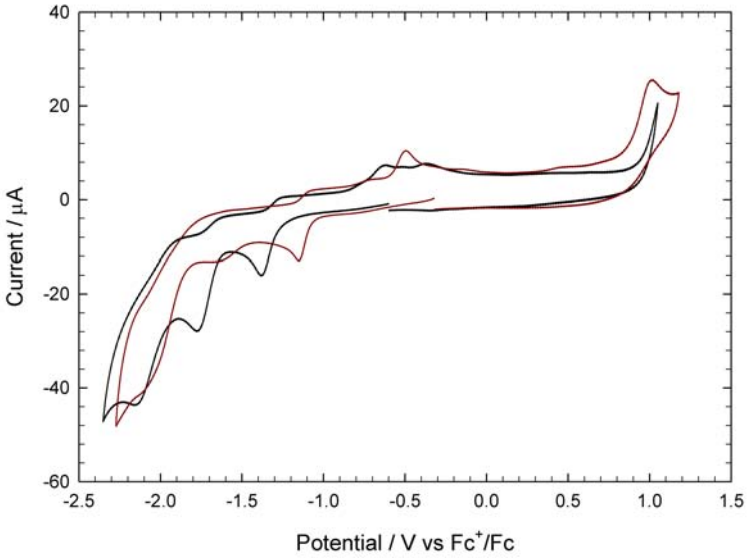

Figure 42: Cyclic voltammetry of $Fe_2(SC_6F_5)_2(CO)_6$ in DCM-$[NBu_4][PF_6]$ (black line) and in MeCN-$[NBu_4][PF_6]$ (red line) in the presence of 10 molar equivalents HOAc (v=0.1 Vs^{-1}, glassy carbon electrode; V vs Fc^+/Fc)

does not occur until after the second reduction of the neutral complex. The first reduction process for the neutral complex is irreversible, which suggests this second process involves species that are not necessarily structurally similar to the neutral complex.

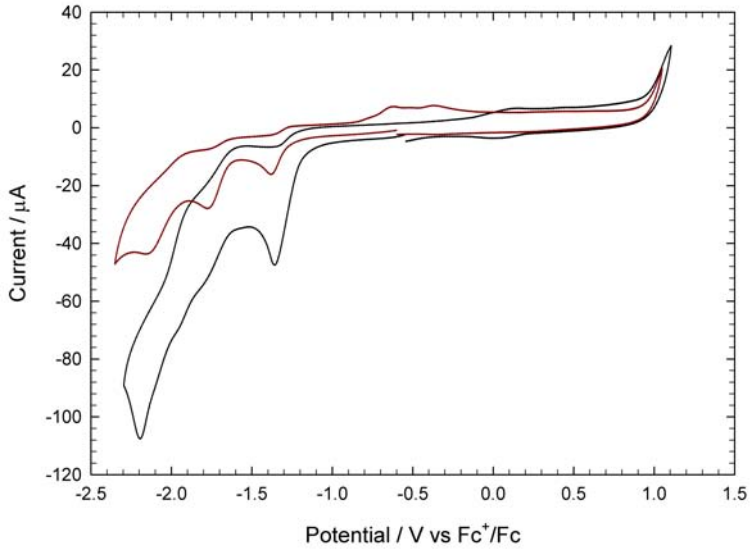

Figure 43: Cyclic voltammetry of $Fe_2(SC_6F_5)_2(CO)_6$ in DCM-$[NBu_4][PF_6]$ in the presence of 10 molar equivalents $HBF_4.Et_2O$ (black line) and 10 molar equivalents HOAc (red line) (v=0.1 Vs^{-1}, glassy carbon electrode; V vs Fc^+/Fc)

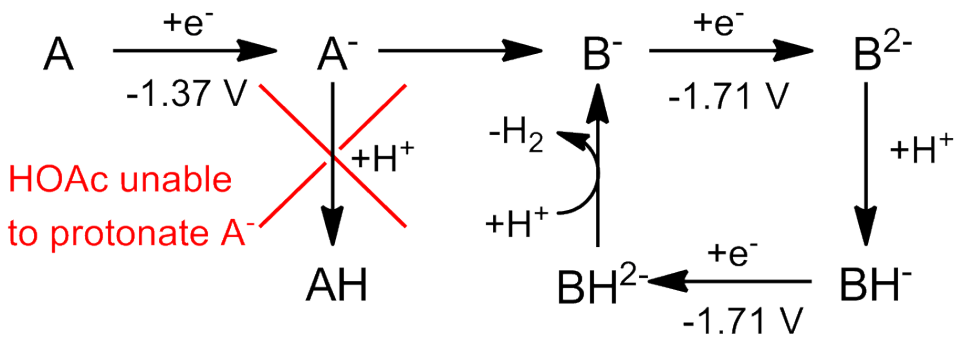

Figure 44: Possible catalytic mechanism of $Fe_2(SC_6F_5)_2(CO)_6$ (denoted A) in the presence of HOAc; B^- denotes the highly catalytic species formed after reduction of the neutral complex; potentials are taken from the CVs obtained in DCM

3.5 Extension: An initial investigation of the di-substituted analogue $Fe_2(SC_6F_5)_2(\mu\text{-}Ph_2PCH_2PPh_2)(CO)_4$

As an extension of the above investigation into the catalytic activity of the hexacarbonyl complex, a small quantity of the di-substituted analogue $Fe_2(SC_6F_5)_2(\mu\text{-}Ph_2PCH_2PPh_2)(CO)_4$ (Figure 45) has been synthesised and investigated to assess whether further investigations would be warranted. As was discussed in Section 1.4, the additional electron density due to the dppm ligand could provide enough electron density on the Fe centres to enable hydride formation as the first step in a catalytic mechanism.

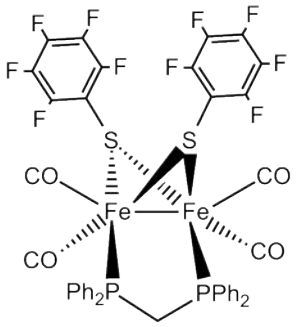

Figure 45: $Fe_2(SC_6F_5)_2(\mu\text{-}Ph_2PCH_2PPh_2)(CO)_4$

3.5.1 Electrochemistry of $Fe_2(SC_6F_5)_2(\mu\text{-}Ph_2PCH_2PPh_2)(CO)_4$ in the absence of protons, in DCM

The CV of the $Fe_2(SC_6F_5)_2(\mu\text{-}Ph_2PCH_2PPh_2)(CO)_4$ in the absence of protons is shown in Figure 46. The first reduction of the complex occurs at -2.0 V, the shape of the peak suggesting this to be two overlapping processes. A second reduction peak of smaller magnitude occurs at -2.21 V. A small re-oxidation peak is present at -0.78 V. The first oxidation of the neutral complex occurs at 0.6 V. As with the first reduction, the broad shape of the peak suggests this may be two overlapping processes.

CVs of the first oxidation of the complex at various scan rates are shown in Figure 47. The oxidation only becomes reversible at scan rates of 1 Vs^{-1} and above. The reduction processes were also investigated at different scan rates and remained irreversible (Figure 48).

3.5.2 Testing for electrocatalytic reduction of protons by $Fe_2(SC_6F_5)_2(\mu\text{-}Ph_2PCH_2PPh_2)(CO)_4$, using the strong acid $HBF_4.Et_2O$ as the proton source, in DCM

An investigation into the catalytic activity of $Fe_2(SC_6F_5)_2(\mu\text{-}Ph_2PCH_2PPh_2)(CO)_4$ has been performed using the proton source $HBF_4.Et_2O$. Figure 49 shows the CVs after additions of the first 10 molar equivalents of acid. After one molar equivalent was added the first reduction peak increased in height. On further additions of acid this peak continued to grow, though at a decreasing rate.

Figure 50 shows CVs taken after the addition of two further additions of 5 molar equivalents

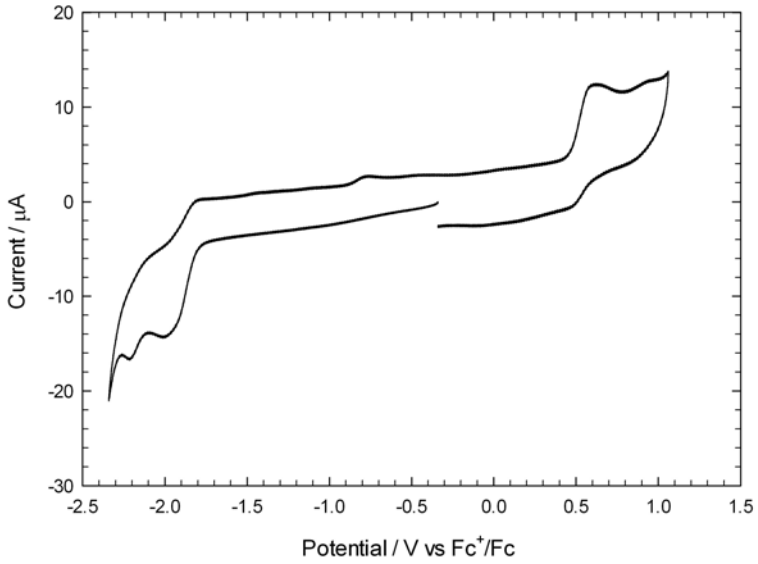

Figure 46: Cyclic voltammetry of $Fe_2(SC_6F_5)_2(\mu\text{-}Ph_2PCH_2PPh_2)(CO)_4$ (0.5 mM) in DCM-$[NBu_4][PF_6]$ (v=0.1 Vs^{-1}, glassy carbon electrode; V vs Fc^+/Fc)

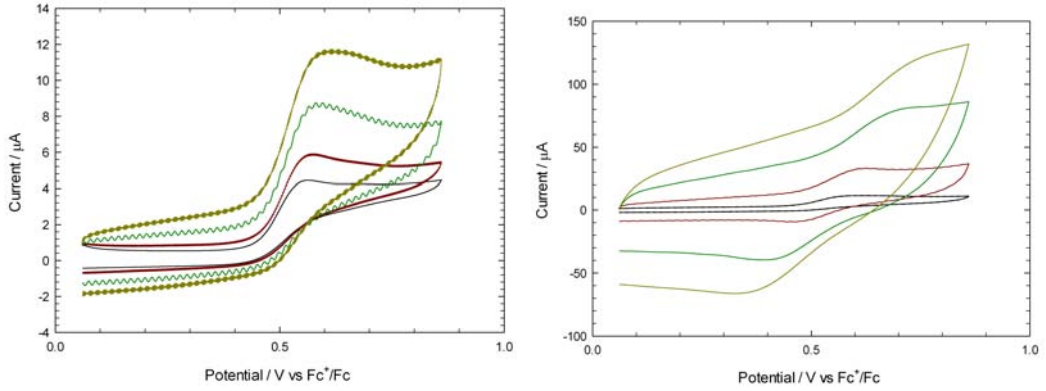

(a) v=0.01, 0.02, 0.05, 0.1 Vs^{-1} (b) v=0.1, 1.0, 5.0, 10.0 Vs^{-1}

Figure 47: Cyclic voltammetry of $Fe_2(SC_6F_5)_2(\mu\text{-}Ph_2PCH_2PPh_2)(CO)_4$ (0.5 mM) in DCM-$[NBu_4][PF_6]$ (glassy carbon electrode; V vs Fc^+/Fc)

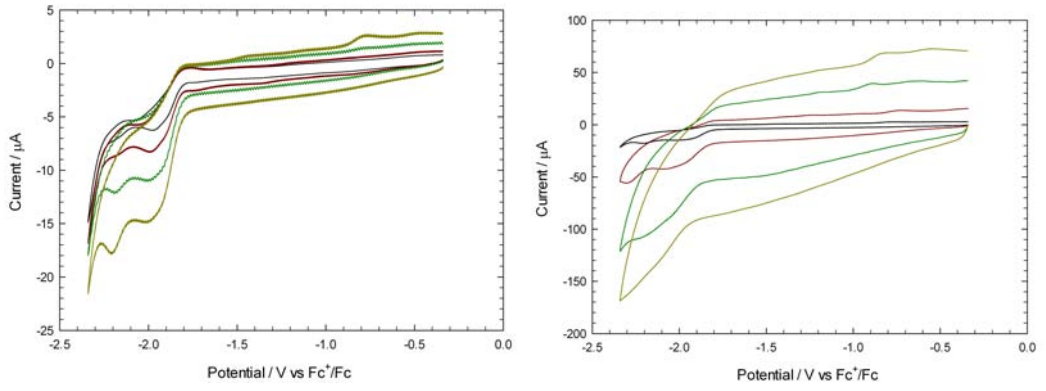

(a) v=0.01, 0.02, 0.05, 0.1 Vs^{-1} (b) v=0.1, 1.0, 5.0, 10.0 Vs^{-1}

Figure 48: Cyclic voltammetry of $Fe_2(SC_6F_5)_2(\mu\text{-}Ph_2PCH_2PPh_2)(CO)_4$ (0.5 mM) in DCM-$[NBu_4][PF_6]$ (glassy carbon electrode; V vs Fc^+/Fc)

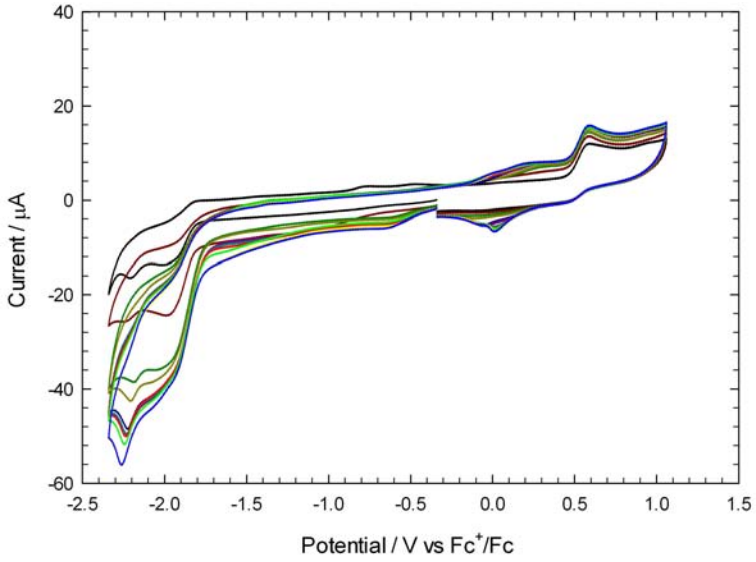

Figure 49: Cyclic voltammetry of $Fe_2(SC_6F_5)_2(\mu\text{-}Ph_2PCH_2PPh_2)(CO)_4$ (0.5 mM) in DCM-$[NBu_4][PF_6]$ in the absence of acid and in the presence of up to 10 molar equivalents $HBF_4.Et_2O$ in steps of 1 molar equivalent (v=0.1 Vs^{-1}, glassy carbon electrode; V vs Fc^+/Fc)

$HBF_4.Et_2O$. The reduction peak does appear to grow, however, it is likely that this is due to the increased direct reduction of acid at the electrode, rather than catalysis. Thus, it appears that the limit of the catalytic mechanism was indeed being approached in Figure 49.

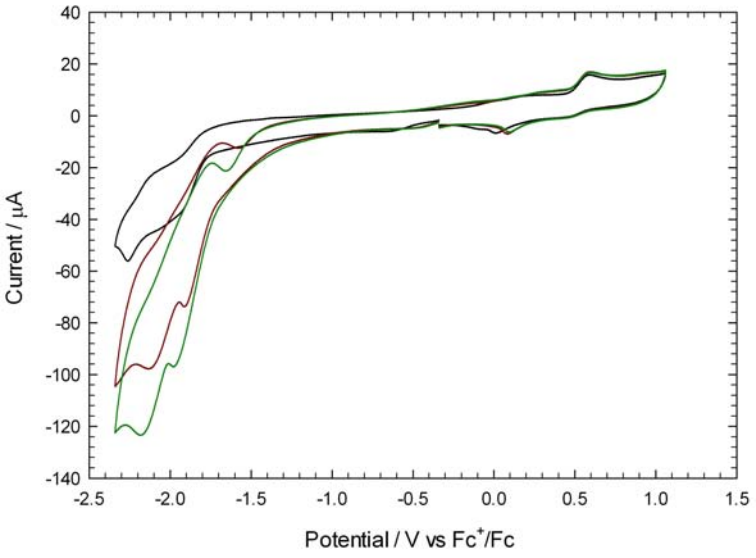

Figure 50: Cyclic voltammetry of $Fe_2(SC_6F_5)_2(\mu\text{-}Ph_2PCH_2PPh_2)(CO)_4$ (0.5 mM) in DCM-$[NBu_4][PF_6]$ in the presence of 10, 15 and 20 molar equivalents $HBF_4.Et_2O$ (v=0.1 Vs^{-1}, glassy carbon electrode; V vs Fc^+/Fc)

These results indicate that the di-substituted complex is catalytic in the presence of $HBF_4.Et_2O$ at the first reduction peak. This catalytic mechanism reaches a limiting rate as 10 molar equivalents concentration is approached.

3.5.3 Summary and discussion

A comparison of the influence of the altered ligand set is shown in Figure 51, which shows CVs of $Fe_2(SC_6F_5)_2(\mu\text{-}Ph_2PCH_2PPh_2)(CO)_4$ and the hexacarbonyl analogue analysed earlier in this chapter. The reduction potential has been shifted 0.5 V negative with the inclusion of the dppm ligand, due to the increased electron density pushed on to the Fe centres. This behaviour is as expected based on similar unsubstituted and di-substituted complexes in the literature.

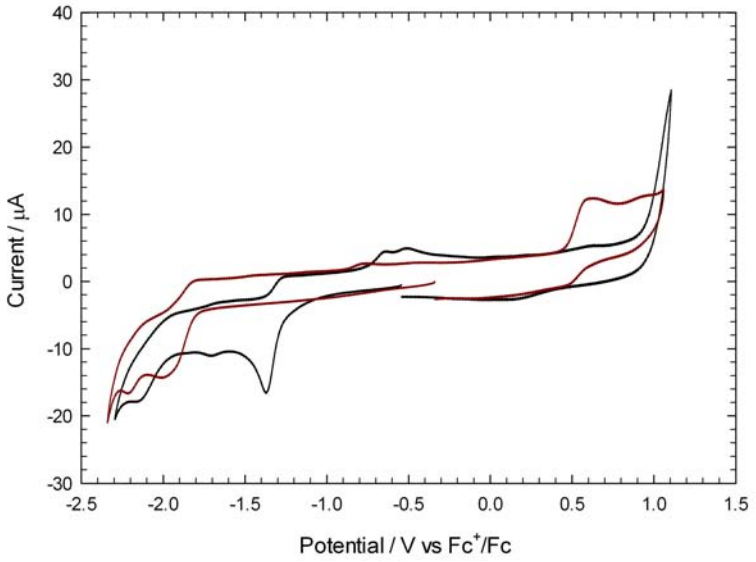

Figure 51: Cyclic voltammetry of $Fe_2(SC_6F_5)_2(CO)_6$ (black line, 0.5 mM) and $Fe_2(SC_6F_5)_2(\mu\text{-}Ph_2PCH_2PPh_2)(CO)_4$ (red line, 0.5 mM) in DCM-$[NBu_4][PF_6]$ (v=0.1 Vs^{-1}, glassy carbon electrode; V vs Fc^+/Fc)

Figure 52 shows the CVs of both the dppm-complex and the hexacarbonyl analogue in the presence of 10 molar equivalents $HBF_4.Et_2O$. It is clear that in this case there is no benefit, at least in terms of catalytic overpotential, of adding the extra basicity to the complex with the ligand set. The increased basicity merely makes the reduction potential more negative. Further basicity would be required for the neutral complex to protonate, and thus reduce the overpotential. This could perhaps be achieved in two ways. Firstly, by making a further substitution, i.e. moving to a tri-substituted phosphine complex. Alternatively, by synthesising the isomeric complex with the dppm ligand in a chelating orientation, which has been found to assist in making the electron density on the Fe centres asymmetric, which increases a complex's susceptibility to protonation. This could also allow for more facile rearrangement of the complex to accommodate protonation. The relative catalytic activity of two isomeric bridging and chelating complexes is investigated in Chapter 6.

3.6 Concluding remarks

The findings presented in this chapter provide further evidence that identity of the dithiolate bridge has a substantial effect on the electron density on the Fe centres of H-cluster mimics. Compared to the analogous pdt-bridged complex, the $(SC_6F_5)_2$ bridged complex has been found to be reduced

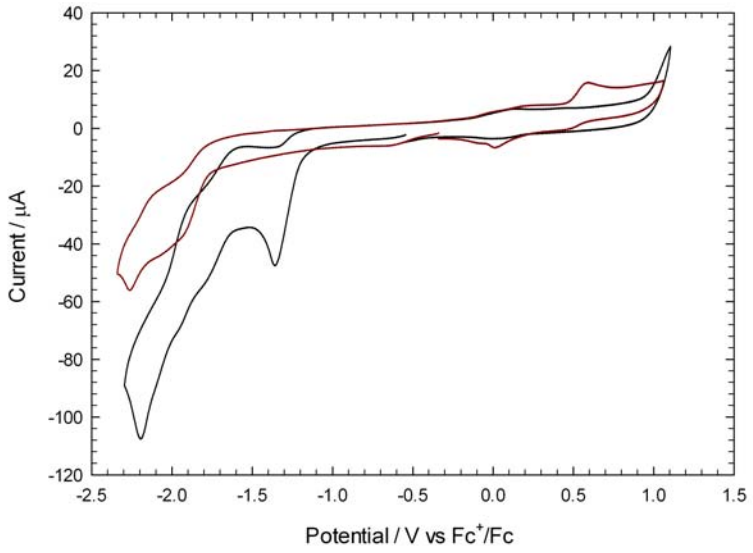

Figure 52: Cyclic voltammetry of $Fe_2(SC_6F_5)_2(CO)_6$ (black line, 0.5 mM) and $Fe_2(SC_6F_5)_2(\mu\text{-}Ph_2PCH_2PPh_2)(CO)_4$ (red line, 0.5 mM) in the presence of 10 molar equivalent $HBF_4.Et_4O$ in DCM-$[NBu_4][PF_6]$ (v=0.1 Vs^{-1}, glassy carbon electrode; V vs Fc^+/Fc)

at a potential 0.49 V less negative in DCM. Indeed, compared to other complexes in the literature $Fe_2(SC_6F_5)_2(CO)_6$ has been found to exhibit one of the mildest reduction potentials (-1.15 V in MeCN), due to the highly electron withdrawing nature of the $(SC_6F_5)_2$ bridge.

As was expected, the neutral $Fe_2(SC_6F_5)_2(CO)_6$ complex would not protonate. This is in keeping with the knowledge that the Fe centres are even less basic than the pdt-bridged complex, which does not protonate. After the first reduction of the neutral complex, however, the reduced species was able to protonate in the presence of $HBF_4.Et_2O$. A catalytic cycle was then available, as described in Section 3.3.3 and re-produced in Figure 53.

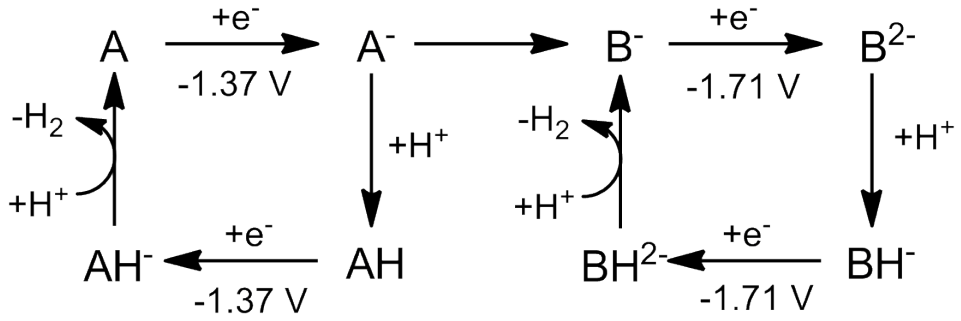

Figure 53: Possible catalytic mechanism of $Fe_2(SC_6F_5)_2(CO)_6$ (denoted A) in the presence of $HBF_4.Et_2O$; B^- denotes the highly catalytic species formed after reduction of the neutral complex; potentials are taken from the CVs obtained in DCM

Perhaps the most intriguing finding of the catalytic mechanism was the minor species (denoted B^- in Figure 53) generated after the first reduction process, which was found to be highly catalytic. The species was not generated when the electrolyte was saturated with CO, suggesting its formation involves CO ligand loss. Also, the catalytic mechanism it exhibits is more limited in MeCN than DCM, suggesting MeCN could be coordinating to the species, decreasing its catalytic activity, or

preventing its formation. By comparison to studies of similar compounds, it is tentatively suggested that B^- is a dimeric species formed in the following steps:

1. Reduction of the neutral complex $Fe_2(SC_6F_5)_2(CO)_6$ (at -1.4 V in DCM)
2. Rearrangement of the singly reduced species and loss of a CO ligand
3. Dimer formation

Two general strategies are available for further research. Firstly, attempts should be made to push the reduction potential even less negative using the dithiolate bridge. It is unlikely that significant gains can be made, compared to such an electron withdrawing bridge used in this chapter, however, any decrease in overpotential is a step forward in creating an efficient catalyst. A second avenue of research is to extend the experiments performed on the di-substituted dppm complex in an attempt to synthesise a complex with the correct ligand set to protonate. An initial investigation should focus on a chelating dppm ligand. If this complex is still unable to protonate, tri- and tetra-substituted complexes should be investigated.

Additionally, it is important to elucidate the structure of the highly catalytic species that was generated after the first reduction of the neutral complex. This could be attempted using spectro-electrochemical approaches. Even in very small concentrations, this species was found to be highly catalytic, and lessons learnt from its structure could lead to synthesis of an excellent catalyst for hydrogen generation.

4 $Fe_2(\mu\text{-X})(CO)_3(\mu,\eta^2\text{-}Ph_2PCH_2CH_2P(Ph)CH_2CH_2PPh_2)$ (X: pdt = $SCH_2CH_2CH_2S$; adt = $SCH_2N(CH_2C_6H_5)CH_2S$; $(SCH_3)_2$): Imparting electronic asymmetry and steric twist through use of the triphos ligand

This chapter describes the susceptibility to protonation, chemical oxidation behaviour, electrochemical behaviour and electrocatalytic activity of $Fe_2(\mu\text{-X})(CO)_3(\mu,\eta^2\text{-}Ph_2PCH_2CH_2P(Ph)CH_2CH_2PPh_2)$ (X: pdt = $SCH_2CH_2CH_2S$; adt = $SCH_2N(CH_2C_6H_5)CH_2S$; $(SCH_3)_2$, Figure 54). As an extension to this work, a small quantity of the edt-bridged complex has been investigated electrochemically (edt = SCH_2CH_2S).

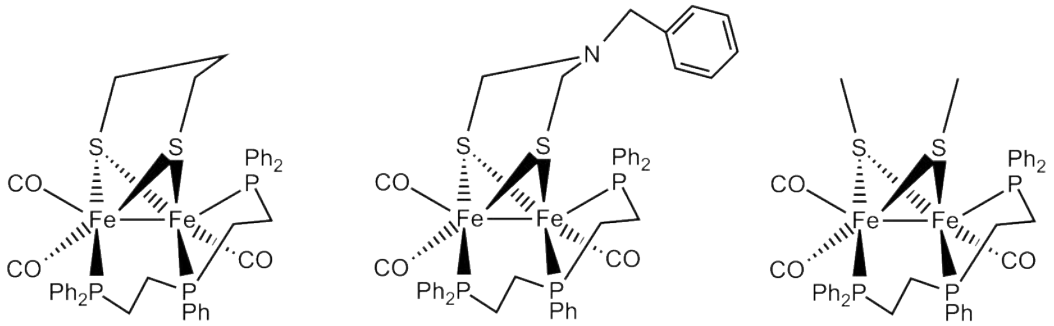

Figure 54: $Fe_2(\mu\text{-X})(CO)_3(\mu,\eta^2\text{-}Ph_2PCH_2CH_2P(Ph)CH_2CH_2PPh_2)$ (X: pdt = $SCH_2CH_2CH_2S$; adt = $SCH_2N(CH_2C_6H_5)CH_2S$; $(SCH_3)_2$)

Hall and co-workers carried out computational studies which suggested that asymmetrical electron distribution and a rotated structure would favour formation of a terminal hydride on protonation, which would be beneficial to catalytic activity. This led Hogarth to synthesise a complex using the triphos ligand to provide both electronic asymmetry and steric twist in an attempt to achieve these objectives, and thus improve catalytic activity [35].

The initial complex was pdt-bridged, and its electrochemistry and electrocatalytic activity shall be reported in this chapter. The chapter shall also report on two analogous complexes that retain the triphos ligand, but vary the dithiolate bridge to $SCH_2N(CH_2C_6H_5)CH_2S$ and $(SCH_3)_2$. As discussed earlier, there has been much interest in having a N atom in the bridge of the complexes, and this is present in the $SCH_2N(CH_2C_6H_5)CH_2S$ bridged complex. Open bridges are of interest as they do not impart strain on the complex during a catalytic mechanism; the complex with the $(SMe)_2$ bridge allows for further understanding of this topic.

As an extension to the analysis of the above, a small quantity of edt-bridged complex has been synthesised and analysed for catalytic activity. The edt bridge exerts more strain on the complex than the other three bridges, and thus was of interest to study.

To our knowledge a systematic analysis of the effect of the electrolyte solution on the electrochemical and electrocatalytic behaviours of mimics of the H-cluster has not been undertaken.

The triphos-ligand complexes have been used to assess the influence of the electrolyte solution on both electrochemistry and electrocatalytic activity. The electrolyte solutions used were DCM-$[NBu_4][PF_6]$, DCM-$[NBu_4][ClO_4]$, DCM-$[NBu_4][BF_4]$ and MeCN-$[NBu_4][PF_6]$.

4.1 Molecular structures of $Fe_2(\mu\text{-X})(CO)_3(\mu,\eta^2\text{-}Ph_2PCH_2CH_2P(Ph)CH_2\text{-}CH_2PPh_2)$ (X: pdt = $SCH_2CH_2CH_2S$; adt = $SCH_2N(CH_2C_6H_5)CH_2S$)

One of the aims of incorporating the triphos ligand was to exert a steric twist in the complexes in order to pull one of the CO ligands into a rotated position, as is observed in the H-cluster. To observe whether or not this has been achieved, XRD molecular structures have been obtained by Graeme Hogarth in University College London for the pdt- and adt-bridged triphos complexes (Figures 55 and 56 respectively).

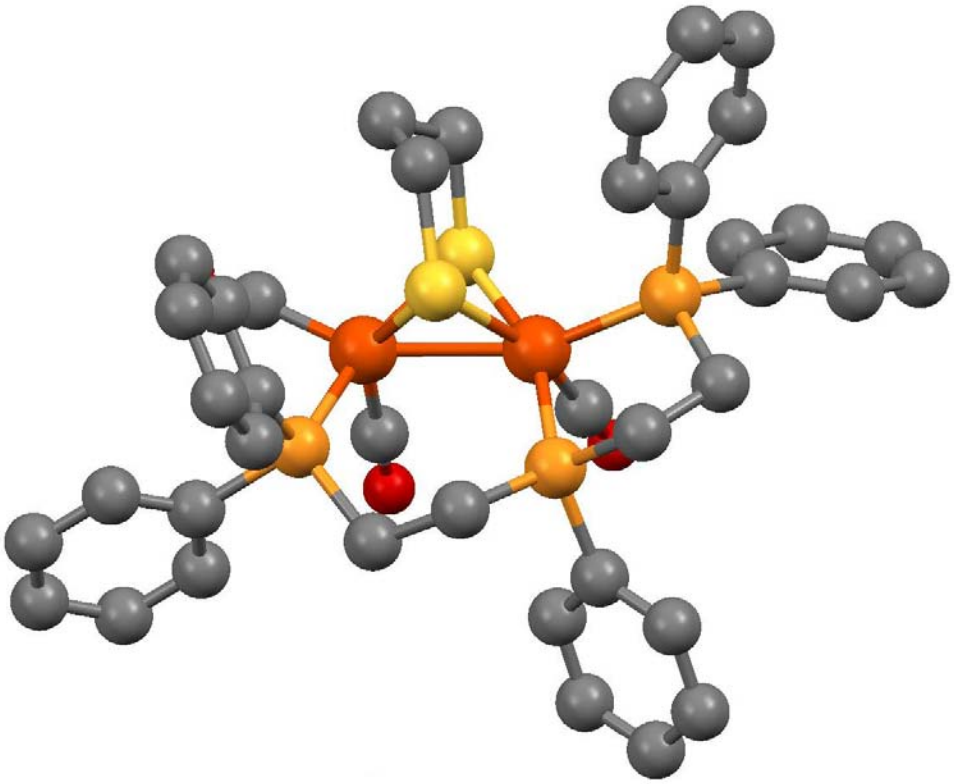

Figure 55: Molecular structure of $Fe_2(\mu\text{-pdt})(CO)_3(\mu,\eta^2\text{-}Ph_2PCH_2CH_2P(Ph)CH_2CH_2PPh_2)$

It appears that the rotated CO ligand objective has not been met, with the complex not sufficiently twisted for the CO to rotate and become semi-bridging in either of the complexes. The structure of the adt-bridged complex does show one similarity with the H-cluster however. If it is assumed that the central atom of the dithiolate bridge in the H-cluster is a N atom, the position at which the N of the adt-bridged triphos complex sits is in a reasonably similar position for where it would need to be to shuttle protons towards the Fe centres. The shortcoming of the adt-bridged complex is that there is not a vacant coordination site at the Fe for a hydride to form because the CO ligand is not rotated. The influence of the molecular structure shall be discussed further throughout

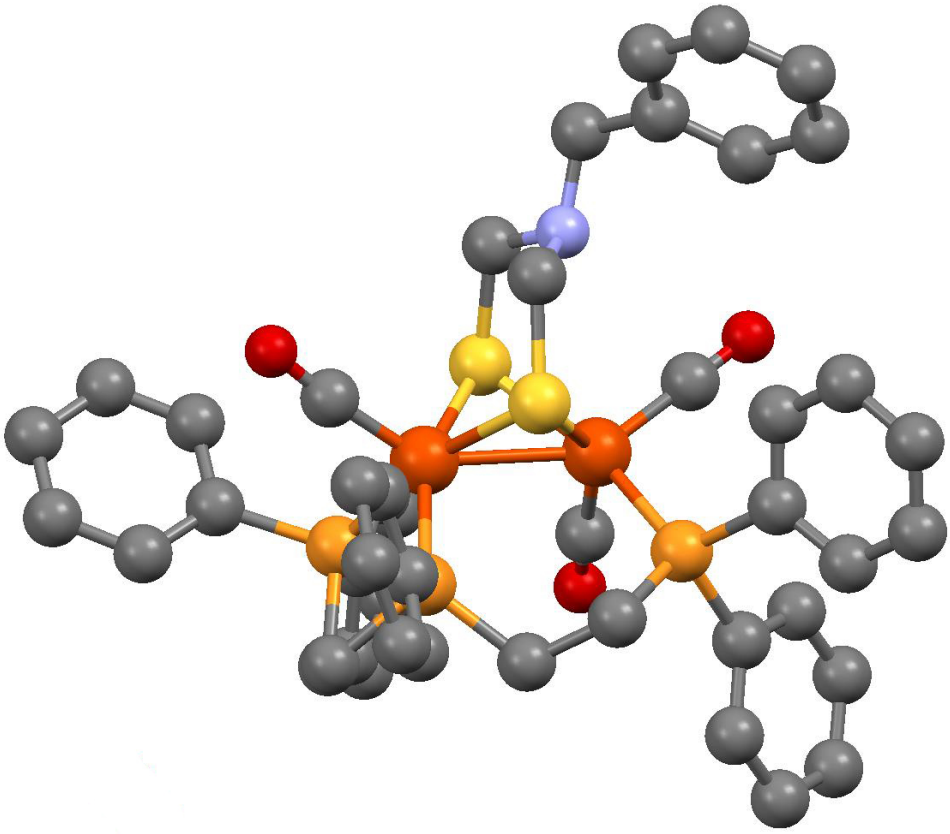

Figure 56: Molecular structure of $Fe_2(\mu\text{-adt})(CO)_3(\mu,\eta^2\text{-}Ph_2PCH_2CH_2P(Ph)CH_2CH_2PPh_2)$

this chapter.

4.2 Susceptibility of $Fe_2(\mu\text{-X})(CO)_3(\mu,\eta^2\text{-}Ph_2PCH_2CH_2P(Ph)CH_2CH_2PPh_2)$ (X: pdt = $SCH_2CH_2CH_2S$; adt = $SCH_2N(CH_2C_6H_5)CH_2S$; $(SMe)_2$ = $(SCH_3)_2$) to protonation

The first step taken to understand any catalytic mechanism the triphos-ligand complexes might exhibit, was to determine whether or not they would protonate in the presence of a Brönsted acid. This aids understanding whether the first step of a catalytic mechanism is a protonation or a reduction process. Protonation was monitored through the IR stretches of the CO ligands (see Chapter 2 for details).

4.2.1 Susceptibility of $Fe_2(\mu\text{-pdt})(CO)_3(\mu,\eta^2\text{-}Ph_2PCH_2CH_2P(Ph)CH_2CH_2PPh_2)$ to protonation

The IR spectrum of $Fe_2(\mu\text{-pdt})(CO)_3(\mu,\eta^2\text{-}Ph_2PCH_2CH_2P(Ph)CH_2CH_2PPh_2)$ in DCM is shown in Figure 57. Bands are seen at 1949 and 1888 cm^{-1}. Next $HBF_4.Et_2O$ was added to the solution (Figure 58). The bands shifted to 2038, 1985 and 1963 cm^{-1}. This shift in wavenumbers suggests that the complex has been protonated by the acid at the FeFe bond.

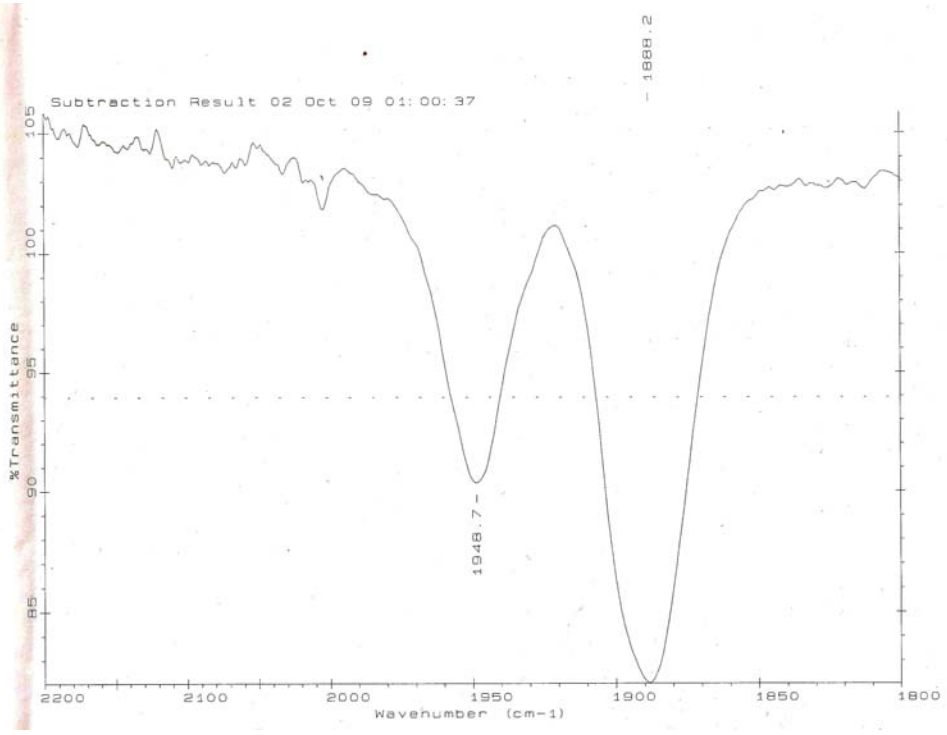

Figure 57: IR spectrum of $Fe_2(\mu\text{-pdt})(CO)_3(\mu,\eta^2\text{-}Ph_2PCH_2CH_2P(Ph)CH_2CH_2PPh_2)$ in DCM

The pdt-bridged complex has also been protonated ex-situ under a N_2 atmosphere and the protonated product crystallised. The IR spectrum of this pre-protonated complex displayed bands at the same positions as in Figure 58.

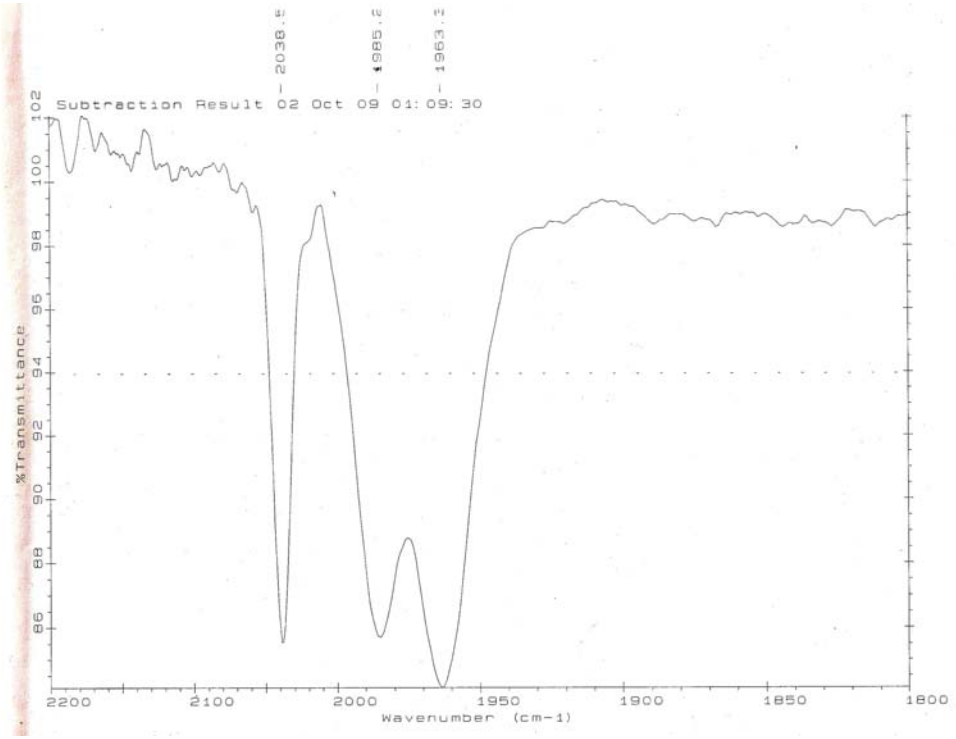

Figure 58: IR spectrum of $Fe_2(\mu\text{-pdt})(CO)_3(\mu,\eta^2\text{-}Ph_2PCH_2CH_2P(Ph)CH_2CH_2PPh_2)$ in DCM in the presence of 3 molar equivalents $HBF_4.Et_2O$

4.2.2 Susceptibility of $Fe_2(\mu\text{-adt})(CO)_3(\mu,\eta^2\text{-}Ph_2PCH_2CH_2P(Ph)CH_2CH_2PPh_2)$ to protonation

The IR experiment above was repeated for $Fe_2(\mu\text{-adt})(CO)_3(\mu,\eta^2\text{-}Ph_2PCH_2CH_2P(Ph)CH_2CH_2PPh_2)$. The spectrum of the neutral complex is shown in Figure 59. Bands are seen at 1951 and 1893 cm^{-1}.

One molar equivalent $HBF_4.Et_2O$ was added to the solution, resulting in signals appearing at 1970, 1922 and 1902 cm^{-1} (Figure 60). Protonation at the nitrogen of the bridge is known to cause a shift in wavenumbers of approximately 10 cm^{-1}, due to electron density being withdrawn from the Fe centres, in contrast to a shift of approximately 100 cm^{-1} for hydride formation at the Fe centres. Thus, the shift observed for the adt complex is assigned to protonation at the N atom of the adt bridge.

Next, a further 1 molar equivalent $HBF_4.Et_2O$ was added to the solution. Bands were now observed at 2097, 2051, 2022, and 1990 cm^{-1} (Figure 61). This larger shift in the wavenumbers suggests that the complex has now been protonated at the Fe centres in the higher concentration of acid. It was therefore concluded that the complex was first protonated at the N of the dithiolate bridge and then at the Fe centres. From electrochemical studies detailed later in this chapter, it is unlikely that the complex is doubly protonated at the N and the Fe centres simultaneously. Rather the protonation is at either position, with the proton associating with the Fe centres at higher acid concentrations.

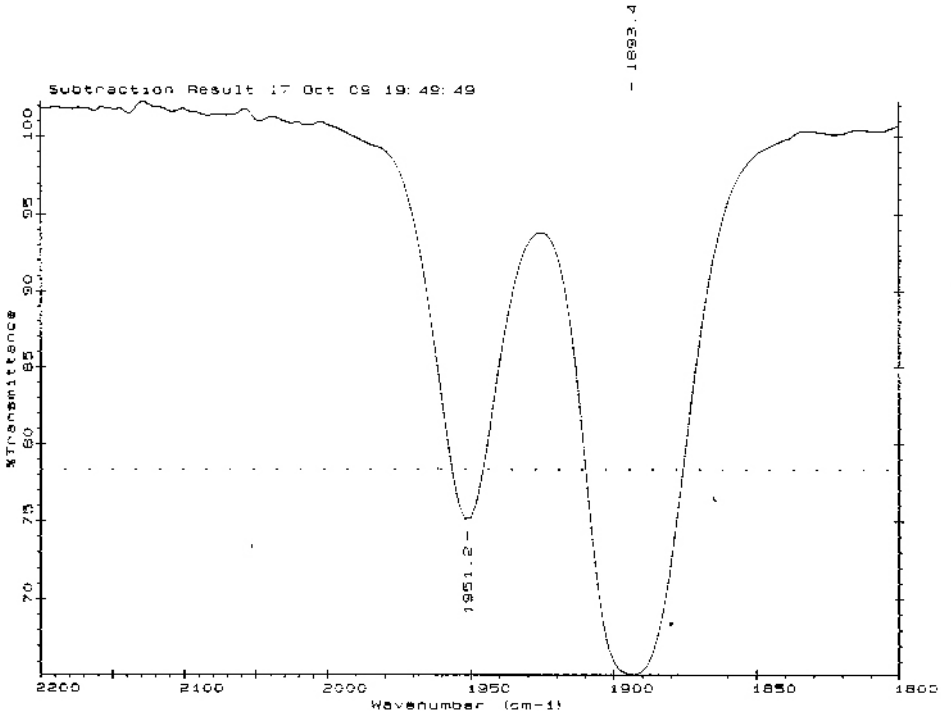

Figure 59: IR spectrum of $Fe_2(\mu\text{-adt})(CO)_3(\mu,\eta^2\text{-}Ph_2PCH_2CH_2P(Ph)CH_2CH_2PPh_2)$ in DCM

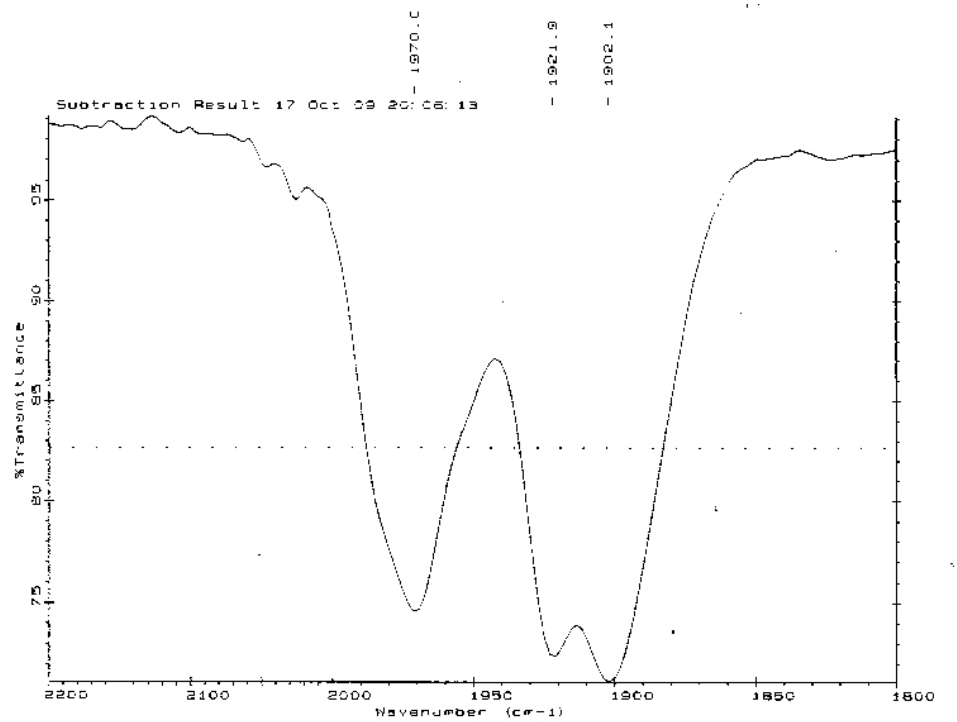

Figure 60: IR spectrum of $Fe_2(\mu\text{-adt})(CO)_3(\mu,\eta^2\text{-}Ph_2PCH_2CH_2P(Ph)CH_2CH_2PPh_2)$ in DCM in the presence of 1 molar equivalent $HBF_4.Et_2O$

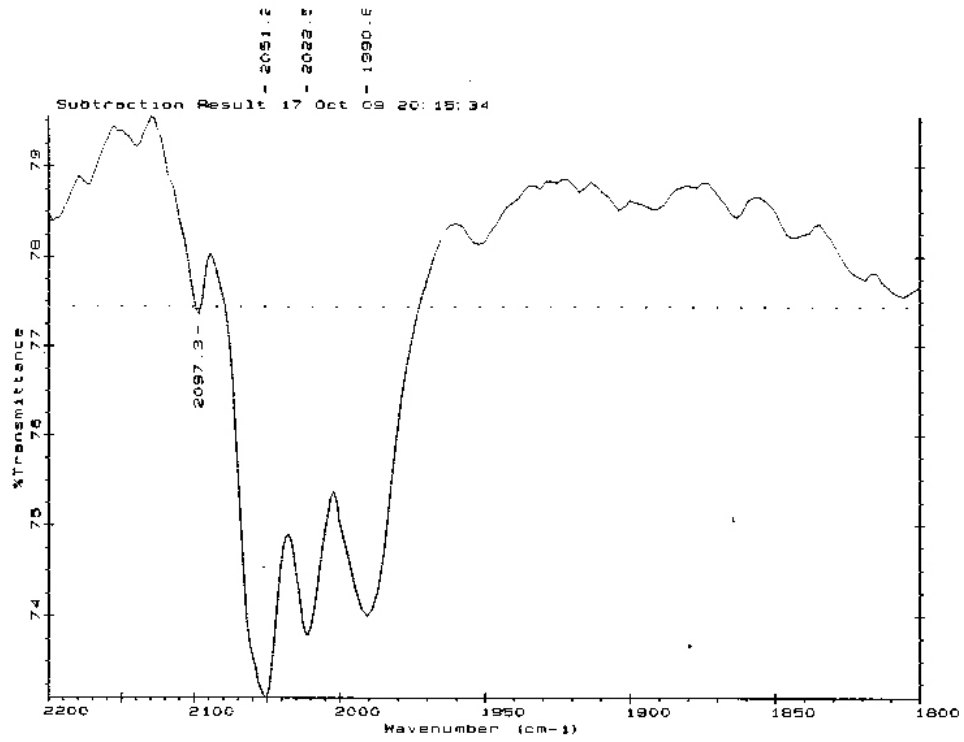

Figure 61: IR spectrum of $Fe_2(\mu\text{-adt})(CO)_3(\mu,\eta^2\text{-}Ph_2PCH_2CH_2P(Ph)CH_2CH_2PPh_2)$ in DCM in the presence of 2 molar equivalents $HBF_4.Et_2O$

4.2.3 Susceptibility of $Fe_2(\mu\text{-}(SMe)_2)(CO)_3(\mu,\eta^2\text{-}Ph_2PCH_2CH_2P(Ph)CH_2CH_2PPh_2)$ to protonation

The IR protonation study seen above for the pdt- and adt- bridged complexes has also been performed on $Fe_2(\mu\text{-}(SMe)_2)(CO)_3(\mu,\eta^2\text{-}Ph_2PCH_2CH_2P(Ph)CH_2CH_2PPh_2)$. The IR spectrum of the complex is shown in Figure 62. Bands are seen at 1944, 1897 cm^{-1}, which is very similar to the pdt-bridged complex.

Next $HBF_4.Et_2O$ was added to the solution (Figure 63). The bands that were seen for the neutral complex have shifted to 2031, 2002 and 1965 cm^{-1}. As with the pdt-bridged complex, this shift in band positions suggests that the $(SMe)_2$-bridged complex has been protonated by the acid at the Fe centres.

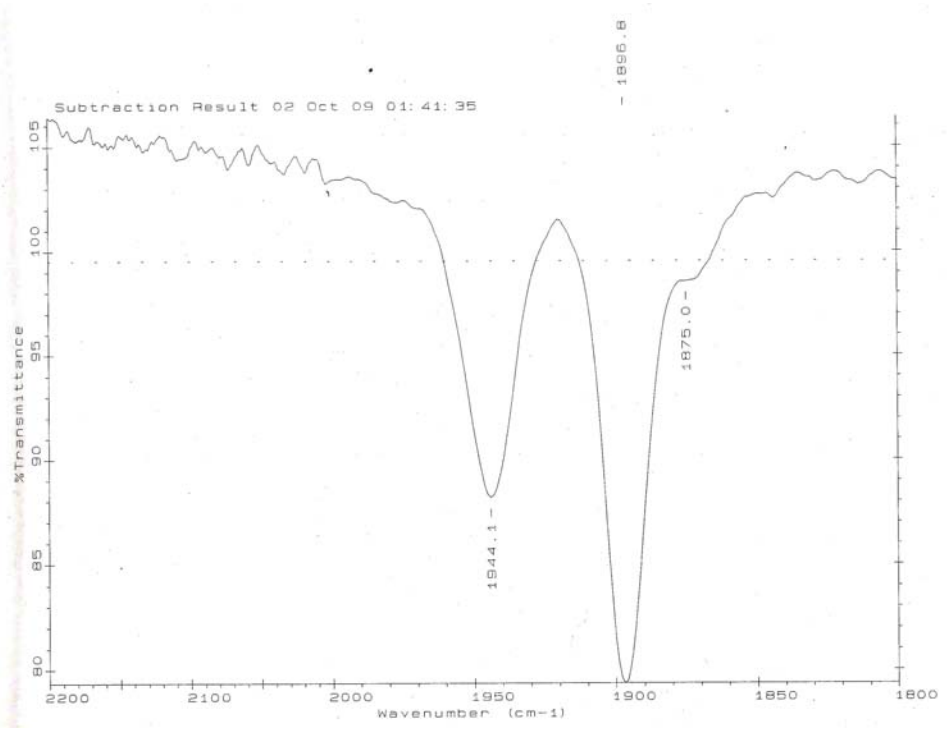

Figure 62: IR spectrum of $Fe_2(\mu\text{-}(SMe)_2)(CO)_3(\mu,\eta^2\text{-}Ph_2PCH_2CH_2P(Ph)CH_2CH_2PPh_2)$ in DCM

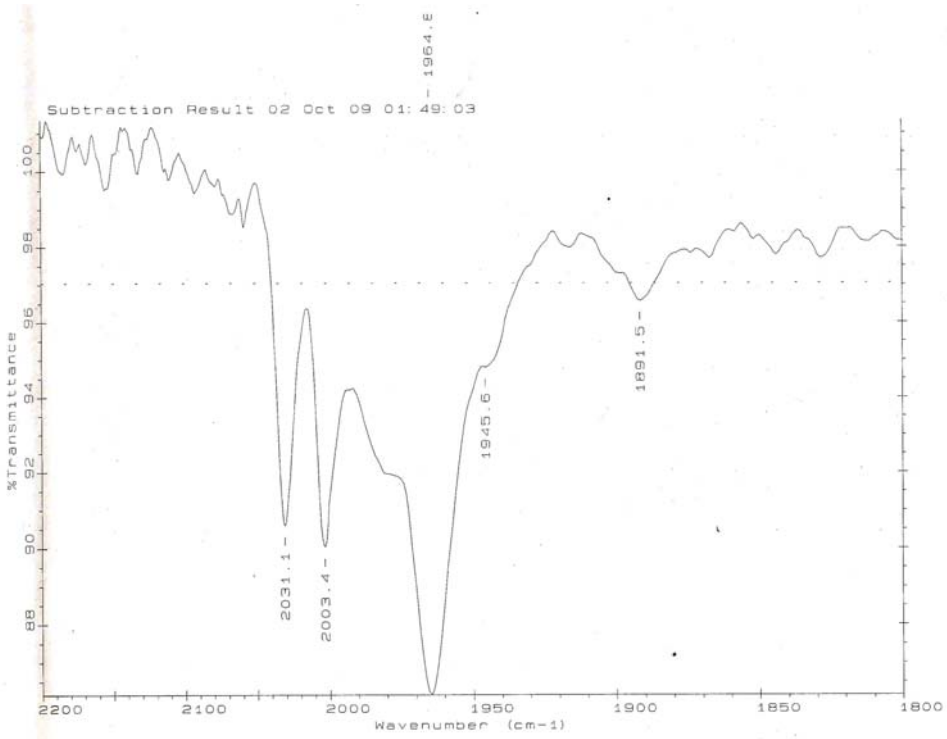

Figure 63: IR spectrum of $Fe_2(\mu\text{-}(SMe)_2)(CO)_3(\mu,\eta^2\text{-}Ph_2PCH_2CH_2P(Ph)CH_2CH_2PPh_2)$ in DCM in the presence of 3 molar equivalents $HBF_4.Et_2O$

4.2.4 Summary and discussion

In summary, the pdt- and $(SMe)_2$ triphos ligand complexes have been found to protonate at the Fe centres. This was expected due to the high electron density on the Fe centres due to the triphos ligand causing them to become basic enough to protonate; indeed the result for the pdt-bridged complex had already been reported by Hogarth and co-workers[35]. In contrast, the adt-bridged complex has been found to first protonate at the N atom in the bridge, and then at the Fe centres in a higher concentration of acid. From these results, and electrochemical studies detailed later in this chapter, it is unlikely that the adt-bridged complex undergoes a double protonation (at the N atom and Fe centres simultaneously), as had been observed for a similar tri-substituted complex reported by Ott, Lomoth and co-workers[15] (though this complex did require specific conditions to observe the various protonation states, which could be investigated in future studies).

The IR bands of the neutral complexes are all at similar wavenumbers, suggesting that each of the complexes will exhibit similar redox potentials, as the electron density on the Fe centres is highly influential in the IR band positions.

4.3 Electrochemistry of $Fe_2(\mu\text{-pdt})(CO)_3(\mu,\eta^2\text{-}Ph_2PCH_2CH_2P(Ph)CH_2CH_2\text{-}PPh_2)$ in the absence of protons in a range of electrolyte solutions

To aid in understanding any catalytic mechanism the triphos-ligand complexes may be found to exhibit, the electrochemistry of the complexes in the absence of protons has been investigated. The pdt-bridged complex has been analysed first.

As was discussed in Chapter 1, many research groups in the field have used only a single electrolyte solution to analyse their range of complexes. It was therefore of interest to analyse whether the electrolyte solution would affect the electrochemical behaviour of the complexes. The triphos-ligand complexes have been used to make this comparison. The four electrolyte solutions used were DCM-$[NBu_4][PF_6]$, DCM-$[NBu_4][ClO_4]$, DCM-$[NBu_4][BF_4]$ and MeCN-$[NBu_4][PF_6]$.

4.3.1 Electrochemistry of $Fe_2(\mu\text{-pdt})(CO)_3(\mu,\eta^2\text{-}Ph_2PCH_2CH_2P(Ph)CH_2CH_2PPh_2)$ in the absence of protons in DCM-$[NBu_4][PF_6]$

The CV of $Fe_2(\mu\text{-pdt})(CO)_3(\mu,\eta^2\text{-}Ph_2PCH_2CH_2P(Ph)CH_2CH_2PPh_2)$ in DCM is shown in Figure 64. On sweeping to negative potentials, no reduction of the complex was observed within the available potential window. The first oxidation of the complex occurs at -0.29 V, and remained reversible over a range of scan rates from 0.01 - 10 Vs^{-1}. An irreversible oxidation process, of similar peak height to the first process, occurs at 0.4 V. This is followed by two further oxidation peaks which are irreversible.

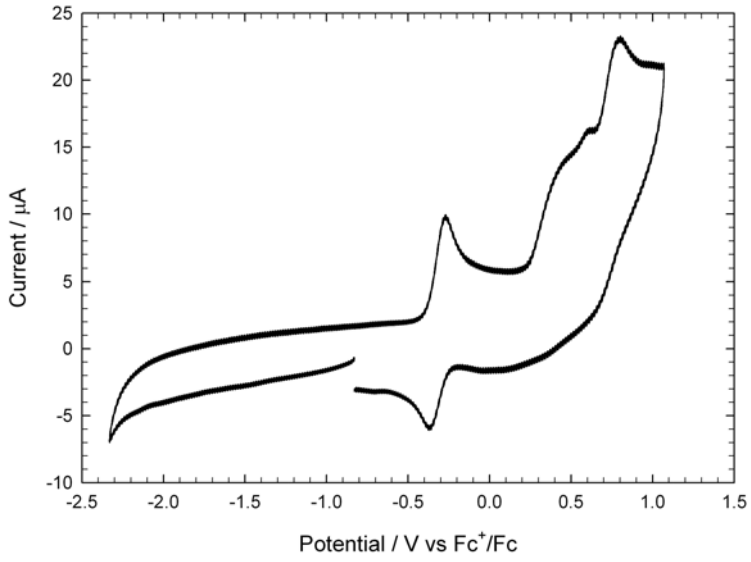

Figure 64: Cyclic voltammetry of $Fe_2(\mu\text{-pdt})(CO)_3(\mu,\eta^2\text{-}Ph_2PCH_2CH_2P(Ph)CH_2CH_2PPh_2)$ (0.5 mM) in DCM-$[NBu_4][PF_6]$ (v=0.1 Vs^{-1}, glassy carbon electrode; V vs Fc^+/Fc)

Bulk chronocoulommetry experiments indicated that the first oxidation is a 1-electron process. Thus, the formal oxidation states of the complex change from Fe(I)Fe(I) to Fe(I)Fe(II). Although it should be noted that a molecular orbital model is a more realistic description for the electronic

structure of these complexes, with the first electron coming from the HOMO upon oxidation. The HOMO for such complexes is usually assumed to be a Fe-Fe σ bonding orbital.

4.3.2 Electrochemistry of $Fe_2(\mu\text{-pdt})(CO)_3(\mu,\eta^2\text{-}Ph_2PCH_2CH_2P(Ph)CH_2CH_2PPh_2)$ in the absence of protons in DCM-$[NBu_4][ClO_4]$

The above section used a DCM-$[NBu_4][PF_6]$ electrolyte solution; this section shall present the results of the same experiments using a DCM-$[NBu_4][ClO_4]$ electrolyte solution. The CV of the pdt-bridged complex in DCM-$[NBu_4][ClO_4]$ is given in Figure 65. When sweeping to negative potentials the first reduction process is not observed within the potential window allowed by the electrolyte solution. The first oxidation of the complex is observed at -0.28 V. A second oxidation process, with a peak height twice that of the first oxidation, occurred at 0.28 V. A third process occurs at 0.69 V.

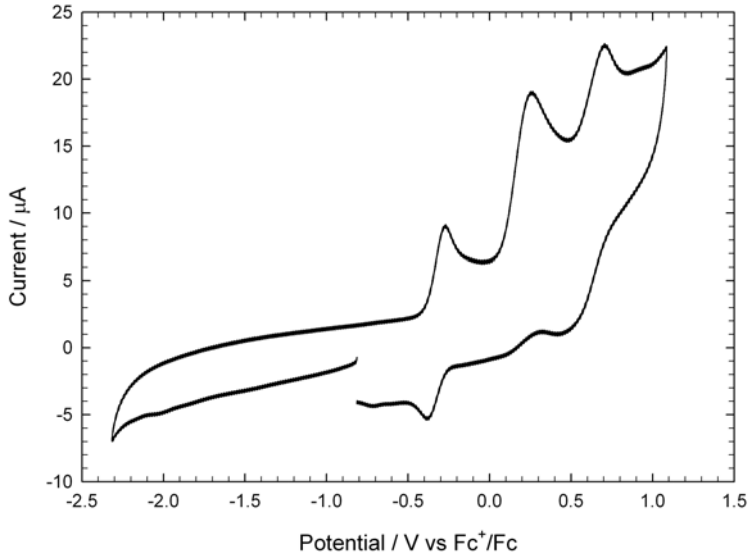

Figure 65: Cyclic voltammetry of $Fe_2(\mu\text{-pdt})(CO)_3(\mu,\eta^2\text{-}Ph_2PCH_2CH_2P(Ph)CH_2CH_2PPh_2)$ (0.5 mM) in DCM-$[NBu_4][ClO_4]$ (v=0.1 Vs^{-1}, glassy carbon electrode; V vs Fc^+/Fc)

4.3.3 Electrochemistry of $Fe_2(\mu\text{-pdt})(CO)_3(\mu,\eta^2\text{-}Ph_2PCH_2CH_2P(Ph)CH_2CH_2PPh_2)$ in the absence of protons in DCM-$[NBu_4][BF_4]$

To extend the investigation a third electrolyte solution was used, namely DCM-$[NBu_4][BF_4]$. The CV of the pdt-bridged complex in this electrolyte solution is shown in Figure 66. Again, no reduction process is observed for the complex. The first oxidation is observed at -0.27 V. Second and third oxidation processes occur at 0.4 and 0.7 V respectively.

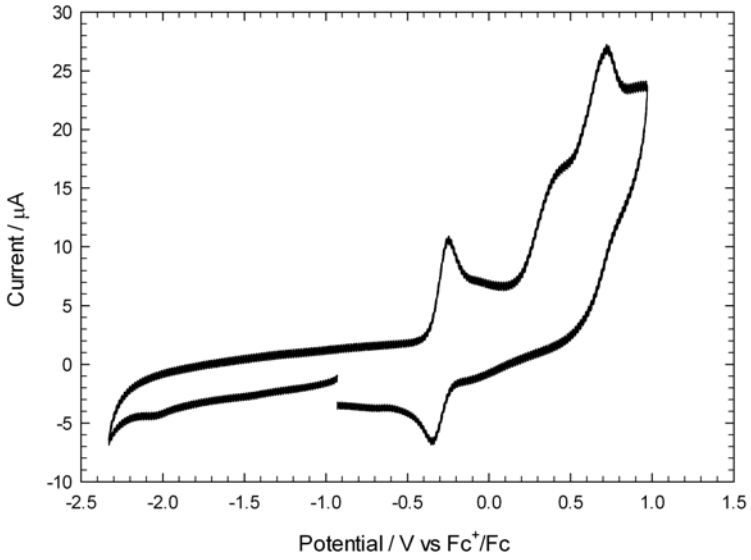

Figure 66: Cyclic voltammetry of $Fe_2(\mu\text{-pdt})(CO)_3(\mu,\eta^2\text{-}Ph_2PCH_2CH_2P(Ph)CH_2CH_2PPh_2)$ (0.5 mM) in DCM-$[NBu_4][BF_4]$ (v=0.1 Vs^{-1}, glassy carbon electrode; V vs Fc^+/Fc)

4.3.4 Electrochemistry of $Fe_2(\mu\text{-pdt})(CO)_3(\mu,\eta^2\text{-}Ph_2PCH_2CH_2P(Ph)CH_2CH_2PPh_2)$ in the absence of protons in MeCN-$[NBu_4][PF_6]$

The pdt-bridged complex has also been analysed in MeCN, to investigate any effect of using a coordinating solvent. The CV of the pdt-bridged complex in MeCN is given in Figure 67. The limit of the potential window prevents detection of the first reduction of the complex. The first oxidation of the complex is observed at -0.2 V. Two smaller oxidation process occur at more positive potentials.

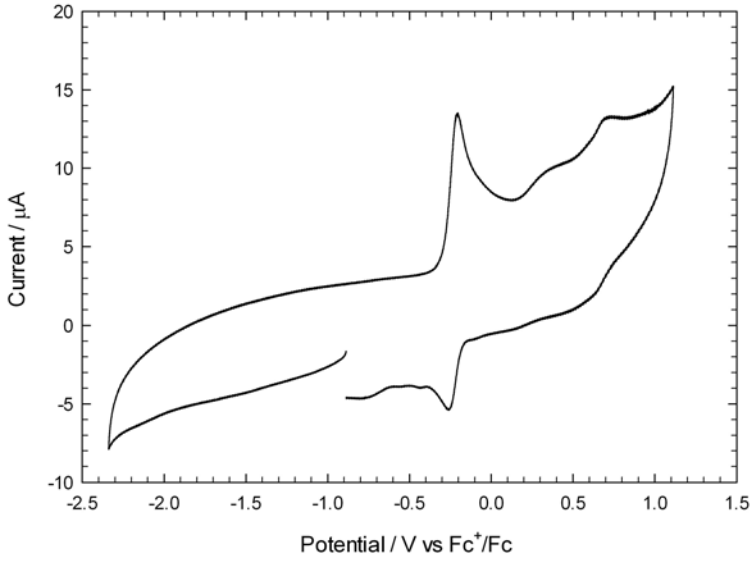

Figure 67: Cyclic voltammetry of $Fe_2(\mu\text{-pdt})(CO)_3(\mu,\eta^2\text{-}Ph_2PCH_2CH_2P(Ph)CH_2CH_2PPh_2)$ (0.5 mM) in MeCN-$[NBu_4][PF_6]$ (v=0.1 Vs^{-1}, glassy carbon electrode; V vs Fc^+/Fc)

Figure 68 looks more closely at the first oxidation at different scan rates. The process remains reversible over this range of scan rates.

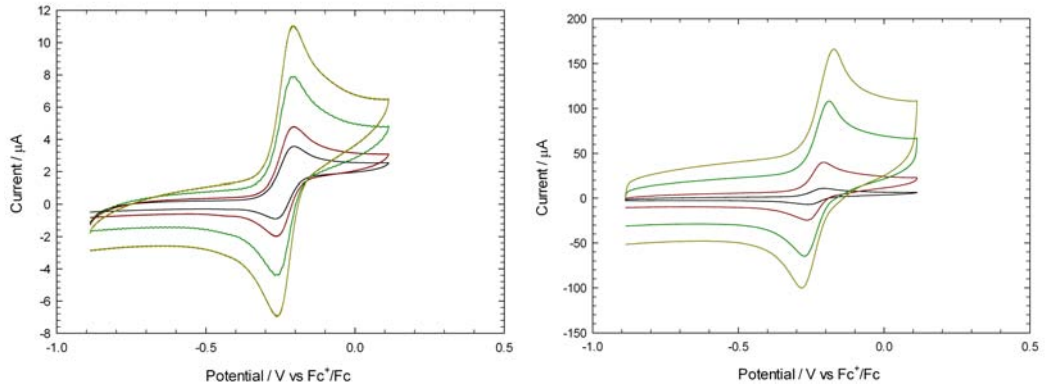

(a) v=0.01, 0.02, 0.05, 0.1 Vs^{-1} (b) v=0.1, 1.0, 5.0, 10.0 Vs^{-1}

Figure 68: Cyclic voltammetry of $Fe_2(\mu\text{-pdt})(CO)_3(\mu,\eta^2\text{-}Ph_2PCH_2CH_2P(Ph)CH_2CH_2PPh_2)$ (0.5 mM) in MeCN-$[NBu_4][PF_6]$ (glassy carbon electrode; V vs Fc^+/Fc)

4.3.5 Summary and discussion

Before comparing the electrochemical behaviour in the various electrolytes, Figure 69 compares the CVs of the pdt-bridged triphos-ligand complex with the analogous pdt-bridged hexacarbonyl complex $Fe_2(\mu\text{-pdt})(CO)_6$ in DCM-$[NBu_4][PF_6]$. The triphos ligand has caused a shift in the oxidation potential of 1.1 V towards negative potentials due to the increased electron density on the Fe centres. This shift is what would be expected based on the negative shift in oxidation potentials of similar substituted complexes. The reduction of the triphos complex is not observed within this potential window, however, it is seen that the hexacarbonyl complex is reduced at -1.87 V. Thus it is anticipated that the first reduction of the triphos-ligand complex would occur at ca. 1 V more negative than this, at about -2.8 V.

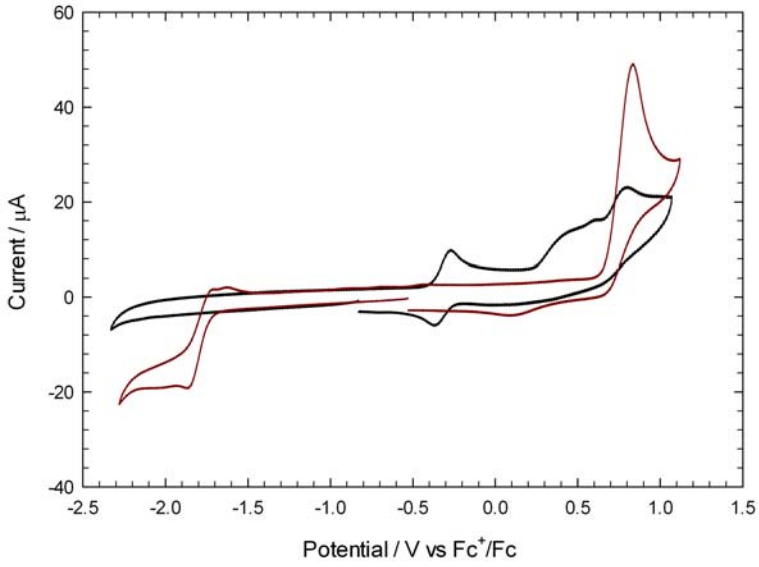

Figure 69: Cyclic voltammetry of $Fe_2(\mu\text{-pdt})(CO)_3(\mu,\eta^2\text{-}Ph_2PCH_2CH_2P(Ph)CH_2CH_2PPh_2)$ (0.5 mM, black line) and $Fe_2(\mu\text{-pdt})(CO)_6$ (0.5 mM, red line) in DCM-$[NBu_4][PF_6]$ (v=0.1 Vs^{-1}, glassy carbon electrode; V vs Fc^+/Fc)

A comparison of the electrochemical behaviour of the pdt-bridged complex in different DCM electrolyte solutions is shown in Figure 70. Although the choice of electrolyte solution makes little difference to the first oxidation of the complex, the fate of the products is changed in the different environments. The significant influence of the choice of electrolyte solution is surprising. It suggests that the oxidised complex interacts with the anion of the electrolyte. This shall be seen to be a common finding throughout the chapter, and shall be discussed further later.

The electrochemical behaviours in DCM and MeCN are compared in Figure 71. The first oxidation process is very similar in both environments, with the oxidation potential 0.05 V more positive in MeCN. The proceeding processes are different in each solvent, suggesting that the oxidised species behaves differently. This is not surprising given the already observed behaviours in different DCM electrolytes, and is explained by the coordinating nature of the MeCN solvent.

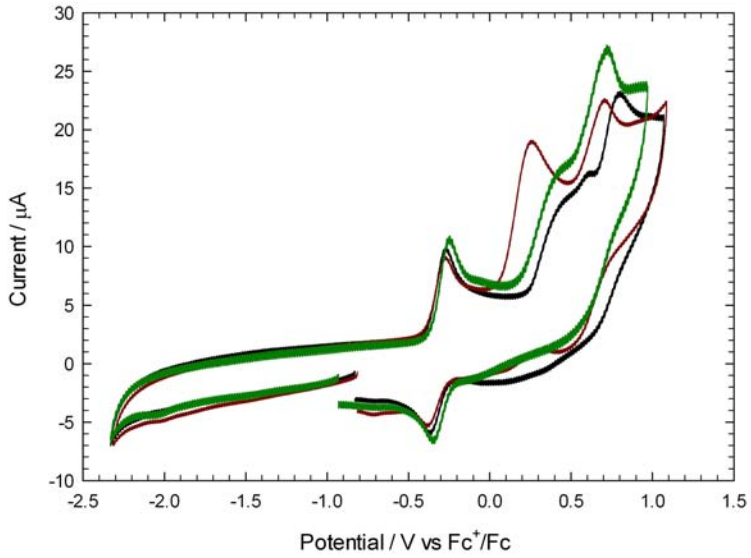

Figure 70: Cyclic voltammetry of $Fe_2(\mu\text{-pdt})(CO)_3(\mu,\eta^2\text{-}Ph_2PCH_2CH_2P(Ph)CH_2CH_2PPh_2)$ (0.5 mM) in DCM-$[NBu_4][PF_6]$ (black line), DCM-$[NBu_4][ClO_4]$ (red line) and DCM-$[NBu_4][BF_4]$ (green line) (v=0.1 Vs^{-1}, glassy carbon electrode; V vs Fc^+/Fc)

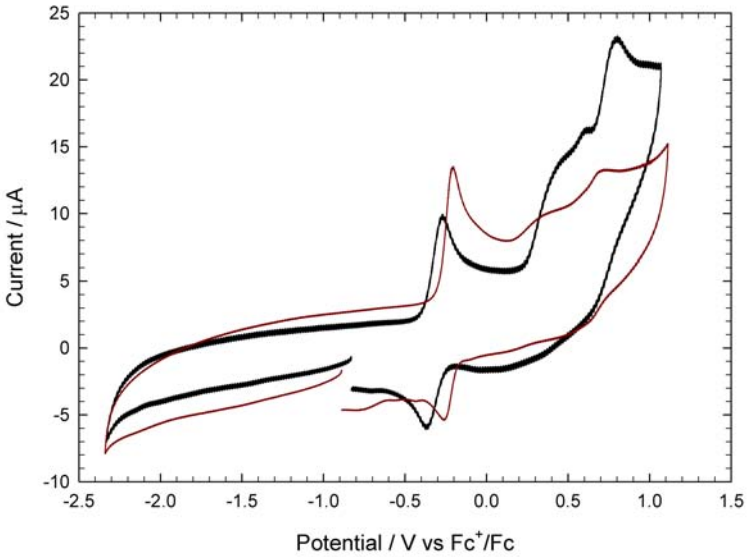

Figure 71: Cyclic voltammetry of $Fe_2(\mu\text{-pdt})(CO)_3(\mu,\eta^2\text{-}Ph_2PCH_2CH_2P(Ph)CH_2CH_2PPh_2)$ (0.5 mM) in DCM-$[NBu_4][PF_6]$ (black line) and MeCN-$[NBu_4][PF_6]$ (red line) (v=0.1 Vs^{-1}, glassy carbon electrode; V vs Fc^+/Fc)

4.4 Attempts to generate a bridging carbonyl ligand through chemical oxidation of $Fe_2(\mu\text{-pdt})(CO)_3(\mu,\eta^2\text{-}Ph_2PCH_2CH_2P(Ph)CH_2CH_2PPh_2)$

As discussed in Chapter 1, the active site of the enzyme exhibits a rotated structure with a semi-bridging CO ligand. Darensbourg and Rauchfuss and their respective co-workers successfully generated complexes with bridging carbonyl ligands through chemical oxidation [30;31]. The electrochemical results presented in the above section indicated that the pdt-bridged complex is oxidised reversibly at a potential less negative than the Fc/Fc^+ couple. Therefore, we attempted to generate the mixed valent oxidation product of the pdt-bridged triphos-ligand complex using $FcPF_6$ as the oxidising agent, and tested to see whether it exhibits a bridging CO ligand. The reaction was followed by IR spectroscopy.

From Section 4.2.1 it was known that the IR spectrum of the complex exhibits bands at 1949 and 1888 cm^{-1}. On addition of $FcPF_6$ one band is present at 1947 cm^{-1} (Figure 72). The IR spectrum gave no evidence for a bridging carbonyl, as no peak was observed the region 1800 to 1600 cm^{-1}. This is likely due to the restrictive nature of the triphos ligand not allowing for a rotation of the CO ligand. Further work is required to elucidate the product of the oxidation reaction. It is thought that the triphos-ligand complex did not undergo rotation due to steric restraint within the complex.

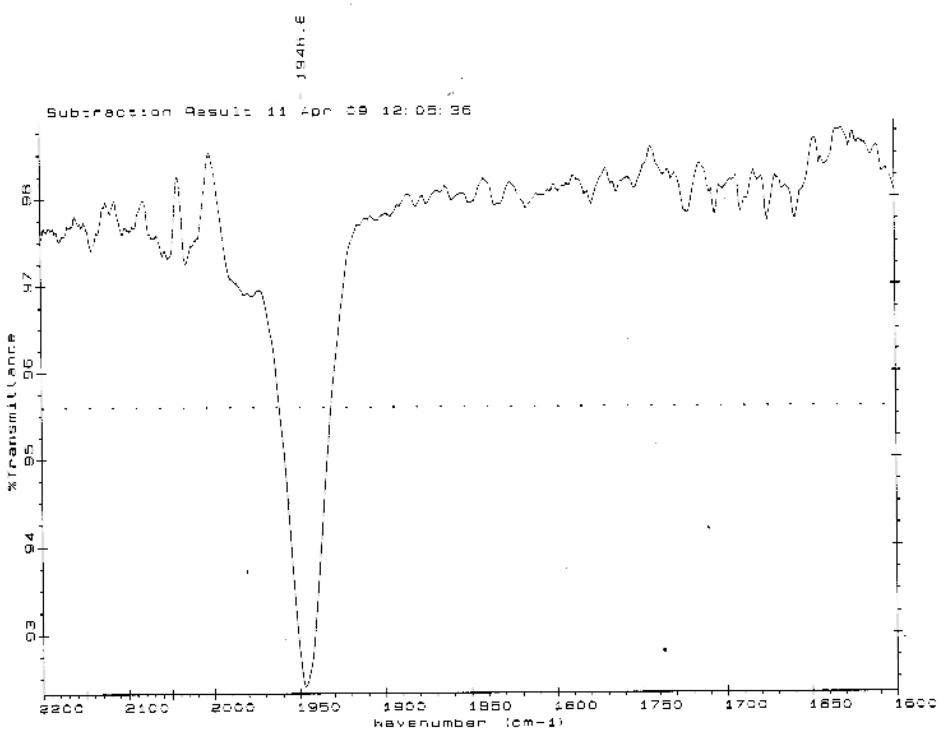

Figure 72: IR spectrum of $Fe_2(\mu\text{-pdt})(CO)_3(\mu,\eta^2\text{-}Ph_2PCH_2CH_2P(Ph)CH_2CH_2PPh_2)$ in DCM after addition of 1 molar equivalent $FcPF_6$

4.5 Electrochemistry of $Fe_2(\mu\text{-adt})(CO)_3(\mu,\eta^2\text{-}Ph_2PCH_2CH_2P(Ph)CH_2CH_2\text{-}PPh_2)$ in the absence of protons in a range of electrolyte solutions

The electrochemical investigations described above have also been performed on the adt-bridged complex.

4.5.1 Electrochemistry of $Fe_2(\mu\text{-adt})(CO)_3(\mu,\eta^2\text{-}Ph_2PCH_2CH_2P(Ph)CH_2CH_2PPh_2)$ in the absence of protons in DCM-$[NBu_4][PF_6]$

The CV of the adt-bridged complex in DCM-$[NBu_4][PF_6]$ is shown in Figure 73. No reduction processes are observed within the potential window of the electrolyte solution. The first oxidation of the complex is observed at -0.29 V, with a second process at -0.08 V. Minor oxidation processes are observed at more positive potentials. From a comparison of the peak height of the first oxidation of the pdt-bridged complex and the peak height of the oxidation process at -0.29 V, the first oxidation of the adt-bridged complex is attributed to a 1-electron process.

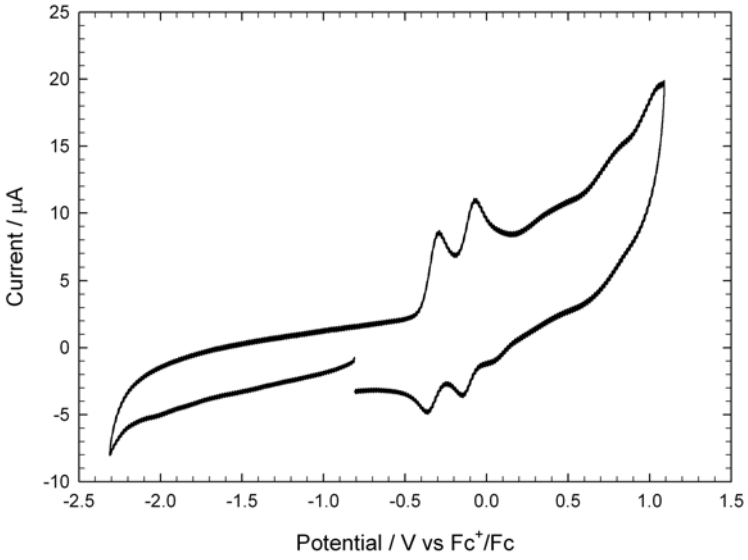

Figure 73: Cyclic voltammetry of $Fe_2(\mu\text{-adt})(CO)_3(\mu,\eta^2\text{-}Ph_2PCH_2CH_2P(Ph)CH_2CH_2PPh_2)$ (0.5 mM) in DCM-$[NBu_4][PF_6]$ (v=0.1 Vs^{-1}, glassy carbon electrode; V vs Fc^+/Fc)

Figure 74 looks at the oxidation processes in more detail. The oxidation peaks were found to be reversible over a range of scan rates. The cause for the second oxidation process so close to the first is not yet known. It is unlikely to be due to steric isomers in solution, as there is such a large difference in oxidation potential. The behaviour is more likely due to two successive electron transfers, i.e. an EE process, with a peak splitting of 0.21 V. The clear separation of the two oxidation peaks indicates that the two electrons are removed from the same HOMO, leading to peak separation due to electrostatic reasons.

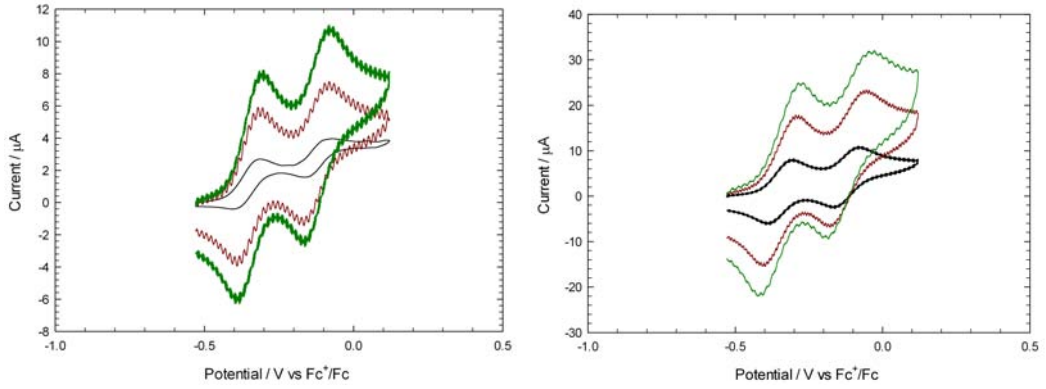

(a) v=0.01, 0.05, 0.1 Vs^{-1} (b) v=0.1, 0.5, 1.0 Vs^{-1}

Figure 74: Cyclic voltammetry of $Fe_2(\mu\text{-adt})(CO)_3(\mu,\eta^2\text{-}Ph_2PCH_2CH_2P(Ph)CH_2CH_2PPh_2)$ (0.5 mM) in DCM-$[NBu_4][PF_6]$ (v=0.1 Vs^{-1}, glassy carbon electrode; V vs Fc^+/Fc)

4.5.2 Electrochemistry of $Fe_2(\mu\text{-adt})(CO)_3(\mu,\eta^2\text{-}Ph_2PCH_2CH_2P(Ph)CH_2CH_2PPh_2)$ in the absence of protons in DCM-$[NBu_4][ClO_4]$

As with the pdt-bridged complex, the adt-bridged complex has also been investigated in a DCM-$[NBu_4][ClO_4]$ electrolyte solution. The CV of the complex in this electrolyte is shown in Figure 75. The first reduction of the complex is not observed within this potential window. The first oxidation of the complex occurs at -0.29 V, with a second oxidation process at -0.11 V. Minor oxidation processes are seen at more positive potentials.

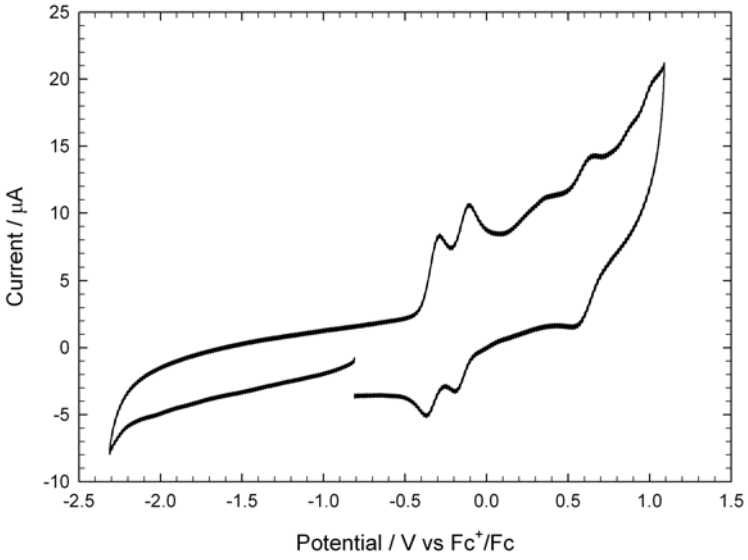

Figure 75: Cyclic voltammetry of $Fe_2(\mu\text{-adt})(CO)_3(\mu,\eta^2\text{-}Ph_2PCH_2CH_2P(Ph)CH_2CH_2PPh_2)$ (0.5 mM) in DCM-$[NBu_4][ClO_4]$ (v=0.1 Vs^{-1}, glassy carbon electrode; V vs Fc^+/Fc)

4.5.3 Electrochemistry of $Fe_2(\mu\text{-adt})(CO)_3(\mu,\eta^2\text{-}Ph_2PCH_2CH_2P(Ph)CH_2CH_2PPh_2)$ in the absence of protons in DCM-$[NBu_4][BF_4]$

The complex has also been investigated in a DCM-$[NBu_4][BF_4]$ electrolyte, as shown in Figure 76. Again, no reduction process is seen within this potential window. The first oxidation of the complex occurs at -0.25 V, with a second oxidation process at -0.08 V. Minor oxidation processes are also seen at more anodic potentials.

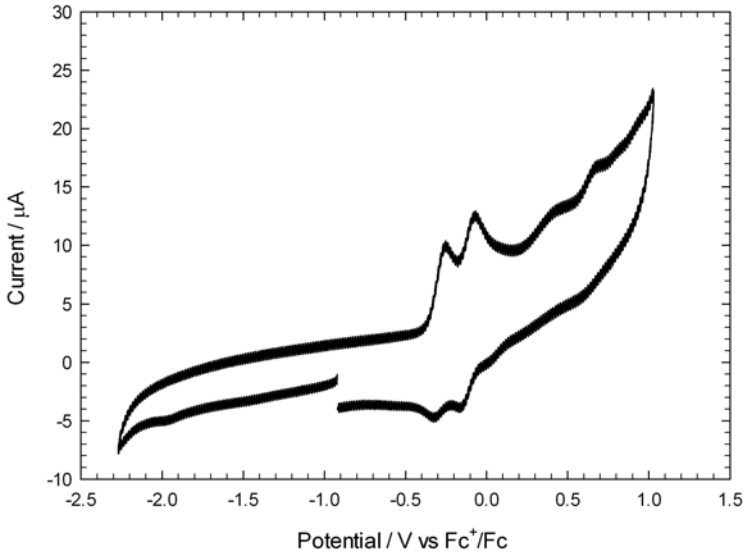

Figure 76: Cyclic voltammetry of $Fe_2(\mu\text{-adt})(CO)_3(\mu,\eta^2\text{-}Ph_2PCH_2CH_2P(Ph)CH_2CH_2PPh_2)$ (0.5 mM) in DCM-$[NBu_4][BF_4]$ (v=0.1 Vs^{-1}, glassy carbon electrode; V vs Fc^+/Fc)

4.5.4 Electrochemistry of $Fe_2(\mu\text{-adt})(CO)_3(\mu,\eta^2\text{-}Ph_2PCH_2CH_2P(Ph)CH_2CH_2PPh_2)$ in the absence of protons in MeCN-$[NBu_4][PF_6]$

As with the pdt-bridged complex, the adt-bridged complex has also been analysed in the coordinating solvent MeCN, as shown in Figure 77. The reduction of the complex is not observable within the potential window of the electrolyte solution. The first oxidation of the complex occurs at -0.22 V. Unlike in the DCM electrolyte solutions, the first oxidation is irreversible, and a second oxidation peak does not follow the first oxidation process.

The first oxidation has been investigated further at different scan rates (Figure 78). At slow scan rates the oxidation is irreversible. At faster scan rates the oxidation becomes more reversible and a second oxidation peak occurs following the first oxidation process. The behaviour at fast scan rates is similar to that observed in DCM. This suggests that at slow scan rates the MeCN is coordinating to the oxidised species, thus making the oxidation process irreversible. At fast scan rates the MeCN coordination process does not have time to occur, and the oxidation process is more reversible.

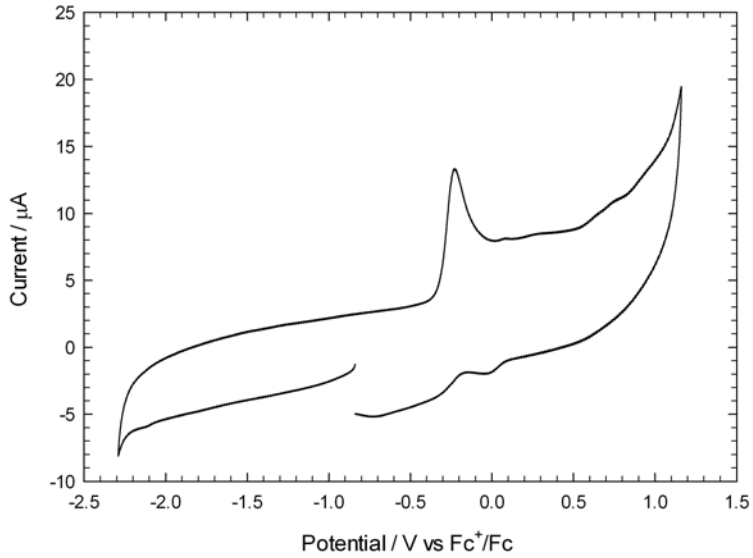

Figure 77: Cyclic voltammetry of $Fe_2(\mu\text{-adt})(CO)_3(\mu,\eta^2\text{-}Ph_2PCH_2CH_2P(Ph)CH_2CH_2PPh_2)$ (0.5 mM) in MeCN-$[NBu_4][PF_6]$ (v=0.1 Vs^{-1}, glassy carbon electrode; V vs Fc^+/Fc)

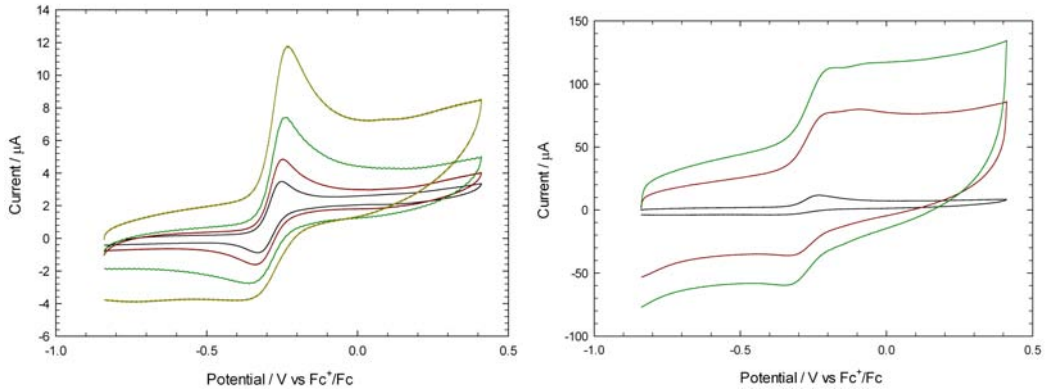

(a) v=0.01, 0.02, 0.05, 0.1 Vs^{-1} (b) v=0.1, 5.0, 10.0 Vs^{-1}

Figure 78: Cyclic voltammetry of $Fe_2(\mu\text{-adt})(CO)_3(\mu,\eta^2\text{-}Ph_2PCH_2CH_2P(Ph)CH_2CH_2PPh_2)$ (0.5 mM) in MeCN-$[NBu_4][PF_6]$ (glassy carbon electrode; V vs Fc^+/Fc)

4.5.5 Summary and discussion

The difference in behaviour due to electrolyte used is not as pronounced as that of the pdt-bridged complex, however some minor differences are evident, as shown in Figure 79. For example, the smaller peaks following the first two oxidation processes are smaller in the DCM-[NBu_4][PF_6] electrolyte compared to the other two electrolytes.

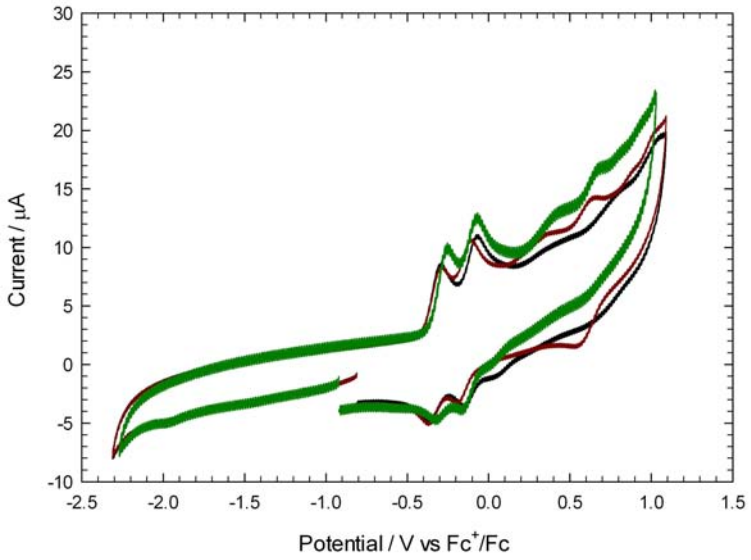

Figure 79: Cyclic voltammetry of $Fe_2(\mu\text{-adt})(CO)_3(\mu,\eta^2\text{-}Ph_2PCH_2CH_2P(Ph)CH_2CH_2PPh_2)$ (0.5 mM) in DCM-[NBu_4][PF_6] (black line), DCM-[NBu_4][ClO_4] (red line) and DCM-[NBu_4][BF_4] (green line) (v=0.1 Vs^{-1}, glassy carbon electrode; V vs Fc^+/Fc)

A comparison of the behaviours in DCM and MeCN is shown in Figure 80. There is a clear difference in the oxidation processes in the two electrolytes. It is thought that in DCM the complex undergoes two reversible one electron oxidation processes. It MeCN however, it is thought that the oxidation peak is irreversible due to the MeCN solvent coordinating to the oxidised species and stabilising it, thus eliminating the second oxidation peak. This result is a clear indication of the significant influence the choice of solvent can have on the electrochemical behaviour of these di-iron complexes.

The adt-bridged complex is compared to the pdt-bridged complex in the three DCM electrolytes in Figures 81, 82 and 83. The first oxidation of each complex is at a very similar potential, indicating that these bridges have comparable electron donating / withdrawing ability. The only major difference in the electrochemical behaviours is in the second oxidation process of the adt complex discussed above.

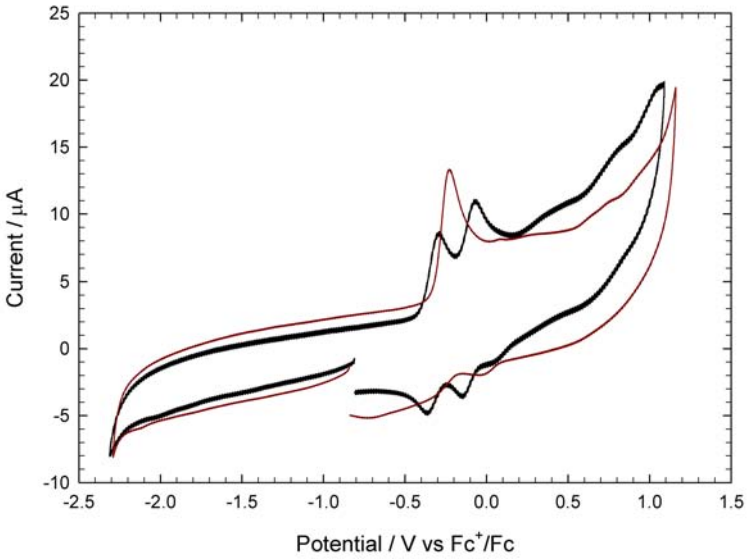

Figure 80: Cyclic voltammetry of $Fe_2(\mu\text{-adt})(CO)_3(\mu,\eta^2\text{-}Ph_2PCH_2CH_2P(Ph)CH_2CH_2PPh_2)$ (0.5 mM) in DCM-$[NBu_4][PF_6]$ (black line) and MeCN-$[NBu_4][PF_6]$ (red line) (v=0.1 Vs^{-1}, glassy carbon electrode; V vs Fc^+/Fc)

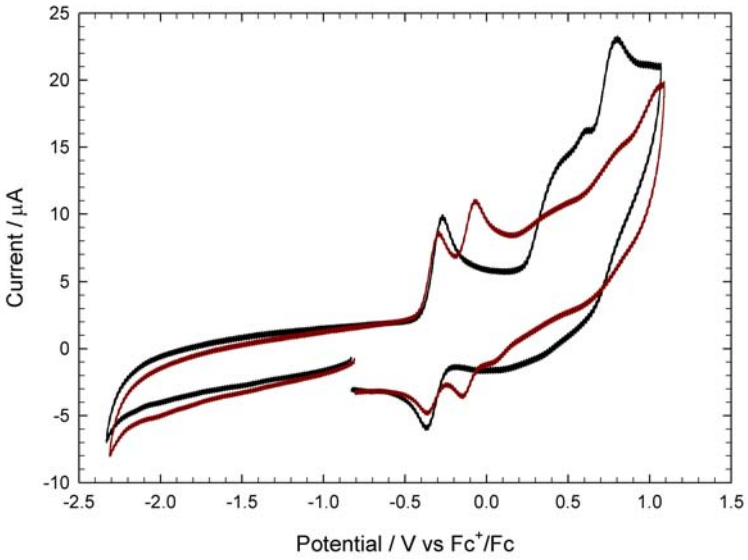

Figure 81: Cyclic voltammetry of $Fe_2(\mu\text{-pdt})(CO)_3(\mu,\eta^2\text{-}Ph_2PCH_2CH_2P(Ph)CH_2CH_2PPh_2)$ (0.5 mM, black line) and $Fe_2(\mu\text{-adt})(CO)_3(\mu,\eta^2\text{-}Ph_2PCH_2CH_2P(Ph)CH_2CH_2PPh_2)$ (0.5 mM, red line) in DCM-$[NBu_4][PF_6]$ (v=0.1 Vs^{-1}, glassy carbon electrode; V vs Fc^+/Fc)

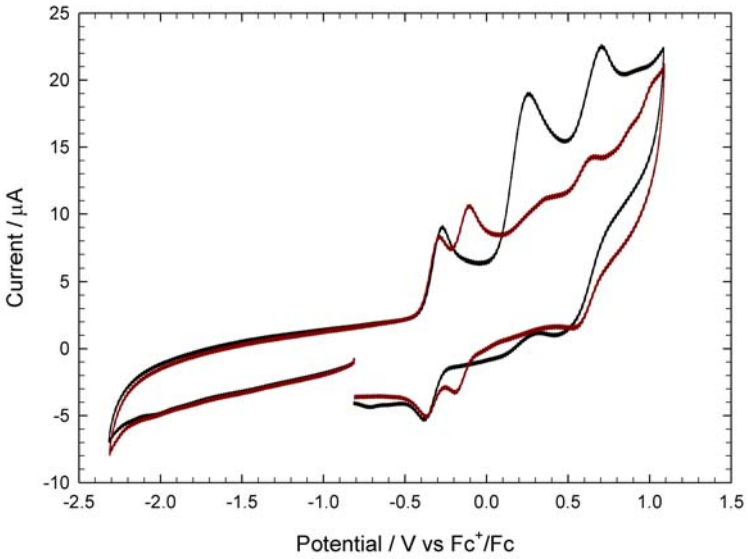

Figure 82: Cyclic voltammetry of $Fe_2(\mu\text{-pdt})(CO)_3(\mu,\eta^2\text{-}Ph_2PCH_2CH_2P(Ph)CH_2CH_2PPh_2)$ (0.5 mM, black line) and $Fe_2(\mu\text{-adt})(CO)_3(\mu,\eta^2\text{-}Ph_2PCH_2CH_2P(Ph)CH_2CH_2PPh_2)$ (0.5 mM, red line) in DCM-$[NBu_4][ClO_4]$ (v=0.1 Vs^{-1}, glassy carbon electrode; V vs Fc^+/Fc)

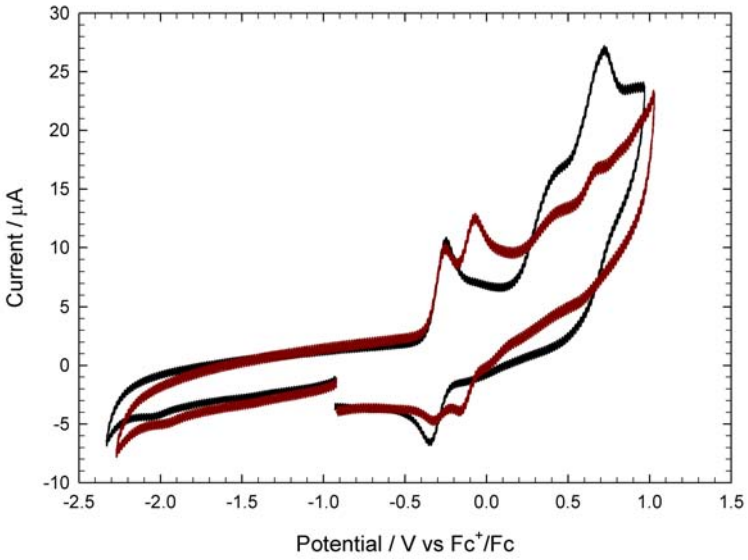

Figure 83: Cyclic voltammetry of $Fe_2(\mu\text{-pdt})(CO)_3(\mu,\eta^2\text{-}Ph_2PCH_2CH_2P(Ph)CH_2CH_2PPh_2)$ (0.5 mM, black line) and $Fe_2(\mu\text{-adt})(CO)_3(\mu,\eta^2\text{-}Ph_2PCH_2CH_2P(Ph)CH_2CH_2PPh_2)$ (0.5 mM, red line) in DCM-$[NBu_4][BF_4]$ (v=0.1 Vs^{-1}, glassy carbon electrode; V vs Fc^+/Fc)

4.6 Electrochemistry of $Fe_2(\mu\text{-}(SMe)_2)(CO)_3(\mu,\eta^2\text{-}Ph_2PCH_2CH_2P(Ph)CH_2CH_2\text{-}PPh_2)$ in the absence of protons in a range of electrolyte solutions

The experiments performed on the pdt- and adt-bridged complexes have been repeated on the $(SMe)_2$-bridged complex.

4.6.1 Electrochemistry of $Fe_2(\mu\text{-}(SMe)_2)(CO)_3(\mu,\eta^2\text{-}Ph_2PCH_2CH_2P(Ph)CH_2CH_2PPh_2)$ in the absence of protons in DCM-$[NBu_4][PF_6]$

Following on from the pdt- and adt-bridged complexes, the electrochemistry of the $(SMe)_2$-bridged complex has been analysed. The CV of the $(SMe)_2$-bridged complex in DCM-$[NBu_4][PF_6]$ is shown in Figure 84. The reduction of the complex is not observed within the potential window offered by the electrolyte solution. The first oxidation of the complex occurs at -0.40 V. Two further oxidation processes occur at 0.48 and 0.78 V.

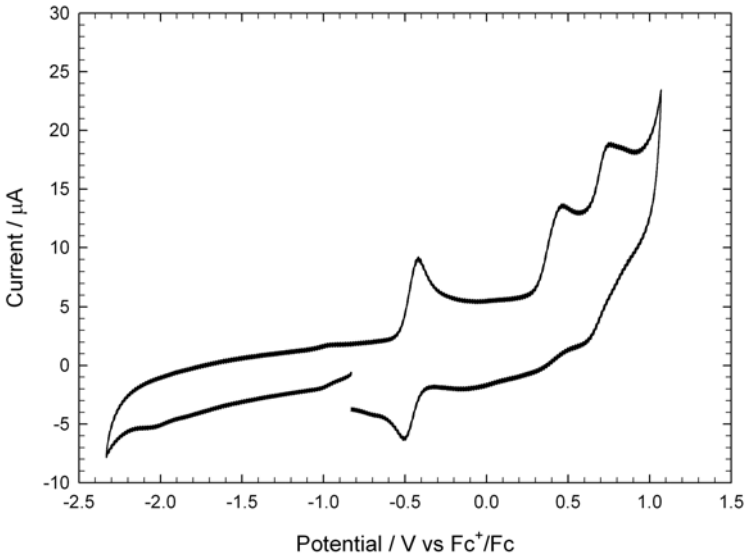

Figure 84: Cyclic voltammetry of $Fe_2(\mu\text{-}(SMe)_2)(CO)_3(\mu,\eta^2\text{-}Ph_2PCH_2CH_2P(Ph)CH_2CH_2PPh_2)$ (0.5 mM) in DCM-$[NBu_4][PF_6]$ (v=0.1 Vs^{-1}, glassy carbon electrode; V vs Fc^+/Fc)

4.6.2 Electrochemistry of $Fe_2(\mu\text{-}(SMe)_2)(CO)_3(\mu,\eta^2\text{-}Ph_2PCH_2CH_2P(Ph)CH_2CH_2PPh_2)$ in the absence of protons in DCM-$[NBu_4][ClO_4]$

As with the pdt- and adt-bridged complexes, the $(SMe)_2$-bridged complex has been analysed in a range of electrolyte solutions. The CV of the complex in DCM-$[NBu_4][ClO_4]$ is given in Figure 85. The reduction of the complex is not observed in this potential window. The first oxidation of the complex occurs at -0.41 V. Further oxidation processes are seen at 0.32, 0.7 and 0.8 V.

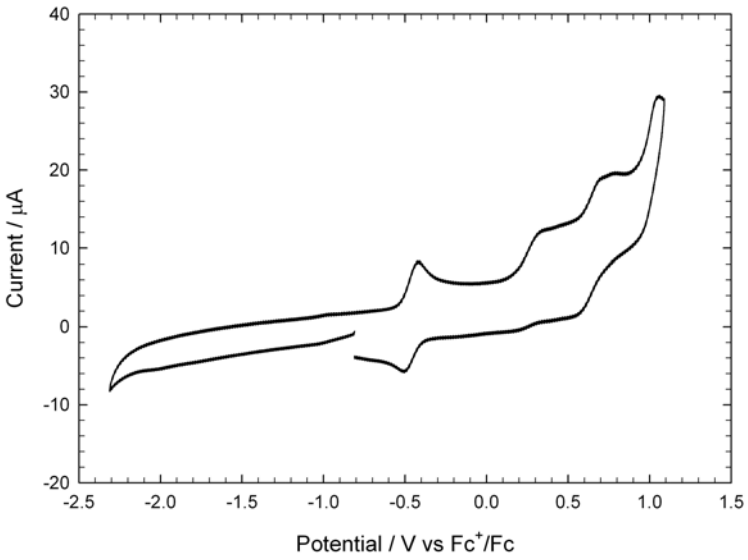

Figure 85: Cyclic voltammetry of $Fe_2(\mu\text{-}(SMe)_2)(CO)_3(\mu,\eta^2\text{-}Ph_2PCH_2CH_2P(Ph)CH_2CH_2PPh_2)$ (0.5 mM) in DCM-$[NBu_4][ClO_4]$ (v=0.1 Vs^{-1}, glassy carbon electrode; V vs Fc^+/Fc)

4.6.3 Electrochemistry of $Fe_2(\mu\text{-}(SMe)_2)(CO)_3(\mu,\eta^2\text{-}Ph_2PCH_2CH_2P(Ph)CH_2CH_2PPh_2)$ in the absence of protons in DCM-$[NBu_4][BF_4]$

The $(SMe)_2$-bridged complex has also been investigated in a DCM-$[NBu_4][BF_4]$ electrolyte solution (Figure 86). The first oxidation of the complex occurs at -0.38 V. Further oxidation process occur at 0.4 and 0.7 V.

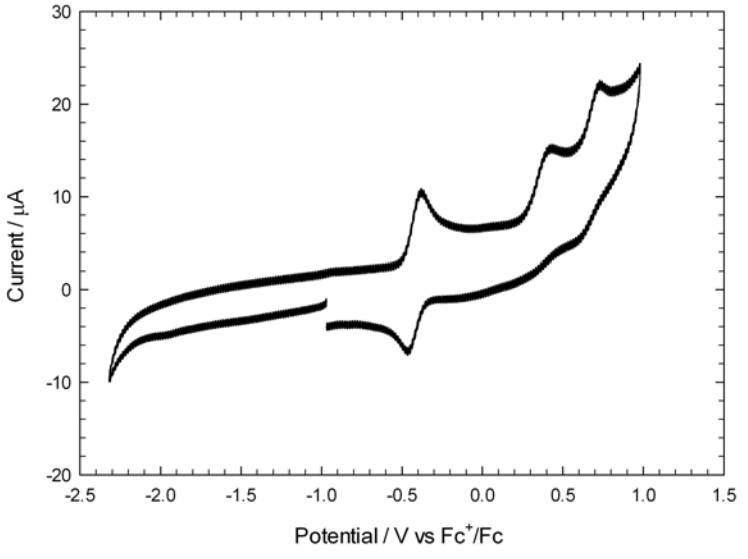

Figure 86: Cyclic voltammetry of $Fe_2(\mu\text{-}(SMe)_2)(CO)_3(\mu,\eta^2\text{-}Ph_2PCH_2CH_2P(Ph)CH_2CH_2PPh_2)$ (0.5 mM) in DCM-$[NBu_4][BF_4]$ (v=0.1 Vs^{-1}, glassy carbon electrode; V vs Fc^+/Fc)

4.6.4 Electrochemistry of $Fe_2(\mu\text{-}(SMe)_2)(CO)_3(\mu,\eta^2\text{-}Ph_2PCH_2CH_2P(Ph)CH_2CH_2PPh_2)$ in the absence of protons in MeCN-$[NBu_4][PF_6]$

As with the pdt- and adt-bridged complexes, the $(SMe)_2$-bridged complex has also been analysed in MeCN (Figure 87). The first oxidation of the complex occurs at -0.35 V. Further oxidation processes occur at -0.14, 0.3 and 1.01 V. On the return scan several clear re-reduction features are observed.

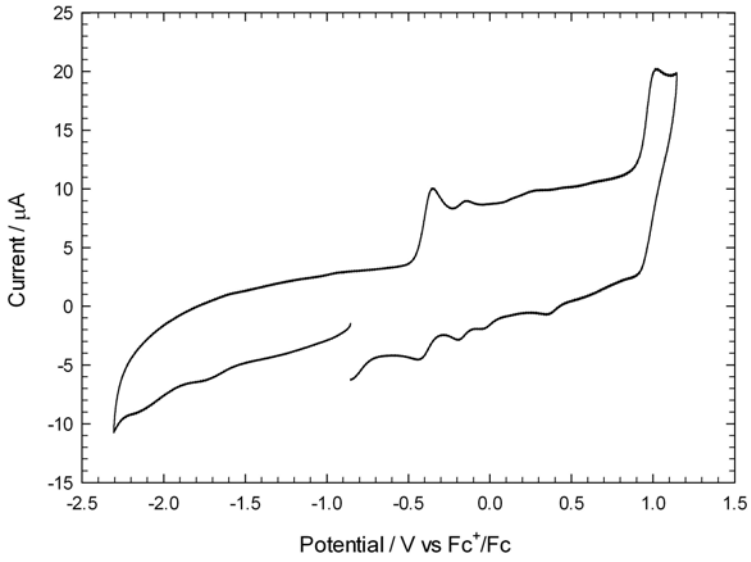

Figure 87: Cyclic voltammetry of $Fe_2(\mu\text{-}(SMe)_2)(CO)_3(\mu,\eta^2\text{-}Ph_2PCH_2CH_2P(Ph)CH_2CH_2PPh_2)$ (0.5 mM) in MeCN-$[NBu_4][PF_6]$ (v=0.1 Vs^{-1}, glassy carbon electrode; V vs Fc^+/Fc)

The first oxidation of the complex was analysed at different scan rates, as shown in Figure 88. At faster scan rates the ratio of the second to the first oxidations increases, suggesting a ECE process. Both oxidation peaks exhibit reversibility.

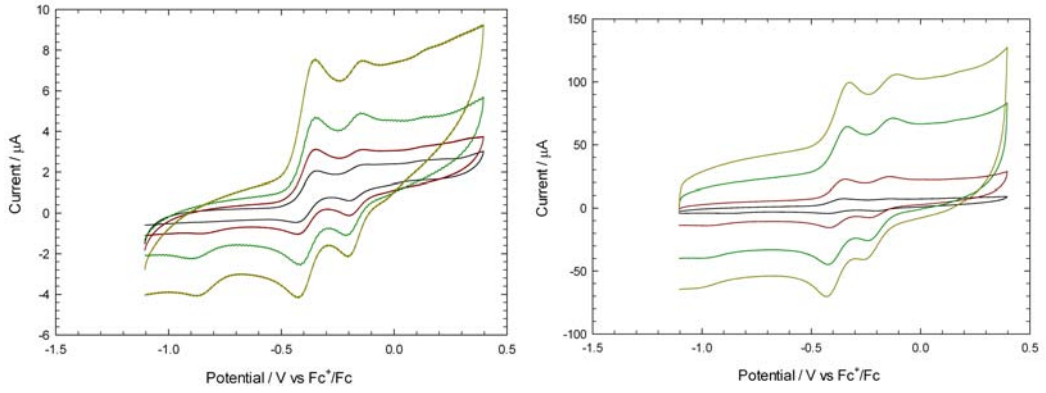

(a) v=0.01, 0.02, 0.05, 0.1 Vs^{-1} (b) v=0.1, 1.0, 5.0, 10.0 Vs^{-1}

Figure 88: Cyclic voltammetry of $Fe_2(\mu\text{-}(SMe)_2)(CO)_3(\mu,\eta^2\text{-}Ph_2PCH_2CH_2P(Ph)CH_2CH_2PPh_2)$ (0.5 mM) in MeCN-$[NBu_4][PF_6]$ (glassy carbon electrode; V vs Fc^+/Fc)

4.6.5 Summary and discussion

The oxidation behaviour of the $(SMe)_2$-bridged complex has been found to be slightly different in each of the different DCM electrolyte solutions, as shown in Figure 89. However, the differences are significantly less than seen for the pdt-bridged complex.

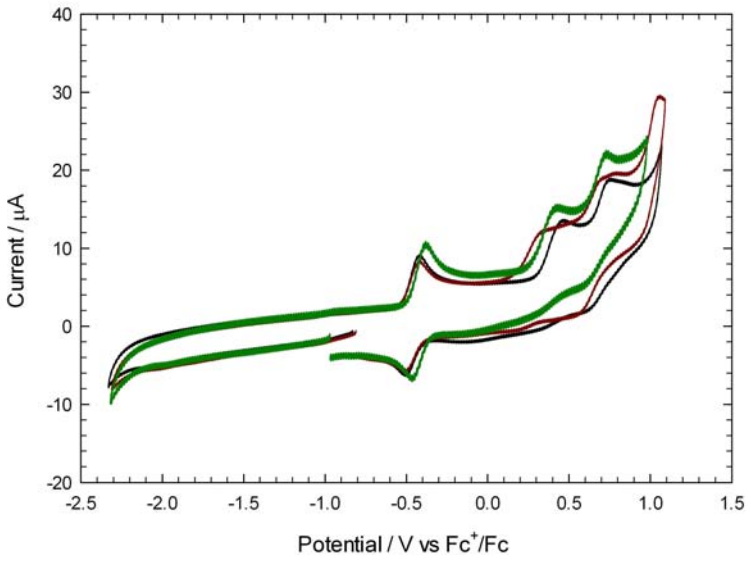

Figure 89: Cyclic voltammetry of $Fe_2(\mu\text{-}(SMe)_2)(CO)_3(\mu,\eta^2\text{-}Ph_2PCH_2CH_2P(Ph)CH_2CH_2PPh_2)$ (0.5 mM) in DCM-$[NBu_4][PF_6]$ (black line), DCM-$[NBu_4][ClO_4]$ (red line) and DCM-$[NBu_4][BF_4]$ (green line) (v=0.1 Vs^{-1}, glassy carbon electrode; V vs Fc^+/Fc)

The differences in the electrochemical behaviour in DCM and MeCN are more significant. In particular, in MeCN once the complex is oxidised a secondary oxidation process follows at 0.2 V more positive; this is not observed in DCM. The generated cation clearly behaves very differently in the DCM and MeCN electrolytes. Possibly the MeCN is involved in a coordination reaction, thus altering the electronic state of the Fe centres. Further work is required to understand this fully.

It is now possible to make a comparison between the influence of the dithiolate bridge on the electrochemistry of the triphos-ligand complexes. CVs of the three triphos-ligand complexes in the absence of protons are shown in Figures 91, 92 and 93. The variation of the dithiolate bridge causes obvious differences in the electrochemical behaviour of the three complexes. In particular, the first oxidation of the $(SMe)_2$-bridged complex occurs at lower potential than the other two bridges. The $(SMe)_2$-bridge is open, and the two SMe moieties are able to orientate themselves with less constraint than the linked pdt and adt bridges. This freedom should raise the reorganisation energy, and therefore stabilise the oxidised state. The other major difference in the three complexes is the additional oxidation process observed for the adt-bridged complex, suggested above to be an EE process. Looking at the structures of the three complexes it is difficult to understand why the adt-bridged complex should readily undergo a second electron transfer and the other complexes should not. Further work, preferably using computation modeling of the molecular orbitals, is required to understand why the adt-bridged complex exhibits this behaviour, while the pdt- and $(SMe)_2$-bridged

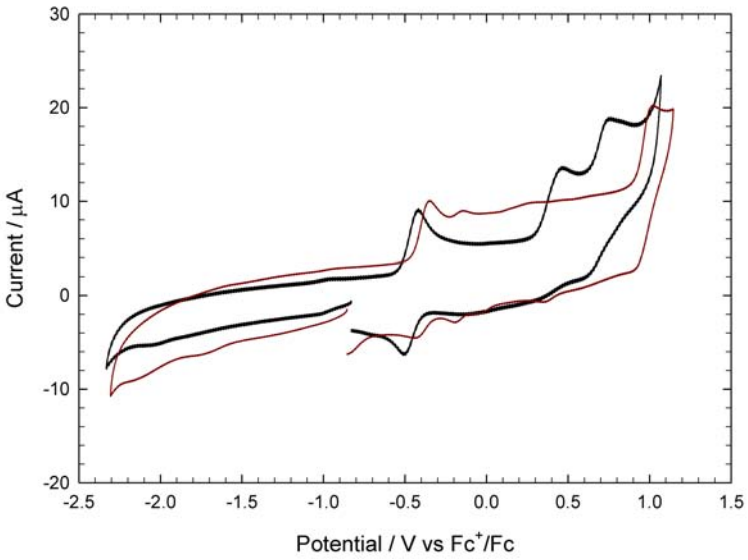

Figure 90: Cyclic voltammetry of $Fe_2(\mu\text{-}(SMe)_2)(CO)_3(\mu,\eta^2\text{-}Ph_2PCH_2CH_2P(Ph)CH_2CH_2PPh_2)$ (0.5 mM) in DCM-$[NBu_4][PF_6]$ (black line) and MeCN-$[NBu_4][PF_6]$ (red line) (v=0.1 Vs^{-1}, glassy carbon electrode; V vs Fc^+/Fc)

complexes do not.

Based on the above hypothesis that a more sterically constraining bridge results in a higher oxidation potential, it is expected that an edt-bridged complex would be harder to oxidise than these three complexes. To test this a small quantity of edt-bridged complex ($Fe_2(\mu\text{-edt})(CO)_3(\mu,\eta^2\text{-}Ph_2PCH_2CH_2P(Ph)CH_2\text{-}CH_2PPh_2)$) has been synthesised and investigated. Due to the limited amount of complex available, the only electrolyte used to date is DCM-$[NBu_4][ClO_4]$.

The CV of the edt-bridged complex is shown in Figure 94. The first reduction of the complex is not observed within the potential window of the electrolyte solution. The first oxidation of the complex is reversible and occurs at -0.21 V. This is followed by a small oxidation peak at -0.08 V. An irreversible oxidation peak of twice the height of the first oxidation occurs at 0.59 V.

The first oxidation of the complex occurs at -0.21 V. Compared to the pdt- (-0.28 V), adt- (-0.29 V) and $(SMe)_2$-bridged (-0.41 V) complexes this is the highest oxidation potential. Thus, the trend is in keeping with the earlier suggestion that a more flexible bridge allows for higher reorganisation energy, making the oxidation potential lower.

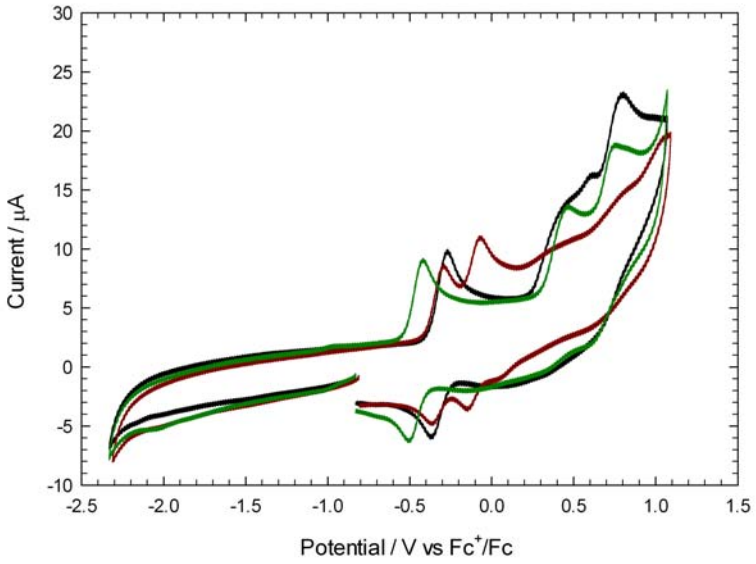

Figure 91: Cyclic voltammetry of $Fe_2(\mu\text{-pdt})(CO)_3(\mu,\eta^2\text{-}Ph_2PCH_2CH_2P(Ph)CH_2CH_2PPh_2)$ (0.5 mM, black line), $Fe_2(\mu\text{-adt})(CO)_3(\mu,\eta^2\text{-}Ph_2PCH_2CH_2P(Ph)CH_2CH_2PPh_2)$ (0.5 mM, red line), and $Fe_2(\mu\text{-}(SMe)_2)(CO)_3(\mu,\eta^2\text{-}Ph_2PCH_2CH_2P(Ph)CH_2CH_2PPh_2)$ (0.5 mM, green line) in DCM-$[NBu_4][PF_6]$ (v=0.1 Vs^{-1}, glassy carbon electrode; V vs Fc^+/Fc)

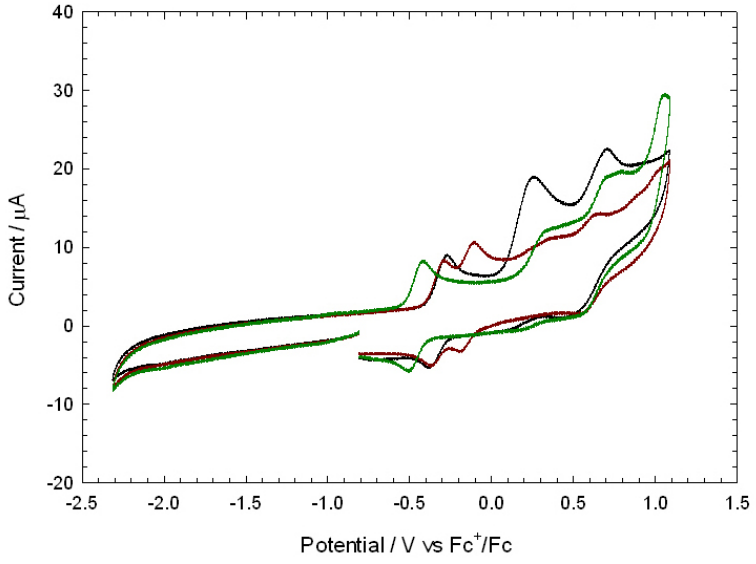

Figure 92: Cyclic voltammetry of $Fe_2(\mu\text{-pdt})(CO)_3(\mu,\eta^2\text{-}Ph_2PCH_2CH_2P(Ph)CH_2CH_2PPh_2)$ (0.5 mM, black line), $Fe_2(\mu\text{-adt})(CO)_3(\mu,\eta^2\text{-}Ph_2PCH_2CH_2P(Ph)CH_2CH_2PPh_2)$ (0.5 mM, red line), and $Fe_2(\mu\text{-}(SMe)_2)(CO)_3(\mu,\eta^2\text{-}Ph_2PCH_2CH_2P(Ph)CH_2CH_2PPh_2)$ (0.5 mM, green line) in DCM-$[NBu_4][ClO_4]$ (v=0.1 Vs^{-1}, glassy carbon electrode; V vs Fc^+/Fc)

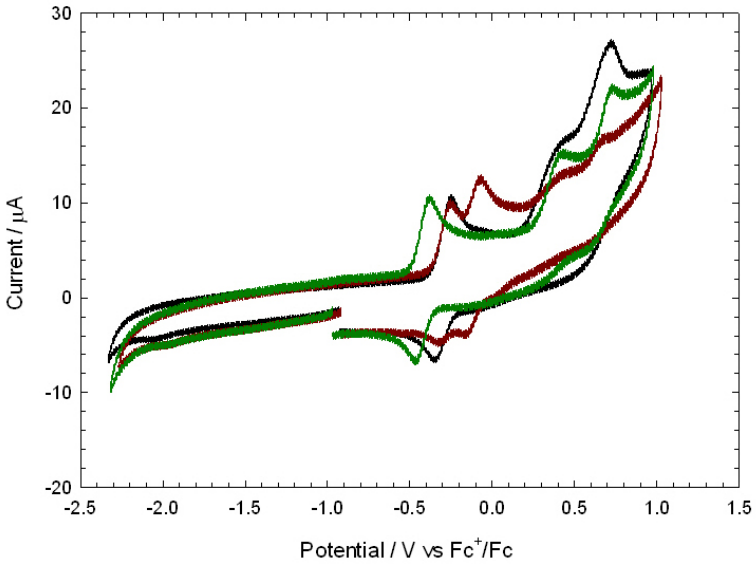

Figure 93: Cyclic voltammetry of $Fe_2(\mu\text{-pdt})(CO)_3(\mu,\eta^2\text{-}Ph_2PCH_2CH_2P(Ph)CH_2CH_2PPh_2)$ (0.5 mM, black line), $Fe_2(\mu\text{-adt})(CO)_3(\mu,\eta^2\text{-}Ph_2PCH_2CH_2P(Ph)CH_2CH_2PPh_2)$ (0.5 mM, red line), and $Fe_2(\mu\text{-}(SMe)_2)(CO)_3(\mu,\eta^2\text{-}Ph_2PCH_2CH_2P(Ph)CH_2CH_2PPh_2)$ (0.5 mM, green line) in DCM-$[NBu_4][BF_4]$ (v=0.1 Vs^{-1}, glassy carbon electrode; V vs Fc^+/Fc)

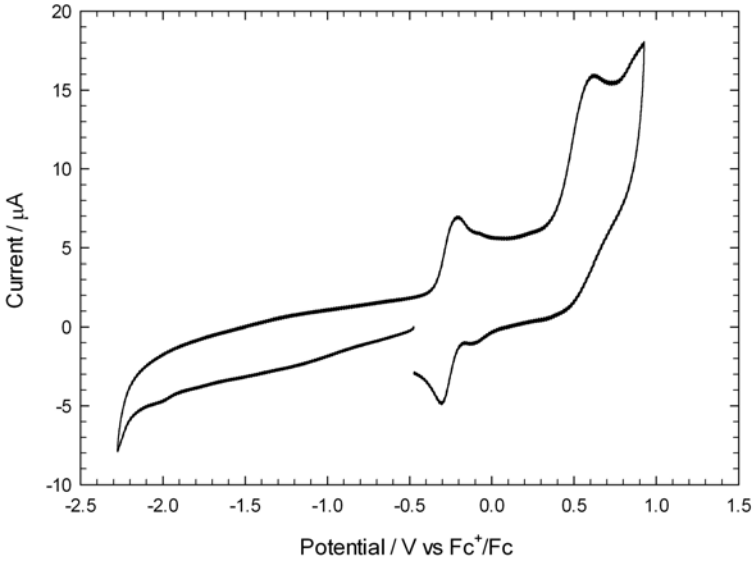

Figure 94: Cyclic voltammetry of $Fe_2(\mu\text{-edt})(CO)_3(\mu,\eta^2\text{-}Ph_2PCH_2CH_2P(Ph)CH_2CH_2PPh_2)$ (0.25 mM) in DCM-$[NBu_4][ClO_4]$ (v=0.1 Vs^{-1}, glassy carbon electrode; V vs Fc^+/Fc)

4.7 Electrochemistry of the singly protonated pdt complex $[Fe_2(\mu\text{-pdt})(CO)_3(\mu,\eta^2\text{-}Ph_2P\text{-}CH_2CH_2P(Ph)CH_2CH_2PPh_2)(\mu\text{-H})]^+$ in the absence of protons in DCM

Hogarth and co-workers reported a stable bridging hydride product after the addition of $HBF_4.Et_2O$ to the pdt-bridged complex[35]. Before moving onto proton reduction catalysis experiments, the singly protonated pdt-bridged complex has been synthesised and analysed electrochemically. The intention was to assess what the oxidation and reduction potentials would be for the protonated species. The method reported by Hogarth was reproduced to synthesise the protonated complex.

Figure 95 (black line) gives the CV of the bridging hydride complex. The first oxidation potential has been shifted by 1.1 V to more positive potentials, compared to the unprotonated complex. This is expected from previous studies which have found that formation of a hydride leads to a shift in potentials of approximately 1 V, due to the Fe centres donating electron density to the hydride. As the peak height is similar to the neutral complex, the oxidation is assumed to be consist a 1-electron transfer. The oxidation process was found to be reversible over a range of scan rates.

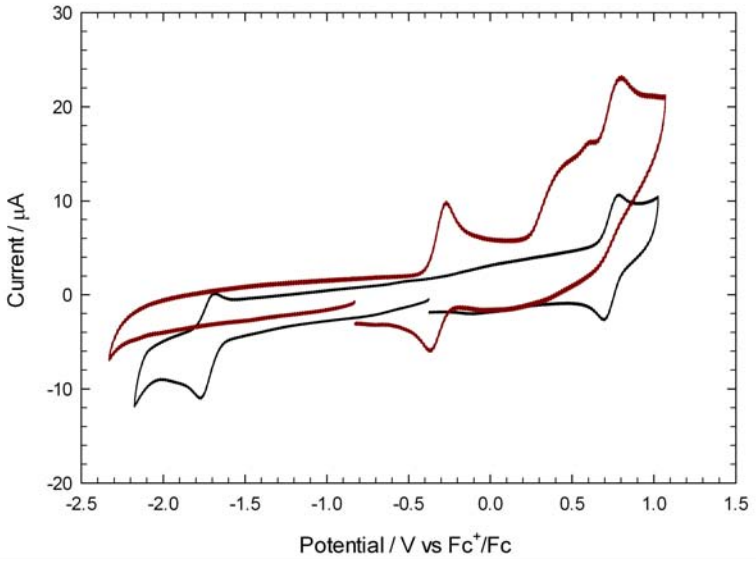

Figure 95: Cyclic voltammetry of $Fe_2(\mu\text{-pdt})(CO)_3(\mu,\eta^2\text{-}Ph_2PCH_2CH_2P(Ph)CH_2CH_2PPh_2)H^+$ (black line, 0.5 mM) and $Fe_2(\mu\text{-pdt})(CO)_3(\mu,\eta^2\text{-}Ph_2PCH_2CH_2P(Ph)CH_2CH_2PPh_2)$ (red line, 0.5 mM) in DCM-$[NBu_4][PF_6]$ (v=0.1 Vs^{-1}, glassy carbon electrode; V vs Fc^+/Fc)

The first reduction of the protonated species can be seen at -1.78 V. As with the oxidation process, this reduction process is reversible, and the peak height suggests it is a 1-electron process. The behaviour was stable over time, suggesting that the protonated complex is stable under an Ar atmosphere.

If the complex is found to be catalytic after the reduction of the protonated complex (resulting in an CECE catalytic mechanism) the positive shift in the reduction potential will imply that the overpotential is better than if catalysis did not occur until after the first reduction (an ECEC

mechanism). However, even the -1.78 V is not a particularly good overpotential compared to other complexes reported in the literature and this dissertation. However, it is possible that the increased basicity compared to these complexes will lead to faster protonation, and thus a faster catalytic turnover, which warrants the investigations presented in the following sections.

Interestingly, the reduction and oxidation processes are both reversible, implying that, on CV timescale, the protonated complex is stable in the 0, +1 and +2 oxidation states.

4.8 Testing for electrocatalytic reduction of protons by $Fe_2(\mu\text{-pdt})(CO)_3(\mu,\eta^2\text{-}Ph_2PCH_2CH_2\text{-}P(Ph)CH_2CH_2PPh_2)$, using the strong acid $HBF_4.Et_2O$ as the proton source

Following on from the analysis of the triphos complexes in the absence of protons, experiments were carried out in the presence of a proton source to analyse whether the complexes are electrocatalysts for proton reduction. The catalytic activity of the complexes was probed by adding $HBF_4.Et_2O$ to the neutral complex in incremental steps. Again a range of electrolyte solutions have been used to probe their influence on the electrocatalytic behaviours of the complexes.

4.8.1 Testing for electrocatalytic reduction of protons by $Fe_2(\mu\text{-pdt})(CO)_3(\mu,\eta^2\text{-}Ph_2P\text{-}CH_2CH_2P(Ph)CH_2CH_2PPh_2)$, using the strong acid $HBF_4.Et_2O$ as the proton source, in DCM-$[NBu_4][PF_6]$

Figure 96 shows the CVs of $Fe_2(\mu\text{-pdt})(CO)_3(\mu,\eta^2\text{-}Ph_2P\text{-}CH_2CH_2P(Ph)CH_2CH_2PPh_2)$ in DCM-$[NBu_4][PF_6]$ after the addition of up to 10 molar equivalents $HBF_4.Et_2O$. On the first addition of acid a reduction peak appears at -1.78 V. This is at the same potential as the singly protonated complex undergoes reduction (Figure 95), suggesting the complex is partially protonated. The first oxidation peak of the complex has diminished, again suggesting the complex is protonating. The oxidation peak of the protonated complex has appeared at 0.79 V.

The complex was not entirely protonated at this stage, as the peaks for the neutral complex are still present. This is because the calculated volume required for 1 molar equivalent acid does not contain 1 molar equivalent $HBF_4.Et_2O$, as the acid was not from a freshly opened bottle. When the same experiment was performed with a fresh bottle of acid, the complex was fully protonated after the addition of 1 molar equivalent acid. The acid used throughout this chapter was of comparable concentration (i.e. from a bottle of a similar age), so comparisons between the complexes are valid.

On further additions of acid the reduction peak of the protonated complex shifted to a potential 0.15 V less negative, and continued to grow with every addition of acid. This indicates that the complex is acting as a catalyst for proton reduction.

4.8.2 Testing for electrocatalytic reduction of protons by $Fe_2(\mu\text{-pdt})(CO)_3(\mu,\eta^2\text{-}Ph_2P\text{-}CH_2CH_2P(Ph)CH_2CH_2PPh_2)$, using the strong acid $HBF_4.Et_2O$ as the proton source, in DCM-$[NBu_4][ClO_4]$

As with the investigation of the complexes in the absence of protons, a range of electrolyte solutions have been used to assess their influence on catalytic behaviour. Figure 97 shows CVs of the pdt-bridged complex after addition of up to 10 equivalents $HBF_4.Et_2O$ in DCM-$[NBu_4][ClO_4]$. On the first addition of acid two reduction peaks appeared at -1.59 and -1.76 V. The first and second oxidation peaks of the neutral complex had diminished slightly. The third oxidation peak grew

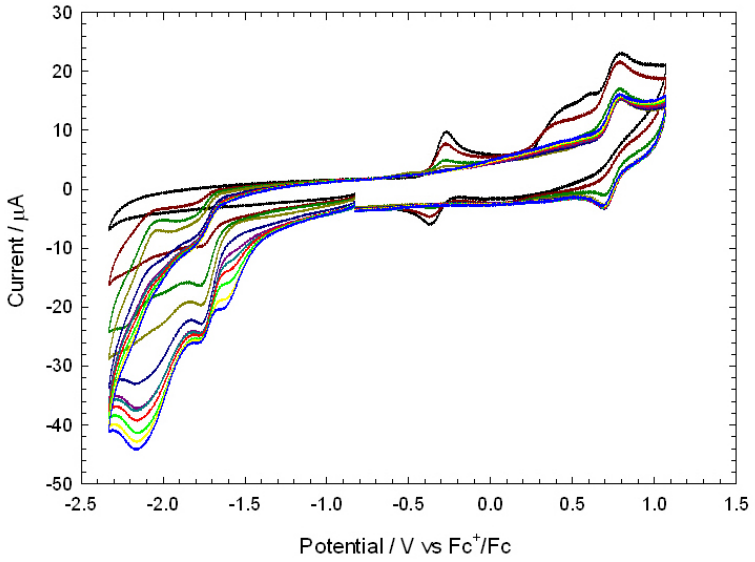

Figure 96: Cyclic voltammetry of $Fe_2(\mu\text{-pdt})(CO)_3(\mu,\eta^2\text{-}Ph_2PCH_2CH_2P(Ph)CH_2CH_2PPh_2)$ (0.5 mM) in DCM-$[NBu_4][PF_6]$ in the absence of acid and in the presence of up to 10 molar equivalents $HBF_4.Et_2O$ in steps of 1 molar equivalent (v=0.1 Vs^{-1}, glassy carbon electrode; V vs Fc^+/Fc)

slightly, presumably due to formation of the protonated complex which is oxidised at this potential.

On further additions of acid the oxidation behaviour becomes that of the fully protonated complex. Also the reduction peaks that appeared after the first addition continued to grow, indicative of catalysis. After the addition of 7 molar equivalents the CVs exhibit a cross-over in the cathodic region, which implies a species is generated at low potentials which remains catalytic on the return scan. A possible identity of this species is the doubly reduced and doubly protonated complex $Fe_2(\mu\text{-pdt})(CO)_3(\mu,\eta^2\text{-}Ph_2PCH_2CH_2P(Ph)CH_2CH_2PPh_2)\text{-}H_2$, which would be expected to be reduced at the potential of the cross-over. If so, this would suggest release of H_2 from the complex could be the rate limiting step of the catalytic mechanism.

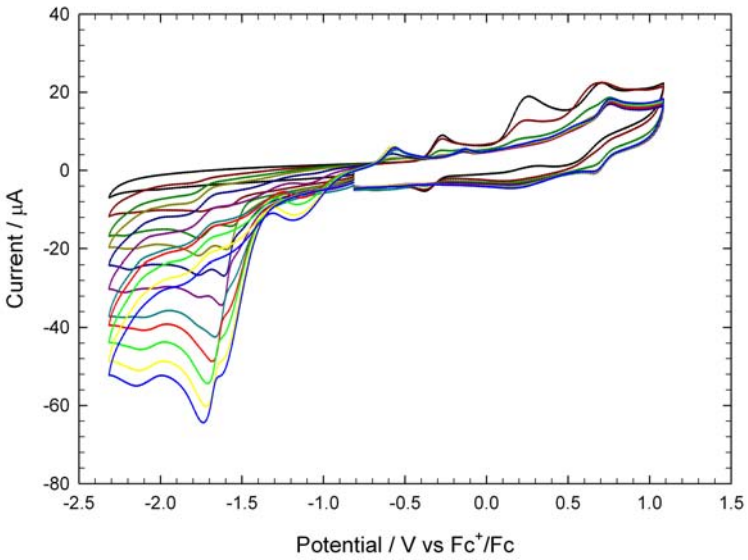

Figure 97: Cyclic voltammetry of $Fe_2(\mu\text{-pdt})(CO)_3(\mu,\eta^2\text{-}Ph_2PCH_2CH_2P(Ph)CH_2CH_2PPh_2)$ (0.5 mM) in DCM-$[NBu_4][ClO_4]$ in the absence of acid and in the presence of up to 10 molar equivalents $HBF_4.Et_2O$ in steps of 1 molar equivalent (v=0.1 Vs^{-1}, glassy carbon electrode; V vs Fc^+/Fc)

4.8.3 Testing for electrocatalytic reduction of protons by $Fe_2(\mu\text{-pdt})(CO)_3(\mu,\eta^2\text{-}Ph_2P\text{-}CH_2CH_2P(Ph)CH_2CH_2PPh_2)$, using the strong acid $HBF_4.Et_2O$ as the proton source, in DCM-$[NBu_4][BF_4]$

The pdt-bridged complex has also been investigated in a DCM-$[NBu_4][BF_4]$ electrolyte solution. The CVs of these investigations are shown in Figure 98. On each addition of acid a peak grows at -1.7 V, which indicates a catalytic mechanism occurs at this potential. The first oxidation of the neutral complex also diminishes, while the first oxidation of the protonated complex grows.

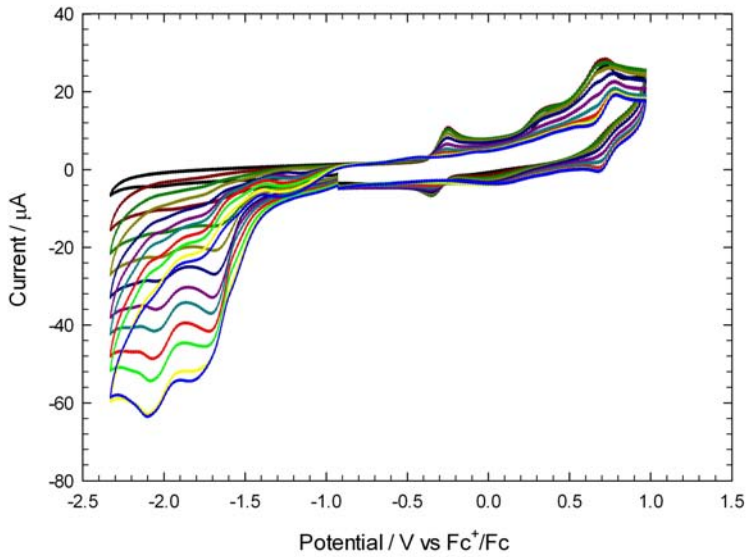

Figure 98: Cyclic voltammetry of $Fe_2(\mu\text{-pdt})(CO)_3(\mu,\eta^2\text{-}Ph_2PCH_2CH_2P(Ph)CH_2CH_2PPh_2)$ (0.5 mM) in DCM-$[NBu_4][BF_4]$ in the absence of acid and in the presence of up to 10 molar equivalents $HBF_4.Et_2O$ in steps of 1 molar equivalent (v=0.1 Vs^{-1}, glassy carbon electrode; V vs Fc^+/Fc)

4.8.4 Testing for electrocatalytic reduction of protons by $Fe_2(\mu\text{-pdt})(CO)_3(\mu,\eta^2\text{-}Ph_2P\text{-}CH_2CH_2P(Ph)CH_2CH_2PPh_2)$, using the strong acid $HBF_4.Et_2O$ as the proton source, in MeCN-$[NBu_4][PF_6]$

The pdt-bridged complex has also been investigated in the coordinating solvent MeCN. The CVs on the addition of up to 10 equivalents $HBF_4.Et_2O$ are shown in Figure 99. On each addition of acid reduction peaks grow at -1.5, -1.7 and -1.8 V, indicative of catalytic mechanisms at these potentials. The results indicate that the overpotential required for catalysis is lower in MeCN than in DCM.

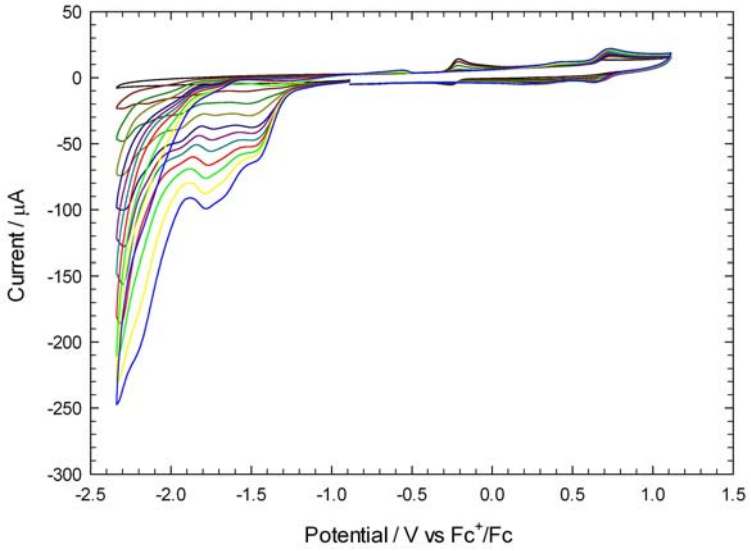

Figure 99: Cyclic voltammetry of $Fe_2(\mu\text{-pdt})(CO)_3(\mu,\eta^2\text{-}Ph_2PCH_2CH_2P(Ph)CH_2CH_2PPh_2)$ (0.5 mM) in MeCN-$[NBu_4][PF_6]$ in the absence of acid and in the presence of up to 10 molar equivalents $HBF_4.Et_2O$ in steps of 1 molar equivalent (v=0.1 Vs^{-1}, glassy carbon electrode; V vs Fc^+/Fc)

4.8.5 Summary and discussion

The pdt-bridged complex has been found to be catalytic in the presence of $HBF_4.Et_2O$. A comparison of the pdt-bridged triphos-ligand complex and pdt-bridged hexacarbonyl complex in the presence of $HBF_4.Et_2O$ is presented in Figure 100. Inclusion of the triphos-ligand into the molecular structure has resulted in a 0.1 V improvement in the overpotential required for catalysis. However, the rate of catalysis (indicated by the peak current) is significantly higher for the hexacarbonyl complex. It is evident from this comparison that there is a balance to be made when using ligands to increase electron density on the Fe centres between susceptibility to protonation and the reduction potential of the complex. In the present case, the increased electron density on the triphos-ligand complex resulted in its first reduction being at a very negative potential, however, it meant that the complex could protonate, and the reduction of the protonated complex was at a lower overpotential than the hexacarbonyl analogue.

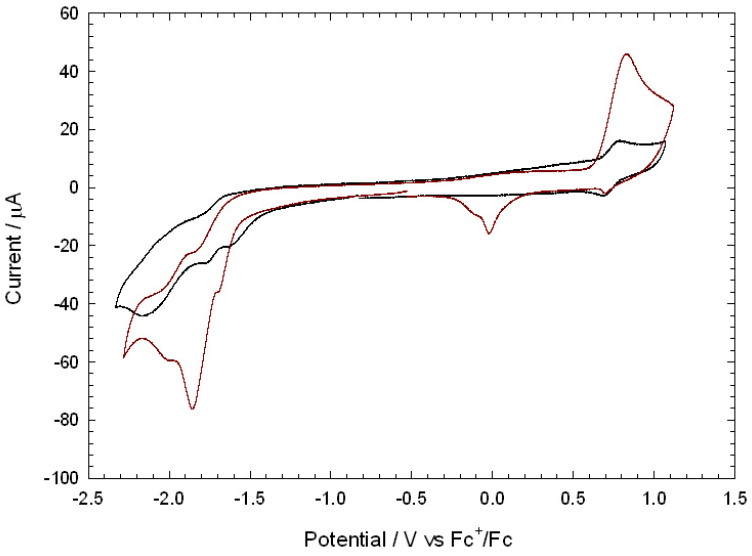

Figure 100: Cyclic voltammetry of $Fe_2(\mu\text{-pdt})(CO)_3(\mu,\eta^2\text{-}Ph_2PCH_2CH_2P(Ph)CH_2CH_2PPh_2)$ (0.5 mM, black line) and $Fe_2(\mu\text{-pdt})(CO)_6$ (0.5 mM, red line) in the presence of 10 molar equivalents $HBF_4.Et_2O$ in DCM-$[NBu_4][PF_6]$ (v=0.1 Vs^{-1}, glassy carbon electrode; V vs Fc^+/Fc)

There is a clear influence of the electrolyte on the catalytic activity of the complex, as illustrated in Figure 101 which shows CVs of the pdt-bridged complex in the presence of 10 molar equivalents $HBF_4.Et_2O$ in DCM-$[NBu_4][PF_6]$, DCM-$[NBu_4][ClO_4]$ and DCM-$[NBu_4][BF_4]$. The catalytic current is three times larger in DCM-$[NBu_4][ClO_4]$ than DCM-$[NBu_4][PF_6]$. The reason for this improvement in the rate of catalysis due to the electrolyte is not yet fully understood. Based on these findings, there is an impact when quantitative comparisons between different complexes in the literature are to be made.

The overpotential has been found to be lower, and the catalytic rate higher, in MeCN compared to DCM, as shown in Figure 102. This is likely due to the fact that the protons can associate with the MeCN ($MeCNH^+$), as opposed to just Et_2O (Et_2OH^+) in DCM.

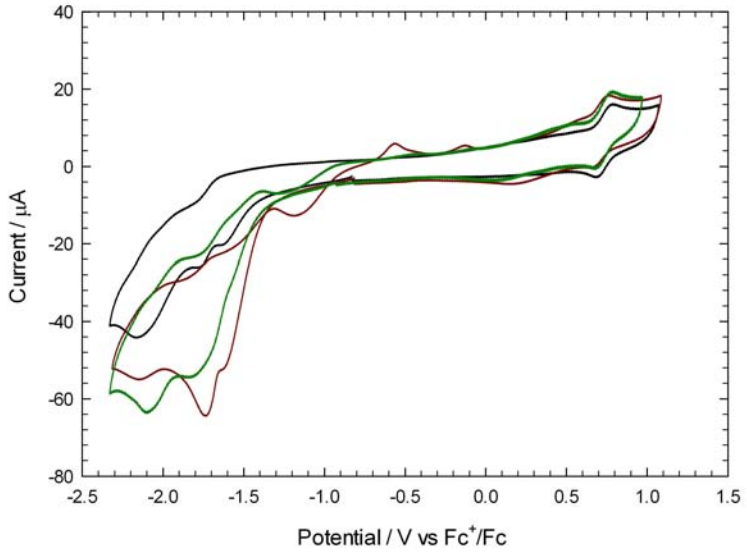

Figure 101: Cyclic voltammetry of $Fe_2(\mu\text{-pdt})(CO)_3(\mu,\eta^2\text{-}Ph_2PCH_2CH_2P(Ph)CH_2CH_2PPh_2)$ (0.5 mM) in DCM-$[NBu_4][PF_6]$ (black line), DCM-$[NBu_4][ClO_4]$ (red line) and DCM-$[NBu_4][BF_4]$ (green line) in the presence of 10 molar equivalents $HBF_4.Et_2O$ (v=0.1 Vs^{-1}, glassy carbon electrode; V vs Fc^+/Fc)

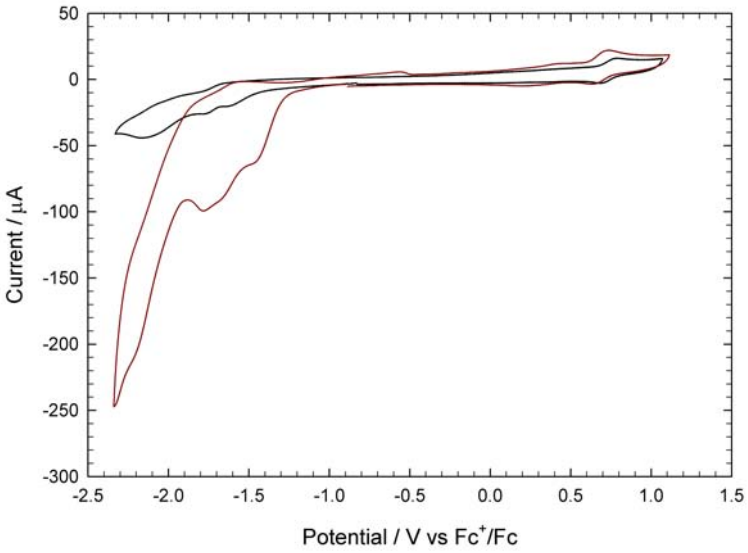

Figure 102: Cyclic voltammetry of $Fe_2(\mu\text{-pdt})(CO)_3(\mu,\eta^2\text{-}Ph_2PCH_2CH_2P(Ph)CH_2CH_2PPh_2)$ (0.5 mM) in DCM-$[NBu_4][PF_6]$ (black line) and MeCN-$[NBu_4][PF_6]$ (red line) in the presence of 10 molar equivalents $HBF_4.Et_2O$ (v=0.1 Vs^{-1}, glassy carbon electrode; V vs Fc^+/Fc)

4.9 Testing for electrocatalytic reduction of protons by $Fe_2(\mu\text{-adt})(CO)_3(\mu,\eta^2\text{-}Ph_2PCH_2CH_2P(Ph)CH_2\text{-}CH_2PPh_2)$, using the strong acid $HBF_4.Et_2O$ as the proton source

Following on from the pdt-bridged complex, the adt-bridged complex has been analysed for electrocatalytic reduction of protons, again using $HBF_4.Et_2O$ as the proton source. To further investigate the influence of electrolyte on the electrocatalytic behaviour, the same range of electrolyte solutions have been used.

4.9.1 Testing for electrocatalytic reduction of protons by $Fe_2(\mu\text{-adt})(CO)_3(\mu,\eta^2\text{-}Ph_2P\text{-}CH_2CH_2P(Ph)CH_2CH_2PPh_2)$, using the strong acid $HBF_4.Et_2O$ as the proton source, in DCM-$[NBu_4][PF_6]$

The CVs of the adt-bridged complex after the addition of up to 10 molar equivalents $HBF_4.Et_2O$ are shown in Figure 103. After addition of one equivalent of acid the first oxidation of the complex moved to 0.1 V, a positive shift of 0.5 V. A second oxidation feature is observed at 0.7 V. On further additions of acid this oxidation peak is unchanged, however a reduction peak grows at -1.8 V. This indicates that a catalytic mechanism occurs at this potential.

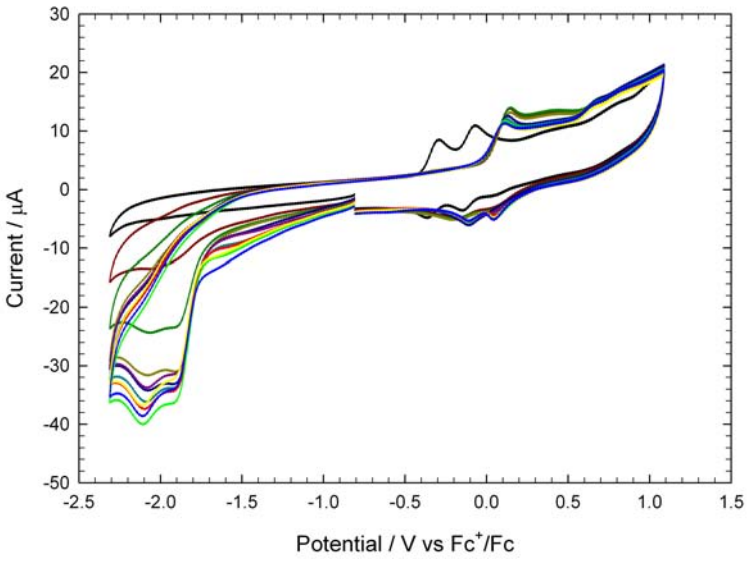

Figure 103: Cyclic voltammetry of $Fe_2(\mu\text{-adt})(CO)_3(\mu,\eta^2\text{-}Ph_2PCH_2CH_2P(Ph)CH_2CH_2PPh_2)$ (0.5 mM) in DCM-$[NBu_4][PF_6]$ in the absence of acid and in the presence of up to 10 molar equivalents $HBF_4.Et_2O$ in steps of 1 molar equivalent (v=0.1 Vs^{-1}, glassy carbon electrode; V vs Fc^+/Fc)

The smaller shift in the oxidation potential (+0.5 V) compared to the pdt-bridged complex (+1.1 V) suggests that the complex has only protonated at the N of the bridge, and not at the Fe centres - a protonation at the Fe centres would result in more electron density being withdrawn from the Fe centres in order to form the hydride bond. Similarly, the reduction peak is at a more negative potential than that seen for protonation at the Fe centres. Interestingly, the IR experiments detailed

in Section 4.2.2 indicated that the complex does protonate at the Fe centres. Indeed, it shall be seen below that the complex does protonate at the Fe centres in the presence of other electrolytes. Thus, the DCM-[NBu_4][PF_6] is clearly playing a role in the protonation behaviour of the complex in solution.

4.9.2 Testing for electrocatalytic reduction of protons by $Fe_2(\mu\text{-adt})(CO)_3(\mu,\eta^2\text{-}Ph_2P\text{-}CH_2CH_2P(Ph)CH_2CH_2PPh_2)$, using the strong acid $HBF_4.Et_2O$ as the proton source, in DCM-[NBu_4][ClO_4]

The above experiment has also been performed in DCM-[NBu_4][ClO_4] (Figure 104). On the first addition of $HBF_4.Et_2O$, small reduction features appear, which on further additions of acid grow into peaks at -1.56, -1.6, and -2.0 V. The first oxidation shifts to 0.06 V, with a second oxidation process at 0.65 V.

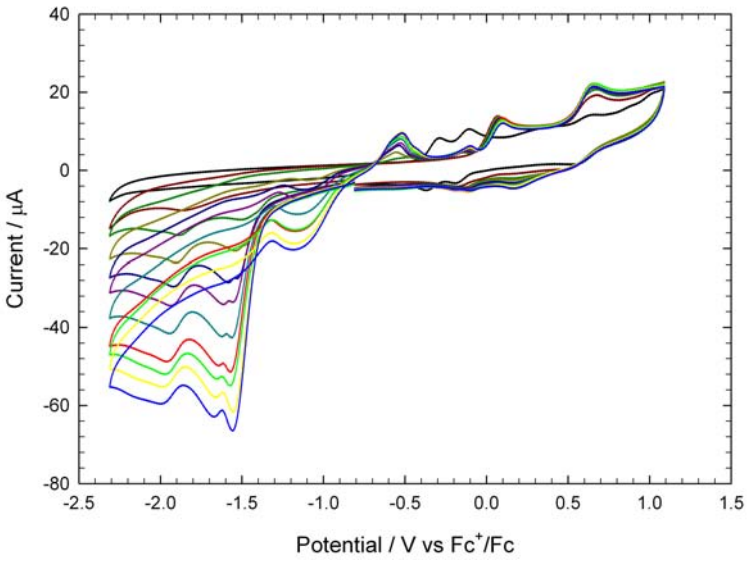

Figure 104: Cyclic voltammetry of $Fe_2(\mu\text{-adt})(CO)_3(\mu,\eta^2\text{-}Ph_2PCH_2CH_2P(Ph)CH_2CH_2PPh_2)$ (0.5 mM) in DCM-[NBu_4][ClO_4] in the absence of acid and in the presence of up to 10 molar equivalents $HBF_4.Et_2O$ in steps of 1 molar equivalent (v=0.1 Vs^{-1}, glassy carbon electrode; V vs Fc^+/Fc)

Interestingly, the oxidation peak is at the potential expected for protonation at the N of the bridge, however the reduction peak is at the potential expected for protonation at the Fe centres. This slightly confusing result could be explained if the proton is moving rapidly between the N in the bridge and the Fe centres. On scanning to positive potentials, the complex is oxidised when the proton is on the N protonation site, i.e. at the lower oxidation potential, and the oxidation peak at the higher potential is not observed as the FeFe protonated complex is not present by this point as the protonated complex has been oxidised. On scanning to negative potentials the FeFe protonation is seen, as this is the first reduction process, and the N protonation is not seen as the complex is gone by that point in the CV. However, further evidence using techniques such as variable temperature

NMR spectroscopy would be required before this explanation could be assumed.

4.9.3 Testing for electrocatalytic reduction of protons by $Fe_2(\mu\text{-adt})(CO)_3(\mu,\eta^2\text{-}Ph_2PCH_2CH_2P(Ph)CH_2CH_2PPh_2)$, using the strong acid $HBF_4.Et_2O$ as the proton source, in DCM-$[NBu_4][BF_4]$

The adt-bridged complex has also been tested as an electrocatalyst in DCM-$[NBu_4][BF_4]$ (Figure 105). On each addition of acid a reduction peak at -1.60 V grew, indicating the complex to be catalytic at this potential. This catalytic reduction peak was followed by a second reduction peak at -1.69 V, and a third at -1.91 V. The first oxidation peak of the neutral complex diminished entirely upon addition of 1 molar equivalent acid, with a new peak appearing at 0.10 V.

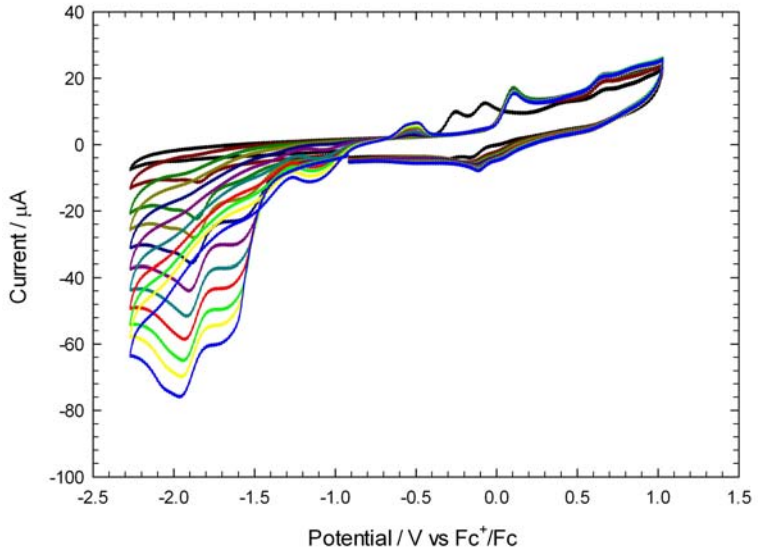

Figure 105: Cyclic voltammetry of $Fe_2(\mu\text{-adt})(CO)_3(\mu,\eta^2\text{-}Ph_2PCH_2CH_2P(Ph)CH_2CH_2PPh_2)$ (0.5 mM) in DCM-$[NBu_4][BF_4]$ in the absence of acid and in the presence of up to 10 molar equivalents $HBF_4.Et_2O$ in steps of 1 molar equivalent (v=0.1 Vs^{-1}, glassy carbon electrode; V vs Fc^+/Fc)

4.9.4 Testing for electrocatalytic reduction of protons by $Fe_2(\mu\text{-adt})(CO)_3(\mu,\eta^2\text{-}Ph_2PCH_2CH_2P(Ph)CH_2CH_2PPh_2)$, using the strong acid $HBF_4.Et_2O$ as the proton source, in MeCN-$[NBu_4][PF_6]$

The CVs of the adt-bridged complex in the presence of $HBF_4.Et_2O$ in MeCN are shown in Figure 106. The behaviour appears to be a combination of those seen in DCM-$[NBu_4][PF_6]$ and DCM-$[NBu_4][ClO_4]$. The first reduction peak is significantly broader than that in DCM-$[NBu_4][ClO_4]$, which could be down to the proton moving more slowly between the N in the bridge and the Fe centres, thus slowing down the catalytic mechanism.

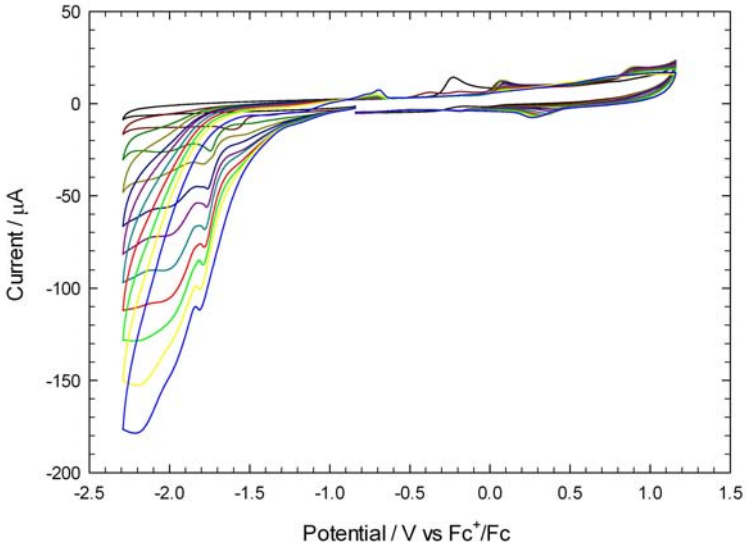

Figure 106: Cyclic voltammetry of $Fe_2(\mu\text{-adt})(CO)_3(\mu,\eta^2\text{-}Ph_2PCH_2CH_2P(Ph)CH_2CH_2PPh_2)$ (0.5 mM) in MeCN-$[NBu_4][PF_6]$ in the absence of acid and in the presence of up to 10 molar equivalents $HBF_4.Et_2O$ in steps of 1 molar equivalent (v=0.1 Vs^{-1}, glassy carbon electrode; V vs Fc^+/Fc)

4.9.5 Summary and discussion

There is a significant difference in catalytic activity based on the choice of electrolyte, as indicated in Figure 107, which shows CVs of the adt-bridged complex in the presence of 10 molar equivalents $HBF_4.Et_2O$ in DCM-$[NBu_4][PF_6]$, DCM-$[NBu_4][ClO_4]$ and DCM-$[NBu_4][BF_4]$. The most significant finding is that the complex appears to be protonated at the Fe centres in the presence of $HBF_4.Et_2O$ in DCM-$[NBu_4][ClO_4]$ and DCM-$[NBu_4][BF_4]$, but not in DCM-$[NBu_4][PF_6]$. The reason for the electrolyte to influence the protonation behaviour so markedly has yet to be conclusively determined.

As with the pdt-bridged complex, the adt-bridged complex exhibited a higher catalytic rate in MeCN compared to DCM. The same explanation as was given for the pdt-bridged complex, is assumed to be the case here also; i.e. protons are able to associate with the MeCN solvent.

A comparison of the pdt- and adt-bridged complexes shall be given in Section 4.10.5.

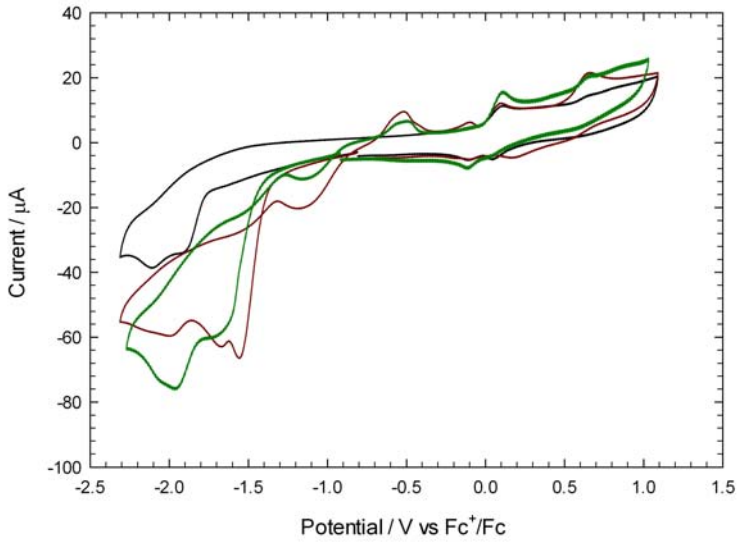

Figure 107: Cyclic voltammetry of $Fe_2(\mu\text{-adt})(CO)_3(\mu,\eta^2\text{-}Ph_2PCH_2CH_2P(Ph)CH_2CH_2PPh_2)$ (0.5 mM) in DCM-$[NBu_4][PF_6]$ (black line), DCM-$[NBu_4][ClO_4]$ (red line) and DCM-$[NBu_4][BF_4]$ (green line) in the presence of 10 molar equivalents $HBF_4.Et_2O$ (v=0.1 Vs^{-1}, glassy carbon electrode; V vs Fc^+/Fc)

4.10 Testing for electrocatalytic reduction of protons by $Fe_2(\mu\text{-}(SMe)_2)(CO)_3(\mu,\eta^2\text{-}Ph_2P\text{-}CH_2CH_2P(Ph)CH_2CH_2PPh_2)$, using the strong acid $HBF_4.Et_2O$ as the proton source

Following on the from the pdt- and adt-bridged complexes, the $(SMe)_2$-bridged complex has been tested for electrocatalytic reduction of protons using $HBF_4.Et_2O$ as the proton source.

4.10.1 Testing for electrocatalytic reduction of protons by $Fe_2(\mu\text{-}(SMe)_2)(CO)_3(\mu,\eta^2\text{-}Ph_2PCH_2CH_2P(Ph)CH_2CH_2PPh_2)$, using the strong acid $HBF_4.Et_2O$ as the proton source, in DCM-$[NBu_4][PF_6]$

The CVs obtained after subsequent additions of $HBF_4.Et_2O$ to the $(SMe)_2$-bridged complex in DCM-$[NBu_4][PF_6]$ are shown in Figure 108. On additions of $HBF_4.Et_2O$ a reduction peak grows at -1.50 V. Two further reduction processes occur at more negative potentials. The first and second oxidations of the neutral complex diminish, while a peak at 0.69 V appears. These results indicate that the complex is protonating in the presence of $HBF_4.Et_2O$. However, any catalytic mechanism which may be happening is slow.

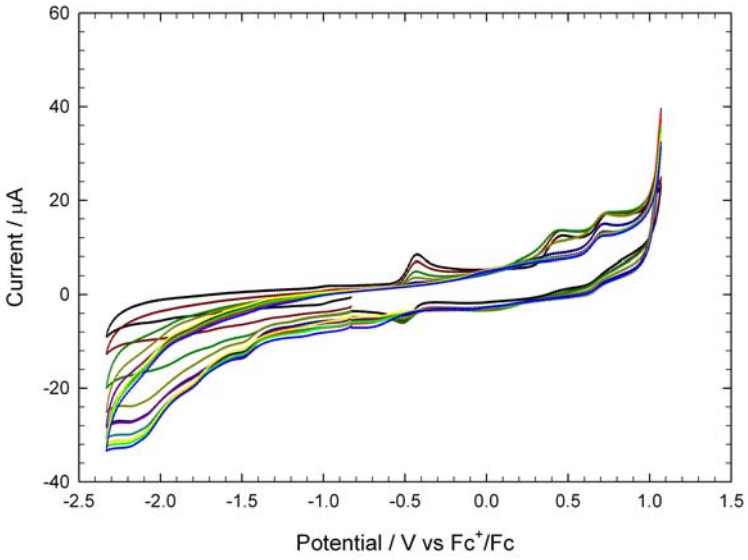

Figure 108: Cyclic voltammetry of $Fe_2(\mu\text{-}(SMe)_2)(CO)_3(\mu,\eta^2\text{-}Ph_2PCH_2CH_2P(Ph)CH_2CH_2PPh_2)$ (0.5 mM) in DCM-$[NBu_4][PF_6]$ in the absence of acid and in the presence of up to 10 molar equivalents $HBF_4.Et_2O$ in steps of 1 molar equivalent (v=0.1 Vs^{-1}, glassy carbon electrode; V vs Fc^+/Fc)

4.10.2 Testing for electrocatalytic reduction of protons by $Fe_2(\mu\text{-}(SMe)_2)(CO)_3(\mu,\eta^2\text{-}Ph_2PCH_2CH_2P(Ph)CH_2CH_2PPh_2)$, using the strong acid $HBF_4.Et_2O$ as the proton source, in DCM-$[NBu_4][ClO_4]$

The above experiment has been repeated in DCM-$[NBu_4][ClO_4]$, as shown in Figure 109. On each addition of acid a reduction peak grows at ca. -1.5 V. A second reduction process follows immediately.

A third process is seen at -2.12 V. The CVs suggest that the first oxidation peak (ca. -0.4 V) remains stable on additions of acid, however this is not the case, as, with acid present, this oxidation peak was only present after the electrode had been scanned past the catalytic reduction peak. This implies that a reduction product is generated which is oxidised at nearly the same potential as the neutral complex. This reduction product could indeed be the neutral complex being regenerated by the catalytic process, however, this has not yet been confirmed.

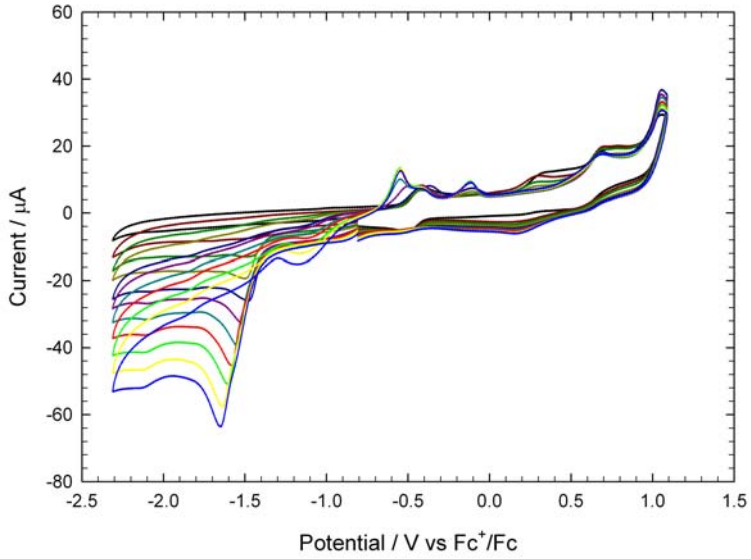

Figure 109: Cyclic voltammetry of $Fe_2(\mu\text{-}(SMe)_2)(CO)_3(\mu,\eta^2\text{-}Ph_2PCH_2CH_2P(Ph)CH_2CH_2PPh_2)$ (0.5 mM) in DCM-$[NBu_4][ClO_4]$ in the absence of acid and in the presence of up to 10 molar equivalents $HBF_4.Et_2O$ in steps of 1 molar equivalent (v=0.1 Vs^{-1}, glassy carbon electrode; V vs Fc^+/Fc)

4.10.3 Testing for electrocatalytic reduction of protons by $Fe_2(\mu\text{-}(SMe)_2)(CO)_3(\mu,\eta^2\text{-}Ph_2PCH_2CH_2P(Ph)CH_2CH_2PPh_2)$, using the strong acid $HBF_4.Et_2O$ as the proton source, in DCM-$[NBu_4][BF_4]$

The $(SMe)_2$-bridged complex has also been tested for electrocatalysis in DCM-$[NBu_4][BF_4]$ (Figure 110). On each addition of $HBF_4.Et_2O$ a reduction peak at -1.5 V grew, and was followed immediately by a reduction process at -1.6 - -1.7 V. These peaks are again indicative of catalysis. As with the CVs taken in DCM-$[NBu_4][ClO_4]$, a species is generated after the electrode has been swept to negative potentials, which is oxidised at close to the potential of the neutral complex. The difference in the oxidation potential suggests this is not the neutral complex generated by the catalytic mechanism, rather a species that coincidentally has a similar oxidation potential to the neutral complex.

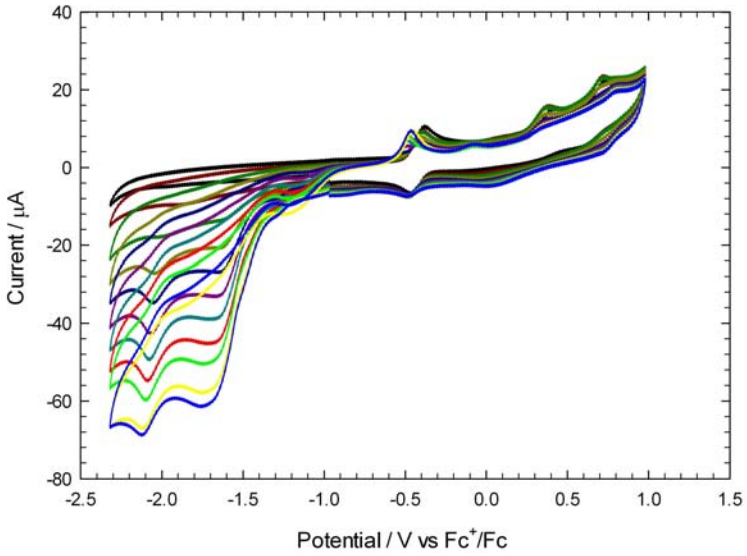

Figure 110: Cyclic voltammetry of $Fe_2(\mu\text{-}(SMe)_2)(CO)_3(\mu,\eta^2\text{-}Ph_2PCH_2CH_2P(Ph)CH_2CH_2PPh_2)$ (0.5 mM) in DCM-$[NBu_4][BF_4]$ in the absence of acid and in the presence of up to 10 molar equivalents $HBF_4.Et_2O$ in steps of 1 molar equivalent (v=0.1 Vs^{-1}, glassy carbon electrode; V vs Fc^+/Fc)

4.10.4 Testing for electrocatalytic reduction of protons by $Fe_2(\mu\text{-}(SMe)_2)(CO)_3(\mu,\eta^2\text{-}Ph_2PCH_2CH_2P(Ph)CH_2CH_2PPh_2)$, using the strong acid $HBF_4.Et_2O$ as the proton source, in MeCN-$[NBu_4][PF_6]$

The complex has also been tested for catalytic activity in MeCN, as shown in Figure 111. The reduction of the complex was at -1.5 V, however this reduction peak reached a limiting current after the addition of 5 molar equivalents acid. A second catalytic process is present at -1.9 V.

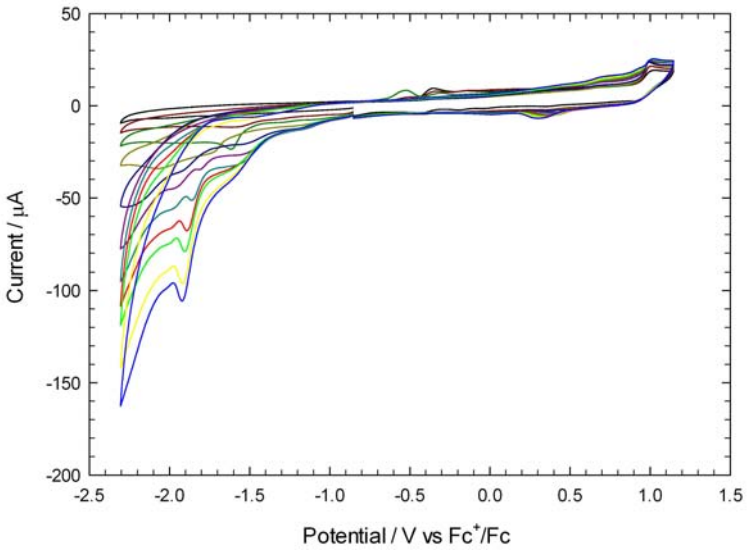

Figure 111: Cyclic voltammetry of $Fe_2(\mu\text{-}(SMe)_2)(CO)_3(\mu,\eta^2\text{-}Ph_2PCH_2CH_2P(Ph)CH_2CH_2PPh_2)$ (0.5 mM) in MeCN-$[NBu_4][PF_6]$ in the absence of acid and in the presence of up to 10 molar equivalents $HBF_4.Et_2O$ in steps of 1 molar equivalent (v=0.1 Vs^{-1}, glassy carbon electrode; V vs Fc^+/Fc)

4.10.5 Summary and discussion

As with the pdt- and adt-bridged complexes, there is a great difference in catalytic activity based on the choice of electrolyte. This is indicated in Figure 112, which shows CVs of the $(SMe)_2$-bridged complex in the presence of 10 molar equivalents $HBF_4.Et_2O$ in DCM-$[NBu_4][PF_6]$, DCM-$[NBu_4][ClO_4]$ and DCM-$[NBu_4][BF_4]$. The rate of catalysis is at least 10 times greater in DCM-$[NBu_4][ClO_4]$ and DCM-$[NBu_4][BF_4]$. Again it is clear is that direct comparisons of catalytic activities of complexes in the literature are not possible unless the electrolyte solutions are identical.

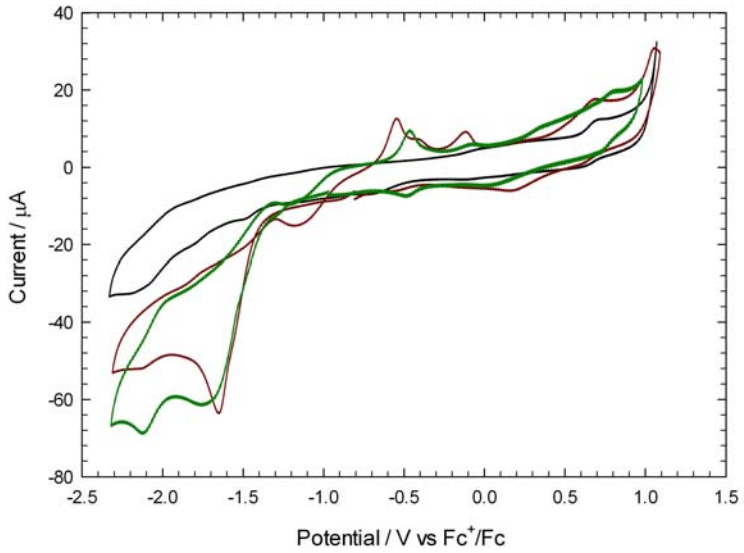

Figure 112: Cyclic voltammetry of $Fe_2(\mu\text{-}(SMe)_2)(CO)_3(\mu,\eta^2\text{-}Ph_2PCH_2CH_2P(Ph)CH_2CH_2PPh_2)$ (0.5 mM) in DCM-$[NBu_4][PF_6]$ (black line), DCM-$[NBu_4][ClO_4]$ (red line) and DCM-$[NBu_4][BF_4]$ (green line) in the presence of 10 molar equivalents $HBF_4.Et_2O$ (v=0.1 Vs^{-1}, glassy carbon electrode; V vs Fc^+/Fc)

All of the CVs required to compare the catalytic activity of the three triphos-ligand complexes are now available, as shown in Figures 113, 114 and 115. The catalytic mechanisms of the three complexes all begin with a protonation step. The following steps are a reduction process, a further protonation and a further reduction; i.e. the mechanisms are CECE processes.

In DCM-$[NBu_4][PF_6]$ the pdt- and $(SMe)_2$-bridged complexes have the lowest overpotential. In DCM-$[NBu_4][ClO_4]$, however, it is the adt-bridged complex which exhibits the lowest overpotential. The reason for this is thought to be that the adt-bridged complex is able to protonate at the Fe centres in this environment, and not in DCM-$[NBu_4][PF_6]$. In DCM-$[NBu_4][BF_4]$ the three complexes have comparable overpotentials, with the adt- and $(SMe)_2$-bridged complexes the lowest.

The overpotential of the triphos-ligand complexes are poor in comparison to many other complexes in the literature. For example, the $(SC_6F_5)_2$-bridged complex analysed in Chapter 3 was catalytic at -1.34 V in DCM-$[NBu_4][PF_6]$, whereas the pdt-bridged triphos-ligand complex is not catalytic until -1.78 V in the same conditions. In general, there is a balance to be made between the electron density that is pushed onto the Fe centres to assist in protonation, and corresponding

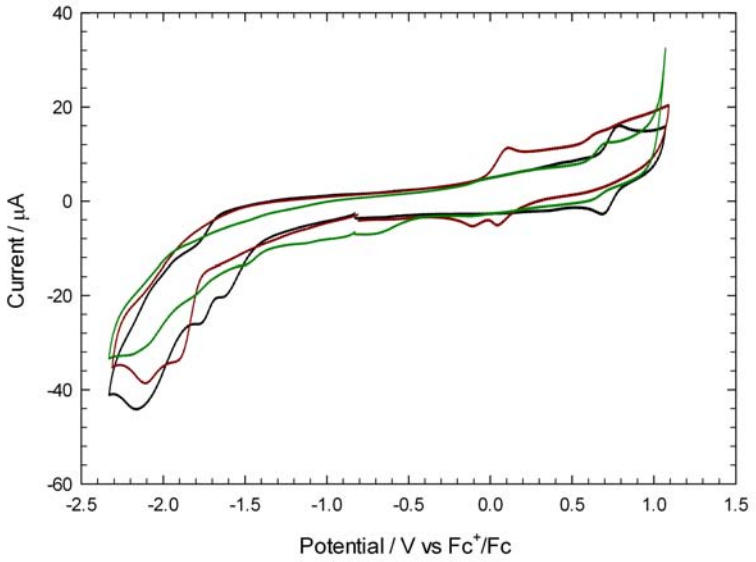

Figure 113: Cyclic voltammetry of $Fe_2(\mu\text{-pdt})(CO)_3(\mu,\eta^2\text{-}Ph_2PCH_2CH_2P(Ph)CH_2CH_2PPh_2)$ (0.5 mM, black line), $Fe_2(\mu\text{-adt})(CO)_3(\mu,\eta^2\text{-}Ph_2PCH_2CH_2P(Ph)CH_2CH_2PPh_2)$ (0.5 mM, red line), and $Fe_2(\mu\text{-}(SMe)_2)(CO)_3(\mu,\eta^2\text{-}Ph_2PCH_2CH_2P(Ph)CH_2CH_2PPh_2)$ (0.5 mM, green line) in the presence of 10 molar equivalent $HBF_4.Et_2O$ in DCM-$[NBu_4][PF_6]$ (v=0.1 Vs^{-1}, glassy carbon electrode; V vs Fc^+/Fc)

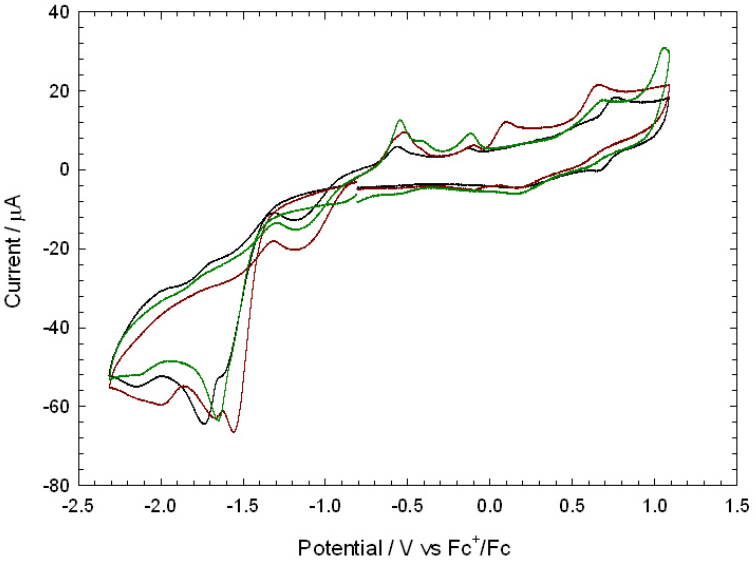

Figure 114: Cyclic voltammetry of $Fe_2(\mu\text{-pdt})(CO)_3(\mu,\eta^2\text{-}Ph_2PCH_2CH_2P(Ph)CH_2CH_2PPh_2)$ (0.5 mM, black line), $Fe_2(\mu\text{-adt})(CO)_3(\mu,\eta^2\text{-}Ph_2PCH_2CH_2P(Ph)CH_2CH_2PPh_2)$ (0.5 mM, red line), and $Fe_2(\mu\text{-}(SMe)_2)(CO)_3(\mu,\eta^2\text{-}Ph_2PCH_2CH_2P(Ph)CH_2CH_2PPh_2)$ (0.5 mM, green line) in the presence of 10 molar equivalent $HBF_4.Et_2O$ in DCM-$[NBu_4][ClO_4]$ (v=0.1 Vs^{-1}, glassy carbon electrode; V vs Fc^+/Fc)

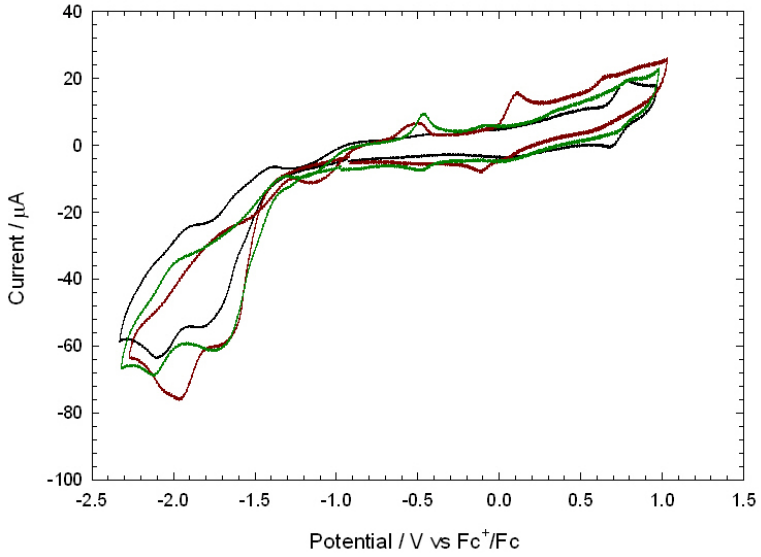

Figure 115: Cyclic voltammetry of $Fe_2(\mu\text{-pdt})(CO)_3(\mu,\eta^2\text{-}Ph_2PCH_2CH_2P(Ph)CH_2CH_2PPh_2)$ (0.5 mM, black line), $Fe_2(\mu\text{-adt})(CO)_3(\mu,\eta^2\text{-}Ph_2PCH_2CH_2P(Ph)CH_2CH_2PPh_2)$ (0.5 mM, red line), and $Fe_2(\mu\text{-}(SMe)_2)(CO)_3(\mu,\eta^2\text{-}Ph_2PCH_2CH_2P(Ph)CH_2CH_2PPh_2)$ (0.5 mM, green line) in the presence of 10 molar equivalent $HBF_4.Et_2O$ in DCM-$[NBu_4][BF_4]$ (v=0.1 Vs^{-1}, glassy carbon electrode; V vs Fc^+/Fc)

reduction potential.

4.11 Extension: Testing for electrocatalytic reduction of protons by $Fe_2(\mu\text{-edt})(CO)_3(\mu,\eta^2\text{-}Ph_2P\text{-}CH_2CH_2P(Ph)CH_2CH_2PPh_2)$, using the strong acid $HBF_4.Et_2O$ as the proton source

Following on the from the pdt-, adt- and $(SMe)_2$-bridged complexes, an initial investigation into the catalytic activity of the edt-bridged complex has been made in DCM-$[NBu_4][ClO_4]$ using $HBF_4.Et_2O$ as the proton source. The CVs obtained after the addition of 6 molar equivalents $HBF_4.Et_2O$ to the complex are shown in Figure 116. The complex is protonated by $HBF_4.Et_2O$, as the oxidation peak of the neutral complex at -0.21 V is diminished on adding the acid. On each addition of acid the reduction peak of the protonated complex grows, indicating a catalytic reaction.

The behaviour of the complex in the presence of protons indicates that a catalytic process is observed at ca. -1.5 V. The catalytic mechanism is initiated by a protonation of the neutral complex; the protonated species is then reduced, protonated and reduced again (an CECE process). Compared to the triphos-ligand complexes presented in this chapter, the edt-bridged complex has a very similar overpotential for proton reduction catalysis. Thus a constrained bridge has not significantly altered the overpotential of the complex. A fair comparison of the turnover frequency (rate of catalysis) is not possible from these CVs due to the different concentrations of acid used. This should be analysed in a future study.

Based on the findings in this chapter, it is expected that using a range of electrolyte solvents would

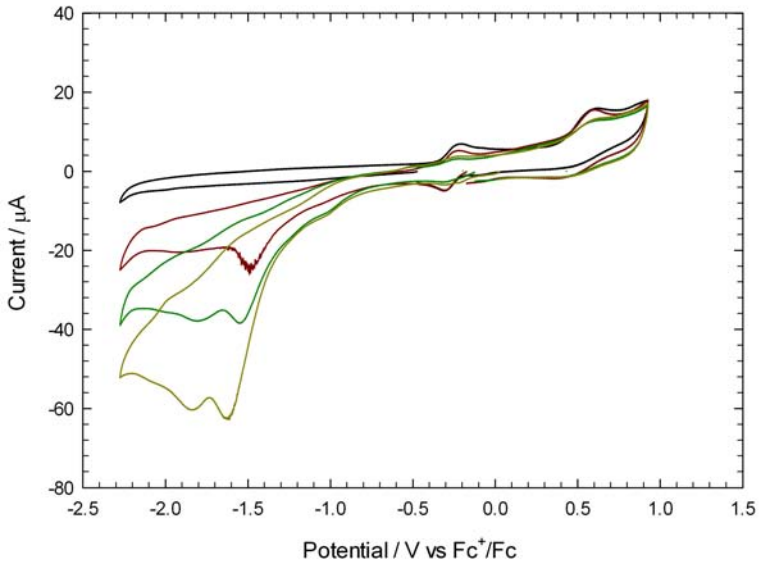

Figure 116: Cyclic voltammetry of $Fe_2(\mu\text{-edt})(CO)_3(\mu,\eta^2\text{-}Ph_2PCH_2CH_2P(Ph)CH_2CH_2PPh_2)$ (0.5 mM) in DCM-$[NBu_4][ClO_4]$ in the absence of acid and in the presence of up to 6 molar equivalents $HBF_4.Et_2O$ in steps of 2 molar equivalents (v=0.1 Vs^{-1}, glassy carbon electrode; V vs Fc^+/Fc)

again have an influence on the electrocatalytic behaviour of the edt-bridged complex. For example, the rate of catalysis would be expected to be greater in DCM-$[NBu_4][ClO_4]$ and DCM-$[NBu_4][BF_4]$, than in DCM-$[NBu_4][PF_6]$. Investigations have not yet been possible, due to the limited amount of complex available.

4.12 Concluding remarks

The aim of this chapter was to assess the catalytic activity of a range of complexes using the triphos ligand to exert a steric twist and electronic asymmetry within the complexes. Each complex had a bridge with a different feature - ranging from a standard pdt bridge, to an adt bridge with a protonation site in it, an open $(SMe)_2$ bridge, and finally the constraining edt bridge. A range of electrolytes have been used to assess the influence these have on the electrochemical and electrocatalytic behaviours of the complexes.

Hogarth had previously reported that the pdt-bridged complex undergoes a protonation at the Fe centres in a bridging orientation[35]. This result has been reproduced herein, and the corresponding results for the adt- and $(SMe)_2$-bridged complexes have been obtained. The pdt- and $(SMe)_2$-bridged complexes protonated at the Fe centres. The adt-bridged complex protonated at the N atom in the bridge, and then at the Fe centres in a higher concentration of $HBF_4.Et_2O$. From the electrochemical investigations limited evidence has been obtained for a rapid shuttling of the proton between the N and the Fe centres in DCM-$[NBu_4][ClO_4]$ and DCM-$[NBu_4][BF_4]$. This would be a major similarity with the H-cluster, and further work should investigate this possible behaviour.

It was found that the triphos-ligand complexes all undergo an electrocatalytic proton reduction mechanism in the presence of excess $HBF_4.Et_2O$. The complexes exhibit a large overpotential for

this mechanism compared to other complexes in the literature and in this dissertation. For example, the $(SC_6F_5)_2$-bridged complex analysed in Chapter 3 was catalytic at -1.34 V in DCM-$[NBu_4][PF_6]$, whereas the pdt-bridged triphos-ligand complex is not catalytic until -1.78 V under the same conditions. This is due to the high electron density put onto the Fe centres by the triphos ligand.

As well as looking at the influence of the triphos ligand, the results also allow for analysis of how the four different bridges affect the electrochemistry and catalytic activity of the complexes. The different bridges did result in substantial differences in electrochemistry of the complexes in the absence of protons, which are somewhat surprising. Computational modeling of the electronic structure of these complexes in neutral, cationic and anionic states would help elucidate and explain differences in the reaction mechanisms. In general, each bridge has been found to have a similar overpotential for catalysis, as was shown in Figure 113, suggesting that these four bridges have similar electron donating / withdrawing capabilities.

The electrolyte solution has been found to play a significant role in the electrochemistry and electrocatalytic response of the complexes tested. For example, the catalytic current of the pdt-bridged complex was approximately three times greater in DCM-$[NBu_4][ClO_4]$ than in DCM-$[NBu_4][PF_6]$. This is a significant result, as it shows that complexes in the literature can not be directly compared unless they were tested under the same experimental conditions, even down to the electrolyte used.

Major differences were also observed between the electrochemical behaviour in DCM and in MeCN. This was put down to the MeCN solvent increasing the proton availability in solution. The difference in behaviour between DCM and MeCN solvents shall be found to be a common theme throughout this dissertation.

Further work should look into the behaviour of different complexes from the literature and this dissertation in a range of electrolyte solutions. It is expected that the behaviour observed is not unique to the triphos ligand complexes. The dramatic increase in catalytic activity under certain conditions is clearly something that is important to understand when it is the catalytic activity of the complexes that is being assessed, and comparisons are being made between complexes tested in different environments in the literature.

5 $Fe_3(\mu\text{-edt})_2(CO)_{7-x}(PPh_3)_x$ ($x = 0, 1, 2$): The effect of using three iron centres instead of two

In this chapter the molecular structure, susceptibility to protonation, electrochemical behaviour and electrocatalytic activity of the three tri-iron complexes $Fe_3(\mu\text{-edt})_2(CO)_{7-x}(PPh_3)_x$ (x = 0, 1, 2) (Figure 117) are presented.

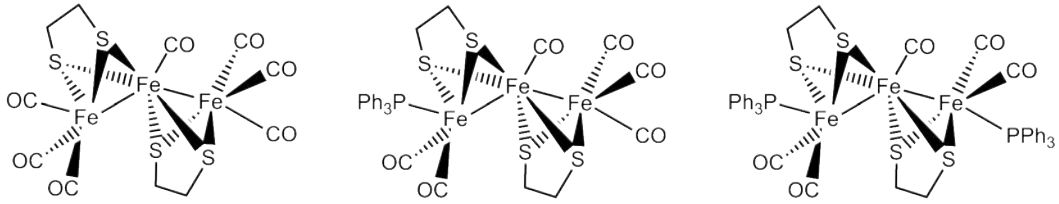

Figure 117: $Fe_3(\mu\text{-edt})_2(CO)_{7-x}(PPh_3)_x$ (x = 0, 1, 2)

As was seen in Chapter 1.5.2, the investigations of Pickett, Best and co-workers of a mixed-valence tetra-iron complex proved fruitful, showing that the tetra-iron complex exhibited an excellent catalytic turnover frequency. In an early paper on the synthesis of di-iron dithiolate complexes, Huttner and co-workers reported that while reaction of $HS(CH_2)_nSH$ (n = 2, 3) with $Fe_3(CO)_{12}$ afforded predominantly the di-iron complexes $Fe_2(\mu\text{-}S(CH_2)_nS)(CO)_6$, in both cases smaller amounts of tri-nuclear materials $Fe_3\mu\text{-}S(CH_2)_nS_2(CO)_7$ could also be isolated[36]. No reports detail these mixed-valence complexes, or their electrocatalytic activity towards proton reduction. Thus, it was of interest to study them to see how they compared to the di-iron and tetra-iron complexes.

Three tri-iron complexes have been investigated each with a slightly different ligand set. The ligands of the simplest complex are all CO; the other two complexes have CO ligands replaced with either one or two PPh_3 ligands. All of the complexes exhibited an edt bridge, thus comparisons could be made with the analogous edt-bridged di-iron and tetra-iron complexes.

5.1 Molecular structures of the tri-iron complexes $Fe_3(\mu\text{-edt})_2(CO)_{7-x}$-$(PPh_3)_x$ ($x = 0, 1, 2$)

The molecular structures of the tri-iron complexes will influence their catalytic activity towards proton reduction, and were therefore analysed.

X-ray diffraction analyses presented in this chapter were performed by Graeme Hogarth in University College London.

5.1.1 Molecular structure of $Fe_3(\mu\text{-edt})_2(CO)_7$

The molecular structure of the unsubstituted complex is given in Figure 118. The molecule exhibits an approximately linear tri-iron core with a Fe(1)-Fe(2)-Fe(3) bond angle of 151.74(3) °. The Fe-Fe distances are 2.5385(8) and 2.5655(8) Å, and the iron-sulfur bond lengths span a range 2.215(1) -

2.263(1) Å. The dithiolate ligands are in an anti arrangement. The formal oxidation states of the Fe centres are Fe(I)Fe(II)Fe(I).

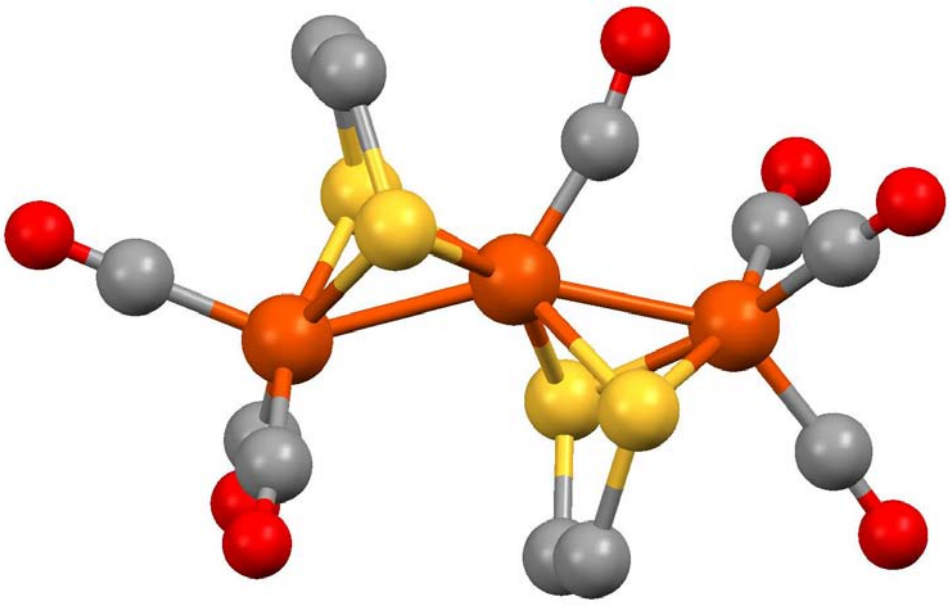

Figure 118: Molecular structure of $Fe_3(\mu\text{-edt})_2(CO)_7$

The iron-iron distances, which vary between 2.5385(8) and 2.5655(8) Å, are consistent with the Fe(I)Fe(II) bond length of 2.543(5) Å found in $Fe_4(CO)_8\mu_3\text{-}(SCH_2)_3CMe_2$, but shorter than the Fe(II)Fe(II) contact of 2.651(9) Å [33].

Adams and Yamamoto have previously prepared the ruthenium analogue, $Ru_3(\mu\text{-edt})_2(CO)_7$, upon addition of 1,2,5,6-tetrathiocyclooctane to $Ru_3(CO)_{12}$ [40]. It exists as two isomers, denoted anti and syn, differing in the relative orientation of the dithiolate bridges, the anti isomer converting into the thermodynamically favoured syn product upon heating. $Fe_3(\mu\text{-edt})_2(CO)_7$ adopts the anti conformation, as seen above, and upon heating no rearrangement was observed.

Adams and Yamamoto have crystallographically characterised the corresponding ruthenium complex anti-$Ru_3(\mu\text{-edt})_2(CO)_7$, the structure of which is very similar to $Fe_3(\mu\text{-edt})_2(CO)_7$. Importantly the Ru-Ru-Ru bond angle of 151.52(3) ° is virtually identical to that in $Fe_3(\mu\text{-edt})_2(CO)_7$, while the central carbonyl is also bent (Ru(2)-C-O 166.4(8) °). This has been attributed to a semi-bridging interaction with a second ruthenium atom (Ru(1)-C 2.713(9) Å). Similar interactions are seen in $Fe_3(\mu\text{-edt})_2(CO)_7$, with Fe(1)-C(3) bond length of 2.576(4) Å. Given the perceived significance of the formation of a semi-bridging carbonyl during the catalytic cycle (see Chapter 1 for details) the observation of this interaction here may be of significance. Indeed it is noted that a number of biomimetic Fe(I)Fe(II) complexes have been shown to contain a semi-bridging carbonyl. For example, Darensbourg has crystallographically characterised $[Fe_2(CO)_3(PMe_3)(IMes)(\mu\text{-CO})(\mu\text{-pdt})][PF_6]$ (IMes = 1,3-bis(2,4,6-trimethylphenyl)imidazol-2-ylidene) containing a semi-bridging carbonyl key structural parameters being: Fe-C 1.864(4) and 2.194(4) Å, Fe-C-O 151.9(3) ° [30]. These can be compared with the related parameters in $Fe_3(\mu\text{-edt})_2(CO)_7$; Fe-C 1.765(4) and 2.576(4) Å,

Fe-C-O 167.6(4) °. Clearly the semi-bridging interaction in $Fe_3(\mu\text{-edt})_2(CO)_7$ is less pronounced although part of this difference may be due to the positive charge on the binuclear complex. The semi-bridging interaction in $Fe_3(\mu\text{-edt})_2(CO)_7$ can also be seen in its IR spectrum (see below), a relatively weak low energy absorption being observed at 1904 cm^{-1}, compared with that at 1861 cm^{-1} seen in $[Fe_2(CO)_3(PMe_3)(IMes)(\mu\text{-CO})(\mu\text{-pdt})][PF_6]$.

It is instructive to consider the mixed-valence complex as a binuclear species with a third Fe(I) "ligand", as illustrated in in Figure 119. Here the Fe(2)-Fe(3) sub-unit looks like a classic non-rotated binuclear complex of the type $Fe_2(\mu\text{-dithiolate})(CO)_4(\kappa^2\text{-chelate})$ with eclipsed ML_3 centres. In contrast, the Fe(1)-Fe(2) sub-unit resembles the rotated structure of mixed-valence Fe(I)-Fe(II) complexes such as $[Fe_2(\mu\text{-pdt})(CO)_3(PMe_3)\text{-}(IMes)][PF_6]$. Thus the two ML_3 fragments are staggered and the adoption of a semi-bridging carbonyl leads to the generation of a vacant coordination site. The semi-bridging CO also means the complex is asymmetrical and the outer Fe centres are inequivalent.

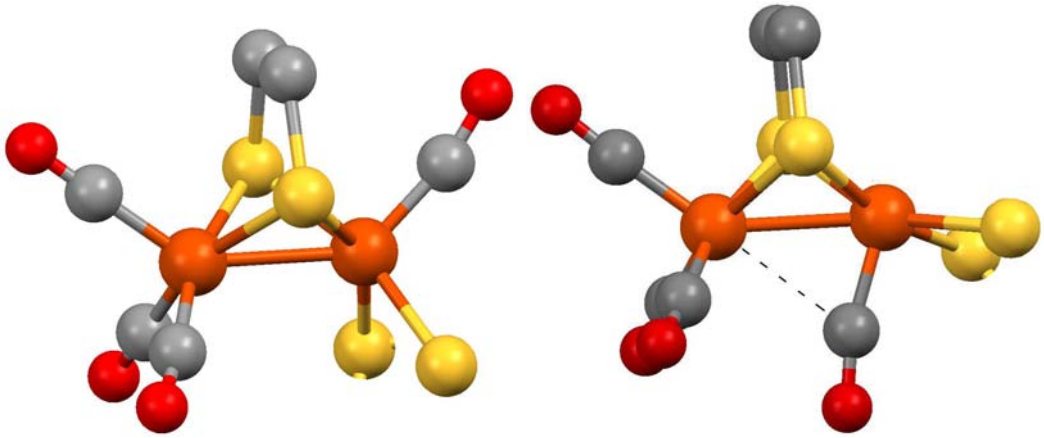

(a) From the left hand side of Figure 118 (b) From the right side of Figure 118 (rotated)

Figure 119: Molecular structure of $Fe_3(\mu\text{-edt})_2(CO)_7$, as two sub-units

5.1.2 Molecular structure of $Fe_3(\mu\text{-edt})_2(CO)_6PPh_3$

The molecular structure of the mono-substituted complex is similar to that of the unsubstituted complex (Figure 120). The molecule exhibits an approximately linear tri-iron core with a bond angle of 151.83(7) °. The Fe-Fe distances are 2.546(2) and 2.584(2) °. The dithiolate ligands are in an anti arrangement. Iron-sulfur bond lengths span a range (2.198(3) - 2.261(3) Å). The phosphine substitution occurs at the apical site of one of the outer Fe centres, and is approximately trans to the metal-metal bond, with an Fe-Fe-P angle of 150.27(9) °. As with the unsubstituted complex, the CO ligand on the central Fe centre is bent to form a semi-bridging CO ligand. The semi-bridging CO bridges towards the Fe centre with the PPh_3 ligand attached, perhaps due to the increased electron density on this Fe centre due to the PPh_3 ligand.

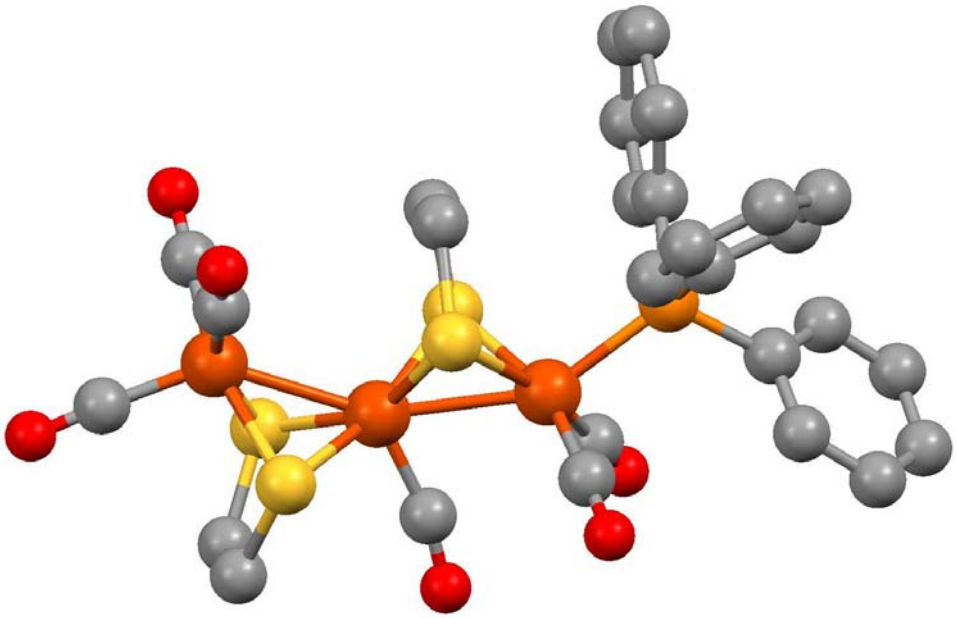

Figure 120: Molecular structure of $Fe_3(\mu\text{-edt})_2(CO)_6PPh_3$

5.1.3 Molecular structure of $Fe_3(\mu\text{-edt})_2(CO)_5(PPh_3)_2$

The molecular structure of the di-substituted complex is again comparable to the unsubstituted and mono-substituted complexes (Figure 121). The molecule exhibits an approximately linear tri-iron core with a bond angle of 151.50(6) °. The Fe-Fe distances are 2.547(2) and 2.546(2) °, and the iron-sulfur bond lengths span a range 2.226(3) - 2.281(3) Å. The dithiolate ligands are in an anti arrangement. The phosphine substitutions both occur at apical sites of the outer Fe centres. They sit approximately trans to the metal-metal bond, with Fe-Fe-P angles of 154.11(8) and 151.03(8) °. As with the unsubstituted and mono-substituted complexes, the CO ligand on the central Fe centre is bent to form a semi-bridging CO ligand. The semi-bridging CO also means the outer Fe centres are inequivalent.

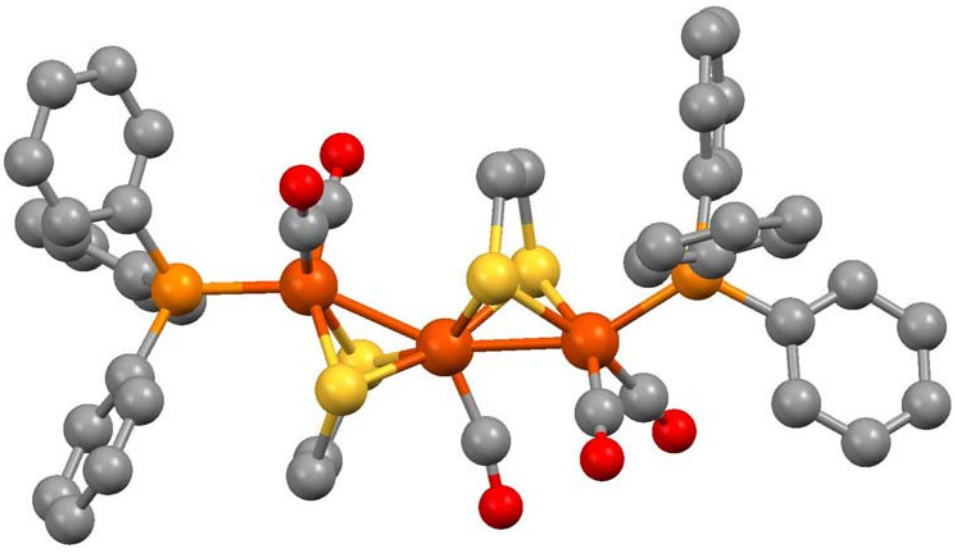

Figure 121: Molecular structure of $Fe_3(\mu\text{-edt})_2(CO)_5(PPh_3)_2$

5.2 Susceptibility of the three tri-iron complexes to protonation

The H-cluster is known to operate through the mixed-valence Fe(I)Fe(II) oxidation states and exhibit a semi-bridging CO ligand. Unlike complexes reported to date, the three tri-iron complexes investigated herein have been found above to display these highly relevant structural elements in their neutral form. (The importance of mixed-valance and semi-bridging carbonyls is discussed in Chapter 1.) It will thus be intriguing to see how these aspects of the tri-iron complexes influence their catalytic activities.

Before testing for catalytic activity, the next step towards understanding any catalytic mechanism the three tri-iron complexes might exhibit was to determine whether or not they would protonate in the presence of a Brönsted acid. This aids understanding of whether the first step of a catalytic mechanism is a protonation or a reduction process. Hexacarbonyl di-iron complexes are not basic enough to bind a proton at the Fe centres and thus phosphine substitution is typically employed in order to increase the proton binding properties of binuclear models. This Chapter will probe whether this also applies for tri-iron complexes.

Protonation was monitored through the IR stretches of the CO ligands. See Chapter 2 for details.

5.2.1 Infrared spectroscopy of $Fe_3(\mu\text{-edt})_2(CO)_7$ in the presence of $HBF_4.Et_2O$

The IR spectrum of $Fe_3(\mu\text{-edt})_2(CO)_7$ in DCM is shown in Figure 122. Bands are seen at 2073, 2040, 2008 and 1975 cm^{-1}. A further broad signal is at 1904 cm^{-1}, consistent with the presence of a semi-bridging CO, as was discussed in Section 5.1.1.

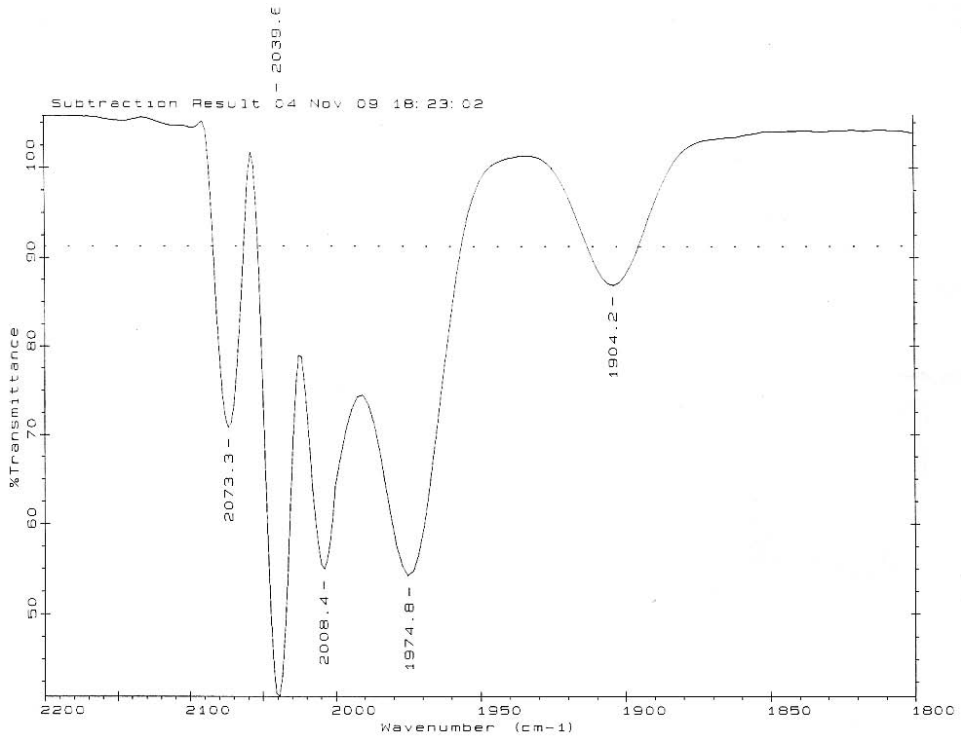

Figure 122: IR spectrum of $Fe_3(\mu\text{-edt})_2(CO)_7$ in DCM

On the addition of one equivalent of $HBF_4.Et_2O$ the bands of the IR spectrum did not change in intensity or position, indicating that the complex did not protonate. Even on the addition of further acid there was no evidence for protonation.

The solution was left for approximately 24 hours (Figure 123). The solution went from dark red to orange, and the bands of the IR spectrum shifted to higher wavenumbers (2108, 2062, 2015 and 1975 cm^{-1}), implying there was a change in the structure of the complex. The signal for the semi-bridging CO had diminished considerably. It was not immediately clear if the shift in the bands was due to protonation, or another chemical process. Indeed, evidence shall be provided below, in the investigations of the mono- and di-substituted complexes, that the molecular rearrangement is due to oxidation or decomposition of the complex rather than protonation.

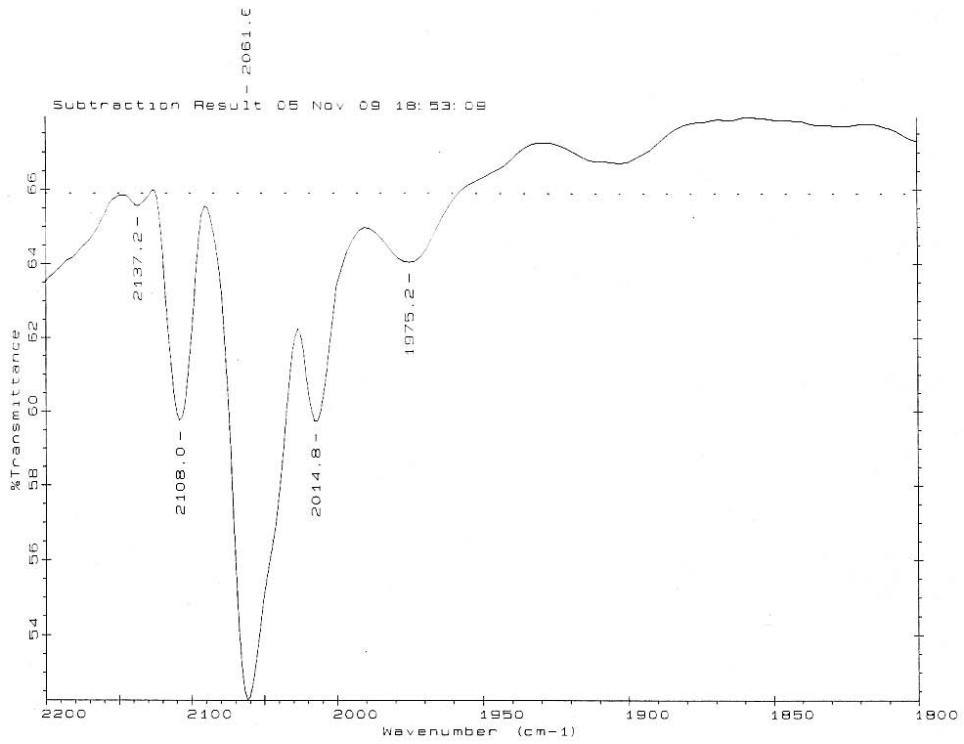

Figure 123: IR spectrum of $Fe_3(\mu\text{-edt})_2(CO)_7$ in DCM in the presence of approximately 5 molar equivalents $HBF_4.Et_2O$ left for 24 hours

5.2.2 Infrared spectroscopy of $Fe_3(\mu\text{-edt})_2(CO)_6PPh_3$ in the presence of $HBF_4.Et_2O$

The above experiment was repeated for the mono-substituted complex $Fe_3(\mu\text{-edt})_2(CO)_6PPh_3$. The IR spectrum of the complex is shown in Figure 124. Bands are seen at 2064, 2035, 2011, 1963 and 1884 cm^{-1}. The bands are at lower wavenumbers than the unsubstituted complex, as would be expected due to the higher electron density on the Fe centres (provided by the PPh_3 ligand) increasing backbonding into CO anti-bonding orbitals, and therefore weakening the CO bond. Again, the broad band at 1884 cm^{-1} supports the suggestion that the complex has a semi-bridging CO ligand.

On the addition of 1 molar equivalent $HBF_4.Et_2O$ there was no significant change in the IR spectrum. However, on adding a further 5 molar equivalents the ratios of the band intensities

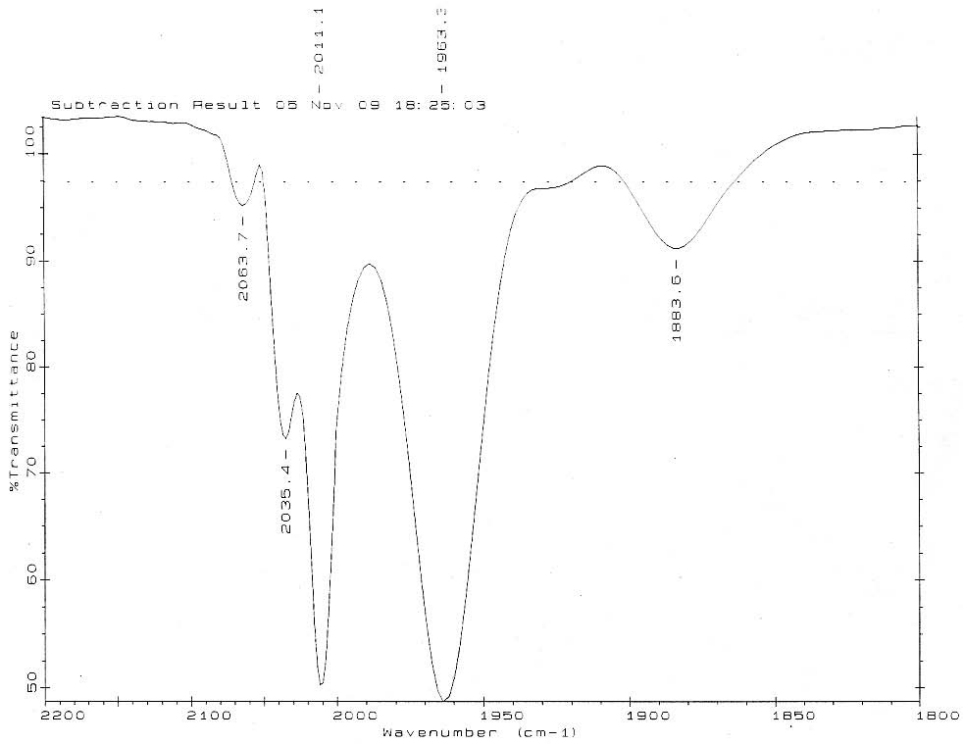

Figure 124: IR spectrum of $Fe_3(\mu\text{-edt})_2(CO)_6PPh_3$ in DCM

changed, although their wavenumbers were unchanged.

The complex was left for 21 hours, after which the IR spectrum shown in Figure 125 was obtained. The bands shifted to 2103, 2039 and 2001 cm^{-1}, implying a clear change in the structure of the complex. The semi-bridging CO signal was no longer present.

As with the unsubstituted complex, this was not sufficient evidence to prove that the complex had protonated. Indeed, evidence shall be provided later that the complex is in fact oxidising, rather than protonating, leading to one or more decomposition products.

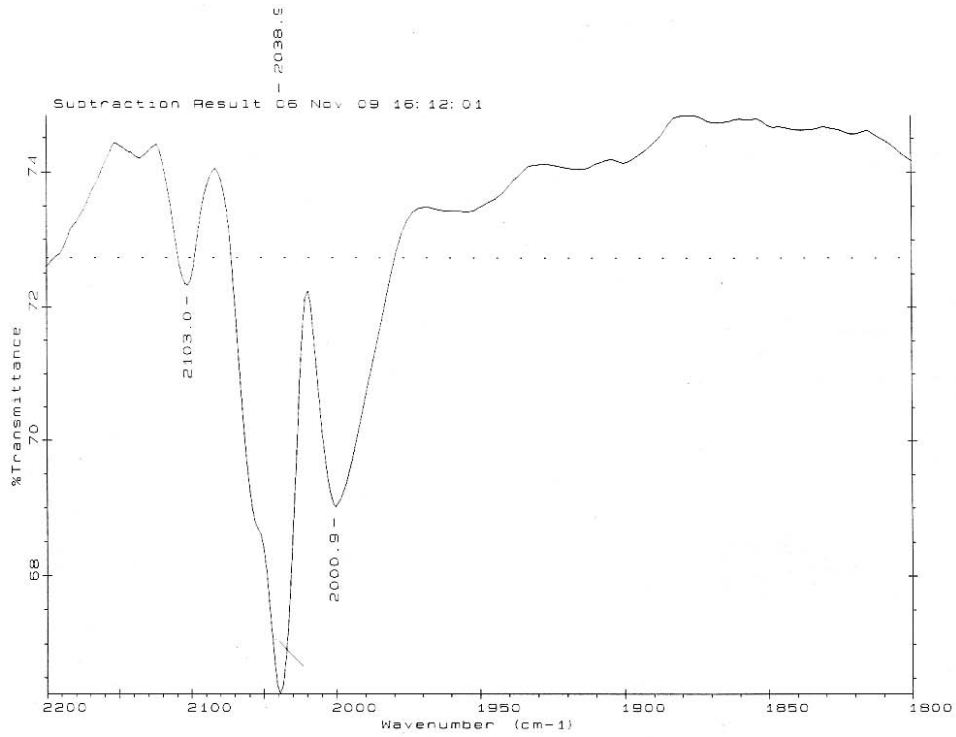

Figure 125: IR spectrum of $Fe_3(\mu\text{-edt})_2(CO)_6PPh_3$ in DCM in the presence of approximately 5 molar equivalents $HBF_4.Et_2O$ left for 21 hours

5.2.3 Infrared spectroscopy of $Fe_3(\mu\text{-edt})_2(CO)_5(PPh_3)_2$ in the presence of $HBF_4.Et_2O$

The IR spectrum of $Fe_3(\mu\text{-edt})_2(CO)_5(PPh_3)_2$ in the absence of protons is shown in Figure 126. Bands are observed at 2042, 2008, 1962 and 1913 cm^{-1}, as well as the broad peak at 1870 cm^{-1} indicative of a semi-bridging CO ligand. The bands are at lower wavenumbers than the unsubstituted and mono-substituted complexes, due to the increased electron density on the Fe centres provided by the two PPh_3 ligands weakening the CO bonds due to increased backbonding into CO anti-bonding orbitals.

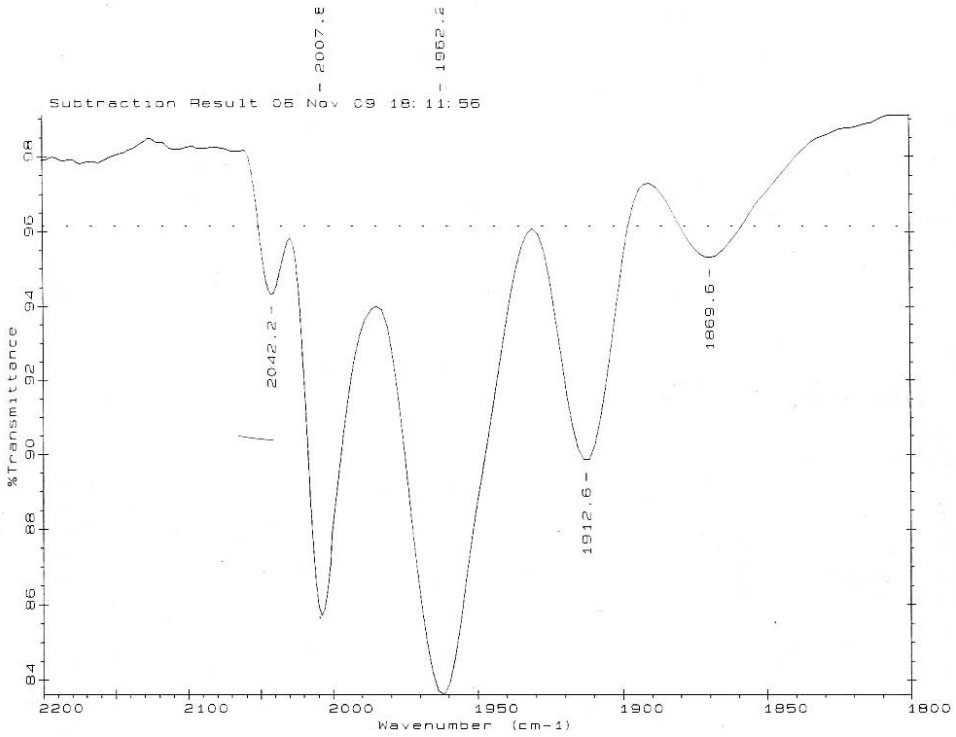

Figure 126: IR spectrum of $Fe_3(\mu\text{-edt})_2(CO)_5(PPh_3)_2$ in DCM

Unlike the unsubstituted and mono-substituted complexes, on the addition of one equivalent $HBF_4.Et_2O$ to the di-substituted complex there was an immediate change in the IR spectrum. The bands of the neutral complex remained, with new bands seen at 2020 and 1989 cm^{-1} which continued to grow in over time.

A second equivalent of $HBF_4.Et_2O$ was added, and the spectrum shown in Figure 127 was obtained. Clear bands were now seen at 2042, 2020 and 1989 cm^{-1}, with no evidence of the neutral complex remaining in solution. On the third and fourth additions of acid the bands did not change further.

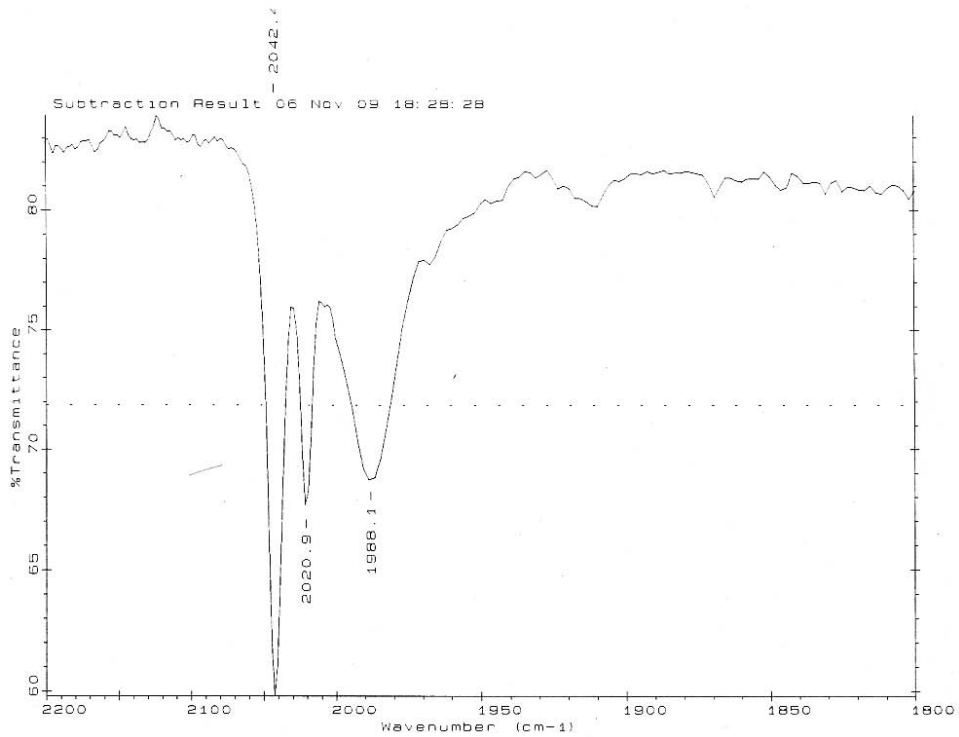

Figure 127: IR spectrum of $Fe_3(\mu\text{-edt})_2(CO)_5(PPh_3)_2$ in DCM in the presence of 2 molar equivalents $HBF_4.Et_2O$

5.2.4 Infrared spectroscopy of $Fe_3(\mu\text{-edt})_2(CO)_5(PPh_3)_2$ in the presence of ferrocenium

The above results suggested the complex had been protonated, however, another possible explanation was that the $HBF_4.Et_2O$ was being reduced to form dihydrogen, with the complex being oxidised rather than protonated. To investigate this possibility the complex was chemically oxidised using ferrocenium and monitored through IR spectroscopy.

After the addition of 1 molar equivalent ferrocenium to a fresh solution of the neutral complex the spectrum shown in Figure 128 was obtained, with a clear transition from the neutral complex to the oxidised form. Bands are now present at 2021 and 1987 cm^{-1}, and the band at 2044 cm^{-1} has grown significantly (the presence of the 2044 cm^{-1} in the spectrum of the neutral complex, shown in Figure 126, suggests that the complex is already partially oxidised in the aerated solution). These band positions are very similar to those seen after the addition of $HBF_4.Et_2O$, thus it seems that addition of acid causes oxidation of the complexes rather than protonation. However, it shall be seen in Section 5.4.5 that the acid does not oxidise the complex under an Ar atmosphere. As the IR investigations were not carried out in deoxygenated solutions, it is suggested that the presence of protons and O_2 leads to the oxidation of the complex, rather than protonation.

Further evidence for this finding has recently been obtained from the NMR spectra. On addition of $HBF_4.Et_2O$ to the complex, the spectrum observed was characteristic of a paramagnetic species, suggesting it has been oxidised.

The IR spectrum for the oxidised complex also indicates that the bridging CO ligand is lost upon oxidation, implying that the oxidised complex does not exhibit a bridging CO ligand.

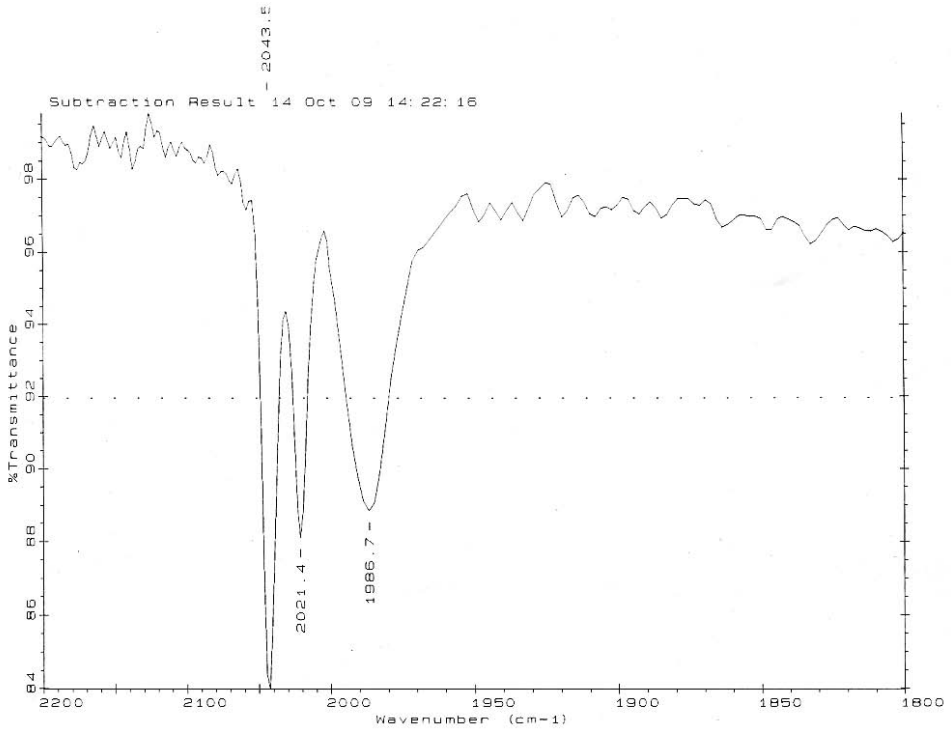

Figure 128: IR spectrum of $Fe_3(\mu\text{-edt})_2(CO)_5(PPh_3)_2$ in DCM after the addition of 1 molar equivalent $[Fc]^+[PF_6]^-$

5.2.5 Infrared spectroscopy of $Fe_3(\mu\text{-edt})_2(CO)_6PPh_3$ in the presence of ferrocenium

As with the di-substituted complex, it was possible that the mono-substituted complex was being oxidised in the presence of $HBF_4.Et_2O$ and O_2. It was therefore important to investigate the IR spectrum of the oxidised complex. One molar equivalent of ferrocenium was added to a fresh solution of the mono-substituted complex, and the spectrum shown in Figure 129 was obtained. New bands had appeared at 2087, 2036, 2012 and 1963 cm^{-1}. These bands do not match those seen after the addition of $HBF_4.Et_2O$, so it is clear that the same oxidation product is not being formed. It is more likely that the acid is either protonating the complex or causing a slow decomposition of the complex. It shall be seen in Section 5.4.4 that the later is the likely case, as there is no evidence for protonation under the experimental conditions employed for electrochemistry.

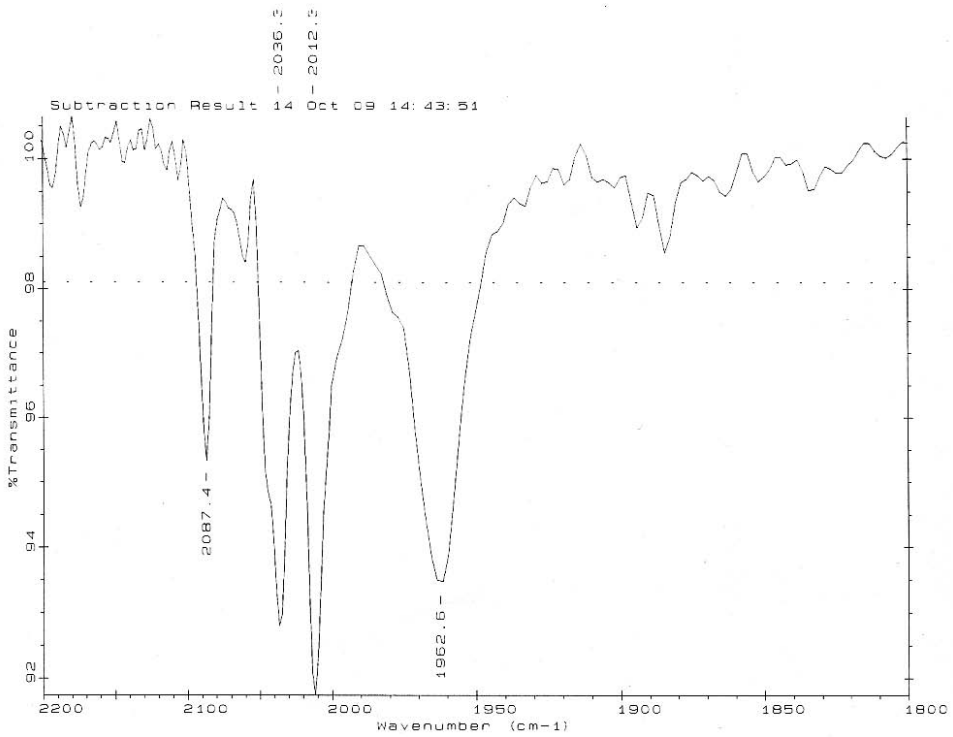

Figure 129: IR spectrum of $Fe_3(\mu\text{-edt})_2(CO)_6PPh_3$ in DCM after the addition of 1 molar equivalent $[Fc]^+[PF_6]^-$

5.2.6 Summary and discussion

The above experiments showed that none of the complexes were basic enough to protonate in the presence of the strong acid $HBF_4.Et_2O$. Thus, it is expected that any catalytic mechanism will require additional basicity put onto the Fe centres through reduction of the complex, and the catalytic mechanism is likely to be ECEC (Figure 6).

The band positions shifted from higher wavenumbers on each substitution, indicating that the oxidation and reduction potentials should shift in a negative direction with each substitution, in a similar way to the di-iron complexes. Also, the di- and mono-substituted complexes have been found to oxidise in the presence of ferrocenium, implying that the oxidation potentials of these complexes

will be negative of the oxidation potential of ferrocene.

In the presence of O_2 the complexes have been found to oxidise when $HBF_4.Et_2O$ is added to the solution. This problem will be avoided in the electrochemical investigations, as the experiments will be carried out in under an Ar atmosphere in the absence of O_2.

5.3 Electrochemistry of the tri-iron complexes in the absence of protons

To further probe the nature of any catalytic activity the tri-iron complexes may exhibit, the electrochemical behaviours of the complexes in the absence of protons have been analysed. As seen above, the complexes do not appear to protonate even in the presence of the strong acid $HBF_4.Et_2O$. Therefore, based on the steps of a generic catalytic mechanism presented in Figure 6, it is expected that the reduction of the complexes will be the first step in a catalytic process, with a mild reduction potential preferred for an efficient catalyst.

5.3.1 Electrochemistry of $Fe_3(\mu\text{-edt})_2(CO)_7$ in the absence of protons, in DCM

The CV of the unsubstituted tri-iron complex in DCM is shown in Figure 130. The complex is reduced at -1.47 V, with a peak current of 9 μA. This is followed by two small reduction peaks at -1.66 and -1.81 V, and another peak of similar magnitude to the first reduction at -2.05 V. On the return scan there are several minor re-oxidation peaks. The first oxidation of the neutral complex occurs at 0.45 V, with a peak current of 9 μA.

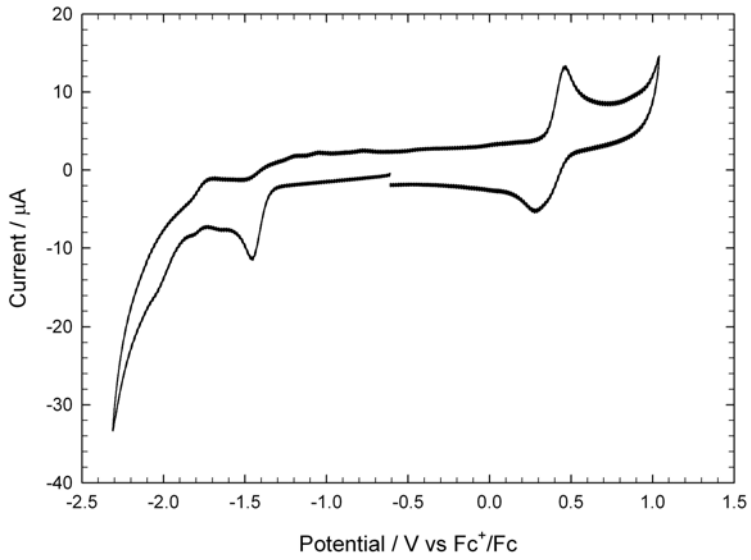

Figure 130: Cyclic voltammetry of $Fe_3(\mu\text{-edt})_2(CO)_7$ (0.5 mM) in DCM-$[NBu_4][PF_6]$ (v=0.1 Vs^{-1}, glassy carbon electrode; V vs Fc^+/Fc)

The oxidation response is shown in detail in Figure 131. The oxidation of the complex is seen at 0.45 V. Two corresponding reduction responses are seen at approximately 0.37 V and 0.28 V. The reversibility of this process was investigated by using a range of scan rates, as shown in Figure 132. The first reduction of the unsubstituted complex is shown in Figure 133. At a scan rate of 0.1 Vs^{-1} the reduction of the complex is seen at -1.47 V. Even at the faster scan rates the reaction does not become electrochemically reversible. These oxidation and reduction behaviours shall be discussed in further detail below.

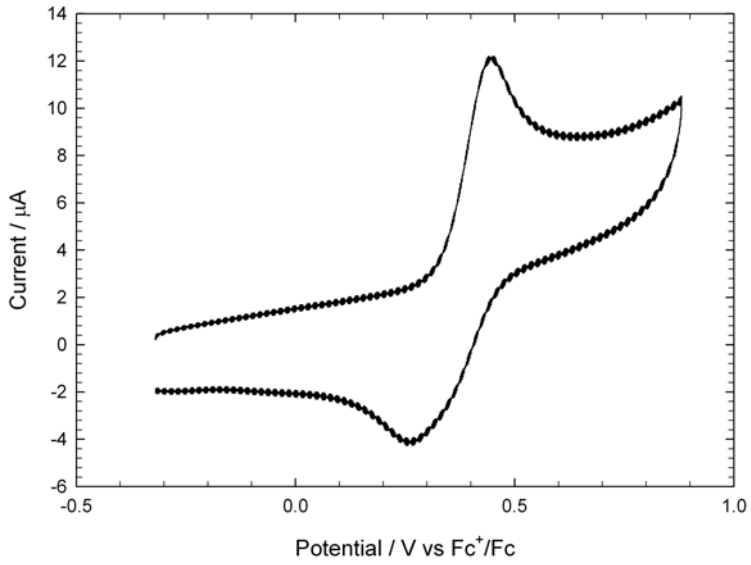

Figure 131: Cyclic voltammetry of $Fe_3(\mu\text{-edt})_2(CO)_7$ (0.5 mM) in DCM-$[NBu_4][PF_6]$ (v=0.1 Vs^{-1}, glassy carbon electrode; V vs Fc^+/Fc)

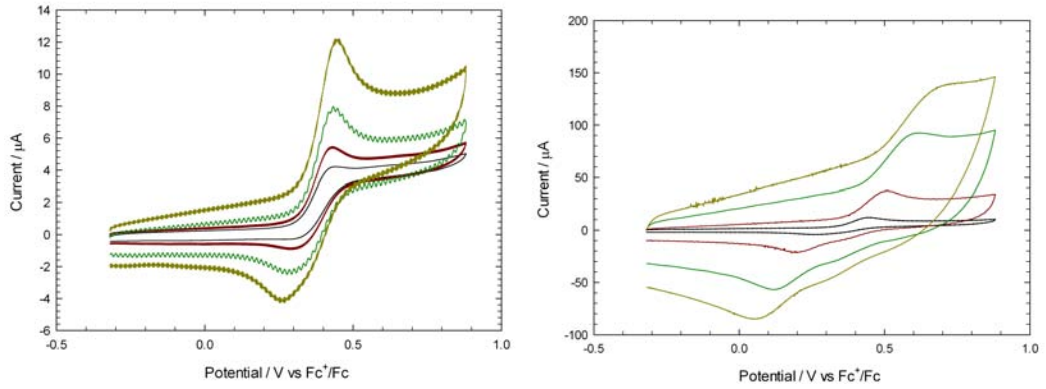

(a) v=0.01, 0.02, 0.05, 0.1 Vs^{-1} (b) v=0.1, 1.0, 5.0, 10.0 Vs^{-1}

Figure 132: Cyclic voltammetry of $Fe_3(\mu\text{-edt})_2(CO)_7$ (0.5 mM) in DCM-$[NBu_4][PF_6]$ (glassy carbon electrode; V vs Fc^+/Fc)

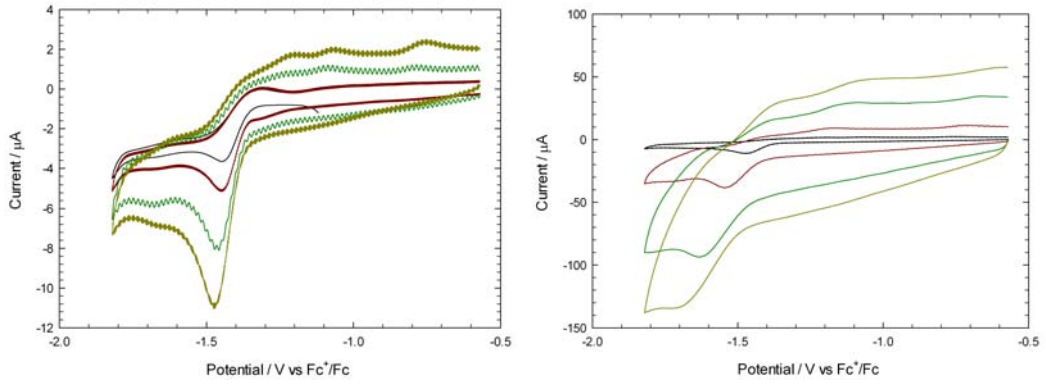

(a) v=0.01, 0.02, 0.05, 0.1 Vs^{-1} (b) v=0.1, 1.0, 5.0, 10.0 Vs^{-1}

Figure 133: Cyclic voltammetry of $Fe_3(\mu\text{-edt})_2(CO)_7$ (0.5 mM) in DCM-$[NBu_4][PF_6]$ (glassy carbon electrode; V vs Fc^+/Fc)

5.3.2 Electrochemistry of $Fe_3(\mu\text{-edt})_2(CO)_7$ in the absence of protons, in CO-saturated DCM

As noted above, the reduction of the unsubstituted complex is irreversible, suggesting a chemical step takes place after the reduction process. A common process that di-iron complexes undergo upon reduction is loss of a CO ligand. Therefore the difference in the electrochemical behaviour of the unsubstituted tri-iron complex in a solution saturated with CO (which would suppress CO ligand loss) was investigated.

The CV obtained under CO is given in Figure 134. The first reduction of the complex is at -1.49 V, the same potential as under Ar. A second reduction process occurs at -1.88 V, with peak current double that of the first reduction. A third reduction process occurs at -2.10 V, again the peak current is double that of the first reduction process. On the return scan, broad re-oxidation peaks occur at -1.70, -0.85, -0.45 and 0 V. The first oxidation of the neutral complex occurs at 0.45 V. This first oxidation has two corresponding re-reduction processes at 0.33 and 0.24 V. A second oxidation process occurs at 0.85 V, with a smaller peak height than the first oxidation. (Note that the small reduction feature at -1.32 V is due to the reduction of trace oxygen.)

Numerous differences between the experiment performed under Ar and the experiment performed under CO are clear. The small reduction feature seen under Ar at -1.71 V is no longer present. The peak at -1.87 V is significantly larger. On the return scan, the re-oxidation peaks appear at different potentials. Scanning to anodic potentials, a second oxidation process occurs under CO at 0.82 V. Importantly, in the presence of CO there is no change to the reversibility or position of the first reduction. This is evidence that the irreversibility of the reduction is not due to CO ligand loss.

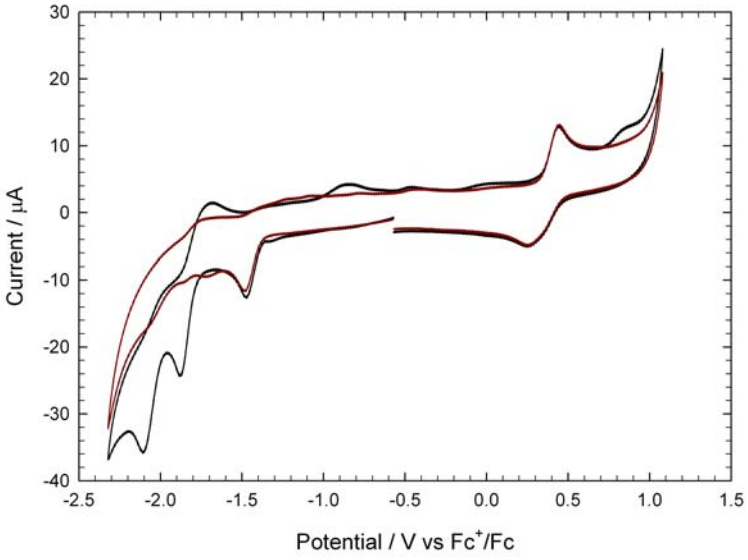

Figure 134: Cyclic voltammetry of $Fe_3(\mu\text{-edt})_2(CO)_7$ (0.5 mM) in DCM-$[NBu_4][PF_6]$ saturated with CO (black line) and Ar (red line) (v=0.1 Vs^{-1}, glassy carbon electrode; V vs Fc^+/Fc)

The first reduction of the complex under CO has been investigated in isolation, as shown in

Figure 135. No improvement in reversibility was observed at fast scan rates.

The species whose reduction causes the new peak observed at -1.87 V has not yet been identified, however, $Fe_2(\mu\text{-edt})(CO)_6$ is known to undergo reduction at this potential (see Figure 150). It is therefore tentatively proposed that after reduction, one of the Fe-Fe-Fe bonds is cleaved, resulting in a di-iron complex and a mono-iron fragment. The vacant coordination site then available is rapidly occupied by a CO ligand, thus forming the di-iron hexacarbonyl which is then reduced at -1.87 V. This bond cleavage mechanism may explain the irreversibility of the first reduction process in both Ar and CO atmospheres. In Ar the coordination site would not be occupied by CO, so further decomposition may be anticipated.

No change in the oxidation response is observed in the CO-saturated solution. Thus CO ligand loss is not occurring during this process either.

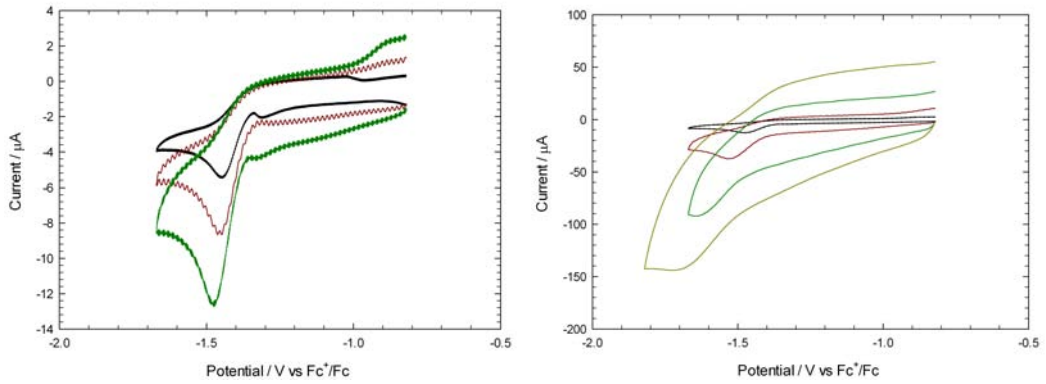

(a) v=0.02, 0.05, 0.1 Vs^{-1} (b) v=0.1, 1.0, 5.0, 10.0 Vs^{-1}

Figure 135: Cyclic voltammetry of $Fe_3(\mu\text{-edt})_2(CO)_7$ (0.5 mM) in DCM-$[NBu_4][PF_6]$ saturated with CO (glassy carbon electrode; V vs Fc^+/Fc)

5.3.3 Electrochemistry of $Fe_3(\mu\text{-edt})_2(CO)_7$ in the absence of protons, in MeCN

Many of the complexes in the literature have been investigated in the coordinating solvent MeCN. To make comparisons with such studies the electrochemistry of the unsubstituted complex was also investigated in MeCN. The change to a coordinating solvent could also provide insights into the structural rearrangement mechanisms which occur upon oxidation and reduction of the complex. If coordination sites become available, then the coordinating solvent is likely to occupy them, thus altering the reaction mechanism.

Figure 136 shows the CV of the unsubstituted complex in MeCN. A reduction peak is observed at -1.27 V. Three small reduction peaks are seen at potentials beyond this, with a reduction of similar magnitude at -2.15 V. The return scan shows several oxidation peaks corresponding to products formed during the reduction. The first oxidation of the complex occurs at 0.39 V, and exhibits no sign of reversibility.

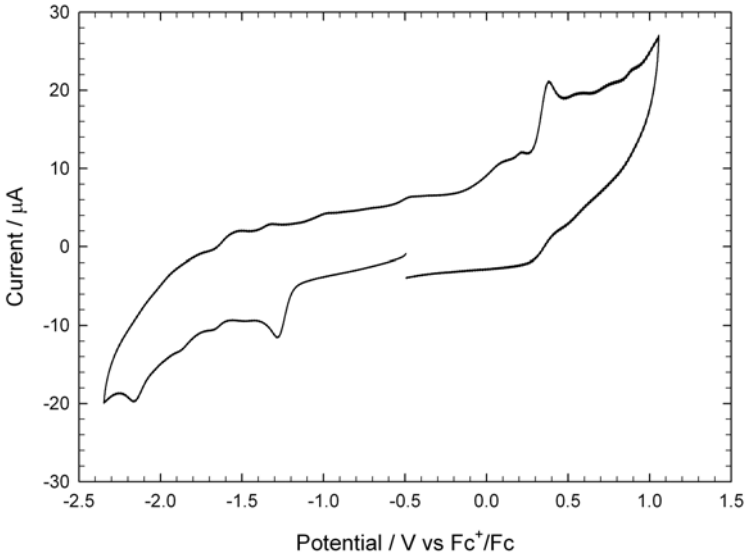

Figure 136: Cyclic voltammetry of $Fe_3(\mu\text{-edt})_2(CO)_7$ (0.5 mM) in MeCN-$[NBu_4][PF_6]$ (v=0.1 Vs^{-1}, glassy carbon electrode; V vs Fc^+/Fc)

The oxidation behaviour of the complex in MeCN is remarkably different to that seen in DCM. It is speculated that the MeCN stabilises the product of the first oxidation process, thus affecting reversibility. However, further work is required to understand this process.

Under the same experimental conditions, the analogous di-iron complex $Fe_2(\mu\text{-edt})(CO)_6$ has been shown to undergo between a one- and two-electron reduction process. Pickett and co-workers studied its reduction chemistry in some detail using spectroelectrochemistry and found that a complex range of products resulted which varied with solvent and CO saturation. The two-electron reduction ultimately led to cleavage of an iron-sulfur bond and structural rearrangement to a bridging carbonyl species. Felton et al recently showed that the reduction of $Fe_2(\mu\text{-edt})(CO)_6$ in MeCN under CO varied from one to two-electron uptake as scan rate was decreased, due to a potential

inversion resulting from this structural rearrangement. Potential inversion occurs during a redox process when the second electron transfer is easier that the first, resulting in a two electron transfer at the potential of the first electron transfer.

Due to the similarity of the unsubstituted tri-iron complex and $Fe_2(\mu\text{-edt})(CO)_6$, the reduction of the tri-iron complex was investigated over a range of scan rates and the resulting normalised currents compared to determine whether potential inversion was taking place in this case, as shown in Figure 137. Each scan rate gives the same normalised reduction current of approximately 18 $\mu As^{1/2}V^{-1/2}$, implying that a potential inversion mechanism does not take place, and the same number of electrons are taken up over the range of scan rates.

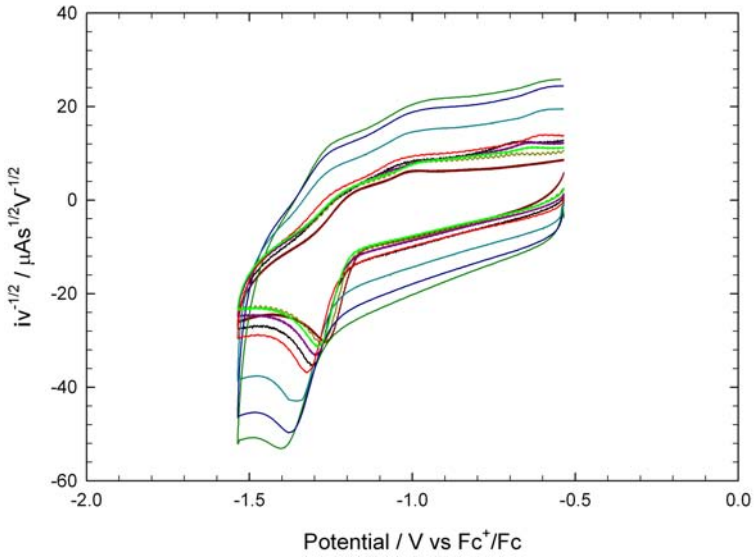

Figure 137: Cyclic voltammetry of $Fe_3(\mu\text{-edt})_2(CO)_7$ (0.5 mM) in MeCN-$[NBu_4][PF_6]$ with current normalised (v=0.02, 0.05, 0.1, 0.2, 0.5, 1, 5, 10, 20 Vs^{-1}, glassy carbon electrode; V vs Fc^+/Fc)

5.3.4 Electrochemistry of $Fe_3(\mu\text{-edt})_2(CO)_6PPh_3$ in the absence of protons, in DCM

A similar set of experiments have been performed on the mono-substituted complex. A CV of the neutral complex in DCM is shown in Figure 138. The reduction of the complex occurs at -1.72 V, 0.25 V more negative than the unsubstituted complex. A small reduction feature is observable at -1.89 V and a larger one at -2.20 V. The complex is oxidised at 0.12 V, compared to 0.45 V for the unsubstituted complex. The corresponding reduction peak on the backward scan is not consistent with reversible behaviour. A large oxidation begins at 0.7 V, which is assumed to involve the complex decomposing.

A closer view of the first oxidation (Figure 139), indicates that the re-reduction peak is indeed associated with the first oxidation and not from the large oxidation that occurs at the more positive potential. Increasing the scan rate to 5 and 10 Vs^{-1} allows detection of two distinct re-reduction peaks at 0.06 and 0.03 V respectively. Even at scan rates up to 10 Vs^{-1} the first reduction showed

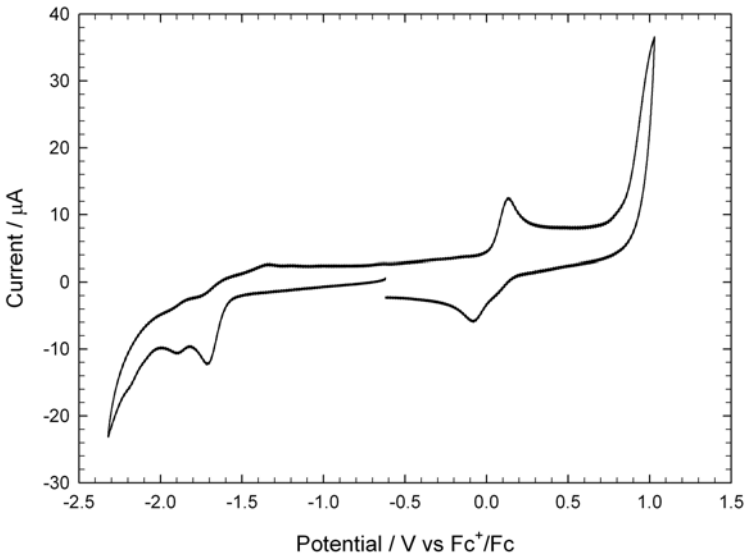

Figure 138: Cyclic voltammetry of $Fe_3(\mu\text{-edt})_2(CO)_6PPh_3$ (0.5 mM) in DCM-$[NBu_4][PF_6]$ (v=0.1 Vs^{-1}, glassy carbon electrode; V vs Fc^+/Fc)

no reversibility (Figure 140).

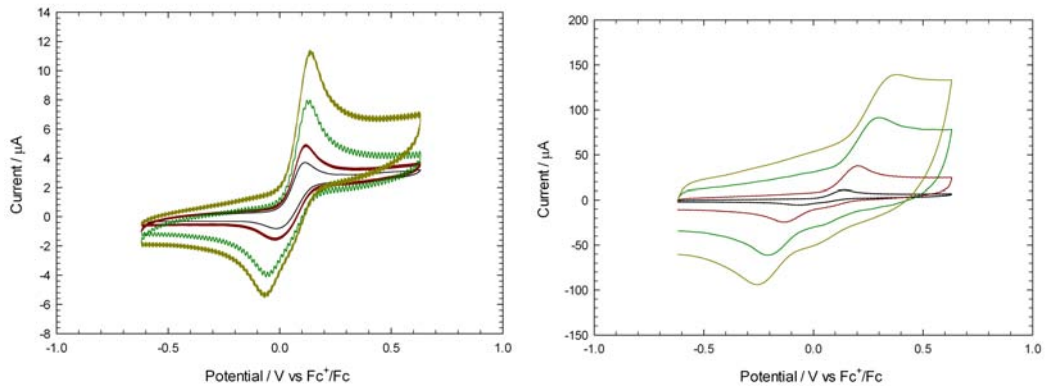

(a) v=0.01, 0.02, 0.05, 0.1 Vs^{-1} (b) v=0.1, 1.0, 5.0, 10.0 Vs^{-1}

Figure 139: Cyclic voltammetry of $Fe_3(\mu\text{-edt})_2(CO)_6PPh_3$ (0.5 mM) in DCM-$[NBu_4][PF_6]$ (glassy carbon electrode; V vs Fc^+/Fc)

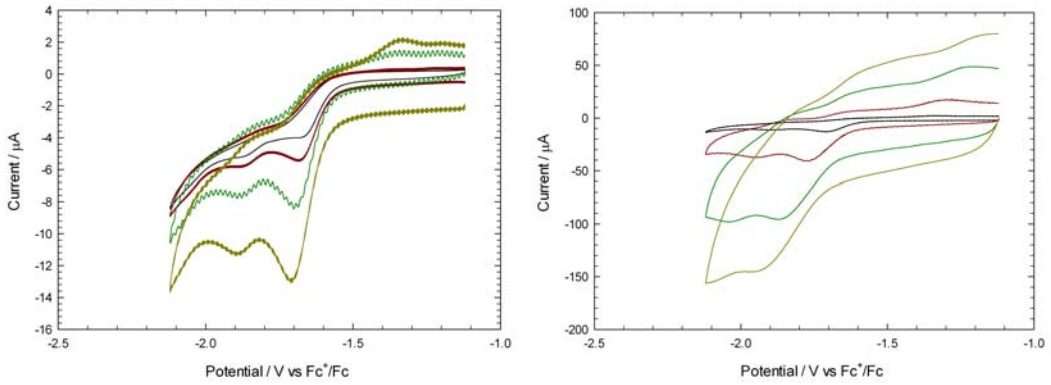

(a) v=0.01, 0.02, 0.05, 0.1 Vs^{-1} (b) v=0.1, 1.0, 5.0, 10.0 Vs^{-1}

Figure 140: Cyclic voltammetry of $Fe_3(\mu\text{-edt})_2(CO)_6PPh_3$ (0.5 mM) in DCM-$[NBu_4][PF_6]$ (glassy carbon electrode; V vs Fc^+/Fc)

5.3.5 Electrochemistry of $Fe_3(\mu\text{-edt})_2(CO)_6PPh_3$ in the absence of protons, in MeCN

The CV of the mono-substituted tri-iron complex has also been obtained in the coordinating solvent MeCN (Figure 141). The first reduction of the complex occurred at -1.49 V. Two small peaks are present at more negative potentials, followed by a larger reduction peak at -2.3 V. On the return scan several small re-oxidation peaks are observed. The sloped oxidation peak at 0.0 V is only present after sweeping to negative potentials first. The first oxidation of the complex occurs at 0.21 V and is irreversible.

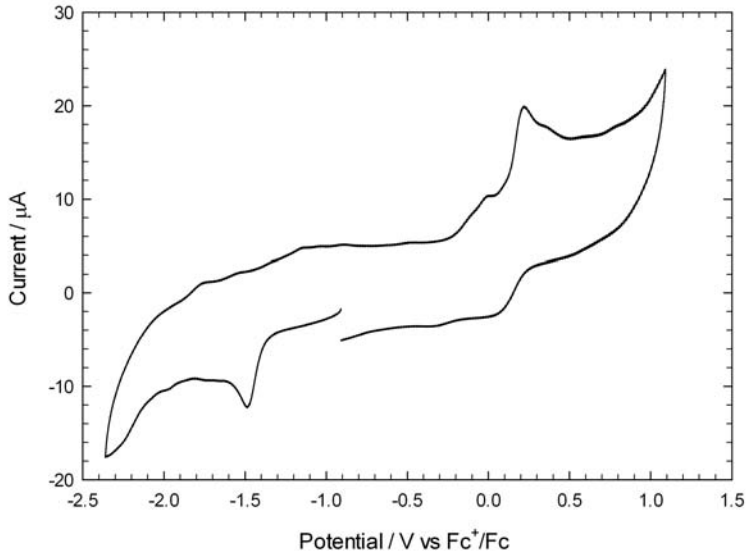

Figure 141: Cyclic voltammetry of $Fe_3(\mu\text{-edt})_2(CO)_6PPh_3$ (0.5 mM) in MeCN-$[NBu_4][PF_6]$ (v=0.1 Vs^{-1}, glassy carbon electrode; V vs Fc^+/Fc)

The first oxidation and reduction of the mono-substituted complex has been analysed at varying scan rates (Figures 142 and 143 respectively). At fast scan rates the oxidation process exhibited a re-reduction peak at ca. -0.05 V, and the behaviour is similar to that observed in the non-coordinating solvent DCM. This indicates that the rate of coordination of MeCN to the oxidation product is slow compared to the fast scan rate used. At fast scan rates, the reduction process exhibited a re-oxidation process at -1.15 V.

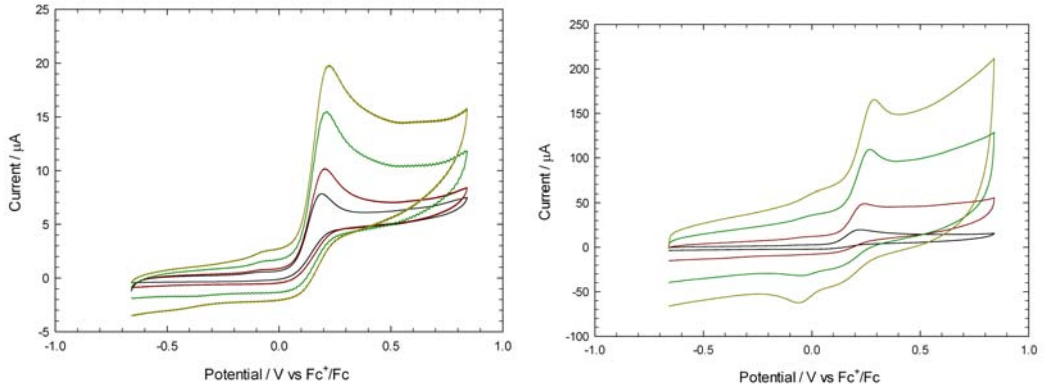

(a) v=0.01, 0.02, 0.05, 0.1 Vs^{-1} (b) v=0.1, 1.0, 5.0, 10.0 Vs^{-1}

Figure 142: Cyclic voltammetry of $Fe_3(\mu\text{-edt})_2(CO)_6PPh_3$ (0.5 mM) in MeCN-$[NBu_4][PF_6]$ (glassy carbon electrode; V vs Fc^+/Fc)

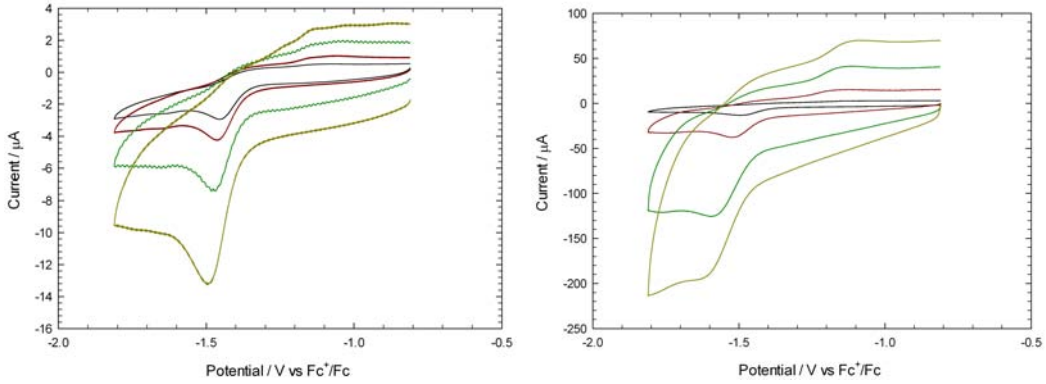

(a) v=0.01, 0.02, 0.05, 0.1 Vs^{-1} (b) v=0.1, 1.0, 5.0, 10.0 Vs^{-1}

Figure 143: Cyclic voltammetry of $Fe_3(\mu\text{-edt})_2(CO)_6PPh_3$ (0.5 mM) in MeCN-$[NBu_4][PF_6]$ (glassy carbon electrode; V vs Fc^+/Fc)

5.3.6 Electrochemistry of $Fe_3(\mu\text{-edt})_2(CO)_5(PPh_3)_2$ in the absence of protons, in DCM

The CV of the di-substituted tri-iron complex $Fe_3(\mu\text{-edt})_2(CO)_5(PPh_3)_2$ in DCM is shown in Figure 144. The oxidation behaviour is remarkably similar to the unsubstituted and mono-substituted complexes, with a shift in the peak positions to lower potentials due to the increased electron density on the Fe centres. However, the reduction behaviour is strikingly different with a peak height consistent with a two electron uptake. The positions of the reductions are further negative than the unsubstituted and mono-substituted complexes due to the two PPh_3 ligands pushing more electron density on to the Fe centres. The first reduction of the complex is at -1.82 V, followed by a small peak at -2.00 V, and a larger reduction process at -2.23 V.

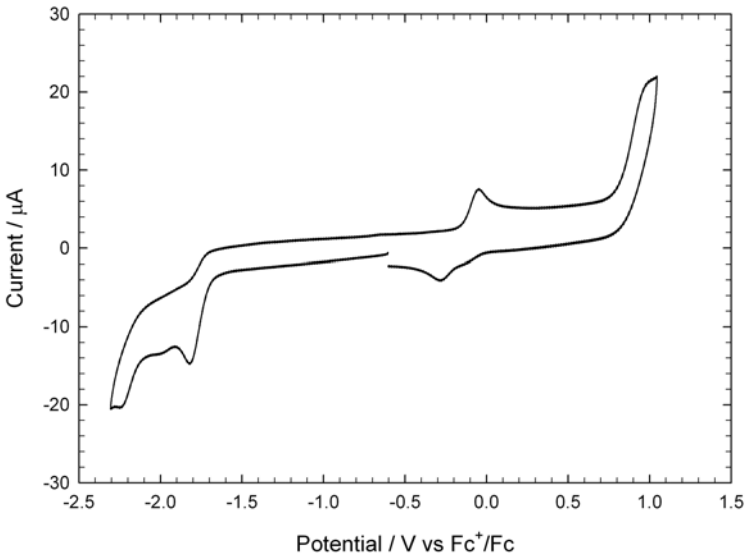

Figure 144: Cyclic voltammetry of $Fe_3(\mu\text{-edt})_2(CO)_5(PPh_3)_2$ (0.5 mM) in DCM-$[NBu_4][PF_6]$ (v=0.1 Vs^{-1}, glassy carbon electrode; V vs Fc^+/Fc)

The peak height of the first oxidation is smaller than that observed for the unsubstituted and mono-substituted complexes of the same concentration (Figure 159 illustrates this clearly). The di-substituted complex was not crystalline, unlike the other two complexes. It is therefore assumed that the sample had some solvents in it, or the complex may have decomposed. Note, the concentrations stated herein assume that the sample was pure complex.

The first oxidation of the complex is shown in Figure 145. The behaviour is similar to that seen for the unsubstituted and mono-substituted tri-iron complexes, with the re-reduction being two overlapping processes.

To probe the nature of the first reduction further the scan rate was varied (Figure 146). Normalising the peak currents indicated that the peak height remained consistent with a 2-electron uptake over the range of scan rates. This indicates that over these electrochemical timescales the di-substituted complex either does not undergo a potential inversion mechanism analogous to that observed for $Fe_2(\mu\text{-edt})(CO)_6$, or the rearrangement is faster than the scan rates used herein al-

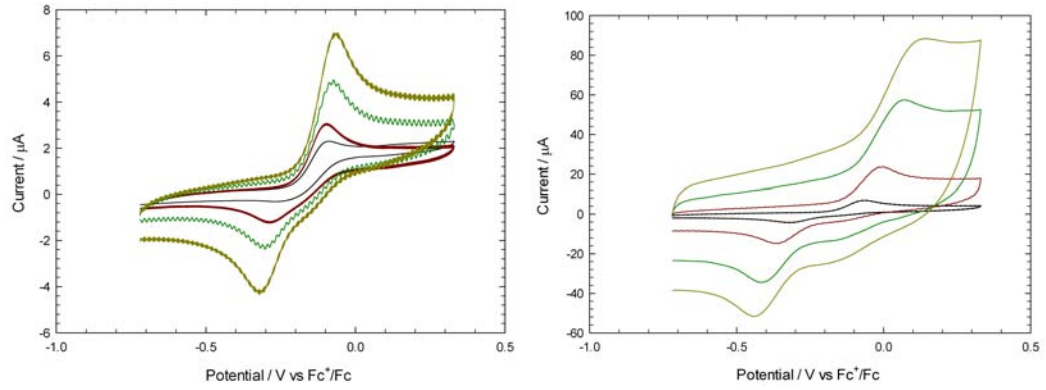

(a) v=0.01, 0.02, 0.05, 0.1 Vs^{-1} (b) v=0.1, 1.0, 5.0, 10.0 Vs^{-1}

Figure 145: Cyclic voltammetry of $Fe_3(\mu\text{-edt})_2(CO)_5(PPh_3)_2$ (0.5 mM) in DCM-$[NBu_4][PF_6]$ (glassy carbon electrode; V vs Fc^+/Fc)

low us to detect. The 2-electron uptake may be due to greater structural rearrangement of the di-substituted complex upon reduction, the greater electron donating ability and steric constraints of the bulky triphenylphosphine group may favour bond cleavage or ligand loss, allowing further electron uptake.

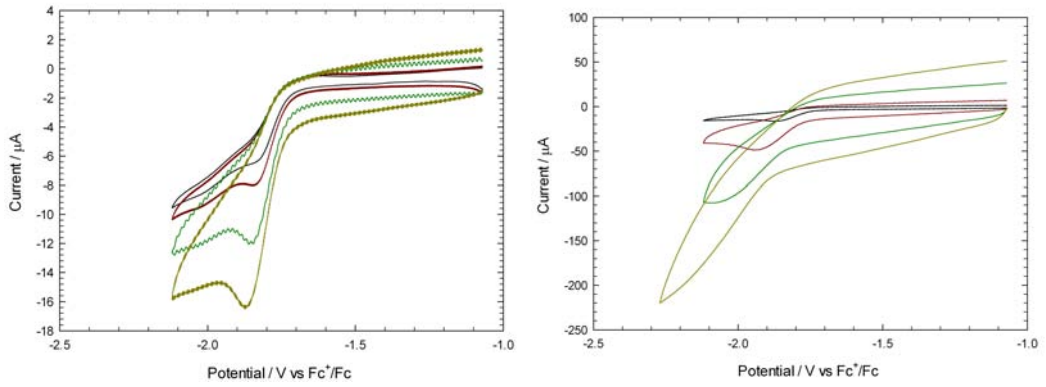

(a) v=0.01, 0.02, 0.05, 0.1 Vs^{-1} (b) v=0.1, 1.0, 5.0, 10.0 Vs^{-1}

Figure 146: Cyclic voltammetry of $Fe_3(\mu\text{-edt})_2(CO)_5(PPh_3)_2$ (0.5 mM) in DCM-$[NBu_4][PF_6]$ (glassy carbon electrode; V vs Fc^+/Fc)

5.3.7 Electrochemistry of $Fe_3(\mu\text{-edt})_2(CO)_5(PPh_3)_2$ in the absence of protons, in CO-saturated DCM

The di-substituted complex has also been analysed under a CO atmosphere (Figure 147). There were minor changes in the behaviour of the complex, such as a more shallow gradient of the first reduction peak, as well as a small reduction peak at -2.05 V. A new oxidation peak is also present at 0.66 V.

The scan rate analysis of the first oxidation and first reduction of the complex were repeated under CO (Figures 148 and 149). There were only minor differences in the behaviours compared to

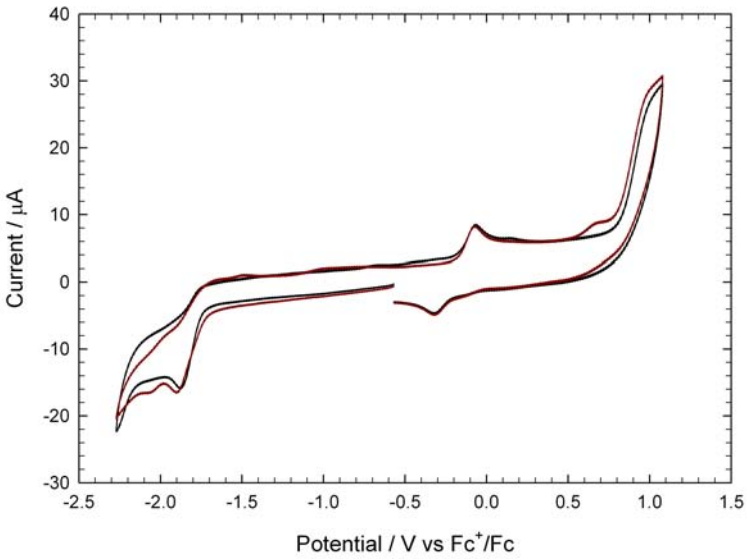

Figure 147: Cyclic voltammetry of $Fe_3(\mu\text{-edt})_2(CO)_5(PPh_3)_2$ (0.5 mM) in DCM-$[NBu_4][PF_6]$ saturated with CO (black line) and Ar (red line) (v=0.1 Vs^{-1}, glassy carbon electrode; V vs Fc^+/Fc)

the Ar saturated system.

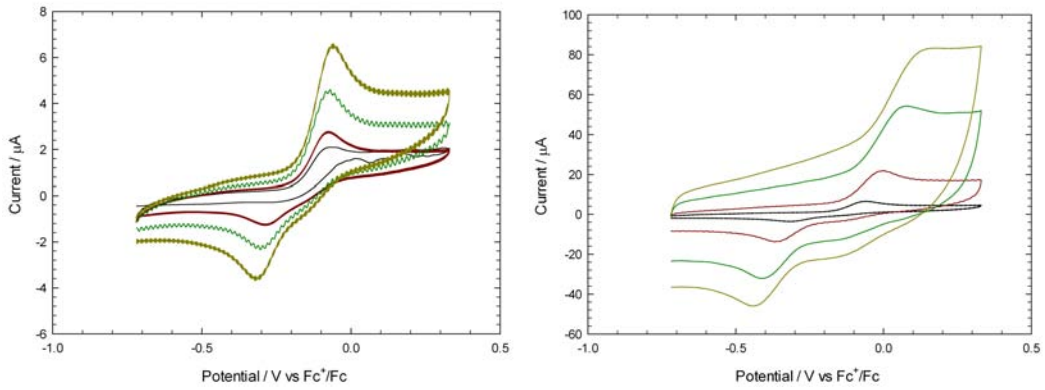

(a) v=0.01, 0.02, 0.05, 0.1 Vs^{-1} (b) v=0.1, 1.0, 5.0, 10.0 Vs^{-1}

Figure 148: Cyclic voltammetry of $Fe_3(\mu\text{-edt})_2(CO)_5(PPh_3)_2$ (0.5 mM) in CO-saturated DCM-$[NBu_4][PF_6]$ (glassy carbon electrode; V vs Fc^+/Fc)

5.3.8 Summary and discussion

To understand the effect of adding the third iron centre, it is useful to compare directly to the analogous edt-bridged di-iron complexes under the same experimental conditions. A comparison between the unsubstituted tri-iron complex, and the analogous unsubstituted di-iron complex $Fe_2(\mu\text{-edt})(CO)_6$ is shown in Figure 150. Moving from a di-iron to a tri-iron system has shifted the first reduction potential 0.44 V less negative. Interestingly the first oxidation of the tri-iron complex also requires less energy than the di-iron complex. This implies that the energy gap between the HOMO and LUMO is smaller in the tri-iron complex than the di-iron complex.

A comparison of the mono-substituted complex and the analogous di-iron complex $Fe_2(\mu\text{-edt})$-

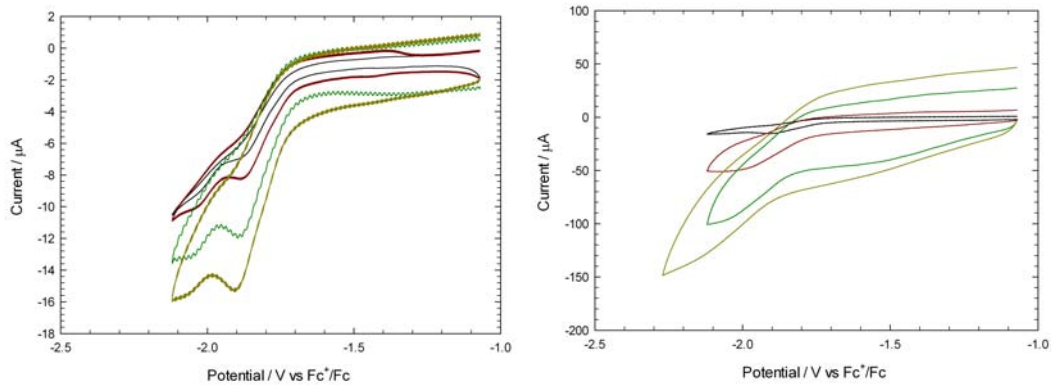

(a) v=0.01, 0.02, 0.05, 0.1 Vs^{-1} (b) v=0.1, 1.0, 5.0, 10.0 Vs^{-1}

Figure 149: Cyclic voltammetry of $Fe_3(\mu\text{-edt})_2(CO)_5(PPh_3)_2$ (0.5 mM) in CO-saturated DCM-$[NBu_4][PF_6]$ (glassy carbon electrode; V vs Fc^+/Fc)

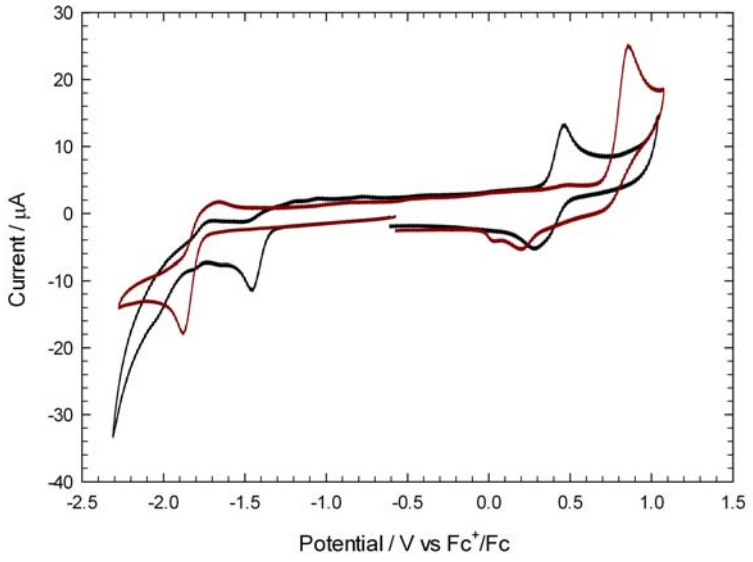

Figure 150: Cyclic voltammetry of $Fe_3(\mu\text{-edt})_2(CO)_7$ (0.5 mM, black line) and $Fe_2(\mu\text{-edt})(CO)_6$ (0.5 mM, red line) in DCM-$[NBu_4][PF_6]$ (v=0.1 Vs^{-1}, glassy carbon electrode; V vs Fc^+/Fc)

$(CO)_5PPh_3$ is shown in Figure 151. As with the unsubstituted complexes, moving from di- to tri-iron results in a positive shift in the reduction potential; the shift is 0.33 V. The HOMO-LUMO gap is again smaller in the tri-iron complex.

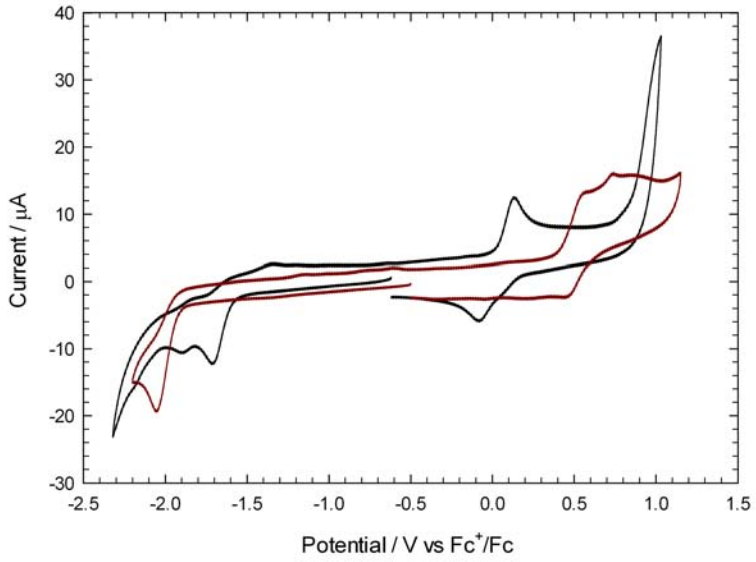

Figure 151: Cyclic voltammetry of $Fe_3(\mu\text{-edt})_2(CO)_6PPh_3$ (0.5 mM, black line) and $Fe_2(\mu\text{-edt})(CO)_5PPh_3$ (0.5 mM, red line) in DCM-$[NBu_4][PF_6]$ (v=0.1 Vs^{-1}, glassy carbon electrode; V vs Fc^+/Fc)

As with the unsubstituted and mono-substituted complexes, a comparison can be made with the analogous di-iron complex $Fe_2(\mu\text{-edt})(CO)_4(PPh_3)_2$ as shown in Figure 152. The tri-iron complex is again reduced at a significantly lower potential than the di-iron, this time the difference is 0.49 V. Also, the HOMO-LUMO gap is smaller in the tri-iron complex.

The related tetra-iron complex $Fe_4(CO)_8\mu_3\text{-}(SCH_2)_3CMe_2$ was found to undergo a reversible one-electron reduction at -1.22 V followed by a quasi-reversible one-electron reduction at -1.58 V in DCM. As the formal assignment of oxidation states for the tetra-iron complex is Fe(I)Fe(II)Fe(II)Fe(I), the first reduction was assigned as the addition of an electron into the anti-bonding σ^* orbital of the inner Fe(II)Fe(II) bond. In reality a shift in the entire IR band profile on reduction indicated that the increased electron density was distributed over all four iron centres, indicating a large degree of delocalisation. The second reduction resulted in the cleavage of the central FeFe bond concomitant with rotation of the carbonyls on the outer iron centres, forming bridging carbonyls across each Fe(inner)Fe(outer) pair. The presence of bridging carbonyls was confirmed using spectroelectrochemistry and recently confirmed as the more energetically favourable product by DFT calculations. The electrochemical quasi-reversibility of the second reduction was consistent with a large structural change between reactant and product. The two-electron reduced product was assigned as a Fe(I)Fe(I)Fe(I)Fe(I) cluster. Formally the oxidation states of the Fe centres of the tri-iron complexes are Fe(I)Fe(II)Fe(I), so addition of the first electron results in an Fe(I)Fe(I)Fe(I) species. It is perhaps most appropriate then to compare the first reduction potential of $Fe_3(\mu\text{-edt})_2(CO)_7$ with the

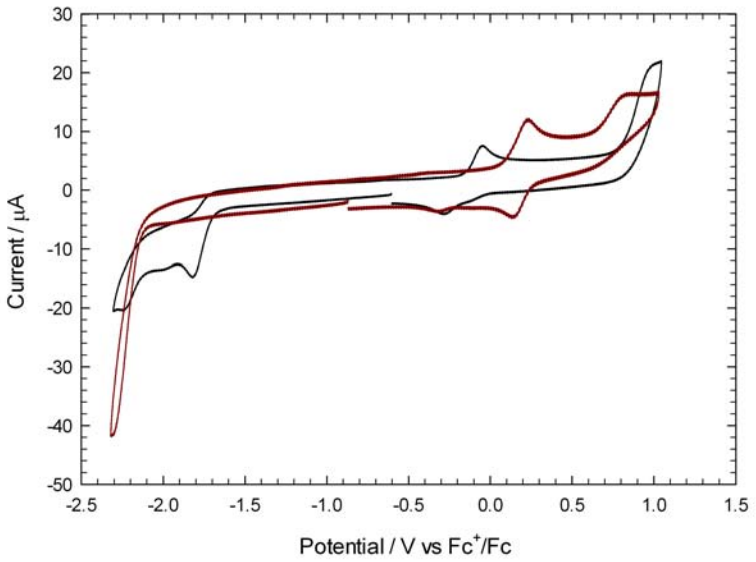

Figure 152: Cyclic voltammetry of $Fe_3(\mu\text{-edt})_2(CO)_5(PPh_3)_2$ (0.5 mM, black line) and $Fe_2(\mu\text{-edt})(CO)_4(PPh_3)_2$ (0.5 mM, red line) in DCM-$[NBu_4][PF_6]$ (v=0.1 Vs^{-1}, glassy carbon electrode; V vs Fc^+/Fc)

second reduction of the tetra-iron complex, as the same oxidation states are under investigation. The first reduction peak of $Fe_3(\mu\text{-edt})_2(CO)_7$ and the second of the tetra-iron complex are found at -1.47 and -1.57 V respectively, which are comparable. Preliminary DFT molecular orbital calculations have now been performed by Michael Richmond at the University of North Texas for the tri-iron complexes (Figures 153 - 158; for the experimental procedure used see Section 2.5). The LUMO of the tri-iron complexes is an anti-bonding orbital delocalised over all three iron centres. The HOMO, on the other hand, is a bonding orbital centred on the Fe-Fe bond away from the semi-bridging CO ligand.

The tri-iron complexes offer a comparison between differing levels of electron donation from ligands. A comparison of the CVs of each of the three tri-iron complexes are shown in Figure 159. The first reduction of the unsubstituted tri-iron complex occurs at -1.47 V. Upon a substitution of one CO with a PPh_3 ligand, the first reduction is shifted 0.25 V more negative. Upon a second substitution, the reduction potential is shifted a further 0.10 V more negative. These shifts in potential are consistent with what has been found for di-iron complexes, such as the edt-bridged di-iron complexes presented.

Interestingly, upon the substitution of the ligand the HOMO and LUMO do not shift by the same degree. On going from the unsubstituted to the mono-substituted complex the HOMO shifts by 0.25 V, whereas the LUMO shifts by 0.33 V; and on going from the mono-substituted to the di-substituted complex the HOMO shifts by 0.10 V, whereas the LUMO shifts by 0.17 V. Thus, the phosphine ligand is having a larger influence on the LUMO than the HOMO. This is consistent with the DFT calculations above, which show that the LUMO is delocalised over the Fe centres, whereas the HOMO is localised on the two Fe centres away from the phosphine substitution in the

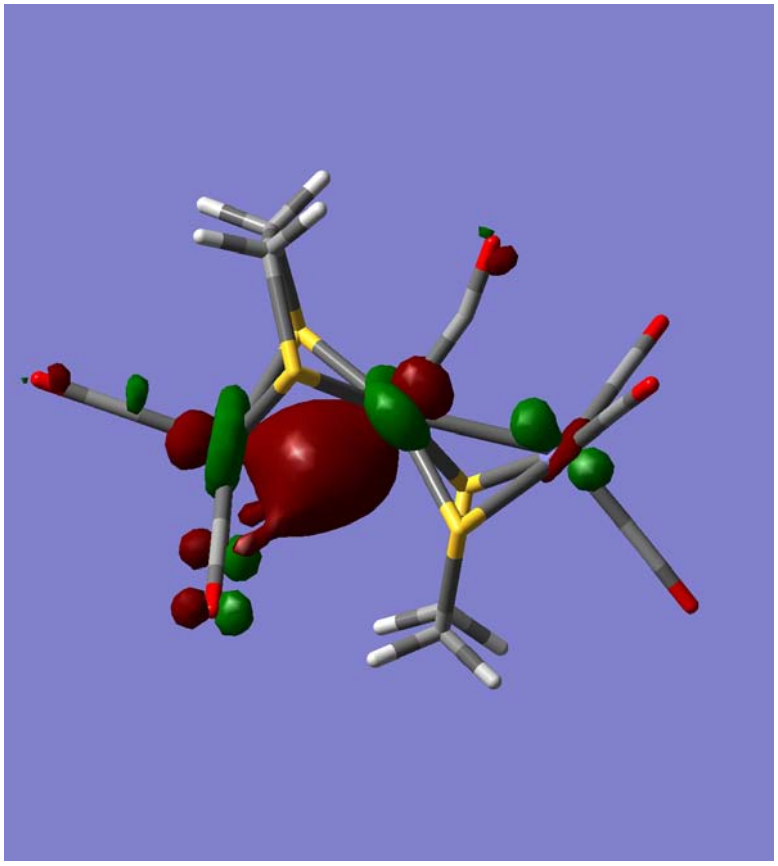

Figure 153: DFT molecular orbital calculation for the HOMO of $Fe_3(\mu\text{-edt})_2(CO)_7$

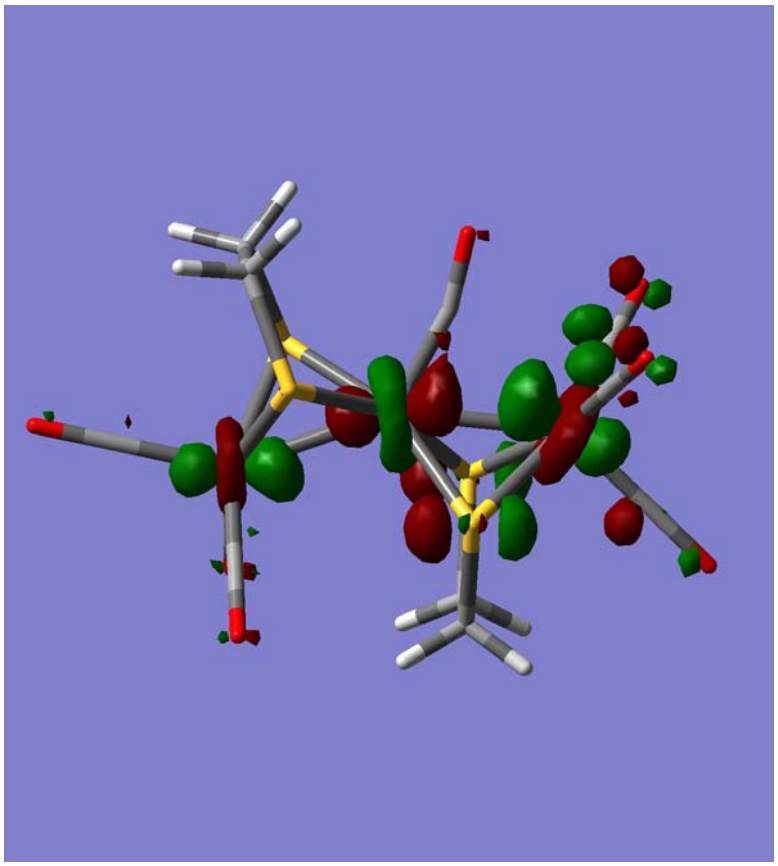

Figure 154: DFT molecular orbital calculation for the LUMO of $Fe_3(\mu\text{-edt})_2(CO)_7$

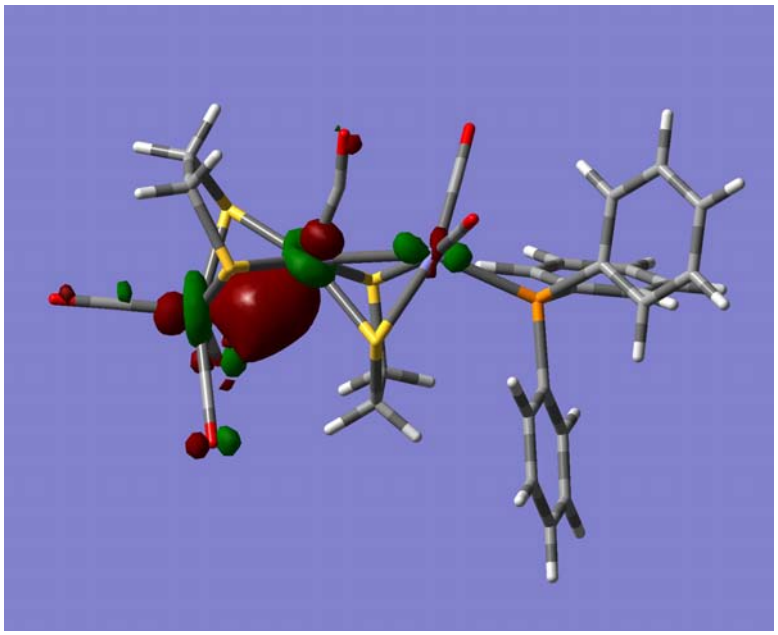

Figure 155: DFT molecular orbital calculation for the HOMO of $Fe_3(\mu\text{-edt})_2(CO)_6PPh_3$

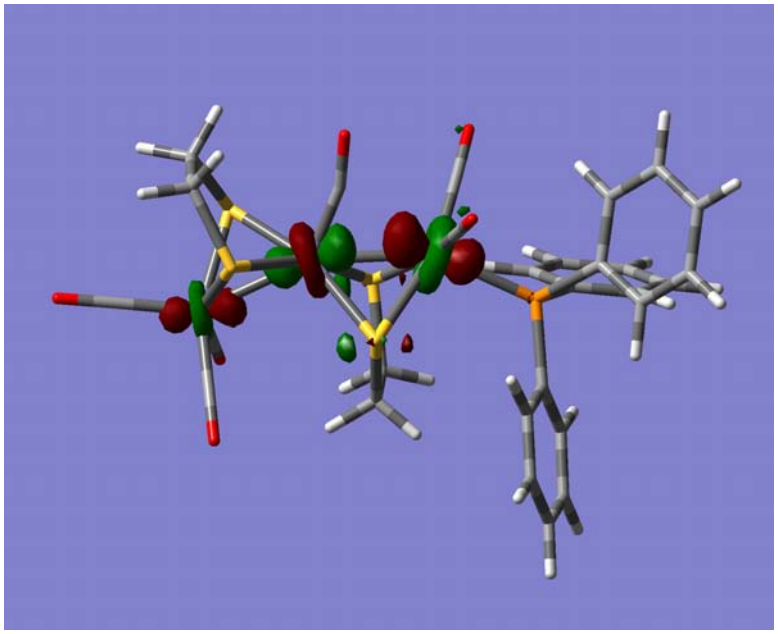

Figure 156: DFT molecular orbital calculation for the LUMO of $Fe_3(\mu\text{-edt})_2(CO)_6PPh_3$

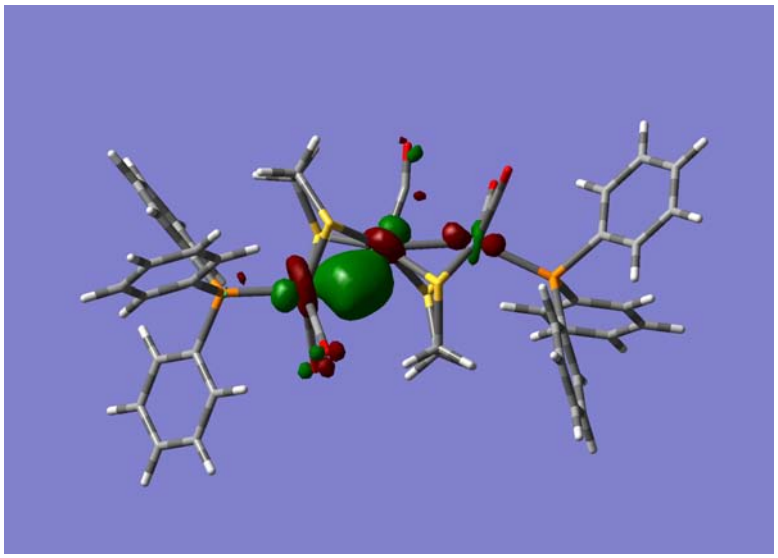

Figure 157: DFT molecular orbital calculation for the HOMO of $Fe_3(\mu\text{-edt})_2(CO)_5(PPh_3)_2$

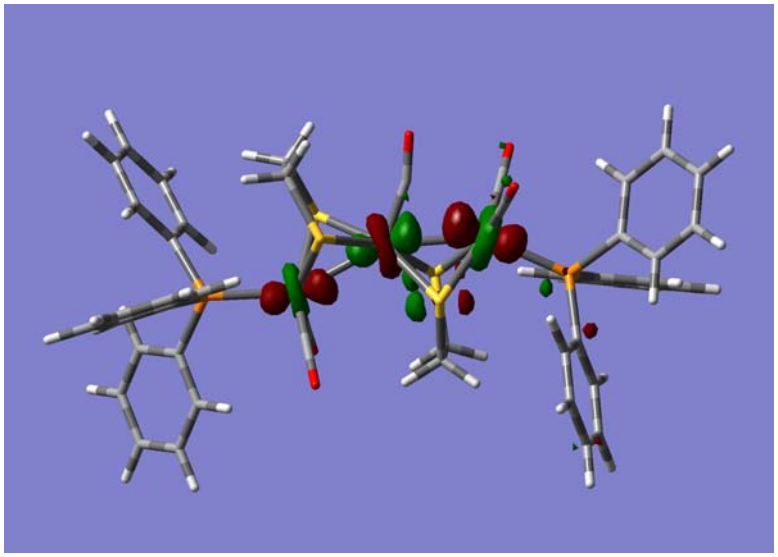

Figure 158: DFT molecular orbital calculation for the LUMO of $Fe_3(\mu\text{-edt})_2(CO)_5(PPh_3)_2$

mono-substituted complex.

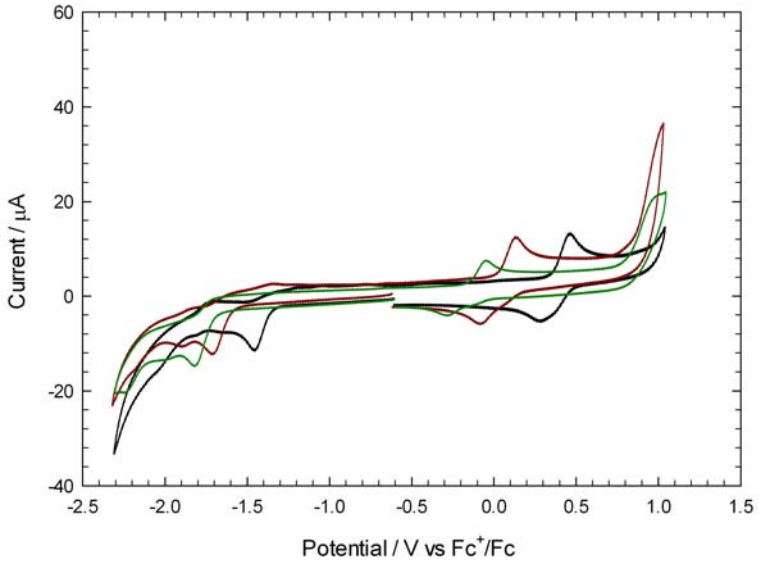

Figure 159: Cyclic voltammetry of $Fe_3(\mu\text{-edt})_2(CO)_7$ (0.5 mM, black line), $Fe_3(\mu\text{-edt})_2(CO)_6PPh_3$ (0.5 mM, red line), and $Fe_3(\mu\text{-edt})_2(CO)_5(PPh_3)_2$ (0.5 mM, green line) in DCM-$[NBu_4][PF_6]$ (v=0.1 Vs^{-1}, glassy carbon electrode; V vs Fc^+/Fc)

The unsubstituted and mono-substituted tri-iron complexes have been found to undergo a 1-electron reduction process to form Fe(I)Fe(I)Fe(I) species, and the di-substituted complex undergoes a 2-electron reduction process. The reduction processes of each complex are irreversible, implying a structural rearrangement of the complex after reduction. Studying the complexes under a CO atmosphere revealed that this rearrangement is not loss of a CO ligand. Interestingly, the irreversibility of the reduction process means that if the complexes are found to be catalytic at the first reduction, it could be the rearranged species which is the catalyst, rather than the singly reduced complex. This will be investigated later in this chapter.

The HOMO-LUMO separation was significantly smaller in the tri-iron complexes than the di-iron analogues. The H-cluster is an exceptional catalyst for both hydrogen oxidation and proton reduction, implying the HOMO-LUMO separation must be small. Thus, along with the mixed valence and semi-bridging CO, the tri-iron complexes exhibit another attribute believed to be important to the functionality of the H-cluster.

It has been found that the complexes exhibit different behaviour in DCM and MeCN. The oxidation of the complexes in MeCN is irreversible, whereas it is quasi-reversible in DCM. The potential of the first reduction process in MeCN is less negative than in DCM. Also, the HOMO-LUMO separation of the complexes is greater in DCM than in MeCN. These factors suggest the relative stabilities of the anion / cation products are different in the different solvent environments.

The shape of the first oxidation couple peak of each of the complexes is not what would be expected for a reversible reaction, as the reduction component appears to be two overlapping processes. This is presumably caused by a minor re-arrangement occurring after oxidation, which leads to the

reduction of the rearranged species taking place at a slightly lower potential than oxidation. Possible reasons that have been investigated for this behaviour are:

- The semi-bridging CO becomes a bridging CO after oxidation, making the complex more stable and therefore more difficult to reduce
- The complex rearranges from the anti- to the syn-arrangement upon oxidation
- Upon oxidation a disproportionation mechanism is established with the singly oxidised complex complex disproportionating into the neutral and dicationic species

The first explanation is unlikely based on the oxidation study of the mono- and di-substituted complexes (Section 5.2), the bridging CO signal is lost upon chemical oxidation by ferrocenium, although this could be explained by the different timescale of the CV compared to the chemical oxidation. The second explanation would explain the loss of the CO-bridging signal from the IR spectrum upon chemical oxidation, and it is feasible that the syn-arrangement would require slightly more energy to be reduced. This rearrangement has been observed for the analogous tri-ruthenium complex on heating, but not for the tri-iron complexes. This suggests that the energy barrier for rotation is too high to make this a feasible explanation. The third explanation is the most favoured at present. Upon oxidation the complex disproportionates as follows:

$[Fe_3]$ - $e^- \longrightarrow [Fe_3]^+$ (oxidation of neutral complex)

$[Fe_3]^+ + [Fe_3]^+ \rightleftharpoons [Fe_3] + [Fe_3]^{2+}$ (disproportionation)

Then on the reduction sweep there are two species at the electrode which are re-reduced at different potentials:

$[Fe_3]^+ + e \longrightarrow [Fe_3]$ (accounts for the reversible re-reduction peak)

$[Fe_3]^{2+} + 2e \longrightarrow [Fe_3]$ (accounts for the quasireversible re-reduction peak, and shifts with scan rate)

Although not necessarily important for the understanding the catalytic activity of these tri-iron complexes, further work would be necessary to completely understand the nature of this oxidation behaviour. A first approach should use an elecrochemical modelling software such as DigiSim.

5.4 Testing for electrocatalytic reduction of protons by the three tri-iron complexes, using the strong acid $HBF_4.Et_2O$ as the proton source

From the above investigations it was now known that the three tri-iron complexes do not protonate. The reduction potentials of the complexes were also known. Next an investigation into whether the complexes are electrocatalysts towards proton reduction was undertaken.

5.4.1 Testing for electrocatalytic reduction of protons by $Fe_3(\mu\text{-edt})_2(CO)_7$, using the strong acid $HBF_4.Et_2O$ as the proton source, in DCM

The electrocatalytic activity of the unsubstituted complex in DCM using $HBF_4.Et_2O$ as the proton source was tested first. The CVs obtained after subsequent additions of $HBF_4.Et_2O$ are shown in Figure 160. In the presence of 1 molar equivalent of $HBF_4.Et_2O$ the peak current of the first reduction process is twice that of the neutral complex. The remaining CV is very similar to that in the absence of acid, bar a new small reduction feature at -1.80 V, and a decrease in the height of the second major reduction process at -2.05 V.

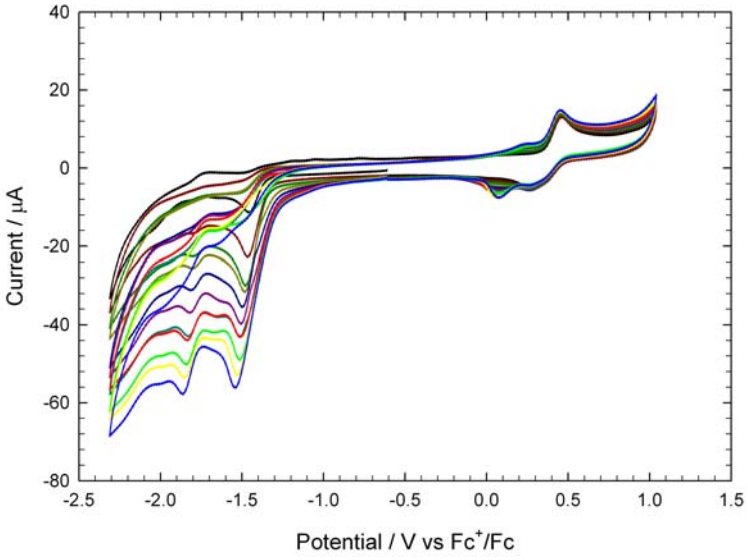

Figure 160: Cyclic voltammetry of $Fe_3(\mu\text{-edt})_2(CO)_7$ (0.5 mM) in DCM-$[NBu_4][PF_6]$ in the absence of acid and in the presence of up to 10 molar equivalents $HBF_4.Et_2O$ in steps of 1 molar equivalent (v=0.1 Vs^{-1}, glassy carbon electrode; V vs Fc^+/Fc)

On further additions of acid the height of the first reduction peak continues to increase, as does the new reduction peak that appeared at -1.80 V after the first addition. The oxidation peak remains largely unchanged from that of the neutral complex. There is a new oxidation feature at 0.23 V and a new reduction feature at 0.08 V. These results indicate that the unsubstituted tri-iron complex is catalytic at ca. -1.5 V. The catalytic mechanism is initiated by the first reduction of the complex.

The oxidation peak of the complex does not shift in potential or change in magnitude in the presence of protons, indicating that protonation of the neutral species does not take place. A shift

in oxidation potential of about +1.0 V would be anticipated upon protonation, due to the removal of electron density from the iron centres on formation of a hydride. The lack of protonation is consistent with the IR study reported in Section 5.2.1 and previous studies, which have shown that all-carbonyl species are not basic enough to protonate in their neutral form. The oxidation and reduction features centred at ca. 0.1 V appear in the presence of excess acid and are believed to be due to an acid-induced decomposition product adsorbing on the electrode.

5.4.2 Testing for electrocatalytic reduction of protons by $Fe_3(\mu\text{-edt})_2(CO)_7$, using the strong acid $HBF_4.Et_2O$ as the proton source, in CO-saturated DCM

It was seen in Section 5.3.2 that voltammetry of the unsubstituted complex under a CO atmosphere revealed numerous differences compared to the experiment performed under Ar. Therefore, as with testing the complex in the absence of protons, the catalytic behaviour has been investigated in a solution saturated with CO (Figure 161). The behaviour was largely the same as under an Ar atmosphere. The main difference being the larger catalytic current at -1.88 V (second reduction process) under CO, suggesting that one of the products of the reduction process is also catalytic in the presence of $HBF_4.Et_2O$. This will be discussed further later in the chapter.

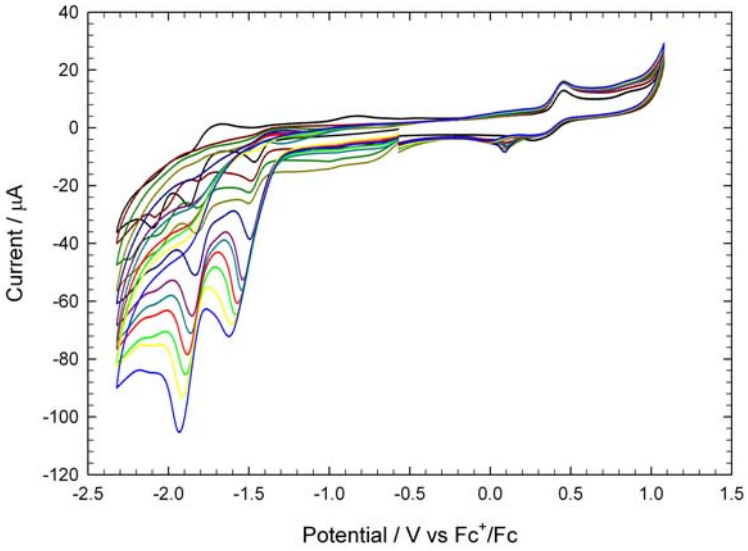

Figure 161: Cyclic voltammetry of $Fe_3(\mu\text{-edt})_2(CO)_7$ (0.5 mM) in DCM-$[NBu_4][PF_6]$ saturated with CO in the absence of acid and in the presence of up to 10 molar equivalents $HBF_4.Et_2O$ in steps of 1 molar equivalent (v=0.1 Vs^{-1}, glassy carbon electrode; V vs Fc^+/Fc)

5.4.3 Testing for electrocatalytic reduction of protons by $Fe_3(\mu\text{-edt})_2(CO)_7$, using the strong acid $HBF_4.Et_2O$ as the proton source, in MeCN

Experiments performed in Section 5.3 indicated that the electrochemical behaviour of the tri-iron complexes differ between the non-coordinating DCM and the coordinating MeCN. To probe these differences further, the additions of $HBF_4.Et_2O$ to the unsubstituted complex were repeated in an

MeCN solvent (under Ar). The CVs obtained are given in Figure 162. On the addition of 1 molar equivalent the first reduction peak height increased. The other reductions are largely unchanged with the exception of a new reduction peak at -1.77 V. The oxidation peak is unchanged, however the second small oxidation peak at 0.55 V has grown.

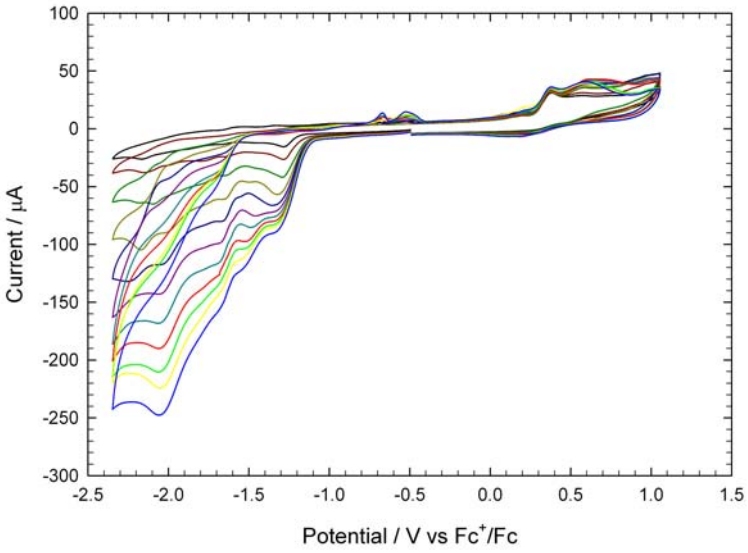

Figure 162: Cyclic voltammetry of $Fe_3(\mu\text{-edt})_2(CO)_7$ (0.5 mM) in MeCN-$[NBu_4][PF_6]$ in the absence of acid and in the presence of up to 10 molar equivalents $HBF_4.Et_2O$ in steps of 1 molar equivalent (v=0.1 Vs^{-1}, glassy carbon electrode; V vs Fc^+/Fc)

On further additions of acid the first reduction continues to grow. The current appears to be approaching a limiting value of approximately 90 μA. As the current approaches this limiting value, a second process appears at -1.47 V and continues to grow on additions of acid. Another reduction process is seen at -1.65 V, which also grows with acid concentration. Finally, there is a further reduction process at -2.05 V, which grows on every addition of acid. Three oxidation features at -0.68, -0.52, and 0.20 V grow with additions of acid. The first oxidation of the complex is unchanged, whereas the second oxidation peak at 0.55 V continues to grow.

These results indicate that the complex is catalytic in the coordinating solvent MeCN. The primary catalytic mechanism is initiated by the reduction of the complex, with the second step of the mechanism presumably a protonation. Once this catalytic mechanism reaches its limiting rate, a second catalytic path is available due to the species which is reduced at ca. -1.47 V.

The differences between DCM and MeCN shall be discussed further in Section 5.4.6.

5.4.4 Testing for electrocatalytic reduction of protons by $Fe_3(\mu\text{-edt})_2(CO)_6PPh_3$, using the strong acid $HBF_4.Et_2O$ as the proton source, in DCM

Electrocatalytic reduction of protons by the mono-substituted complex was tested for next, again using $HBF_4.Et_2O$ as the proton source. The CVs obtained in DCM after additions of the acid are shown in Figure 163. On the first addition of acid the first reduction peak increased considerably.

There is very little else changed in the CV. On further additions of acid the first reduction peak continued to grow with no indication of reaching a limiting current even after 10 molar equivalents were added. In the higher concentrations of acid the second small reduction feature of the neutral complex at -1.90 V now begins to grow. The reduction peak at -0.02 V grows on increasing acid concentration, suggesting there is a process occurring which requires the presence of a strong acid. This peak appears to be present only after scanning to potentials beyond the second oxidation peak.

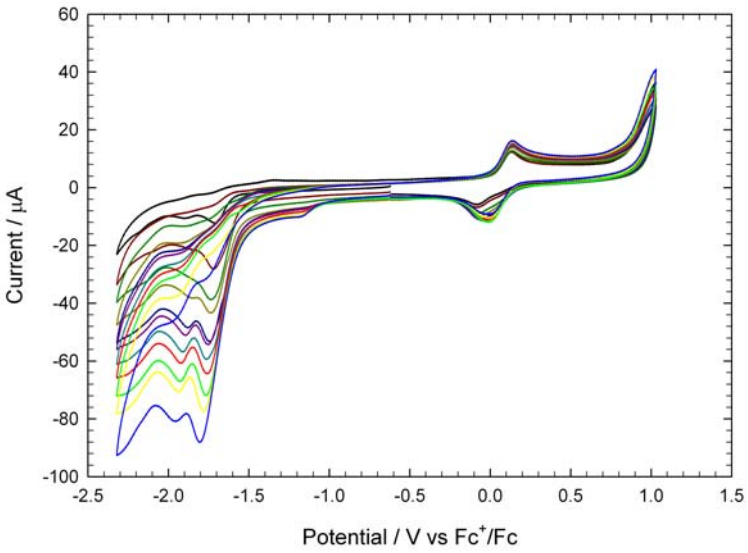

Figure 163: Cyclic voltammetry of $Fe_3(\mu\text{-edt})_2(CO)_6PPh_3$ (0.5 mM) in DCM-$[NBu_4][PF_6]$ in the absence of acid and in the presence of up to 10 molar equivalents $HBF_4.Et_2O$ in steps of 1 molar equivalent (v=0.1 Vs^{-1}, glassy carbon electrode; V vs Fc^+/Fc)

The peak catalytic current is approximately double that of the unsubstituted complex after the addition of 10 molar equivalents $HBF_4.Et_2O$. This indicates that the singly-reduced mono-substituted complex is more readily protonated than the singly-reduced unsubstituted complex, which is consistent with the increased basicity of the Fe centres on the phosphine substitution.

5.4.5 Testing for electrocatalytic reduction of protons by $Fe_3(\mu\text{-edt})_2(CO)_5(PPh_3)_2$, using the strong acid $HBF_4.Et_2O$ as the proton source, in DCM

The CVs of the di-substituted tri-iron complex in DCM after additions of $HBF_4.Et_2O$ are shown in Figure 164. On the first addition of acid the first reduction peak becomes more broad, and grows slightly. The remainder of the CV is largely the same as in the absence of protons.

On further additions of acid a new reduction peak appears at approximately -1.1 V. The first reduction seems to include a shoulder at 0.25 V less negative than the reduction of the neutral complex. On the return scan there is a new oxidation feature growing with additions of acid at 0.2 V, as well as a reduction feature at 0.08 V, which is presumably caused by the oxidation processes.

The protonation study presented in Section 5.2 suggested that $HBF_4.Et_2O$ oxidises the di-substituted complex in the presence of O_2. These electrochemical investigations provide further

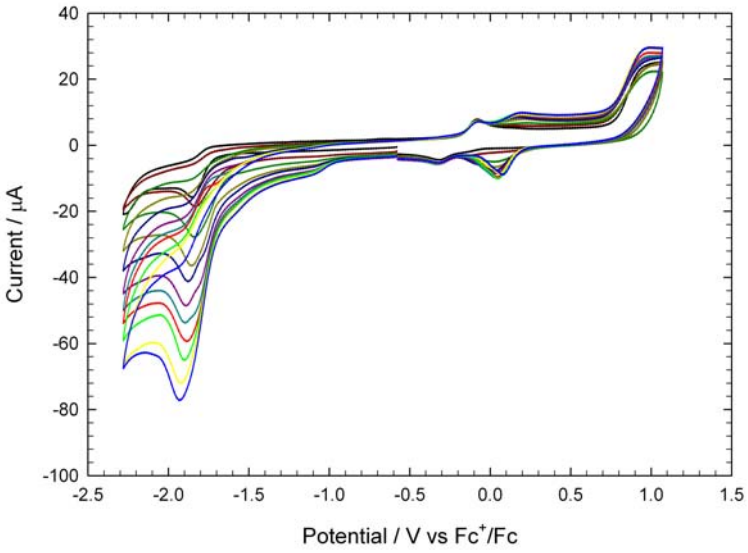

Figure 164: Cyclic voltammetry of $Fe_3(\mu\text{-edt})_2(CO)_5(PPh_3)_2$ (0.5 mM) in DCM-$[NBu_4][PF_6]$ in the absence of acid and in the presence of up to 10 molar equivalents $HBF_4.Et_2O$ in steps of 1 molar equivalent (v=0.1 Vs^{-1}, glassy carbon electrode; V vs Fc^+/Fc)

evidence firstly that $HBF_4.Et_2O$ does not protonate the di-substituted complex, and secondly that O_2 is required for the oxidation of the complex by the acid. If either protonation or oxidation were occurring the potential of the first oxidation of the complex would shift in a positive direction. Note, when the electrochemical experiment was repeated without saturating the solution with Ar, the potential of the oxidation peak did shift positive, implying that O_2 is required for the oxidation mechanism observed in Section 5.2.3.

The reduction peak observed at -1.1 V is in a position that would be expected if the complex had protonated, however, the fact that the first oxidation of the complex remains unchanged negates this explanation of the cause of this peak. It is possible that a small proportion of the complex is indeed protonated and can be catalytic at this potential, thus causing the reduction peak at -1.1 V to grow on additions of acid, and the very slight decrease in the first oxidation peak.

The addition of $HBF_4.Et_2O$ to the di-substituted complex has also been performed in CO-saturated DCM. The CVs obtained were very similar to those obtained under an Ar atmosphere.

5.4.6 Summary and discussion

In summary, the reduced states of the three tri-iron complexes are catalysts for the reduction of protons, the catalytic overpotential being sensitive to the degree of phosphine substitution. As was seen in the protonation study earlier, the complexes were found to not protonate in the presence of $HBF_4.Et_2O$. Thus, the first step of the catalytic mechanism must be a reduction process.

The catalytic activity of the unsubstituted tri-iron complex is compared to that of the analogous di-iron complex $Fe_2(\mu\text{-edt})(CO)_6$ in Figure 165. Both complexes are catalytic after their first reduction. Thus, due to the lower reduction potential of the tri-iron complex, moving from two to three

Fe centres has resulted in a ca. 0.4 V improvement in the overpotential for catalysis.

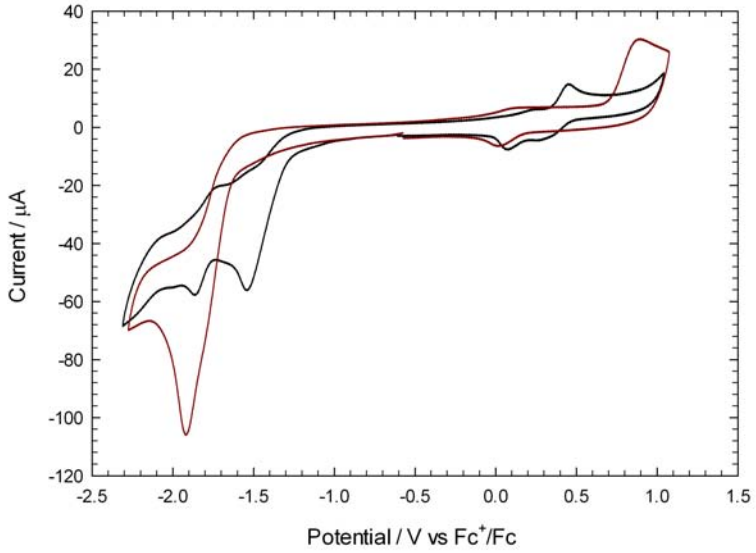

Figure 165: Cyclic voltammetry of $Fe_3(\mu\text{-edt})_2(CO)_7$ (0.5 mM, black line) and $Fe_2(\mu\text{-edt})(CO)_6$ (0.5 mM, red line) in the presence of 10 molar equivalents $HBF_4.Et_2O$ in DCM-$[NBu_4][PF_6]$ (v=0.1 Vs^{-1}, glassy carbon electrode; V vs Fc^+/Fc)

Pickett and co-workers found the catalytic reduction potential of the tetra-iron complex $(Fe_2(CO)_4(MeC(CH_2S)_3))_2$ in the presence of LuH^+ to be -1.2 V vs Ag/AgCl[33]. Assuming the conversion from Ag/AgCl to Fc^+/Fc to be -0.437 V (for MeCN)[21], the tri-iron complex is reduced at ca. 0.13 V less negative than the tetra-iron complex. However, a direct comparison of catalytic performance is not possible due to the different acid used.

A comparison of mono-substituted di-iron and mono-substituted tri-iron complexes is made in Figure 166. As with the unsubstituted complex, due to the less negative reduction potential of the tri-iron complex, the tri-iron complex is catalytic at a lower overpotential than the di-iron complex; again, the improvement is ca. 0.4 V. A comparison with the analogous tetra-iron complex is not yet possible, as investigations in to substituted tetra-iron complexes are not yet available.

The di-substituted complex is compared to the di-iron analogue in Figure 167. As with the unsubstituted and mono-substituted complexes, the overpotential is lower for the tri-iron complex than the di-iron complex. In this case, the improvement is ca. 0.25 V.

A comparison of the catalytic activity of the three tri-iron complexes in the presence of $HBF_4.Et_2O$ is shown in Figure 168. None of the complexes are catalytic until after their first reduction; implying the unsubstituted complex has the lowest overpotential for catalysis. However, the mono-substituted complex has a higher catalytic current in the presence of 10 molar equivalent acid. This is put down to the increased basicity allowing for a faster protonation in the catalytic mechanism. This increased rate of protonation can also be seen in the gradient of the reduction peaks - the mono-substituted is steeper than the unsubstituted complex. It is not possible to make a fair comparison with the di-substituted complex, due the difference in concentration, however it appears that the complex

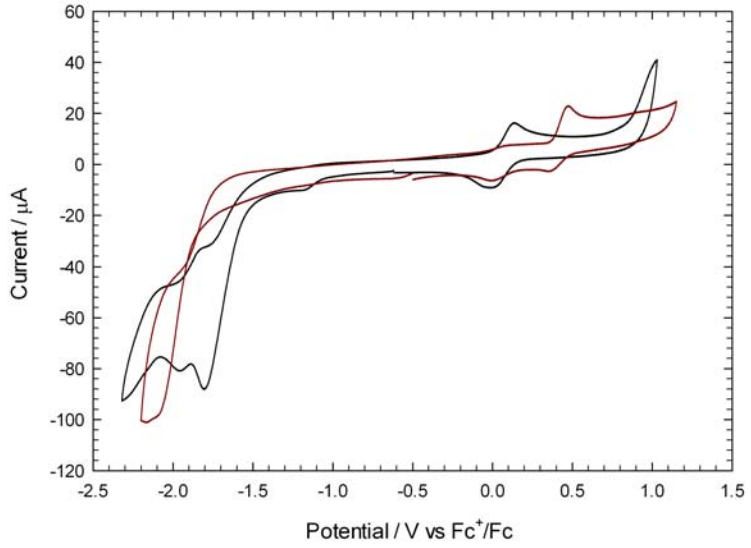

Figure 166: Cyclic voltammetry of $Fe_3(\mu\text{-edt})_2(CO)_6PPh_3$ (0.5 mM, black line) and $Fe_2(\mu\text{-edt})(CO)_5PPh_3$ (0.5 mM, red line) in the presence of 10 molar equivalents $HBF_4.Et_2O$ in DCM-$[NBu_4][PF_6]$ (v=0.1 Vs^{-1}, glassy carbon electrode; V vs Fc^+/Fc)

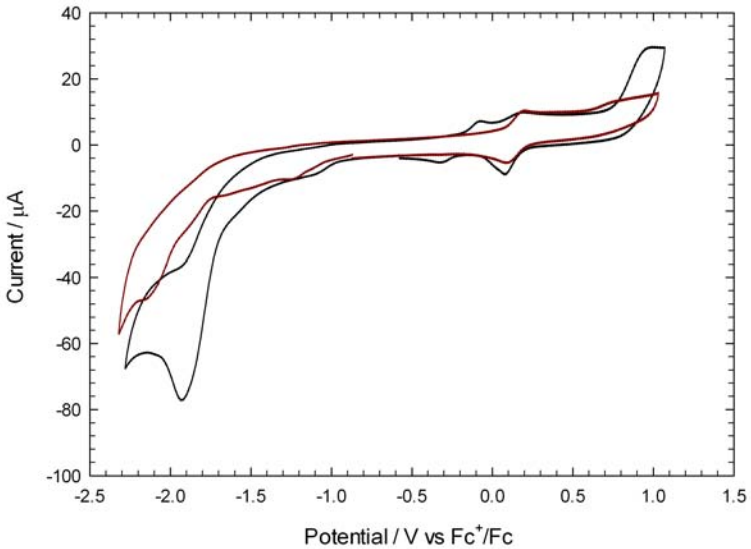

Figure 167: Cyclic voltammetry of $Fe_3(\mu\text{-edt})_2(CO)_5(PPh_3)_2$ (0.5 mM, black line) and $Fe_2(\mu\text{-edt})(CO)_4(PPh_3)_2$ (0.5 mM, red line) in the presence of 10 molar equivalents $HBF_4.Et_2O$ in DCM-$[NBu_4][PF_6]$ (v=0.1 Vs^{-1}, glassy carbon electrode; V vs Fc^+/Fc)

would have an even higher current than the mono-substituted complex. Again, this is likely due to the higher basicity of the iron centres due to the electron donating phosphine ligands.

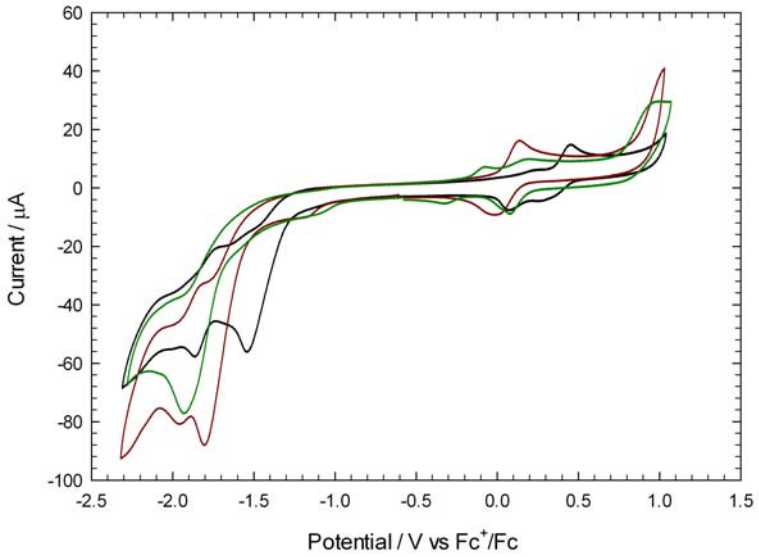

Figure 168: Cyclic voltammetry of $Fe_3(\mu\text{-edt})_2(CO)_7$ (0.5 mM, black line), $Fe_3(\mu\text{-edt})_2(CO)_6PPh_3$ (0.5 mM, red line), and $Fe_3(\mu\text{-edt})_2(CO)_5(PPh_3)_2$ (0.5 mM, green line) in the presence of 10 molar equivalent $HBF_4.Et_2O$ in DCM-$[NBu_4][PF_6]$ (v=0.1 Vs^{-1}, glassy carbon electrode; V vs Fc^+/Fc)

The catalytic mechanism of the unsubstituted complex was simulated using DigiSim and the ECEC catalytic mechanism shown in Figure 169. The simulated mechanism was kept deliberately simple in order to model the first electrocatalytic process only. Even so, the results for the simulation and experiment match well for the parameters shown in Figure 169 and linear plots of the simulated and experimental data are shown in Figure 170. Any discrepancy may be due to the concentration of available protons being slightly less than expected from the volume of $HBF_4.Et_2O$ added, as some HF is lost from solution by evaporation over time. The form of the CVs and the simulation parameters suggest that the rate-determining step is the protonation of the singly reduced complex, rather than the elimination of H_2.

The catalytic mechanism of the mono-substituted complex has also been modeled in DigiSim using the same ECEC mechanism used for the unsubstituted complex. All parameters were kept unchanged, except for the rate constants for the protonation steps which were increased to account for the additional basicity on the Fe centres. The simulated CVs then fit the experimental behaviour well. This gives further evidence that the increased rate of catalysis is due to the increased basicity on the Fe centres. This finding again indicates that there is a balance to be made when increasing the basicity on the Fe centres - although the rate of protonation is improved, the overpotential is worsened.

Performing the experiments on the unsubstituted complex under a CO atmosphere has shown that CO does not inhibit the catalytic mechanism. Indeed, under CO a second catalytic mechanism is also available after the second reduction process at ca. -1.9 V. It was suggested earlier that this

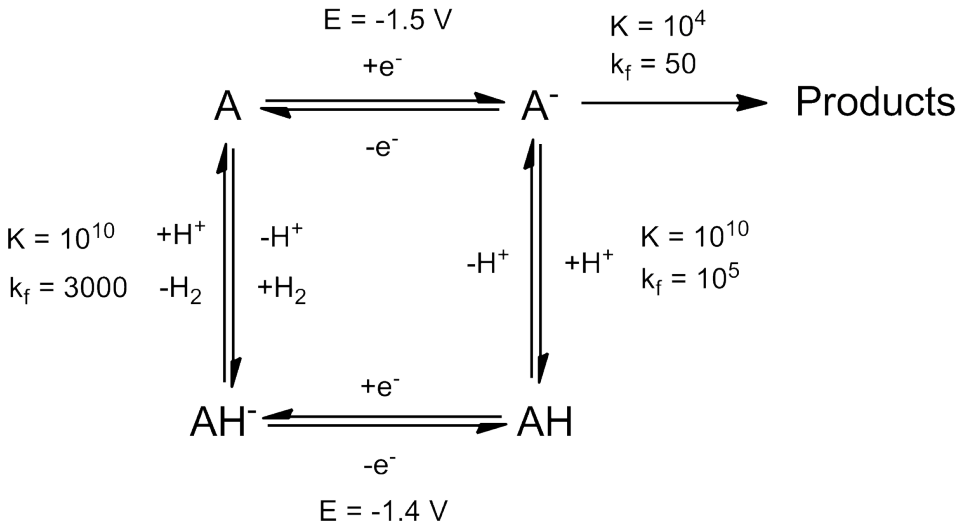

Figure 169: Catalytic mechanism used for DigiSim simulation of $Fe_3(\mu\text{-edt})_2(CO)_7$ (0.5 mM; v=0.1 Vs^{-1}; D = 1x10^{-5} cm^2/s; ; denoted A) in DCM-[NBu_4][PF_6] in the presence of $HBF_4.Et_2O$

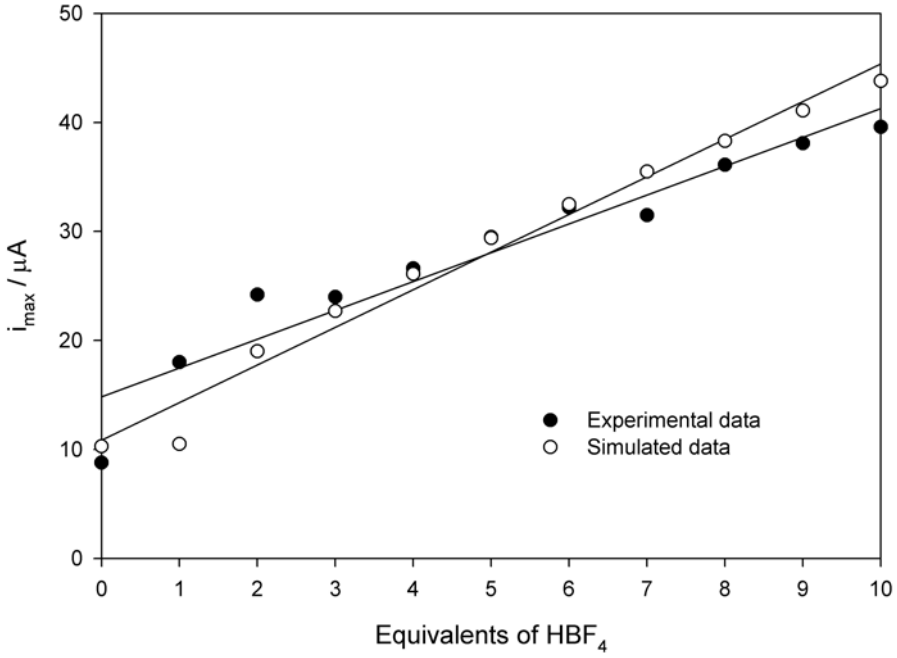

Figure 170: Plots of catalytic peak current from DigiSim simulations and experimentally obtained data of $Fe_3(\mu\text{-edt})_2(CO)_7$ in DCM-[NBu_4][PF_6] in the presence of $HBF_4.Et_2O$ (the straight lines are a guide for the eye)

second reduction process is due to di-iron species generated by the decomposition of the tri-iron complex upon reduction.

The first reductions of the tri-iron complexes are irreversible, this suggests there is a rearrangement in the molecule after reduction. This rearrangement has not yet been identified. It is evident from the experiments performed under CO, that the rearrangement is unlikely to involve CO ligand loss. One possibility is that one of the Fe-Fe bonds is cleaved, perhaps generating mono- and di-iron species. Alternatively, the semi-bridging CO is able to become a bridging CO. The rearrangement could be significant, as it is after the first reduction that the complex is catalytic. This significance would depend upon the lifetime of the singly reduced (not yet rearranged) complex and its rate of protonation.

5.5 Testing for electrocatalytic reduction of protons by the three tri-iron complexes, using the weaker acid HOTs as the proton source

It was now known that the tri-iron complexes are catalytic in the presence of a strong acid, thus it was of interest to investigate whether or not the complexes could catalyse proton reduction in the presence of the weaker acid HOTs.

MeCN has been used as the solvent, as HOTs is not soluble in DCM. Due to limited availability of the the di-substituted complex, only the unsubstituted and mono-substituted complexes have been analysed in the presence of HOTs.

5.5.1 Testing for electrocatalytic reduction of protons by $Fe_3(\mu\text{-edt})_2(CO)_7$, using the weaker acid HOTs as the proton source

The CVs of the unsubstituted complex after additions of HOTs are shown in Figure 171. On the addition of 1 molar equivalent HOTs there is an increase in the current at the potential of the first reduction. On the return scan there is a small oxidation peak at -0.77 V. The features at potentials less negative than the first oxidation of the neutral complex are diminished.

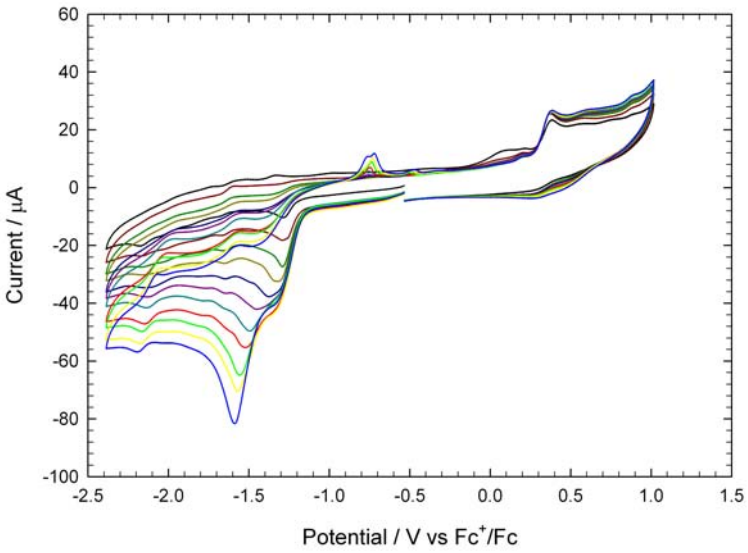

Figure 171: Cyclic voltammetry of $Fe_3(\mu\text{-edt})_2(CO)_7$ (0.5 mM) in MeCN-$[NBu_4][PF_6]$ in the absence of acid and in the presence of up to 10 molar equivalents HOTs in steps of 1 molar equivalent (v=0.1 Vs^{-1}, glassy carbon electrode; V vs Fc^+/Fc)

On further additions of HOTs the first reduction peak continues to grow, reaching a limiting current of -44 μA (including any background current contribution). This limit was confirmed with further additions of HOTs, as shown in Figure 172. Once the limiting current is reached, a second reduction process grows at more negative potentials on further additions of acid. On the return scan, the new oxidation peak at -0.77 V continues to grow; the shape of the peak indicates that it is due to a "stripping" of adsorbed species formed on the electrode surface during reduction.

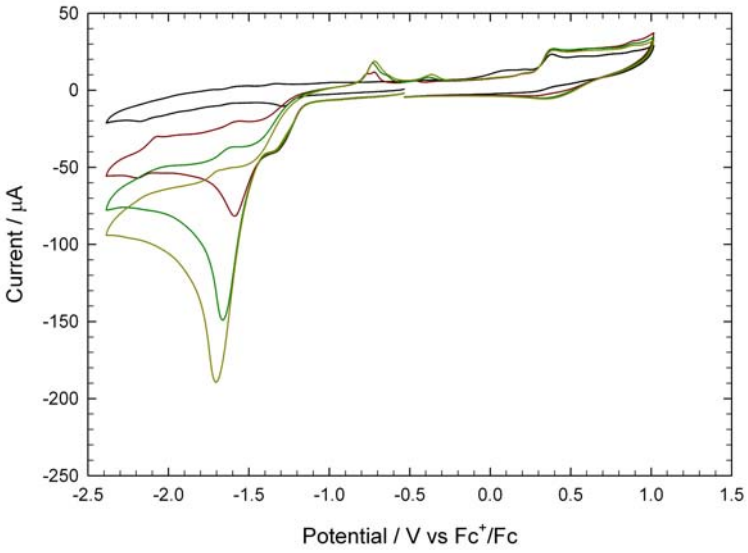

Figure 172: Cyclic voltammetry of $Fe_3(\mu\text{-edt})_2(CO)_7$ (0.5 mM) in MeCN-$[NBu_4][PF_6]$ in the absence of acid and in the presence of 10, 20, 30 molar equivalents HOTs (v=0.1 Vs^{-1}, glassy carbon electrode; V vs Fc^+/Fc)

5.5.2 Testing for electrocatalytic reduction of protons by $Fe_3(\mu\text{-edt})_2(CO)_6PPh_3$, using the weaker acid HOTs as the proton source

The CVs of the mono-substituted complex after additions of HOTs are shown in Figure 173. On the addition of the first equivalent of HOTs the peak current of the first reduction increased. The features at potentials less negative than the first oxidation of the neutral complex are diminished.

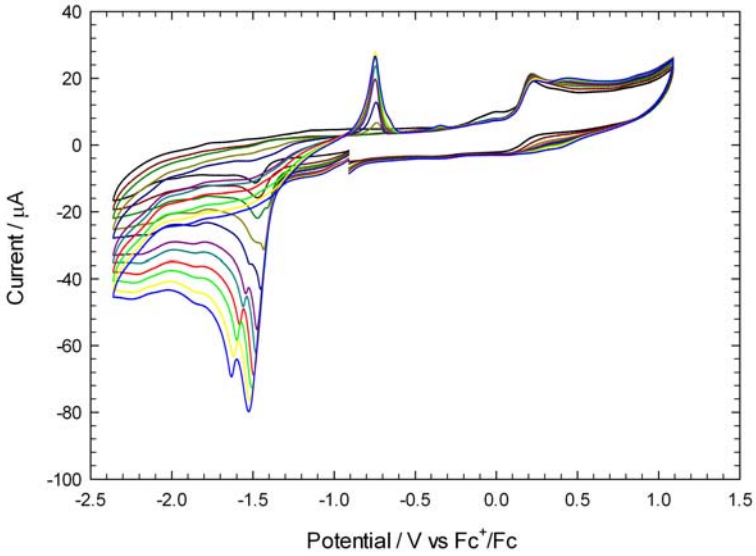

Figure 173: Cyclic voltammetry of $Fe_3(\mu\text{-edt})_2(CO)_6PPh_3$ (0.5 mM) in MeCN-$[NBu_4][PF_6]$ in the absence of acid and in the presence of up to 10 molar equivalents HOTs in steps of 1 molar equivalent (v=0.1 Vs^{-1}, glassy carbon electrode; V vs Fc^+/Fc)

On further additions of HOTs the first reduction peak continues to grow. A second reduction process is also present at slightly more negative potentials. On the return scan a peak at -0.75 V

grows with each addition of acid; as with the unsubstituted complex, the shape of this peak is indicative of a stripping process.

Up to 50 molar equivalents of HOTs were added to the solution (Figure 174). The trends identified above continued. The first reduction peak reached a limit at ca. -100 μA; whereas the second reduction process continued to grow with every addition of acid.

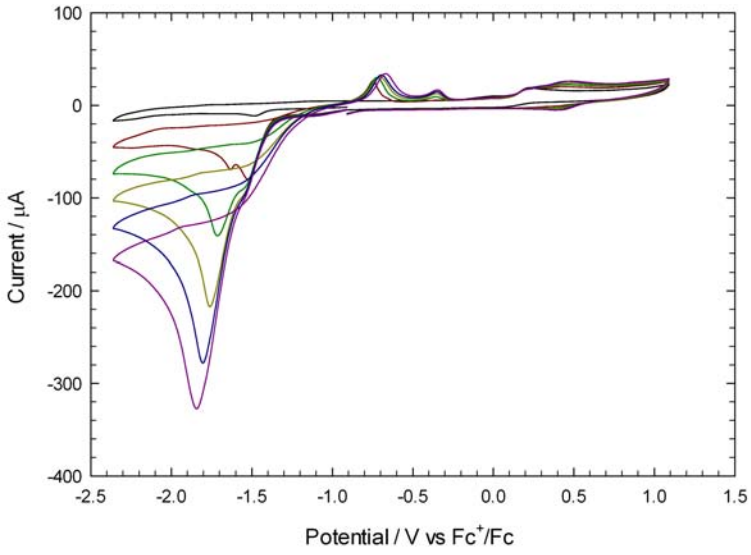

Figure 174: Cyclic voltammetry of $Fe_3(\mu\text{-edt})_2(CO)_6PPh_3$ (0.5 mM) in MeCN-$[NBu_4][PF_6]$ in the absence of acid and in the presence of 10, 20, 30 molar equivalents HOTs (v=0.1 Vs^{-1}, glassy carbon electrode; V vs Fc^+/Fc)

5.5.3 Summary and discussion

The unsubstituted and mono-substituted tri-iron complexes have been found to be catalytic towards proton reduction when the proton source is HOTs. The CVs of the two complexes after the addition of 10 molar equivalents HOTs are shown in Figure 175. As was found for the experiments adding $HBF_4.Et_2O$, there is a balance to be made when adding basicity to the complex - the overpotential is lower for the unsubstituted complex, however the rate of catalysis is also lower.

The CVs of the unsubstituted complex in the presence of $HBF_4.Et_2O$ and in the presence of HOTs are compared in Figure 176. This comparison indicates that the catalytic peaks are the same potentials in the presence of both acids, thus the catalytic mechanisms are the same.

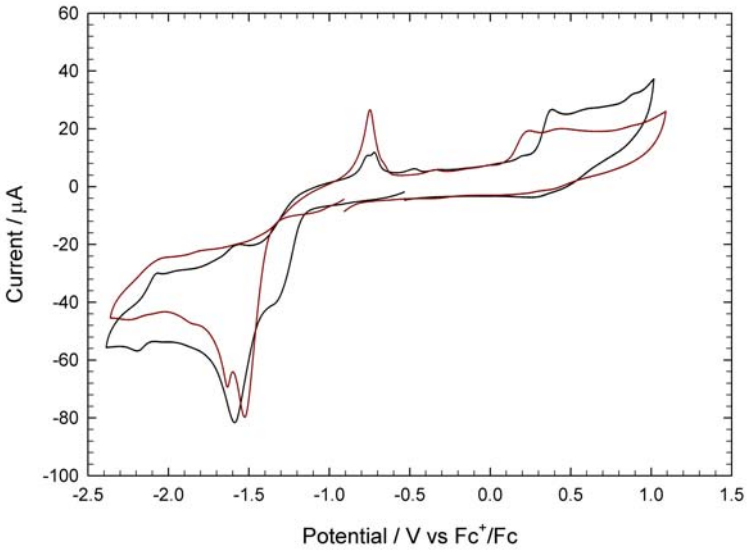

Figure 175: Cyclic voltammetry of $Fe_3(\mu\text{-edt})_2(CO)_7$ (0.5 mM, black line) and $Fe_3(\mu\text{-edt})_2(CO)_6PPh_3$ (0.5 mM, red line) in the presence of 10 molar equivalent HOTs in MeCN-$[NBu_4][PF_6]$ (v=0.1 Vs^{-1}, glassy carbon electrode; V vs Fc^+/Fc)

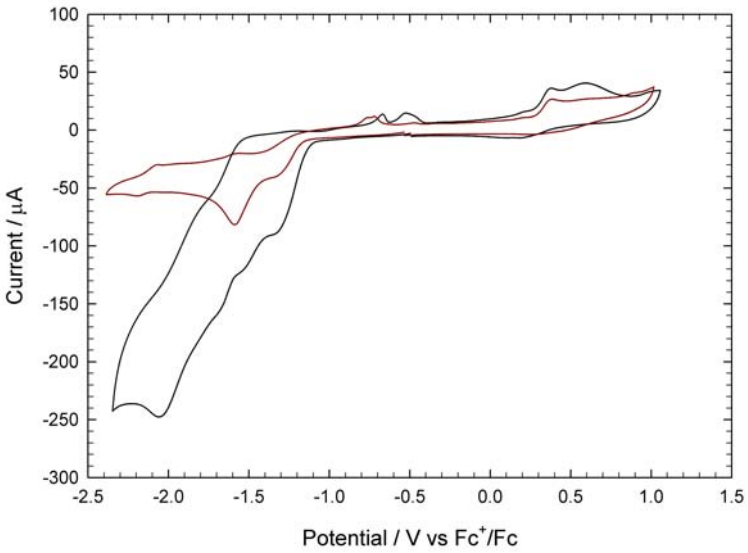

Figure 176: Cyclic voltammetry of $Fe_3(\mu\text{-edt})_2(CO)_7$ (0.5 mM) in the presence of 10 molar equivalent $HBF_4.Et_2O$ (black line) and HOTs (red line) in MeCN-$[NBu_4][PF_6]$ (v=0.1 Vs^{-1}, glassy carbon electrode; V vs Fc^+/Fc)

5.6 Testing for electrocatalytic reduction of protons by the three tri-iron complexes, using the weak acid HOAc as the proton source

The three tri-iron complexes have also been tested for electrocatalytic proton reduction using the significantly weaker acetic acid, HOAc, as the proton source.

5.6.1 Testing for electrocatalytic reduction of protons by $Fe_3(\mu\text{-edt})_2(CO)_7$, using the weak acid HOAc as the proton source, in DCM

The CVs obtained after additions of HOAc in DCM are shown in Figure 177. On the addition of 1 molar equivalent HOAc the first reduction peak is slightly larger. On the return scan the oxidation peak at -1.75 V is no longer present, suggesting a new reduction process is happening in the presence of HOAc, which consumes the product that was being re-oxidised. In addition, a new reduction product is present, which is re-oxidised at -0.59 V. The remainder of the CV is unchanged. On further additions of acid, the second reduction of the neutral complex grows steadily. The remainder of the CV remains unchanged from the behaviour in the presence of 1 equivalent HOAc.

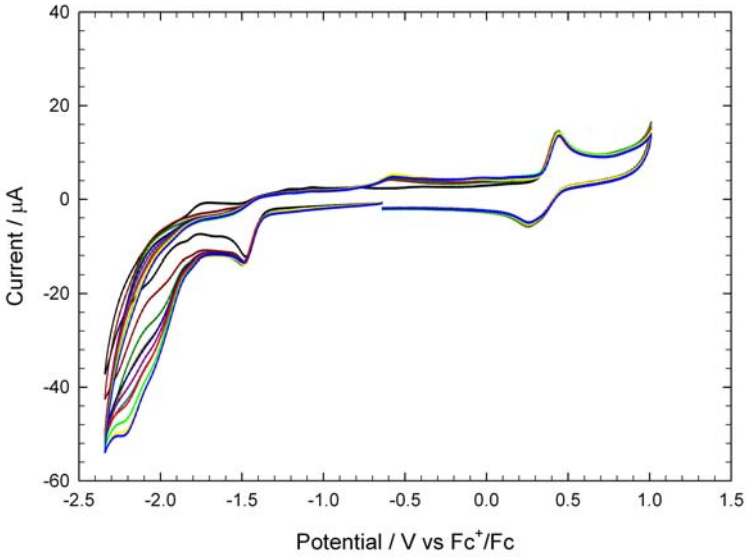

Figure 177: Cyclic voltammetry of $Fe_3(\mu\text{-edt})_2(CO)_7$ (0.5 mM) in DCM-$[NBu_4][PF_6]$ in the absence of acid and in the presence of up to 10 molar equivalents HOAc in steps of 1 molar equivalent (v=0.1 Vs^{-1}, glassy carbon electrode; V vs Fc^+/Fc)

On additions of up to 50 molar equivalents (Figure 178) the reduction at -2.05 V grows, with a suggestion that the peak is reaching a limiting current. The rest of the CV is largely unchanged.

These results indicate that the unsubstituted tri-iron complex is not catalytic after its first reduction. However, a catalytic process does occur at more negative potentials. This catalytic process is initiated by a species formed after the reduction of the complex. The singly reduced complex is not basic enough to be protonated by the weaker HOAc.

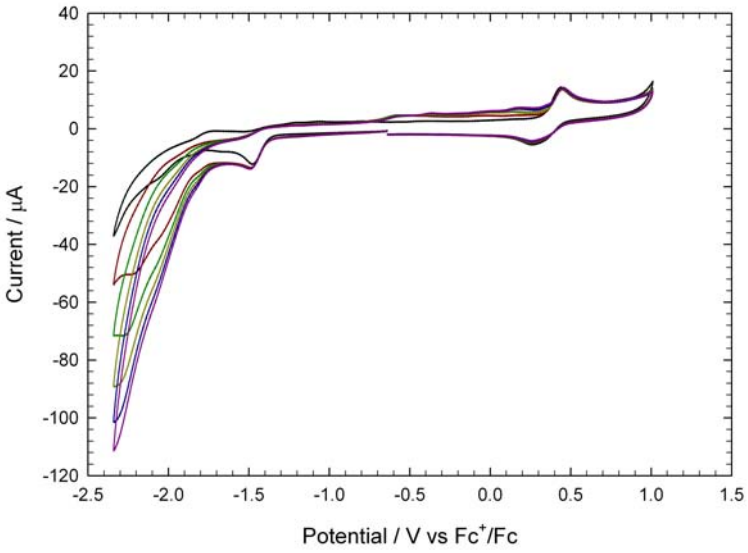

Figure 178: Cyclic voltammetry of $Fe_3(\mu\text{-edt})_2(CO)_7$ (0.5 mM) in DCM-$[NBu_4][PF_6]$ in the absence of acid and in the presence of up to 50 molar equivalents HOAc in steps of 10 molar equivalent (v=0.1 Vs^{-1}, glassy carbon electrode; V vs Fc^+/Fc)

5.6.2 Testing for electrocatalytic reduction of protons by $Fe_3(\mu\text{-edt})_2(CO)_7$, using the weak acid HOAc as the proton source, in MeCN

The same experiment has been performed in MeCN (Figures 179 and 180). On the addition of 1 molar equivalent there was a slight increase in the height of the first reduction. Also, the features at -1.82 and -2.05 V grew appreciably. On the return scan the small oxidation features diminished, however a new peak occurs at -0.48 V. On further additions of acid the first reduction currents increase slightly. The two peaks that grew appreciably, continue to increase on additions of acid; as does the new oxidation feature. The first oxidation peak of the complex also increases in height.

After 40 molar equivalents of acid had been added, the two reduction peaks that grew reached a limiting current (Figure 180). The peak at the edge of the potential window continued to increase, which could be attributed to direct reduction of the acid at the electrode surface. The oxidation feature at -0.48 V increases, as does the peak before the first oxidation of the neutral complex.

As with the DCM results, these findings indicate that the complex is not catalytic after its first reduction in the presence of HOAc; however, unidentified species formed after this reduction are themselves catalysts once they are reduced.

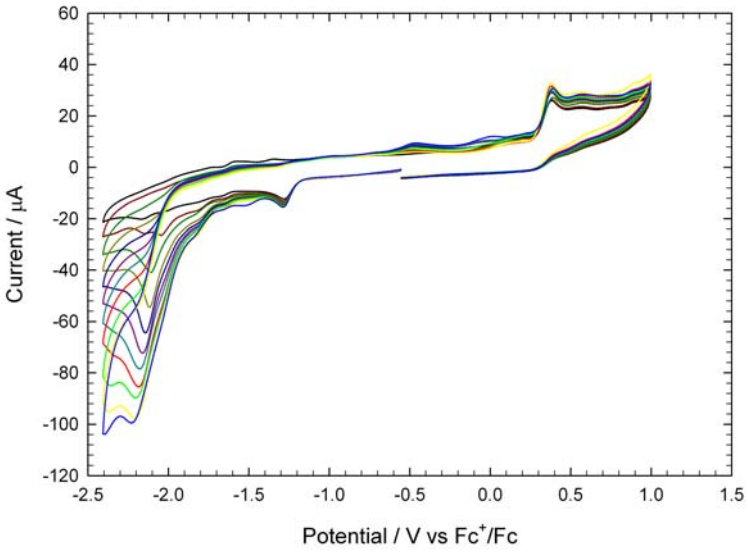

Figure 179: Cyclic voltammetry of $Fe_3(\mu\text{-edt})_2(CO)_7$ (0.5 mM) in MeCN-$[NBu_4][PF_6]$ in the absence of acid and in the presence of up to 10 molar equivalents HOAc in steps of 1 molar equivalent (v=0.1 Vs^{-1}, glassy carbon electrode; V vs Fc^+/Fc)

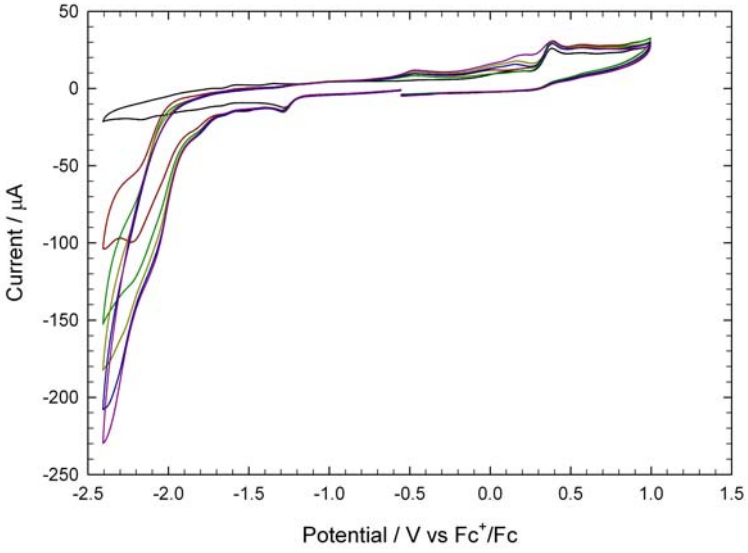

Figure 180: Cyclic voltammetry of $Fe_3(\mu\text{-edt})_2(CO)_7$ (0.5 mM) in MeCN-$[NBu_4][PF_6]$ in the absence of acid and in the presence of up to 50 molar equivalents HOAc in steps of 10 molar equivalents (v=0.1 Vs^{-1}, glassy carbon electrode; V vs Fc^+/Fc)

5.6.3 Testing for electrocatalytic reduction of protons by $Fe_3(\mu\text{-edt})_2(CO)_6PPh_3$, using the weak acid HOAc as the proton source, in DCM

The mono-substituted complex in the presence of HOAc in DCM is shown in Figures 181 and 182. On the first addition of acid the current at the potential of the first reduction increases. The remainder of the CV is unchanged.

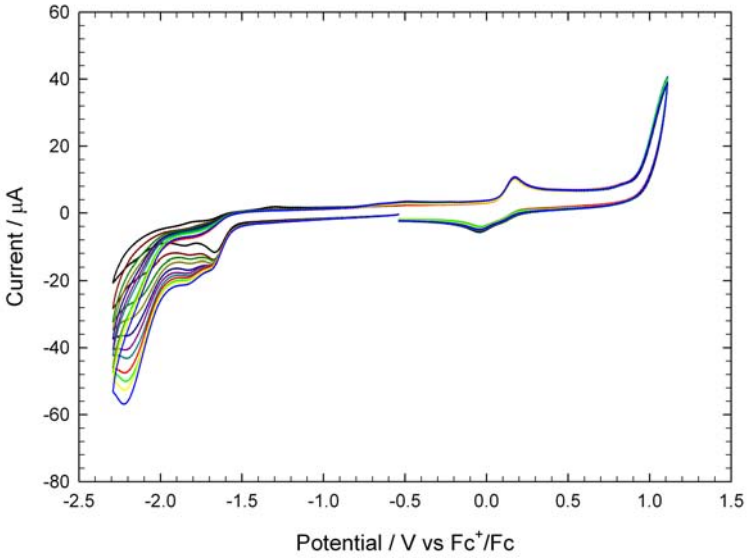

Figure 181: Cyclic voltammetry of $Fe_3(\mu\text{-edt})_2(CO)_6PPh_3$ (0.5 mM) in DCM-$[NBu_4][PF_6]$ in the absence of acid and in the presence of up to 10 molar equivalents HOAc in steps of 1 molar equivalent (v=0.1 Vs^{-1}, glassy carbon electrode; V vs Fc^+/Fc)

On further additions of acid the first reduction peak continues to increase. The second reduction feature at -1.85 V grows. As does the reduction at -2.22 V. Again, the return scan is unchanged even at 10 molar equivalents.

On additions of further acid (Figure 182), the first reduction continues to increase, suggesting it has not yet reached a limiting current. The second and third reduction currents also grow. Again, the return scan is largely unchanged.

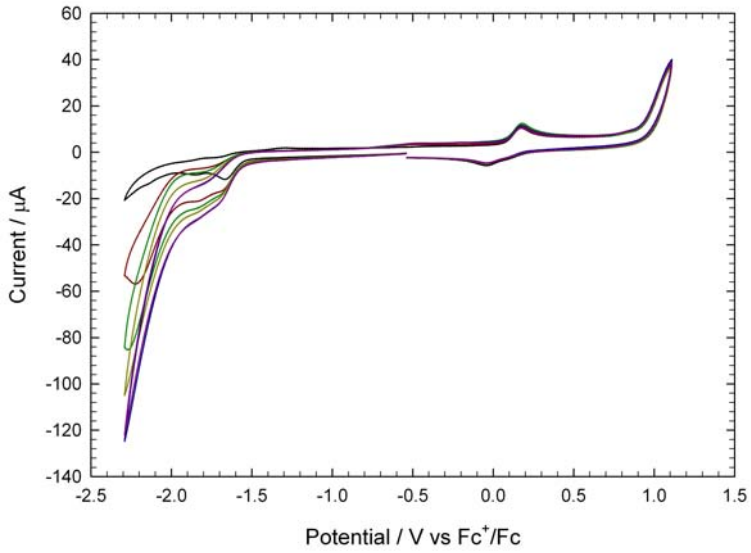

Figure 182: Cyclic voltammetry of $Fe_3(\mu\text{-edt})_2(CO)_6PPh_3$ (0.5 mM) in DCM-$[NBu_4][PF_6]$ in the absence of acid and in the presence of up to 50 molar equivalents HOAc in steps of 10 molar equivalent (v=0.1 Vs^{-1}, glassy carbon electrode; V vs Fc^+/Fc)

5.6.4 Testing for electrocatalytic reduction of protons by $Fe_3(\mu\text{-edt})_2(CO)_6PPh_3$, using the weak acid HOAc as the proton source, in MeCN

The mono-substituted complex in the presence of HOAc in MeCN is shown in Figures 183 and 184. On the first addition of acid the first reduction of the complex is unchanged. Small reduction peaks appear at -1.68 and -2.15 V, along with a larger peak at -1.95 V.

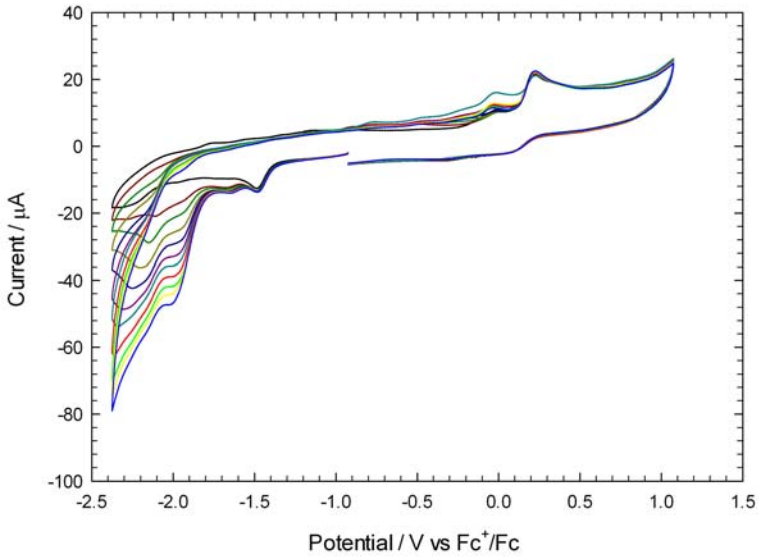

Figure 183: Cyclic voltammetry of $Fe_3(\mu\text{-edt})_2(CO)_6PPh_3$ (0.5 mM) in MeCN-$[NBu_4][PF_6]$ in the absence of acid and in the presence of up to 10 molar equivalents HOAc in steps of 1 molar equivalent (v=0.1 Vs^{-1}, glassy carbon electrode; V vs Fc^+/Fc)

On further additions of HOAc the first reduction peak of the complex and the peak that appeared at -1.68 V remain the same height. The peaks at -1.95 V and -2.15 V grow with each addition of acid. This trend continues for every concentration of acid tested.

Interestingly the reduction process that initiates proton reduction catalysis is that of a minor species in solution. This implies that the minor species is highly catalytic. This species has yet to be identified.

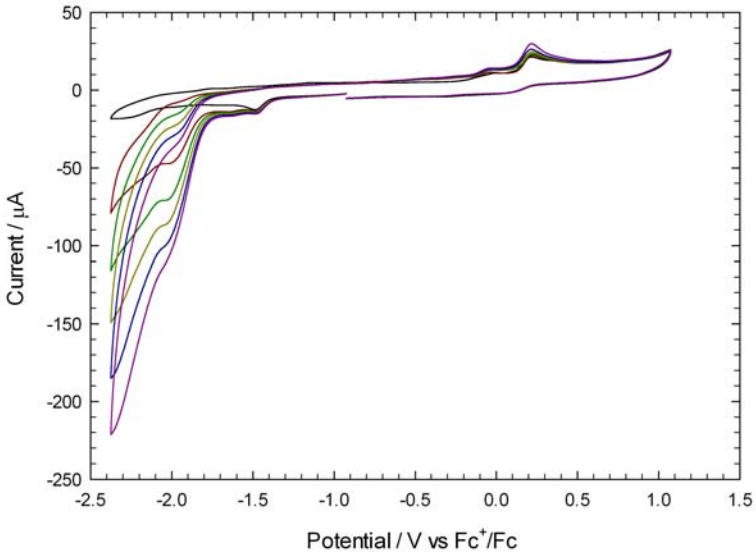

Figure 184: Cyclic voltammetry of $Fe_3(\mu\text{-edt})_2(CO)_6PPh_3$ (0.5 mM) in MeCN-$[NBu_4][PF_6]$ in the absence of acid and in the presence of up to 50 molar equivalents HOAc in steps of 10 molar equivalent (v=0.1 Vs^{-1}, glassy carbon electrode; V vs Fc^+/Fc)

5.6.5 Testing for electrocatalytic reduction of protons by $Fe_3(\mu\text{-edt})_2(CO)_5(PPh_3)_2$, using the weak acid HOAc as the proton source, in DCM

The behaviour of the di-substituted complex was analysed in the presence of the weak acid HOAc (Figures 185 and 186). On the first addition of acid there is almost no change in the CV of the complex. As further additions of acid are made, the CV still remains unchanged, the only new feature being a small oxidation peak at -0.67 V. Adding up to 50 equivalents indicated that a catalytic response at the first reduction could be observed. This was followed by a further reduction current that is presumably direct reduction of the acid.

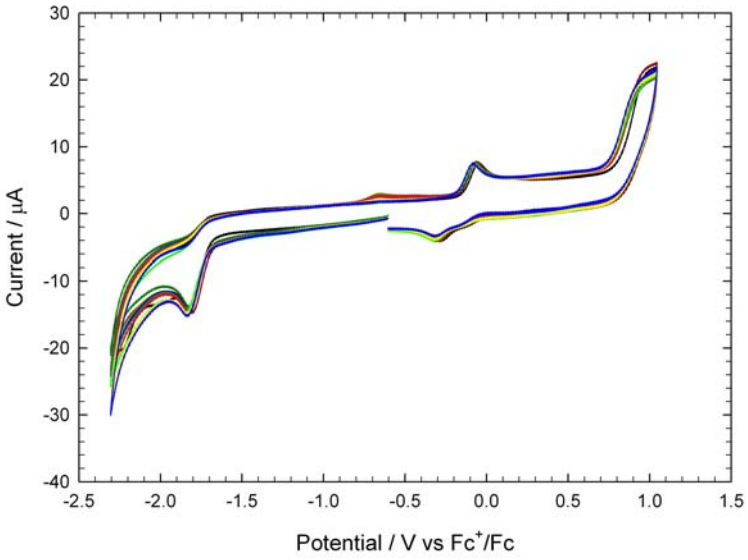

Figure 185: Cyclic voltammetry of $Fe_3(\mu\text{-edt})_2(CO)_5(PPh_3)_2$ (0.5 mM) in DCM-$[NBu_4][PF_6]$ in the absence of acid and in the presence of up to 10 molar equivalents HOAc in steps of 1 molar equivalent (v=0.1 Vs^{-1}, glassy carbon electrode; V vs Fc^+/Fc)

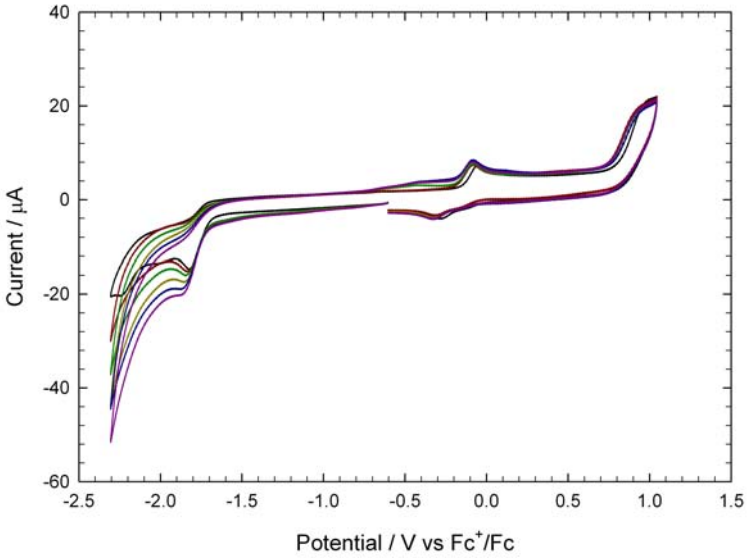

Figure 186: Cyclic voltammetry of $Fe_3(\mu\text{-edt})_2(CO)_5(PPh_3)_2$ (0.5 mM) in DCM-$[NBu_4][PF_6]$ in the absence of acid and in the presence of up to 50 molar equivalents HOAc in steps of 10 molar equivalent (v=0.1 Vs^{-1}, glassy carbon electrode; V vs Fc^+/Fc)

5.6.6 Summary and discussion

The CVs of the unsubstituted tri-iron complex and the unsubstituted di-iron complex in the presence of 10 molar equivalents HOAc are shown in Figure 187. Both complexes are not catalytic at the first reduction of the complex - catalysis is initiated by a species generated after the first reduction. The overpotential of catalysis is improved when using a tri-iron, rather than the di-iron, centre. Figure 188 shows a similar comparison of the mono-substituted tri-iron complex and the equivalent di-iron complex. As with the unsubstituted complexes, neither are catalytic upon their first reduction, however, species generated after reduction are catalytic.

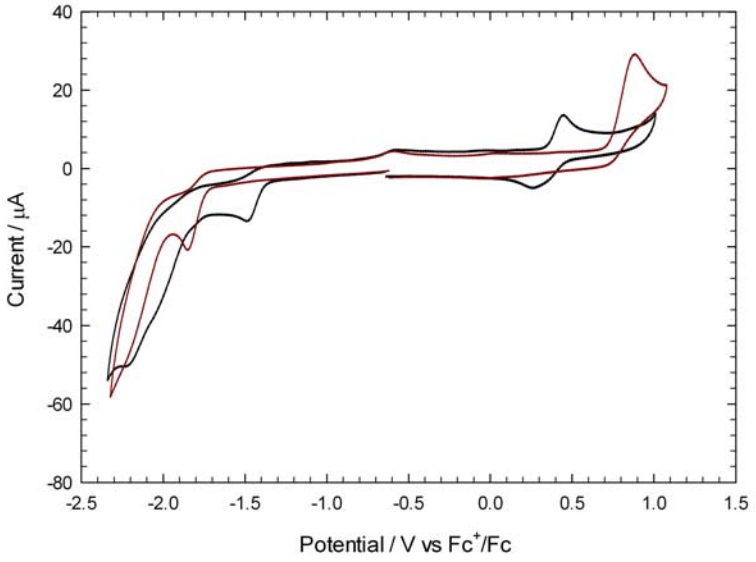

Figure 187: Cyclic voltammetry of $Fe_3(\mu\text{-edt})_2(CO)_7$ (0.5 mM, black line) and $Fe_2(\mu\text{-edt})(CO)_6$ (0.5 mM, red line) in the presence of 10 molar equivalents HOAc in DCM-$[NBu_4][PF_6]$ (v=0.1 Vs^{-1}, glassy carbon electrode; V vs Fc^+/Fc)

The CVs of the three tri-iron complexes in the presence of 10 molar equivalents HOAc are shown in Figure 189. The unsubstituted complex CV shows a slight increase in reduction current suggesting a catalytic process, however, this is severely limited. The mono-substituted complex showed no extra reduction peak after the first catalytic peak, as has been seen for similar di-iron complexes. It is surprising that the di-substituted complex is less catalytic at the first reduction than the mono-substituted complex. It would be expected that the increased electron density on the Fe centres from the two PPh_3 ligands would lead to enhanced catalysis. This may be because the electron-density is extensively delocalised throughout the structure and distributed more symmetrically than in the mono-substituted complex.

A comparison of the behaviour of the unsubstituted complex in the presence of $HBF_4.Et_2O$ and in the presence of HOAc is given in Figure 190. The catalytic mechanism is clearly different in the presence of HOAc to that seen when the proton source was $HBF_4.Et_2O$ or HOTs. The singly reduced complex is protonated by $HBF_4.Et_2O$, which opens a catalytic pathway via a reduction, further protonation, reduction and liberation of H_2. The weaker acid HOAc, however, is unable

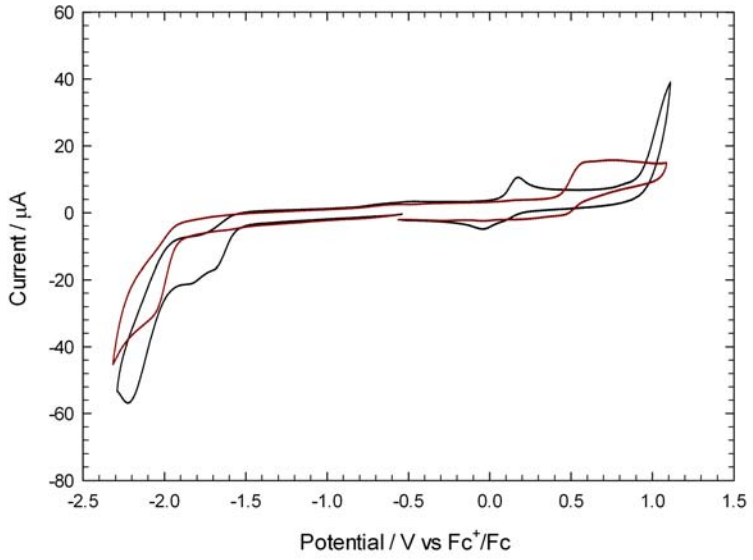

Figure 188: Cyclic voltammetry of $Fe_3(\mu\text{-edt})_2(CO)_6PPh_3$ (0.5 mM, black line) and $Fe_2(\mu\text{-edt})(CO)_5PPh_3$ (0.5 mM, red line) in the presence of 10 molar equivalents HOAc in DCM-$[NBu_4][PF_6]$ (v=0.1 Vs^{-1}, glassy carbon electrode; V vs Fc^+/Fc)

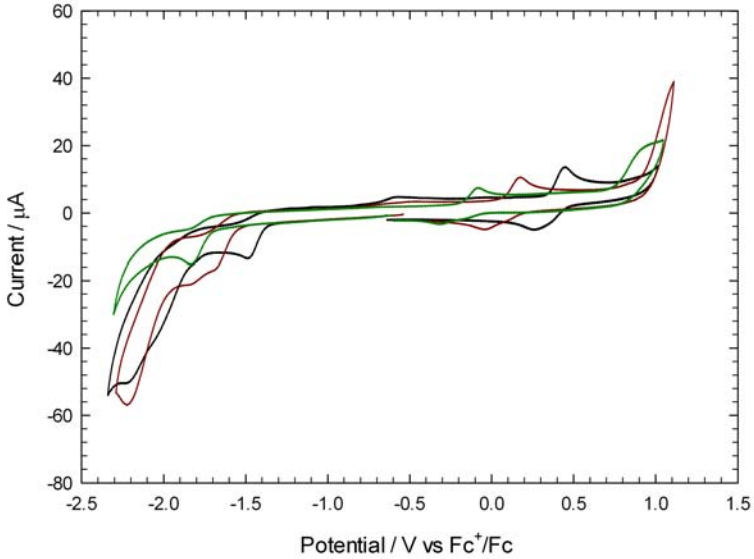

Figure 189: Cyclic voltammetry of $Fe_3(\mu\text{-edt})_2(CO)_7$ (0.5 mM, black line), $Fe_3(\mu\text{-edt})_2(CO)_6PPh_3$ (0.5 mM, red line), and $Fe_3(\mu\text{-edt})_2(CO)_5(PPh_3)_2$ (0.5 mM, green line) in the presence of 10 molar equivalent HOAc in DCM-$[NBu_4][PF_6]$ (v=0.1 Vs^{-1}, glassy carbon electrode; V vs Fc^+/Fc)

to protonate the singly reduced complex, so this catalytic mechanism is unavailable and the singly reduced species must be further reduced, or decompose to smaller fragments, to initiate a catalytic mechanism. Similar comparisons in Figures 191 and 192 give the same conclusion for the mono- and di-substituted complexes.

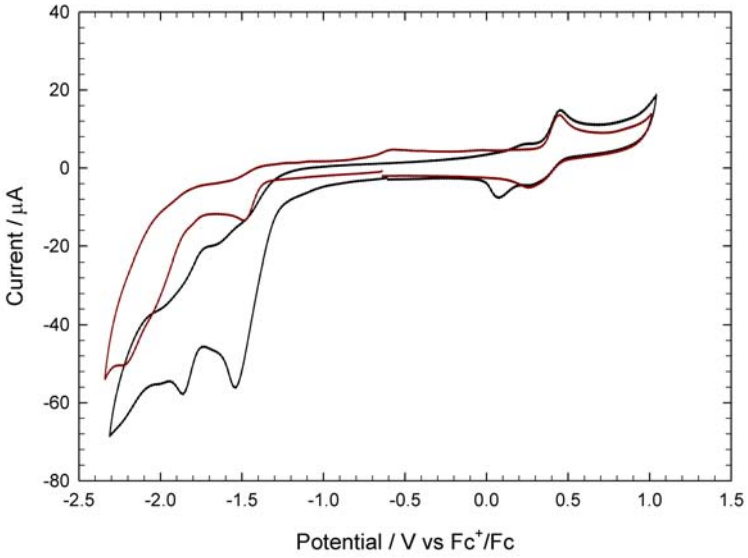

Figure 190: Cyclic voltammetry of $Fe_3(\mu\text{-edt})_2(CO)_7$ (0.5 mM) in the presence of 10 molar equivalent $HBF_4.Et_2O$ (black line) and HOAc (red line) in DCM-$[NBu_4][PF_6]$ (v=0.1 Vs^{-1}, glassy carbon electrode; V vs Fc^+/Fc)

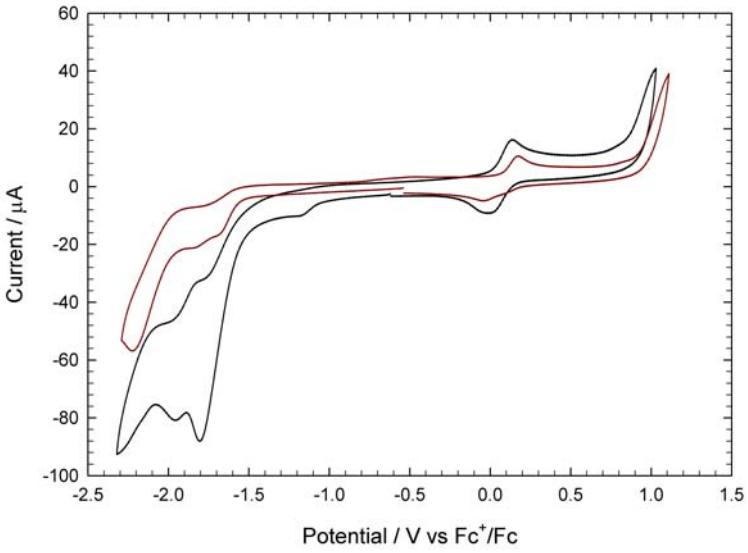

Figure 191: Cyclic voltammetry of $Fe_3(\mu\text{-edt})_2(CO)_6PPh_3$ (0.5 mM) in the presence of 10 molar equivalent $HBF_4.Et_2O$ (black line) and HOAc (red line) in DCM-$[NBu_4][PF_6]$ (v=0.1 Vs^{-1}, glassy carbon electrode; V vs Fc^+/Fc)

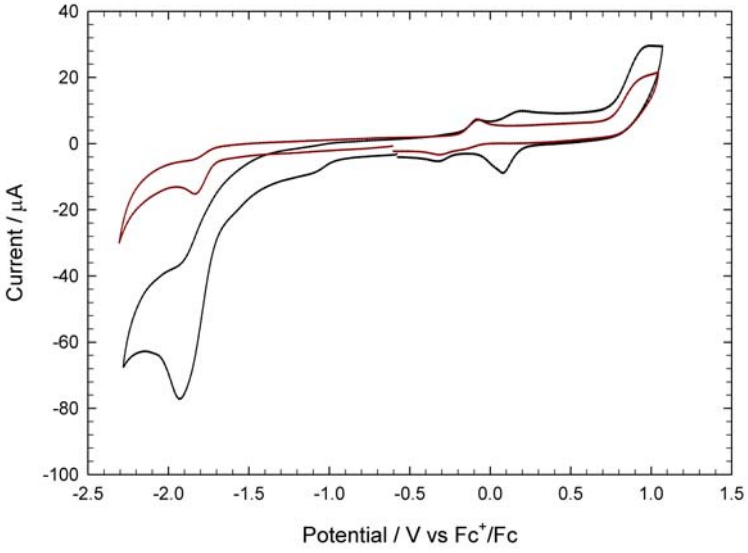

Figure 192: Cyclic voltammetry of $Fe_3(\mu\text{-edt})_2(CO)_5(PPh_3)_2$ (0.5 mM) in the presence of 10 molar equivalent $HBF_4.Et_2O$ (black line) and HOAc (red line) in DCM-$[NBu_4][PF_6]$ (v=0.1 Vs^{-1}, glassy carbon electrode; V vs Fc^+/Fc)

5.7 Concluding remarks

This chapter has presented the investigation into the synthesis, molecular structure, susceptibility to protonation, electrochemical behaviour and electrocatalytic activity of the three tri-iron complexes $Fe_3(\mu\text{-edt})_2\text{-}(CO)_{7-x}(PPh_3)_x$ (x = 0, 1, 2). The tri-iron complexes have been found to be both mixed valence and exhibit a semi-bridging carbonyl in their neutral forms. This is a significant step towards closer mimicking the structural elements of the hydrogenase active site that are thought to be important in their catalytic activity.

The additional Fe centre results in a less negative reduction potential over the di-iron analogues. For example the unsubstituted complex is reduced at 0.44 V less negative than the equivalent di-iron complex. Interestingly the HOMO-LUMO separation is smaller in the tri-iron complex than in the di-iron complex. The difference in potential between the first oxidation and first reduction of the unsubstituted complex is 1.9 V, in contrast to 2.7 V for the di-iron equivalent. Similarly the values are 1.8 V for the mono-substituted complex compared to 2.6 V for the di-iron equivalent, and 1.9 V for the di-substituted complex compared to 2.5 V for the di-iron complex. In the enzyme the catalysis of proton reduction and hydrogen oxidation takes place reversibly and close to the thermodynamic potential, thus the difference in energy between the HOMO and LUMO must be very small. By designing biomimetics with a smaller HOMO-LUMO gap it is hoped to come closer to the catalytic performance of the enzyme.

Each of the complexes was catalytic towards proton reduction in the presence of $HBF_4.Et_2O$. As the reduction potential of the neutral complex is 0.44 V less negative than the di-iron analogue, this resulted in a significant improvement in the overpotential for catalysis when three iron centres are used instead of two. Although a direct comparison with the tetra-iron complex is not possible due to the different experimental conditions used, using three iron centres appears to result in an overpotential improvement over using four iron centres.

Substitution with one or two PPh_3 ligands does not increase the basicity of the complexes sufficiently to allow protonation of the neutral molecule. The first step in the catalytic cycle is therefore always reduction of the complex. The usual rationale for designing hydrogenase mimic complexes with electron-donating ligands is that this increases the basicity of the metal-metal bond, allowing protonation of the neutral complex. The benefit of this is that reduction of the protonated species (and hence catalysis) can occur at up to 1 V less negative potential than the reduction of the neutral complex, which is a significant energy gain. However, in this case it is found that protonation of the neutral mono- and di-substituted complexes does not take place, even with the strongest acid, thus no overpotential advantage is gained from substitution. In fact, the catalysis is pushed to more negative potentials as the increased electron-density makes the complexes more difficult to reduce. However one advantage of substitution seems to be the higher catalytic currents that can be achieved with the substituted complex indicating a faster turnover.

There are two key avenues for further research. Firstly, the pursuit of protonation of neutral

tri-iron complexes should be continued. This may be possible by moving to a chelating phosphine ligand, or by moving to tri-substituted complexes. Secondly, the literature, and work presented in Chapter 3, has found that the reduction potential of di-iron complexes can be dramatically improved by using an electron withdrawing bridge. Moving from two to three iron centres has already improved the reduction potential considerably, thus also incorporating an electron withdrawing bridge would be expected to make further improvements to the reduction potential and perhaps present a catalyst for proton reduction with an excellent overpotential.

6 $Fe_2(\mu\text{-pdt})(CO)_4(\mu\text{-}(Ph_2PN(CH_2CHCH_2)PPh_2))$ and $Fe_2(\mu\text{-pdt})(CO)_4(\kappa\text{-}(Ph_2PN(CH_2\text{-}CHCH_2)PPh_2))$: An investigation into a ligand in both bridging and chelating orientations

This chapter presents the susceptibility to protonation, electrochemical behaviour, electron transfer catalysis investigation and electrocatalytic activity of two isomeric, di-substituted complexes with a basic site in the bridging or chelating ligand: $Fe_2(\mu\text{-pdt})(CO)_4(\mu\text{-}(Ph_2PN(CH_2CH\text{-}CH_2)PPh_2))$ and $Fe_2(\mu\text{-pdt})(CO)_4(\kappa\text{-}(Ph_2PN(CH_2CHCH_2)PPh_2))$ (Figure 193).

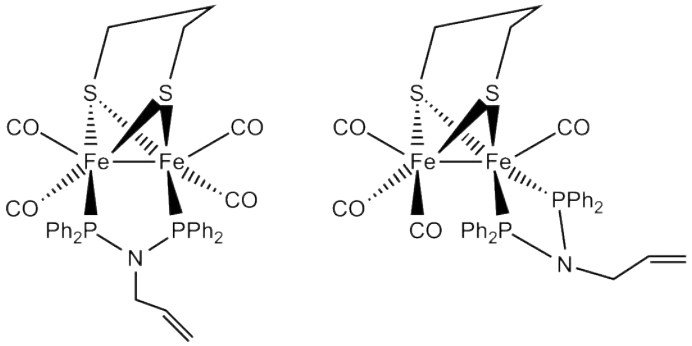

Figure 193: $Fe_2(\mu\text{-pdt})(CO)_4(\mu\text{-}(Ph_2PN(CH_2CHCH_2)PPh_2))$ (left) and $Fe_2(\mu\text{-pdt})(CO)_4(\kappa\text{-}(Ph_2P\text{-}N(CH_2CHCH_2)P\text{-}Ph_2))$ (right)

As discussed in Section 1.4, one of the key ways to vary the catalytic performance of H-cluster mimics is to vary the ligand set. The two complexes $Fe_2(\mu\text{-pdt})(CO)_4(\mu\text{-}(Ph_2PN(CH_2CHCH_2)PPh_2))$ and $Fe_2(\mu\text{-pdt})(CO)_4(\kappa\text{-}(Ph_2PN(CH_2CHCH_2)P\text{-}Ph_2))$ allow for investigation of the whether this ligand set provides sufficient basicity on the Fe centres to enable protonation, and the influence of the orientation of the ligand set (bridging or chelating) on the electrocatalytic activity of the complexes.

As the complexes are di-substituted with electron donating ligands, it is likely that the electron density on the Fe centres would be sufficient to allow hydride formation. The complexes differ in that the ligand is either bridging or chelating, which allows for further understanding about the influence of asymmetrical electron density on catalytic activity. The complexes were designed with a N in the ligand to provide a protonation site that could shuttle electrons to the Fe centres; however our studies suggest that this site is not basic enough to be protonated.

Talarmin and co-workers found that the chelating ligand of $Fe_2(\mu\text{-}SCH_2XCH_2S)(CO)_4(\kappa\text{-}(Ph_2(CH_2CH_2)PPh_2))$ rearranges to become a bridging ligand upon its first reduction via an electron transfer catalysis mechanism. As an additional study, the chelating-ligand complex $Fe_2(\mu\text{-pdt})(CO)_4(\kappa\text{-}(Ph_2PN(CH_2CHCH_2)PPh_2))$ has been tested to see if it will rearrange to the bridging-ligand isomer upon electrochemical reduction.

6.1 Susceptibility of $Fe_2(\mu\text{-pdt})(CO)_4(\mu\text{-}(Ph_2PN(CH_2CHCH_2)PPh_2))$ and $Fe_2(\mu\text{-pdt})(CO)_4(\kappa\text{-}(Ph_2PN(CH_2CHCH_2)PPh_2))$ to protonation

The first step taken towards understanding any catalytic mechanism the two complexes might exhibit was to determine whether or not they would protonate in the presence of a Brönsted acid. As discussed in Chapter 1, this aids understanding of whether the first step of a catalytic mechanism is a protonation or a reduction process. As in earlier chapters, protonation was monitored through the IR stretches of the CO ligands.

6.1.1 Susceptibility of $Fe_2(\mu\text{-pdt})(CO)_4(\mu\text{-}(Ph_2PN(CH_2CHCH_2)PPh_2))$ to protonation

The IR spectrum of $Fe_2(\mu\text{-pdt})(CO)_4(\mu\text{-}(Ph_2PN(CH_2CHCH_2)PPh_2))$ is shown in Figure 194. Bands are present at 1927, 1964, 1994 cm^{-1}. The band at 1927 cm^{-1} exhibits a shoulder. After adding $HBF_4.Et_2O$ to the solution, the IR spectrum in Figure 195 was obtained. The bands of the neutral complex have diminished, and new bands have appeared at 2000, 2011, 2044 and 2055 cm^{-1}. This suggests that complex has been partially protonated in the presence of $HBF_4.Et_2O$.

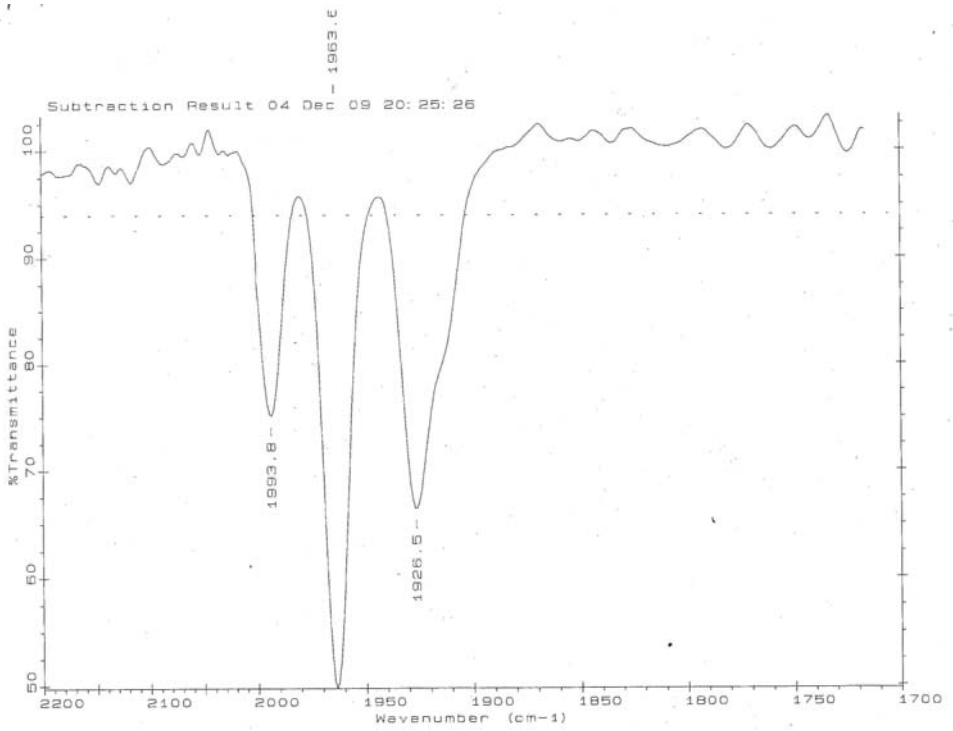

Figure 194: IR spectrum of $Fe_2(\mu\text{-pdt})(CO)_4(\mu\text{-}(Ph_2PN(CH_2CHCH_2)PPh_2))$ in DCM

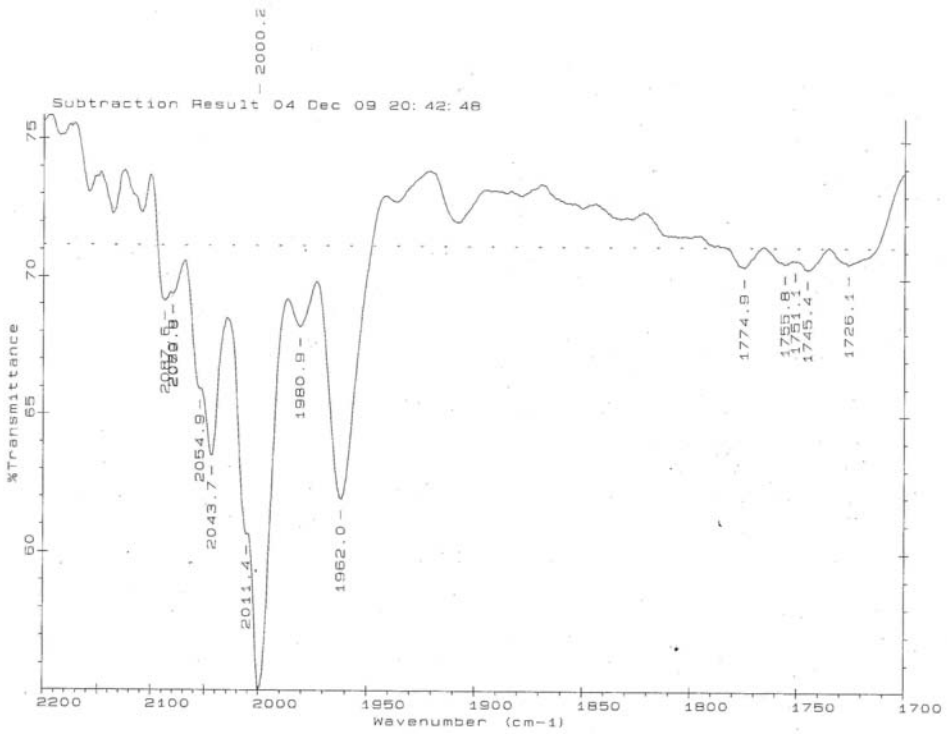

Figure 195: IR spectrum of $Fe_2(\mu\text{-pdt})(CO)_4(\mu\text{-}(Ph_2PN(CH_2CHCH_2)PPh_2))$ in DCM in the presence of $HBF_4.Et_2O$

6.1.2 Susceptibility of $Fe_2(\mu\text{-pdt})(CO)_4(\kappa\text{-}(Ph_2PN(CH_2CHCH_2)PPh_2))$ to protonation

The above procedure was repeated with the chelating ligand complex. Figure 196 shows the spectrum of the neutral complex. Two equivalents $HBF_4.Et_2O$ were added to the solution, the resulting IR spectrum is shown in Figure 197. The bands shifted to higher wavenumbers, again suggesting that electron density had been withdrawn from the Fe centres due to protonation.

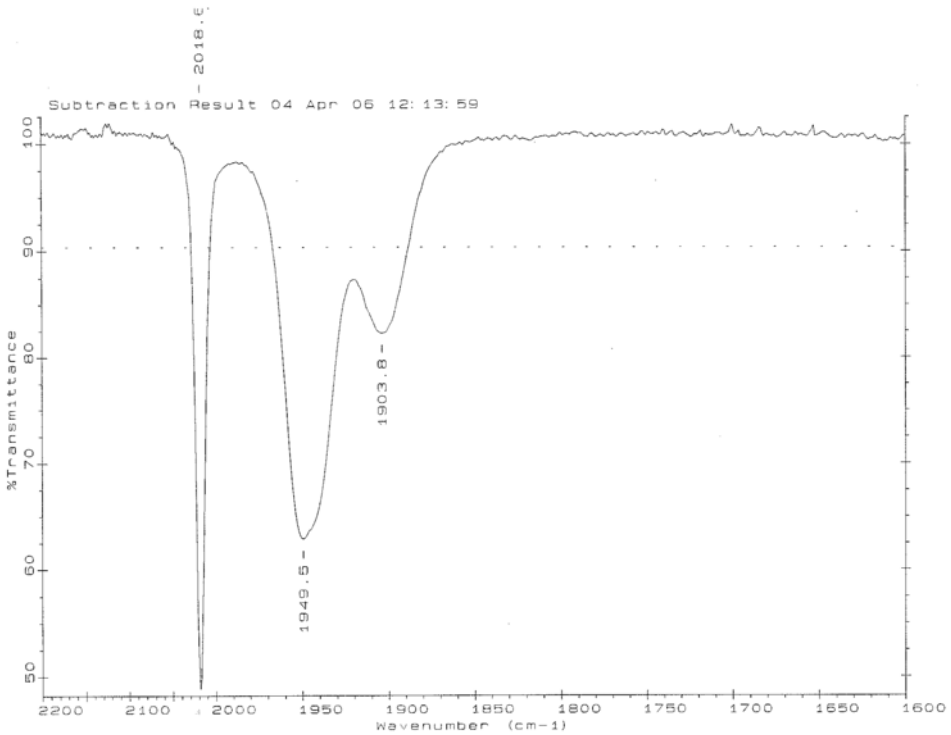

Figure 196: IR spectrum of $Fe_2(\mu\text{-pdt})(CO)_4(\kappa\text{-}(Ph_2PN(CH_2CHCH_2)PPh_2))$ in DCM

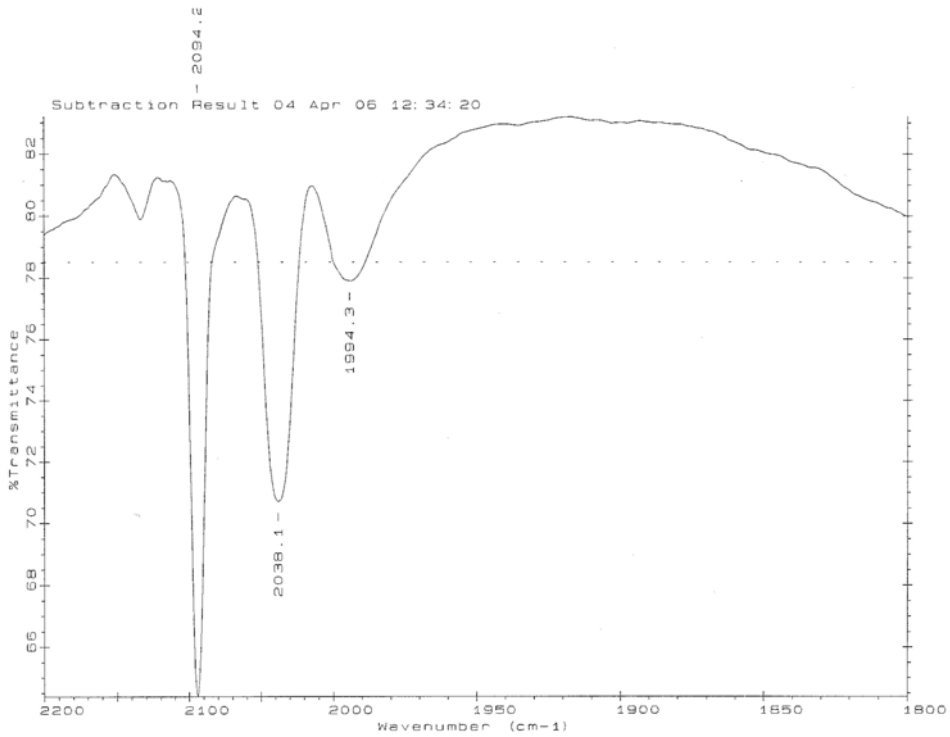

Figure 197: IR spectrum of $Fe_2(\mu\text{-pdt})(CO)_4(\kappa\text{-}(Ph_2PN(CH_2CHCH_2)PPh_2))$ in DCM in the presence of $HBF_4.Et_2O$

6.1.3 Summary and discussion

The bridging ligand complex has been found to only partially protonate in the presence of $HBF_4.Et_2O$, whereas the chelating ligand complex protonates cleanly. This provides further evidence that an asymmetry of electron density over the iron centres can assist in the protonation of di-iron complexes. Earlier in this dissertation, the tri-substituted triphos-ligand complexes were found to protonate readily, whereas unsubstituted and mono-substituted complexes were found to not protonate, the di-substituted complexes presented in this chapter therefore provide a level of substitution where protonation is only just able to occur. As well as the asymmetry of electron density on the Fe centres, another factor in the unclean protonation of the bridging isomer could be the kinetic rearrangement required to accommodate a hydride bridging the Fe centres - whereas the chelating isomer is likely to be able to rearrange fairly readily, the bridging isomer is considerably more rigid.

No evidence was observed for protonation at the N of the bridging or chelating ligand. This could suggest that the proton moved too quickly from the N to the Fe centres to be observed, however, it is more likely that the N was not basic enough to protonate.

These results indicate that any catalytic mechanism these complexes may exhibit in $HBF_4.Et_2O$ is unlikely to be the same for each complex, as the chelating complex protonates rapidly in the presence of the acid, whereas the bridging-ligand complex is only partially protonated. The electrocatalytic activity of the two isomers shall be investigated later in this chapter.

6.2 Electrochemistry of $Fe_2(\mu\text{-pdt})(CO)_4(\mu\text{-}(Ph_2PN(CH_2CHCH_2)PPh_2))$ and $Fe_2(\mu\text{-pdt})(CO)_4(\kappa\text{-}(Ph_2PN(CH_2CHCH_2)PPh_2))$ in the absence of protons

The electrochemical behaviour of the two isomers in the absence of protons has been analysed. This will aid in understanding the nature of any catalytic activity the two complexes may exhibit. The main focus is the difference between the electrochemical behaviour of the symmetrical and asymmetrical complexes. All of the results presented were performed in MeCN.

6.2.1 Electrochemistry of $Fe_2(\mu\text{-pdt})(CO)_4(\mu\text{-}(Ph_2PN(CH_2CHCH_2)PPh_2))$ in the absence of protons, in MeCN

The bridging-ligand complex has been investigated in the coordinating solvent MeCN (Figure 198). The first reduction of the complex occurs at -2.15 V, and is irreversible. A small feature occurs at -0.81 V, which is assumed to be the re-oxidation of a product of the reduction process. The first oxidation of the neutral complex occurs at 0.31 V. A second oxidation process occurs at 0.71 V. Both oxidation processes exhibit minor re-reduction peaks.

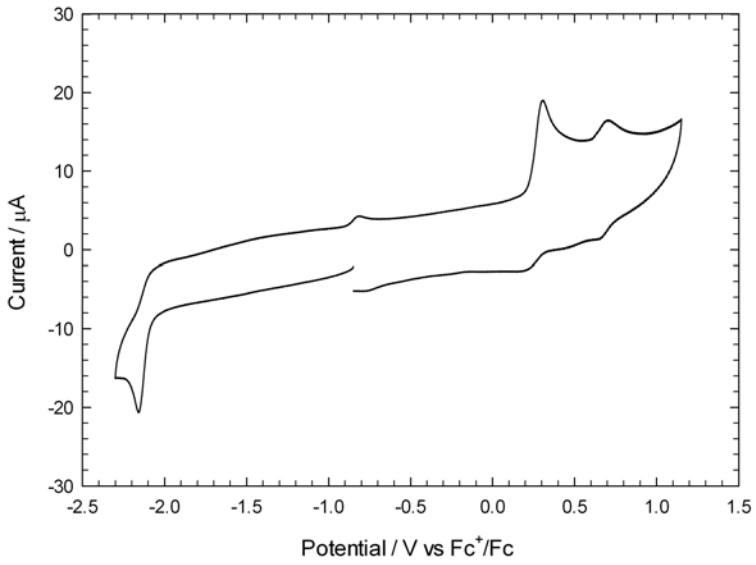

Figure 198: Cyclic voltammetry of $Fe_2(\mu\text{-pdt})(CO)_4(\mu\text{-}(Ph_2PN(CH_2CHCH_2)PPh_2))$ (0.5 mM) in MeCN-$[NBu_4][PF_6]$ (v=0.1 Vs^{-1}, glassy carbon electrode; V vs Fc^+/Fc)

Using other complexes presented in this thesis as benchmarks, the oxidation process appears consistent with a transfer of more than one electron. As the oxidation is irreversible, this process is likely to involve significant structural rearrangement in the complex. The reduction process is of a similar magnitude to the oxidation process, suggesting this also consists of more than one electron, and involves a structural rearrangement.

To probe the behaviour of the oxidation and reduction processes further, the scan rate was varied. Figure 199 shows the analysis of the first oxidation peak at different scan rates. The reversibility of

the first oxidation peak is marginally improved at the faster scan rates. This suggests that the first oxidation is a one electron process and is quasi-reversible, but a rearrangement leads to a product which is oxidised further. The reduction process has also been analysed at various scan rates (Figure 200). The reduction showed no sign of reversibility over the scan rates used.

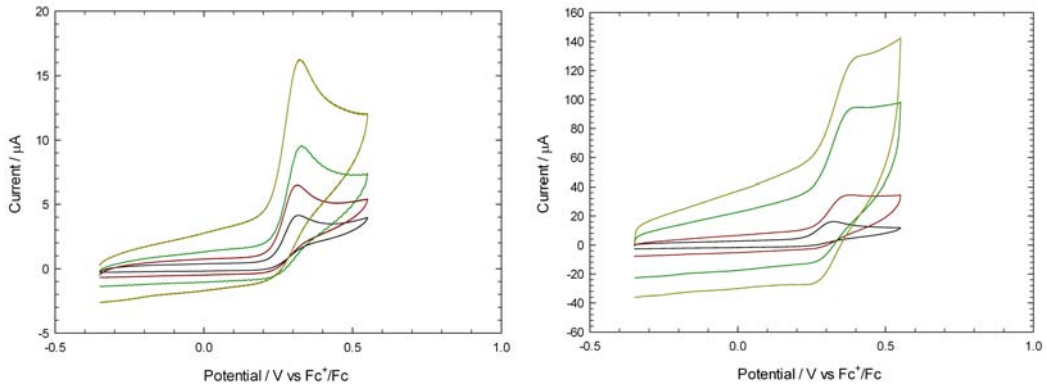

(a) v=0.01, 0.02, 0.05, 0.1 Vs^{-1} (b) v=0.1, 1.0, 5.0, 10.0 Vs^{-1}

Figure 199: Cyclic voltammetry of $Fe_2(\mu\text{-pdt})(CO)_4(\mu\text{-}(Ph_2PN(CH_2CHCH_2)PPh_2))$ (0.5 mM) in MeCN-$[NBu_4][PF_6]$ (glassy carbon electrode; V vs Fc^+/Fc)

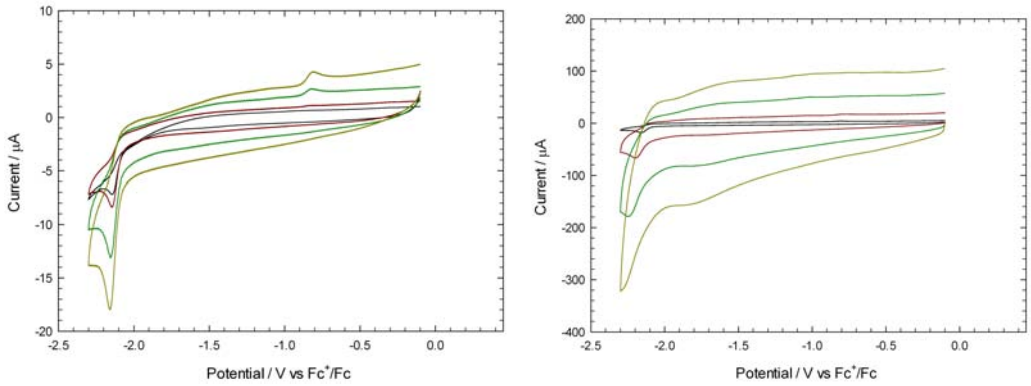

(a) v=0.01, 0.02, 0.05, 0.1 Vs^{-1} (b) v=0.1, 1.0, 5.0, 10.0 Vs^{-1}

Figure 200: Cyclic voltammetry of $Fe_2(\mu\text{-pdt})(CO)_4(\mu\text{-}(Ph_2PN(CH_2CHCH_2)PPh_2))$ (0.5 mM) in MeCN-$[NBu_4][PF_6]$ (glassy carbon electrode; V vs Fc^+/Fc)

6.2.2 Electrochemistry of $Fe_2(\mu\text{-pdt})(CO)_4(\kappa\text{-}(Ph_2PN(CH_2CHCH_2)PPh_2))$ in the absence of protons, in MeCN

The electrochemistry of the chelating-ligand complex is shown in Figure 201. The first reduction of the complex occurs at -2.19 V, this is preceded by a small shoulder. On returning towards positive potentials, a small re-oxidation peak is observed at -0.80 V. The first oxidation of the neutral complex occurs at -0.10 V, and is irreversible. Three further irreversible oxidation processes take place at 0.10, 0.31 and 0.69 V.

As with the bridging-ligand complex, comparing the peak height of the oxidation of the chelating-

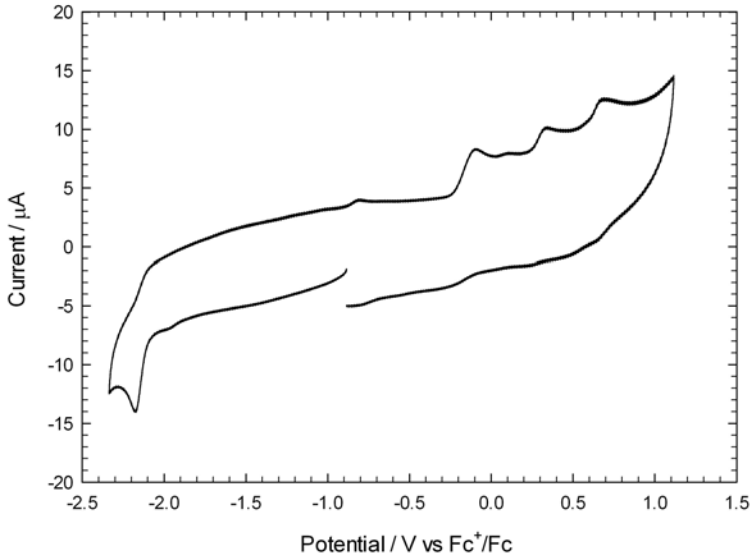

Figure 201: Cyclic voltammetry of $Fe_2(\mu\text{-pdt})(CO)_4(\kappa\text{-}(Ph_2PN(CH_2CHCH_2)PPh_2))$ (0.5 mM) in MeCN-$[NBu_4][PF_6]$ (v=0.1 Vs^{-1}, glassy carbon electrode; V vs Fc^+/Fc)

ligand complex with other complexes presented in this dissertation suggests the oxidation is a one electron process. The reduction peak height is larger than the first oxidation, suggesting this is between a one and two electron process.

The oxidation processes have been analysed at various scan rates (Figure 202). The first oxidation process becomes more reversible at faster scan rates, although the corresponding re-reduction appears to be a double peak suggesting the process is not a simple 1-electron oxidation and reduction. The three processes at more positive potentials remain irreversible. The reduction process of the chelating-ligand complex has also been investigated at various scan rates. No improvement in reversibility was seen over the range of scan rates tested.

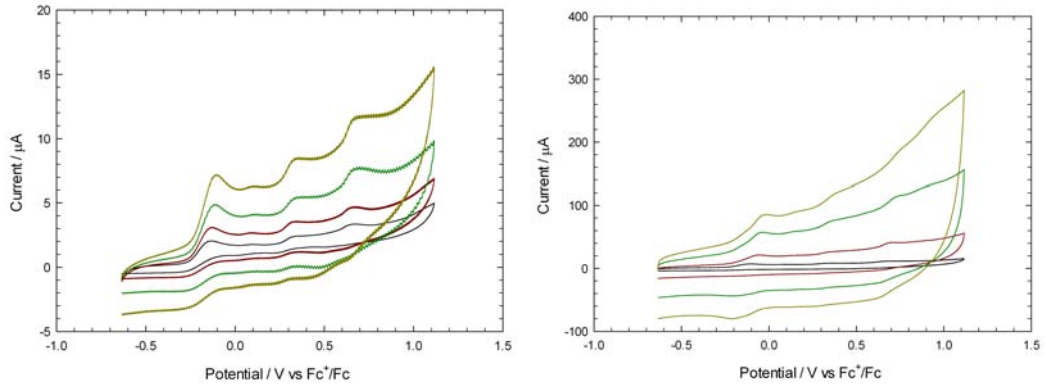

(a) v=0.01, 0.02, 0.05, 0.1 Vs^{-1} (b) v=0.1, 1.0, 5.0, 10.0 Vs^{-1}

Figure 202: Cyclic voltammetry of $Fe_2(\mu\text{-pdt})(CO)_4(\kappa\text{-}(Ph_2PN(CH_2CHCH_2)PPh_2))$ (0.5 mM) in MeCN-$[NBu_4][PF_6]$ (glassy carbon electrode; V vs Fc^+/Fc)

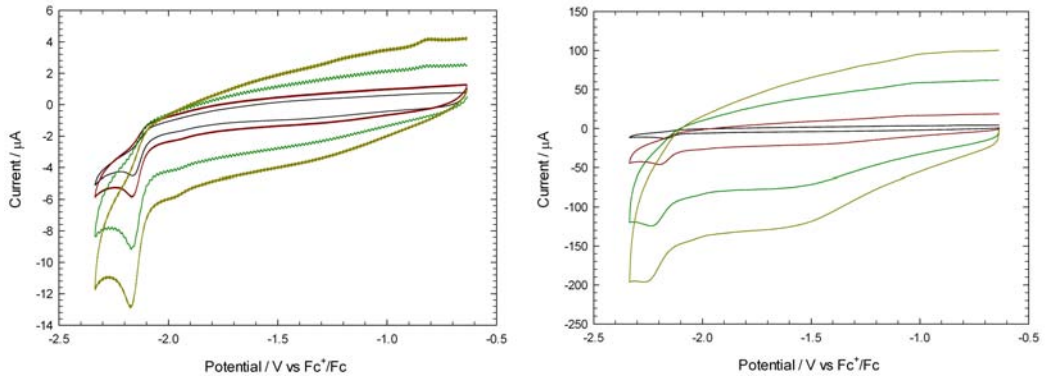

(a) v=0.01, 0.02, 0.05, 0.1 Vs^{-1} (b) v=0.1, 1.0, 5.0, 10.0 Vs^{-1}

Figure 203: Cyclic voltammetry of $Fe_2(\mu\text{-pdt})(CO)_4(\kappa\text{-}(Ph_2PN(CH_2CHCH_2)PPh_2))$ (0.5 mM) in MeCN-$[NBu_4][PF_6]$ (glassy carbon electrode; V vs Fc^+/Fc)

6.2.3 Summary and discussion

The CVs of the bridging- and chelating-ligand isomers are compared in Figure 204. The chelating-ligand complex is oxidised at a potential 0.41 V less positive than the bridging-ligand complex, implying that the binding position of the ligand clearly has a large influence in the electrochemical behaviour of the complexes. This is presumably due to the bias of electron density on one iron centre rather than the other, showing that significant electronic asymmetry within di-iron complexes is possible. We can assume that the HOMO of the chelating-ligand complex has a greater contribution from the di-substituted Fe centre, whereas the HOMO of the bridging-ligand complex is evenly distributed over the two Fe centres. Interestingly, whereas the HOMO energy (from which the electron is removed on oxidation) differs depending on whether the ligand is bridging or chelating, the LUMO energy (related to the potential of the first reduction) appears similar for both complexes because the reduction potentials are the same. Thus the binding position of the ligand has less influence on the LUMO energy. The binding position clearly does alter the reduction mechanism, however, as the number of electrons transferred is different for each complex. Another explanation for the two complexes exhibiting reduction process at the same potential, is the rapid conversion of chelating ligand to a bridging orientation upon reduction, which will be ruled out in the next Section.

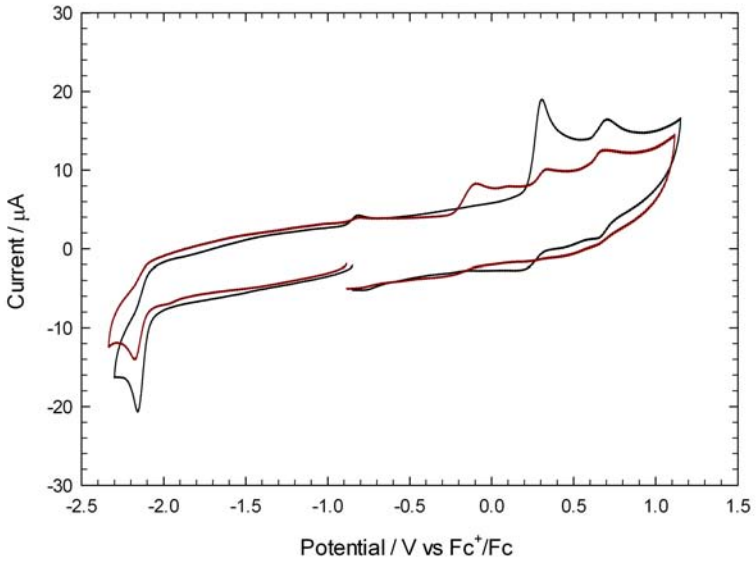

Figure 204: Cyclic voltammetry of $Fe_2(\mu\text{-pdt})(CO)_4(\mu\text{-}(Ph_2PN(CH_2CHCH_2)PPh_2))$ (0.5 mM, black line) and $Fe_2(\mu\text{-pdt})(CO)_4(\kappa\text{-}(Ph_2PN(CH_2CHCH_2)PPh_2))$ (0.5 mM, red line) in MeCN-$[NBu_4][PF_6]$ (v=0.1 Vs^{-1}, glassy carbon electrode; V vs Fc^+/Fc)

6.3 Investigation into whether the chelating-ligand complex undergoes electron transfer catalysis to form the bridging-ligand complex

Talarmin and co-workers have reported an electron transfer catalysis (ETC) process in which the chelating-ligand complex $Fe_2(\mu\text{-}SCH_2XCH_2S)(CO)_4(\kappa\text{-}(Ph_2P(CH_2CH_2)PPh_2))$ rearranges to a bridging-ligand isomer upon reduction. The CVs showing this behaviour and the corresponding mechanism are shown in Figure 205. It was found that when the chelating-ligand complex (1) is reduced (seen as the small reduction peak at -2.05 V in Figure 205) it rapidly rearranges to the bridging-ligand isomer (2^-). As the reduction potential of this newly formed bridging-ligand isomer was more negative than -2.05 V, it was oxidised at the electrode surface and by surrounding chelating-ligand complex, to form the neutral bridging-ligand complex (2). The neutral bridging ligand complex (2) was then reduced at -2.2 V (the larger reduction peak in Figure 205).

This ETC process was demonstrated by holding the electrode potential at -2.05 V for 10 seconds (scan b in Figure 205), and then scanning back to positive potentials. The oxidation peak, and therefore concentration, of the chelating-ligand complex had diminished, and that of the bridging-ligand complex had increased. Thus the chelating-ligand complex was rearranging to the bridging-ligand complex.

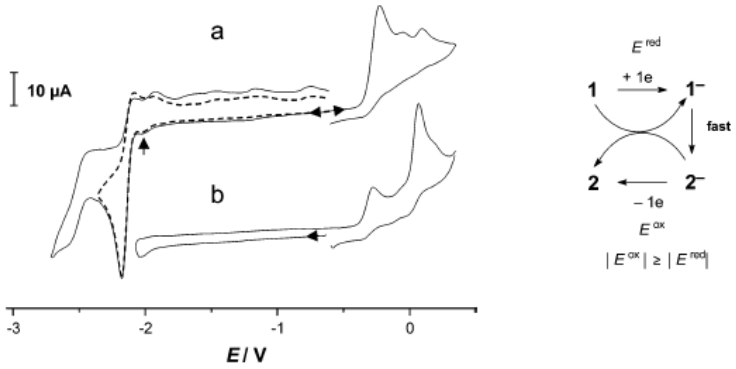

Figure 205: The cyclic voltammetry of $Fe_2(\mu\text{-}SCH_2N(^iPr)CH_2S)(CO)_4(\kappa\text{-}(Ph_2P(CH_2CH_2)PPh_2))$ (left) and the mechanism for electron transfer catalysis rearrangement from the chelating-ligand complex to the bridging-ligand isomer upon the first reduction process (right)

It was of interest to assess whether the chelating-ligand complex presented in this chapter, $Fe_2(\mu\text{-}pdt)(CO)_4(\kappa\text{-}(Ph_2PN(CH_2CHCH_2)PPh_2))$, would undergo a similar ETC rearrangement upon reduction to form the bridging-ligand isomer, $Fe_2(\mu\text{-}pdt)(CO)_4(\mu\text{-}(Ph_2PN(CH_2CHCH_2)PPh_2))$.

Analysis of the CVs of the chelating-ligand complex (Figure 201) indicates that there is a small reduction feature which precedes the larger reduction process. If an ETC process is occurring in a similar way to that reported by Talarmin and co-workers, this, rather than the larger peak at -2.19 V, would be the reduction peak for the chelating-ligand complex. The larger peak at -2.19 V would then be assigned to reduction of the bridging-ligand complex, which had been generated after the ETC rearrangement of the chelating-ligand complex.

The experiment to assess whether the chelating-ligand complex does indeed undergo an ETC

rearrangement is shown in Figure 206 using the same method as Talarmin and co-workers. The black line is the CV of the chelating complex at 0.2 Vs^{-1}. The red line is the CV of the complex under the same conditions, with the electrode held at a potential beyond the small reduction feature (-2.05 V) for 20 seconds. On the return scan the height of the first oxidation peak corresponding to the chelating-ligand complex has not decreased, implying that the concentration of the chelating-ligand complex at the electrode surface is the same. As the concentration of the chelating-ligand complex has not diminished, it has not been converted to the bridging-ligand isomer, and therefore an ETC rearrangement has not occurred.

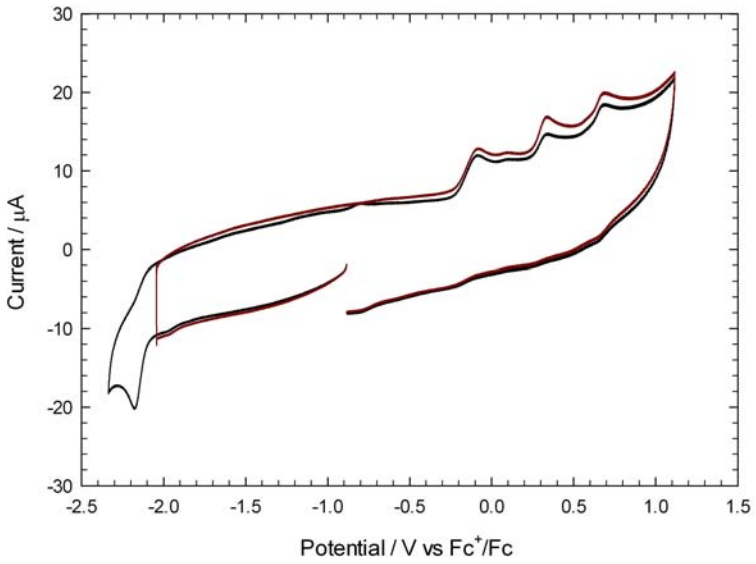

Figure 206: Cyclic voltammetry of $Fe_2(\mu\text{-pdt})(CO)_4(\kappa\text{-}(Ph_2PN(CH_2CHCH_2)PPh_2))$ (0.5 mM) in MeCN-$[NBu_4][PF_6]$ (black line) and electrode potential held at -2.05 V for 20 seconds (red line) (v=0.2 Vs^{-1}, glassy carbon electrode; V vs Fc^+/Fc)

It is not surprising that the chelating-ligand complex does not undergo an ETC rearrangement to the bridging-ligand isomer, whereas the complex investigated by Talarmin and co-workers does, because ETC mechanisms are rare. A possible explanation is that the chelating ligand of the complex presented herein is more bulky than that presented by Talarmin and co-workers, which could prevent rearrangement of the chelating ligand to the bridging-ligand isomer. Additionally the ligand herein has a smaller bite angle, which constrains the angle of the P-N-P bond, whereas the complex investigated by Talarmin and co-workers contains a more flexible P-C-C-P chain.

6.4 Testing for electrocatalytic reduction of protons by $Fe_2(\mu\text{-pdt})(CO)_4$-($\mu$-($Ph_2PN(CH_2CHCH_2)PPh_2$)) and $Fe_2(\mu\text{-pdt})(CO)_4$($\kappa$-($Ph_2PN(CH_2CHCH_2)PPh_2$)), using the strong acid $HBF_4.Et_2O$ as the proton source

Following on from the analysis of the two complexes in the absence of protons, experiments were carried out in the presence of a proton source to analyse if the complexes are catalysts towards proton reduction. The first set of experiments used the strong acid $HBF_4.Et_2O$ as the proton source.

6.4.1 Testing for electrocatalytic reduction of protons by $Fe_2(\mu\text{-pdt})(CO)_4$($\mu$-($Ph_2PN(CH_2CHCH_2)PPh_2$)), using the strong acid $HBF_4.Et_2O$ as the proton source, in MeCN

The CVs of the bridging-ligand complex with up to 10 molar equivalents of $HBF_4.Et_2O$ in MeCN are shown in Figure 207. After the first addition of acid (dark red line) a new reduction peak occurs at -1.79 V. A broad feature at -2.1 V is also present. On further additions of acid a reduction peak at ca. -1.6 V grows. The peaks that appeared after the first addition of acid continue to increase with acid concentration.

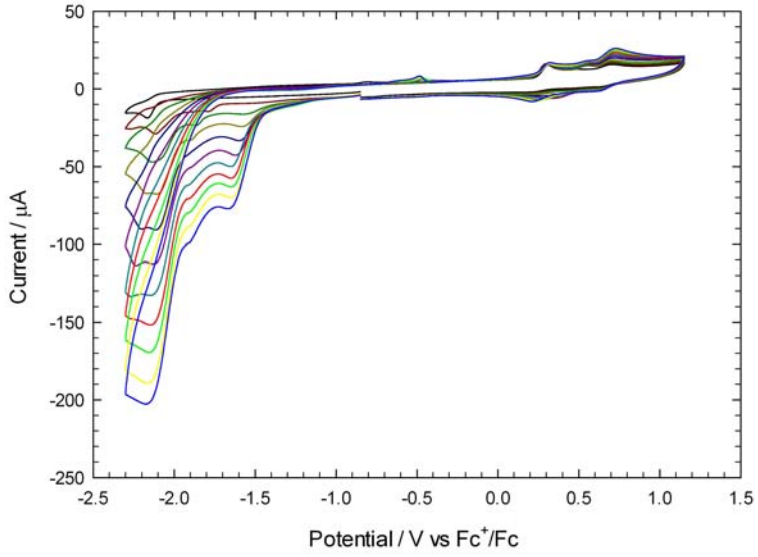

Figure 207: Cyclic voltammetry of $Fe_2(\mu\text{-pdt})(CO)_4(\mu\text{-}(Ph_2PN(CH_2CHCH_2)PPh_2))$ (0.5 mM) in MeCN-$[NBu_4][PF_6]$ in the absence of acid and in the presence of up to 10 molar equivalents $HBF_4.Et_2O$ in steps of 1 molar equivalent (v=0.1 Vs^{-1}, glassy carbon electrode; V vs Fc^+/Fc)

The oxidation peak of the complex is changed very little throughout the additions of $HBF_4.Et_2O$. This suggests that a significant proportion of the neutral complex remains unprotonated after the addition of acid. This is in keeping with observations in Section 6.1.1, in which only a partial protonation on addition of $HBF_4.Et_2O$ was observed.

The reduction peak at ca. -1.6 V grows on each addition of $HBF_4.Et_2O$, implying a catalytic mechanism. The position of the peak is where the reduction of the protonated complex would be

expected. As there is only a small amount of protonated complex in the bulk solution (as indicated by the oxidation peak being only slightly diminished), the catalytic mechanism must rely on the small quantity of the protonated complex being reduced, and establishing a catalytic cycle.

6.4.2 Testing for electrocatalytic reduction of protons by $Fe_2(\mu\text{-pdt})(CO)_4(\kappa\text{-}(Ph_2PN\text{-}(CH_2CHCH_2)PPh_2))$, using the strong acid $HBF_4.Et_2O$ as the proton source, in MeCN

The above experiments have been repeated for the chelating-ligand isomer. Figure 208 shows the CVs after additions of $HBF_4.Et_2O$ in MeCN. On the first addition of acid (dark red line) the first reduction peak has decreased and a new reduction peak has appeared at -1.59 V. The first oxidation peak has also decreased, with a new peak appearing at 0.71 V. This behaviour suggests protonation has occurred at the Fe centres (as earlier predicted by IR spectroscopy) - the diminishing peaks due to the diminishing concentration of the neutral complex, and the growing peaks due to the growing concentration of the protonated complex.

On further additions of acid the first reduction peak continues to grow. Two further reduction peaks also grow at ca. -1.9 V and ca. -2.2 V. These results indicate that protonation occurs under these conditions, and that the reduction of the protonated complex initiates a catalytic mechanism.

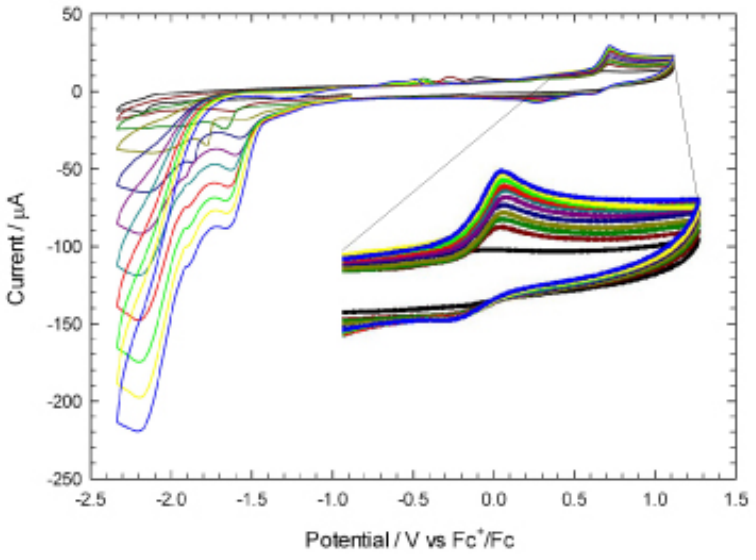

Figure 208: Cyclic voltammetry of $Fe_2(\mu\text{-pdt})(CO)_4(\kappa\text{-}(Ph_2PN(CH_2CHCH_2)PPh_2))$ (0.5 mM) in MeCN-$[NBu_4][PF_6]$ in the absence of acid and in the presence of up to 10 molar equivalents $HBF_4.Et_2O$ in steps of 1 molar equivalent (v=0.1 Vs^{-1}, glassy carbon electrode; V vs Fc^+/Fc)

6.4.3 Summary and discussion

A comparison of the bridging- and chelating-ligand complexes in MeCN in the presence of 10 molar equivalents $HBF_4.Et_2O$ is shown in Figure 209. The chelating-ligand complex exhibits a higher catalytic current, presumably due to its more rapid protonation in the presence of the acid. This

difference is emphasised in Figure 210, which shows the current due to the chelating-ligand complex (red line in Figure 209) minus the current due to the bridging-ligand complex (black line in Figure 209). These experiments give further evidence that there is a benefit of using a chelating ligand, rather than a bridging ligand, to make the electron density asymmetric, which enables a more rapid protonation of the complex and therefore a faster rate of catalysis. Compared to other complexes in the literature the reduction potential for catalysis is reasonable, however due to the slow protonation compared to complexes with higher electron density on the Fe centres the rate of catalysis is slow. An indicative mechanism for the chelating complex is shown in Figure 211.

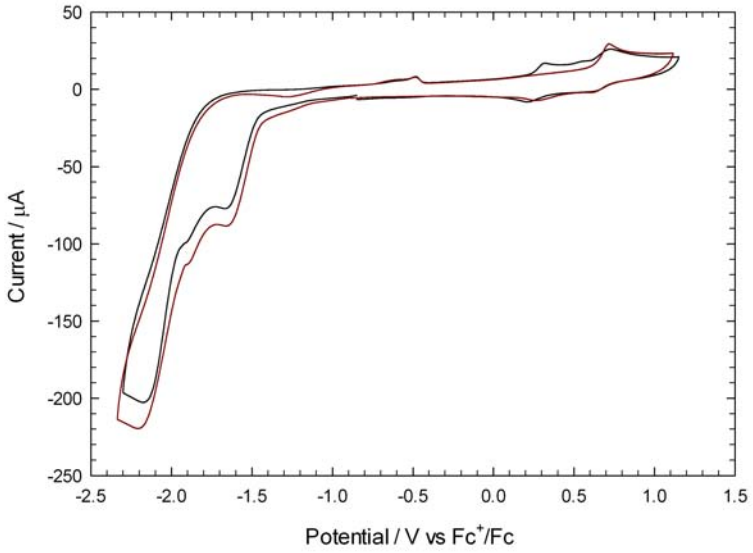

Figure 209: Cyclic voltammetry of $Fe_2(\mu\text{-pdt})(CO)_4(\mu\text{-}(Ph_2PN(CH_2CHCH_2)PPh_2))$ (0.5 mM, black line) and $Fe_2(\mu\text{-pdt})(CO)_4(\kappa\text{-}(Ph_2PN(CH_2CHCH_2)PPh_2))$ (0.5 mM, red line) in the presence of 10 molar equivalents $HBF_4.Et_2O$ in MeCN-$[NBu_4][PF_6]$ (v=0.1 Vs^{-1}, glassy carbon electrode; V vs Fc^+/Fc)

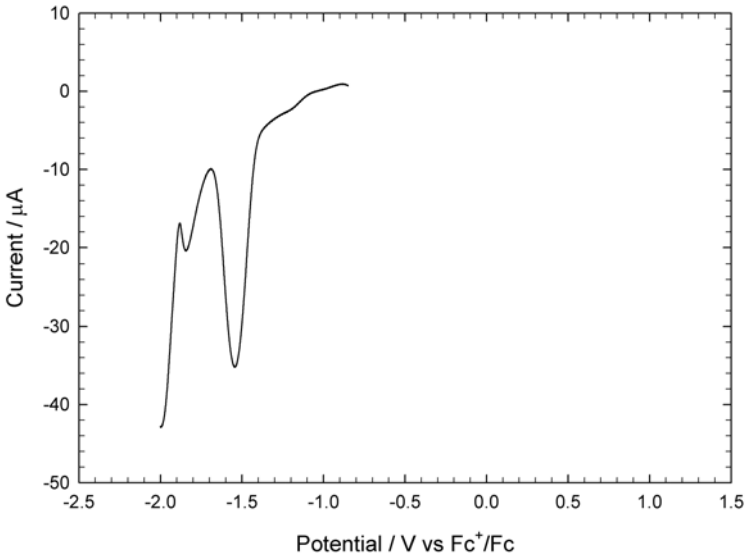

Figure 210: Current from CV of $Fe_2(\mu\text{-pdt})(CO)_4(\kappa\text{-}(Ph_2PN(CH_2CHCH_2)PPh_2))$ (0.5 mM, red line in Figure 209) minus current from CV of $Fe_2(\mu\text{-pdt})(CO)_4(\mu\text{-}(Ph_2PN(CH_2CHCH_2)PPh_2))$ (0.5 mM, black line in Figure 209), both in the presence of 10 molar equivalents $HBF_4.Et_2O$ in MeCN-$[NBu_4][PF_6]$ (v=0.1 Vs^{-1}, glassy carbon electrode; V vs Fc^+/Fc)

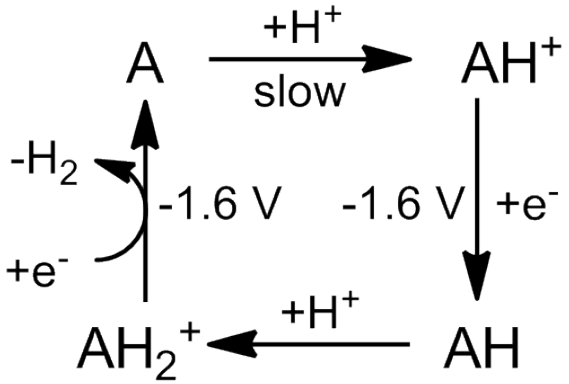

Figure 211: Possible catalytic mechanism of $Fe_2(\mu\text{-pdt})(CO)_4(\kappa\text{-}(Ph_2PN(CH_2CHCH_2)PPh_2))$ (denoted A) in the presence of $HBF_4.Et_2O$; potentials are taken from the cyclic voltammograms obtained in MeCN

6.5 Testing for electrocatalytic reduction of protons by $Fe_2(\mu\text{-pdt})(CO)_4(\mu\text{-}(Ph_2PN(CH_2CH\text{-}CH_2)PPh_2))$ and $Fe_2(\mu\text{-pdt})(CO)_4(\kappa\text{-}(Ph_2PN(CH_2CH\text{-}CH_2)PPh_2))$, using the weak acid HOAc as the proton source

It is clear that the weaker acid HOAc would be unable to protonate the neutral complexes, as the significantly stronger acid $HBF_4.Et_2O$ was only able to protonate the chelating complex slowly, however it was unknown whether HOAc would protonate the reduced form of the complexes, possibly leading to a ECEC catalytic mechanism. The first reduction of both complexes were observable within the potential window of the MeCN-$[NBu_4][PF_6]$ (Figure 204), therefore, an investigation has been performed using the weaker acid HOAc as the proton source.

6.5.1 Testing for electrocatalytic reduction of protons by $Fe_2(\mu\text{-pdt})(CO)_4(\mu\text{-}(Ph_2PN(CH_2CHCH_2)PPh_2))$, using the weak acid HOAc as the proton source, in MeCN

The CVs of the bridging-ligand complex in MeCN adding HOAc are shown in Figure 212. On the first addition of acid the first reduction peak shifts to a slightly more positive potential and increases in height. The oxidation peaks are largely unchanged. On further additions of acids the reduction peak continues to grow in height, indicating that the complex is catalytic towards proton reduction after the first reduction of the complex. Up to 50 molar equivalents of HOAc were added to the solution (Figure 213). The catalytic peak continued to grow.

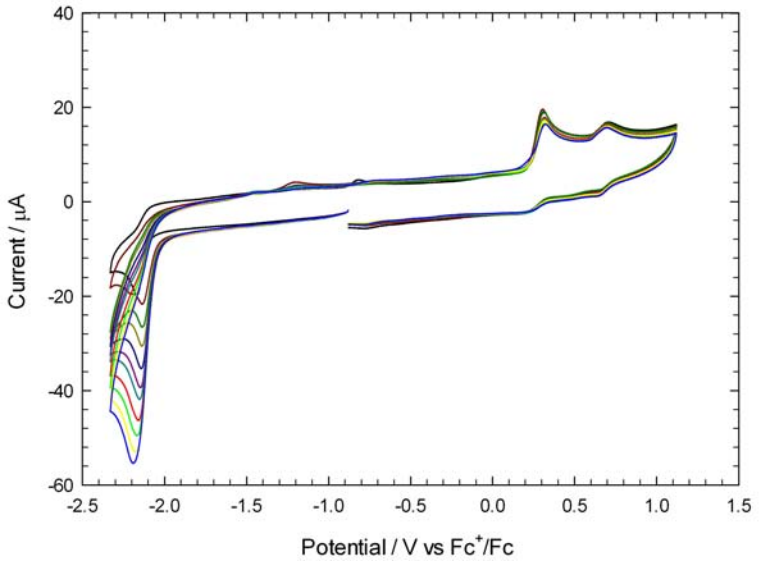

Figure 212: Cyclic voltammetry of $Fe_2(\mu\text{-pdt})(CO)_4(\mu\text{-}(Ph_2PN(CH_2CHCH_2)PPh_2))$ (0.5 mM) in MeCN-$[NBu_4][PF_6]$ in the absence of acid and in the presence of up to 10 molar equivalents HOAc in steps of 1 molar equivalent (v=0.1 Vs^{-1}, glassy carbon electrode; V vs Fc^+/Fc)

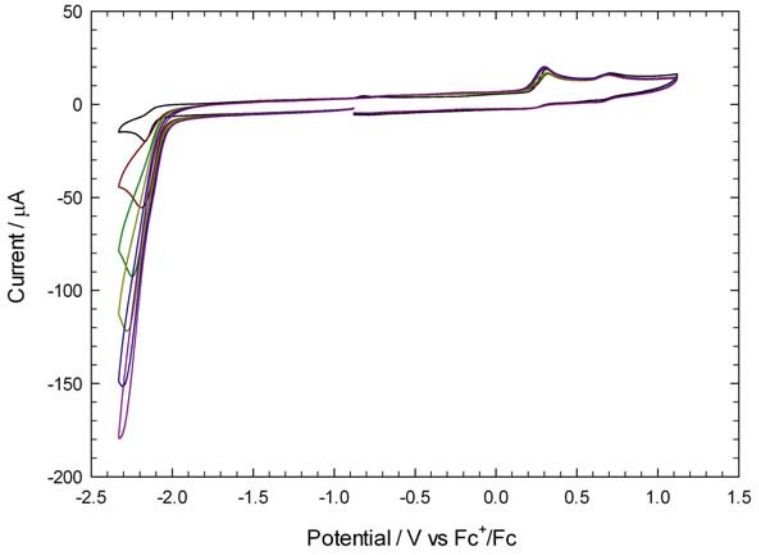

Figure 213: Cyclic voltammetry of $Fe_2(\mu\text{-pdt})(CO)_4(\mu\text{-}(Ph_2PN(CH_2CHCH_2)PPh_2))$ (0.5 mM) in MeCN-$[NBu_4][PF_6]$ in the absence of acid and in the presence of up to 50 molar equivalents HOAc in steps of 10 molar equivalent (v=0.1 Vs^{-1}, glassy carbon electrode; V vs Fc^+/Fc)

6.5.2 Testing for electrocatalytic reduction of protons by $Fe_2(\mu\text{-pdt})(CO)_4(\kappa\text{-}(Ph_2PN\text{-}(CH_2CHCH_2)PPh_2))$, using the weak acid HOAc as the proton source, in MeCN

The chelating-ligand complex has also been investigated with additions of HOAc as the proton source in MeCN. The CVs of the additions up to 10 equivalents of acid are shown in Figure 214. On the first addition of acid the first reduction peak shifts to a slightly less negative potential and increases in height. The oxidation behaviour is unchanged from the neutral complex. On further additions of acid the first reduction peak continues to grow, indicating that the complex is catalytic after it has been reduced. Up to 50 molar equivalents HOAc were added in total, as shown in Figure 215.

6.5.3 Summary and discussion

Comparing the CVs of the bridging- and chelating-ligand complexes after addition of HOAc (Figure 216), it is clear that there is no advantage in using one isomer over the other when the proton source is HOAc. As was found in Section 6.2.3 the two complexes are reduced at similar potentials, as it is this reduction which initiates the catalytic mechanism the complexes are catalytic at similar potentials.

The behaviours of each complex in the presence of HOAc and $HBF_4.Et_2O$ in MeCN are compared in Figures 217 and 218. The overpotential is certainly greater for the weaker acid.

The catalytic mechanism in the presence of HOAc can be assumed to be the same for both the bridging- and chelating-ligand complexes, and is shown in Figure 219. This mechanism differs fundamentally from that suggested for the chelating-ligand complex in the presence of $HBF_4.Et_2O$ (Figure 211) in that the first step is a reduction process, rather than a protonation.

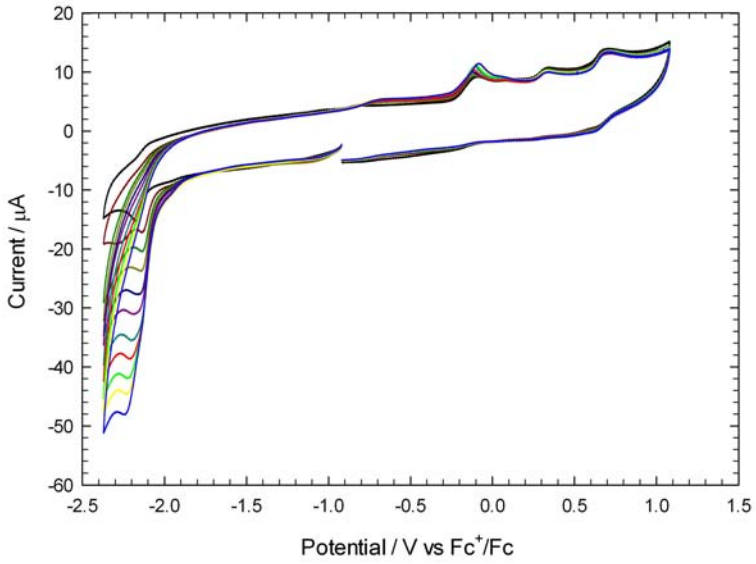

Figure 214: Cyclic voltammetry of $Fe_2(\mu\text{-pdt})(CO)_4(\kappa\text{-}(Ph_2PN(CH_2CHCH_2)PPh_2))$ (0.5 mM) in MeCN-$[NBu_4][PF_6]$ in the absence of acid and in the presence of up to 10 molar equivalents HOAc in steps of 1 molar equivalent (v=0.1 Vs^{-1}, glassy carbon electrode; V vs Fc^+/Fc)

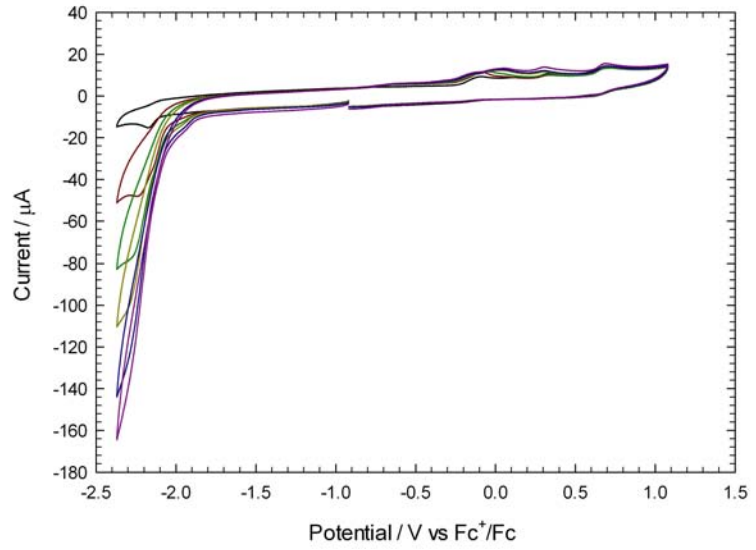

Figure 215: Cyclic voltammetry of $Fe_2(\mu\text{-pdt})(CO)_4(\kappa\text{-}(Ph_2PN(CH_2CHCH_2)PPh_2))$ (0.5 mM) in MeCN-$[NBu_4][PF_6]$ in the absence of acid and in the presence of up to 50 molar equivalents HOAc in steps of 10 molar equivalent (v=0.1 Vs^{-1}, glassy carbon electrode; V vs Fc^+/Fc)

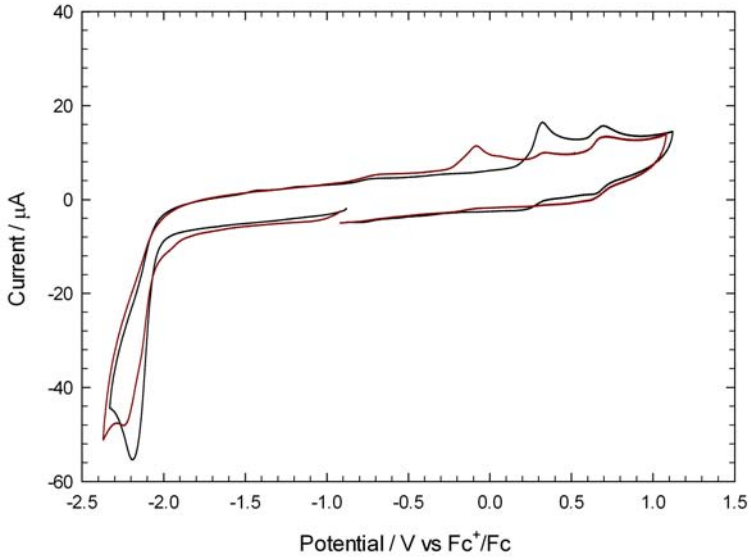

Figure 216: Cyclic voltammetry of $Fe_2(\mu\text{-pdt})(CO)_4(\mu\text{-}(Ph_2PN(CH_2CHCH_2)PPh_2))$ (0.5 mM, black line) and $Fe_2(\mu\text{-pdt})(CO)_4(\kappa\text{-}(Ph_2PN(CH_2CHCH_2)PPh_2))$ (0.5 mM, red line) in the presence of 10 molar equivalents HOAc in MeCN-$[NBu_4][PF_6]$ (v=0.1 Vs^{-1}, glassy carbon electrode; V vs Fc^+/Fc)

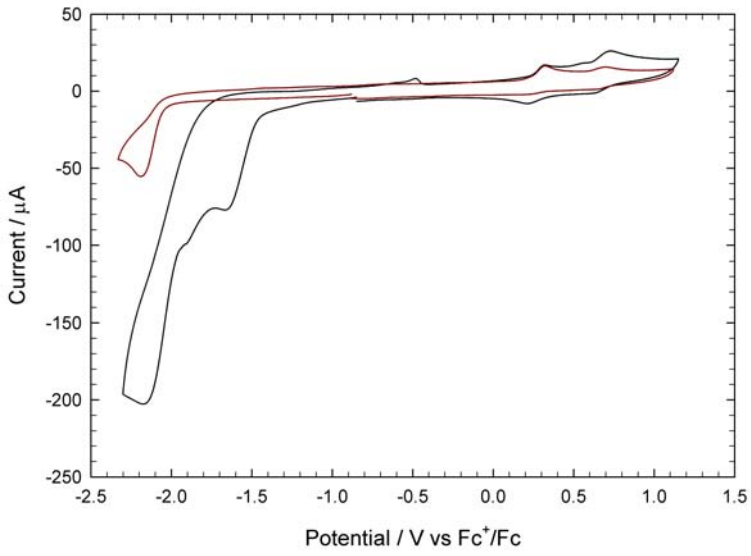

Figure 217: Cyclic voltammetry of $Fe_2(\mu\text{-pdt})(CO)_4(\mu\text{-}(Ph_2PN(CH_2CHCH_2)PPh_2))$ (0.5 mM) in the presence of 10 molar equivalents $HBF_4.Et_2O$ (black line) and HOAc (red line) in MeCN-$[NBu_4][PF_6]$ (v=0.1 Vs^{-1}, glassy carbon electrode; V vs Fc^+/Fc)

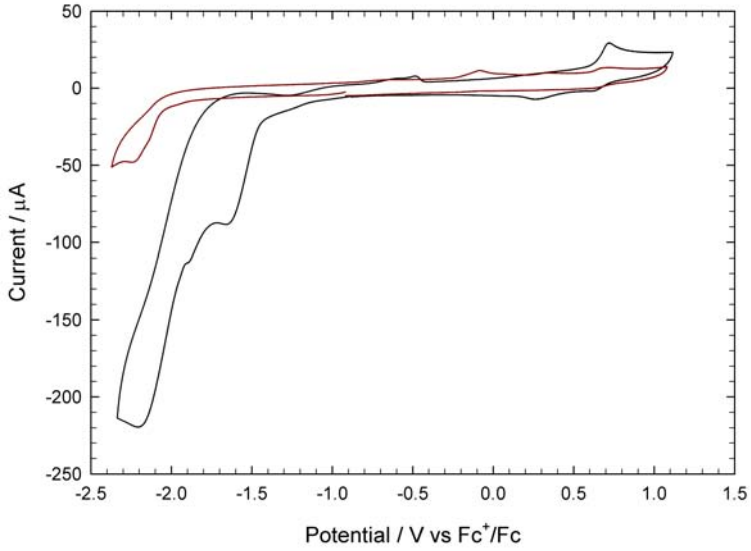

Figure 218: Cyclic voltammetry of $Fe_2(\mu\text{-pdt})(CO)_4(\kappa\text{-}(Ph_2PN(CH_2CHCH_2)PPh_2))$ (0.5 mM) in the presence of 10 molar equivalents $HBF_4.Et_2O$ (black line) and HOAc (red line) in MeCN-$[NBu_4][PF_6]$ (v=0.1 Vs^{-1}, glassy carbon electrode; V vs Fc^+/Fc)

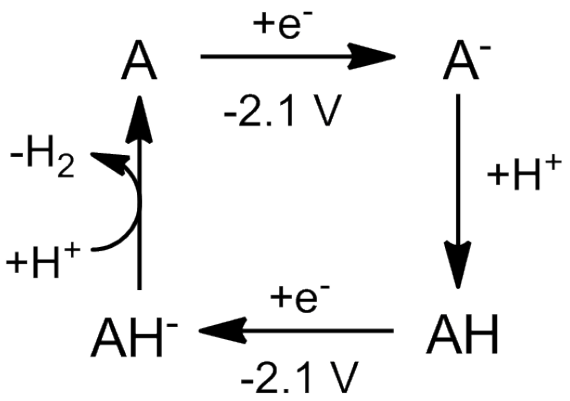

Figure 219: Possible catalytic mechanism of $Fe_2(\mu\text{-pdt})(CO)_4(\mu\text{-}(Ph_2PN(CH_2CHCH_2)PPh_2))$ and $Fe_2(\mu\text{-pdt})(CO)_4(\kappa\text{-}(Ph_2PN(CH_2CHCH_2)PPh_2))$ (denoted A) in the presence of HOAc; potentials are taken from the cyclic voltammograms obtained in MeCN

6.6 Summary and discussion

The chelating-ligand complex has been found to protonate in the presence of $HBF_4.Et_2O$, leading to a slow catalytic mechanism. The bridging-ligand complex on the other hand was only partially protonated by this acid, leading to a slower catalytic mechanism. This is further confirmation that the asymmetry of electron density caused by the chelating ligand is able to favour protonation, and increase the rate of catalysis of proton reduction. Interestingly, the reduction processes of both complexes occur at a very similar potential in MeCN, and at this potential the complex was catalytic towards reduction of HOAc.

No evidence has been found for protonation at the N atom in the ligand. This suggests that N atom is not sufficiently basic to protonate.

The ETC mechanism observed by Talarmin and co-workers for their similar chelating complex has not been observed for the chelating complex analysed herein.

Further work should aim to increase electron density at the iron centres of the chelating-ligand complex. The complex has been shown to undergo a catalytic mechanism, however the rate is slow due to the slow rate of protonation of the Fe centres. Increasing electron density on the Fe centres would increase the rate of the protonation step of the catalytic mechanism, and thus improve the rate of catalysis. One novel way this could be attempted is through use of an electron donating bridge. Many bridges have been analysed in the literature which withdraw electron density in order to decrease a complex's reduction potential. This could be an opportunity to attempt the opposite, i.e. to increase the basicity of the Fe centres.

7 Conclusion

The aim of this dissertation was to investigate electrocatalytic reduction of protons to hydrogen by complexes inspired by the FeFe hydrogenase enzyme active site (H-cluster). The research has generated several conclusions, as detailed in the relevant chapters. Some of the major findings shall be outlined below. As with the introduction presented in Chapter 1, the conclusions shall be grouped in to the major structural themes: the influence of varying the dithiolate bridge, the influence of varying the ligand set, and the influence of varying the Fe centres. A fourth theme has been exposed by the research presented, namely the influence of the electrolyte environment.

7.1 Varying the dithiolate bridge

As was discussed in Section 1.3, the dithiolate bridge was already known to have an influence on the catalytic activity of H-cluster mimics. The bridge influences the electron density on the Fe centres of the complex, thus controlling both its reduction potential and its susceptibility to protonation. Further reasons the bridge has been used include to host a basic site for protonation, or to exert a steric influence on the complex. The results presented in this thesis have built on the current understanding of the influence of the dithiolate bridge.

Chapter 3 analysed the influence of the highly electron withdrawing bridge $(SC_6F_5)_2$. The bridge withdrew electron density from the Fe centres, resulting in a very mild reduction potential of the neutral complex compared to other complexes in this thesis and the literature. Although the complex was unable to protonate, the benefit of the electron withdrawing bridge could be seen in the milder reduction potential of the complex (-1.37 V in DCM and -1.15 V in MeCN). A comparison with the analogous di-iron pdt hexacarbonyl complex, $Fe_2(\mu\text{-pdt})(CO)_6$, indicated that the $(SC_6F_5)_2$ bridge had caused a positive shift in the reduction potential of 0.49 V. Compared to other complexes in the literature this is one of the mildest overpotentials for proton reduction recorded.

Chapter 4 also probed the influence of varying the dithiolate bridge. On to the triphos-ligand complexes were placed four differing bridges: pdt = $SCH_2CH_2CH_2S$; adt = $SCH_2N(CH_2C_6H_5)CH_2S$; $(SCH_3)_2$); and SCH_2CH_2S. The varying of the bridge had only a slight influence on the redox potentials of the neutral complexes. For example, the unlinked $(SMe)_2$-bridged was oxidised at ca. 0.2 V lower than the pdt- and adt-bridged complex; this is thought to be due to the unconstraining bridge allowing for greater orbital overlap and therefore easier oxidation. In the presence of protons the varying bridges were found to have only minor influence on the electrocatalytic activity of the complexes.

7.2 Varying the ligand set

Section 1.4 introduced the influence of the ligand set on catalytic activity. All of the complexes presented in this dissertation have features that contribute to the understanding of this topic.

The first complex presented was $Fe_2(SC_6F_5)_2(CO)_6$ (Chapter 3). As an extension to the investigations into this complex, the analogous complex with a bridging dppm ligand ($Fe_2(SC_6F_5)_2(\mu$-$Ph_2PCH_2PPh_2)(CO)_4$) was synthesised and analysed. As expected from the literature, the inclusion of the dppm ligand resulted in a shift in the redox potentials in a negative direction, due to electron density donated to the Fe centres from the ligand. The inclusion of the ligand did not allow for the complex to protonate, thus the inclusion of the ligand resulted in no benefit in the catalysis - indeed, it pushed the reduction potential more negative. Further research is required to investigate if the complex could be made basic enough to protonate either with a chelating ligand or a further substitution. Even so there is a balance to be made, as protonation may not counteract the negative shift in reduction potential.

Chapter 4 aimed to analyse how the triphos ligand, used to exert steric twist and electronic asymmetry, influenced electrocatalytic activity. The triphos ligand provided sufficient electron density to the Fe centres for the complexes to protonate. The reduction potentials of the neutral complexes were very negative. The protonation of the complexes did cause the first reduction potentials to shift positive, however even after this positive shift, the overpotential was still poor compared to other complexes presented in this dissertation and the literature. This again shows that there is a balance to be made when adding electron density to the Fe centres, between the benefit of protonation versus the negative shift in the reduction potential.

A range of ligands, going from a heptacarbonyl system to mono- and di-PPh_3 systems, were used on the tri-iron complexes investigated in Chapter 5. The electrochemistry of each complex was similar, however, on addition of each PPh_3 ligand the oxidation and reduction potentials shifted in a negative direction due to the additional electron density on the Fe centres due to the phosphine ligands. Even the di-substituted complex was not basic enough to protonate. Thus, the complexes were only able to catalyse proton reduction after they had been reduced. Future work could attempt to put further electron density on the Fe centres by further substitutions.

The final complexes presented (Chapter 6) allowed for a comparison of bridging versus chelating ligands. The bridging-ligand complex protonated more slowly than the chelating-ligand, due to an asymmetry in the electron density of the chelating-ligand complex. This resulted in the chelating-ligand complex being a superior catalyst.

7.3 Varying the Fe centres

Section 1.5 presented the current understanding of the influence of the iron centres on catalytic activity. Chapter 5 reported the effect of switching from di- and tetra-iron complexes, to a tri-iron system. In the neutral state the tri-iron complexes are mixed valence, as with the H-cluster in its catalytic state. Structural analysis of the tri-iron complexes revealed that they exhibit a semi-bridging CO ligand, again a key feature of the H-cluster. The reduction potential of the tri-iron complexes were significantly less negative than the corresponding di-iron complexes. The

tri-iron complexes were unable to protonate. The complexes were found to be catalytic after their first reduction, and the potentials at which this occurred were significantly milder than the di-iron analogues. Comparisons between the tri- and tetra-iron systems are hampered by the differing conditions used, however, the results presented herein suggest the tri-iron system is catalytic at a slightly milder reduction potential than the tetra-iron system.

7.4 Varying the electrolyte environment

Throughout this dissertation the complexes have been investigated in differing electrolyte environments. These environments have been found to significantly influence the electrochemical behaviour of the complexes, which implies that great care should be taken when comparing behaviours of complexes reported in the literature.

The first complex investigated ($Fe_2(\mu\text{-}(SC_6F_5)_2))(CO)_6$) showed a difference in reduction potential of 0.22 V when moving from DCM to MeCN. Unlike in the experiments performed in DCM, the catalysis due to the minor species formed after reduction of the complex is severely limited in MeCN. One possible reason for this is that the vacant coordination site generated after CO ligand loss is being occupied by the MeCN solvent, thus limiting the formation of the highly catalytic species.

In Chapter 4 the electrolyte solution was varied extensively, using DCM-[NBu_4][PF_6], DCM-[NBu_4][ClO_4], DCM-[NBu_4][BF_4] and MeCN-[NBu_4][PF_6]. The differences affected the oxidation behaviour of the complexes; for example, the products of the first oxidation process which appeared to be stabilised by some of the electrolytes and not by others. The electrolyte solution had an unexpected influence on the catalytic activity of the complexes. For example, when testing the pdt-bridged complex in the presence of 10 molar equivalents $HBF_4.Et_2O$, the catalytic current was three times larger in DCM-[NBu_4][ClO_4] than DCM-[NBu_4][PF_6]. The reason for this improvement in the rate of catalysis is not yet fully understood.

A Synthesis of the complexes investigated

The following sections outline the procedures followed to synthesise the complexes that have been investigated in this research. All of the complexes, with the exception of $Fe_2(\mu\text{-}((SCH_3)_2))(CO)_3(\mu,\eta^2\text{-}Ph_2PCH_2CH_2P(Ph)CH_2CH_2PPh_2)$, have been performed by other people as stated.

A.1 Synthesis of $Fe_2(SC_6F_5)_2(CO)_6$

$Fe_3(CO)_{12}$ (1.50 g, 2.98 mmol) and C_6F_5SH (1.79 ml, 5.96 mmol) were refluxed in toluene for 1 h, the dark green solution turning deep red. The solution was cooled to room temperature and removal of volatiles yielded a red oily solid (2.71 g, 90 %). The solid was dissolved in hexane and filtered, removal of volatiles from the clear red filtrate gave a bright red solid (0.842 g, 0.570 mmol, 29 %). The solid caught in the filter paper was dissolved in CH_2Cl_2, and on removal of volatiles yielded a bright red solid (1.605 g, 2.370 mmol, 52 %). IR analysis confirmed the two solids to be the same compound, giving the overall yield (2.447 g, 3.610 mmol, 81 %).

The synthesis was performed by Faith Ridley and Graeme Hogarth in University College London.

A.2 Synthesis of $Fe_2(SC_6F_5)_2(\mu\text{-}Ph_2PCH_2PPh_2)(CO)_4$

$Fe_2(CO)_6(\mu\text{-}SC_6F_5)_2$ (0.329 g, 0.480 mmol) and dppm (0.21 g, 0.546 mmol) were refluxed in toluene for 2 h, the dark red solution turning a deeper red. The solution was cooled to room temperature and volatiles were removed yielding a dark red oily solid (0.534 g, 0.420 mmol, 43 %). The solid was washed with hexane and recrystallised from CH_2Cl_2-MeOH giving deep red block crystals.

The synthesis was performed by Faith Ridley and Graeme Hogarth in University College London.

A.3 Synthesis of $Fe_2(\mu\text{-pdt})(CO)_3(\mu,\eta^2\text{-}Ph_2PCH_2CH_2P(Ph)CH_2CH_2PPh_2)$

$Fe_2(CO)_6(\mu\text{-pdt})$ (0.20 g, 0.518 mmol) and triphos (0.277 g, 0.518 mmol) were heated in toluene for 16 h. After removal of volatiles the solids were washed with hexane (3 x 10 ml) and diethyl ether (3 x 5 ml) and dried. Crystallization from CH_2Cl_2-MeOH afforded the product as a brown solid (0.36 g, 83 %).

The synthesis was performed by Graeme Hogarth in University College London.

A.4 Synthesis of $Fe_2(\mu\text{-}(SCH_2N(CH_2C_6H_5)CH_2S))(CO)_3(\mu,\eta^2\text{-}Ph_2PCH_2CH_2P(Ph)CH_2CH_2PPh_2)$

$Fe_2(CO)_6\mu\text{-}SCH_2N(Bz)CH_2S$ (0.237 g, 0.499 mmol) and triphos (0.200 g, 0.499 mmol) were refluxed in toluene for 19 h, the clear dark red solution turning deep red on heating and reflux. The solution was allowed to cool to room temperature and volatiles were removed giving a dark red oily solid which was washed with hexane. The washed solid was redissolved in CH_2Cl_2 and the product crashed out on addition of hexane. Removal of volatiles gave a red solid (0.479 g, 0.518 mmol, 104 %).

The synthesis was performed by Faith Ridley and Graeme Hogarth in University College London.

A.5 Synthesis of $Fe_2(\mu\text{-}((SCH_3)_2))(CO)_3(\mu,\eta^2\text{-}Ph_2PCH_2CH_2P(Ph)CH_2CH_2PPh_2)$

$Fe_2(CO)_6\mu$-$((SCH_3)_2)$ (0.100 g, 0.190 mmol) and triphos (0.122 g, 0.288 mmol) were refluxed in toluene for 4 h. The solution was allowed to cool to room temperature and volatiles were removed giving a dark yellow / green oily solid which was washed with hexane. The washed solid was crystallised in CH_2Cl_2-MeOH to form thin crystals.

The synthesis was performed with the assistance of Graeme Hogarth in University College London.

A.6 Synthesis of $Fe_2(\mu\text{-edt})(CO)_3(\mu,\eta^2\text{-}Ph_2PCH_2CH_2P(Ph)CH_2CH_2PPh_2)$

$Fe_2(CO)_6(\mu$-edt) (0.068 g, 0.187 mmol) and triphos (0.100 g, 0.187 mmol) with 2 equiv. $Me_3NO.2H_2O$ (0.042 g, 0.347 mmol) were refluxed in toluene for 40 h, the initial red-orange solution turning deep red-brown on heating and resulting in a dark brown solution after 40 h reflux. The solution was allowed to cool to room temperature and solvent removed in vacuo giving a dark brown sticky solid (0.174 g, 0.214 mmol, 114 %).

Alternatively, $Fe_2(CO)_6(\mu$-edt) (0.136 g, 0.347 mmol) and triphos (0.200 g, 0.374 mmol) with 2 equiv. $Me_3NO.2H_2O$ (0.084 g, 0.748 mmol) were refluxed in toluene for 20 h, the initial red-orange solution turning deep red-brown on heating and resulting in a dark brown solution over the course of the reflux. The solution was allowed to cool to room temperature and solvent removed in vacuo giving a dark brown sticky solid which was washed with hexane and Et_2O to give a dark brown solid (0.173 g, 0.214 mmol, 57 %). This was recrystallised by slow diffusion of MeOH into a concentrated CH_2Cl_2 solution giving clumps of dark brown crystals.

The synthesis was performed by Faith Ridley and Graeme Hogarth in University College London.

A.7 Synthesis of $Fe_3(\mu\text{-edt})_2(CO)_7$

To a suspension of $Na_2[Fe(CO)_4]$, (ca. 2.183 g, 10.20 mmol) in THF (30 ml) was added drop-wise a solution of 1,2-ethanedithiol (0.479 g, 5.10 mmol) in THF (30 ml). After stirring for 24 h at room temperature, the solvent was removed in vacuo and the residue extracted with hexane and filtered on Kieselguhr. The filtrate was concentrated under reduced pressure to give a reddish-yellow gummy mass, which was chromatographed by TLC on silica gel. Elution with hexane developed to bands. The faster moving reddish-yellow band gave $Fe_2(CO)_6(\mu$-edt) (512 mg, 27 %) and red crystals after recrystallisation from hexane/CH_2Cl_2 at 4 °C.

The synthesis was performed by Shariff Kabir, Shishir Ghosh and Ahibur Rahaman in Jahangirnagar University, Bangladesh.

A.8 Synthesis of $Fe_3(\mu\text{-edt})_2(CO)_6PPh_3$ and $Fe_3(\mu\text{-edt})_2(CO)_5(PPh_3)_2$

A benzene solution (20 ml) of $Fe_3(CO)_7(\mu\text{-edt})_2$ (75 mg, 0.137 mmol) and PPh_3 (36 mg, 0.137 mmol) was heated to reflux for 15 h. The solvent was removed under reduced pressure and the residue chromatographed by TLC on silica gel. Elution with hexane/CH_2Cl_2 (v/v 9:1) developed five bands. The first and last band was unreacted [$Fe_3(CO)_7(\mu\text{-edt})_2$] (trace). The second to fifth band afforded the following compounds in order of elution: [$Fe_2(CO)_5(PPh_3)(\mu\text{-edt})$] (18 mg, 22 %) as red crystals, [$Fe_3(CO)_6(PPh_3)(\mu\text{-edt})_2$][$Fe_3(CO)_7(\mu\text{-edt})_2$] (25 mg, 23 %) as orange crystals, [$Fe_3(CO)_5(PPh_3)_2(\mu\text{-edt})_2$] (16 mg, 12 %) as red crystals and Ph_3PS (15 mg, 30 %) as white crystals after recrystallisation from hexane/CH_2Cl_2 at -20 °C.

The synthesis was performed by Shariff Kabir, Shishir Ghosh and Ahibur Rahaman in Jahangirnagar University, Bangladesh.

A.9 Synthesis of $Fe_2(\mu\text{-pdt})(CO)_4(\mu\text{-}(Ph_2PN(CH_2CHCH_2)PPh_2))$

$Fe_2(CO)_6(\mu\text{-pdt})$ (0.20 g, 0.518 mmol) and $Ph_2PN(allyl)PPh_2$ (0.42 g, 0.570 mmol) were dissolved into toluene (approx. 50 ml). The brick red solution was refluxed for three hours, the solution darkened to brown. The solvent was removed giving an oily residue. CH_2Cl_2 (approx. 10 ml) and hexane (approx. 10 ml) were added so that on the final solvent removal a dry red-brown solid resulted. The crude was washed with hexane (3 x 5 ml / deep brown) and Et_2O (3 x 5 ml / even deeper brown).

The synthesis was performed by Graeme Hogarth in University College London.

A.10 Synthesis of $Fe_2(\mu\text{-pdt})(CO)_4(\kappa\text{-}(Ph_2P\text{-}N(CH_2CHCH_2)PPh_2))$

$Fe_2(CO)_6(\mu\text{-pdt})$ (0.10 g, 0.255 mmol) and $Ph_2PN(allyl)PPh_2$ (0.15 g, 0.350 mmol) were dissolved into MeCN (approx. 25 ml) to give a crimson solution. Separately $Me_3NO.2H_2O$ (0.08 g, 0.721 mmol) was dissolved into MeCN (approx. 20 ml), solution was a light yellow. On addition the Me_3NO solution to the mixture the colour went immediately very dark. After two hours mixing the solvent was removed and a dark brown black solid remained. The crude was given a wash with hexane (2 x 10 ml). The hexane washes were left to slowly evaporate giving small crystals.

The synthesis was performed by Graeme Hogarth in University College London.

References

[1] S. Ghosh, G. Hogarth, K. B. Holt, S. E. Kabir, A. Rahaman and D. G. Unwin, *Chemical Communications*, 2011, **47**, 11222–11224.

[2] Y. Nicolet, C. Piras, P. Legrand, C. E. Hatchikian and J. C. Fontecilla-Camps, *Structure with Folding and Design*, 1999, **7**, 13–23.

[3] J. W. Peters, W. N. Lanzilotta, B. J. Lemon and L. C. Seefeldt, *Science*, 1998, **282**, 1853–1858.

[4] B. J. Lemon and J. W. Peters, *Biochemistry*, 1999, **38**, 12969–12973.

[5] C. Greco, M. Bruschi, L. De Gioia and U. Ryde, *Inorganic Chemistry*, 2007, **46**, 5911–5921.

[6] K. A. Vincent, A. Parkin and F. A. Armstrong, *Chemical Reviews*, 2007, **107**, 4366–4413.

[7] D. S. Chong, I. P. Georgakaki, R. Mejia-Rodriguez, J. Samabria-Chinchilla, M. P. Soriaga and M. Y. Darensbourg, *Dalton Transactions*, 2003, 4158–4163.

[8] S. J. Borg, T. Behrsing, S. P. Best, M. Razavet, X. M. Liu and C. J. Pickett, *Journal of the American Chemical Society*, 2004, **126**, 16988–16999.

[9] J. F. Capon, F. Gloaguen, P. Schollhammer and J. Talarmin, *Journal of Electroanalytical Chemistry*, 2004, **566**, 241–247.

[10] K. Charreteur, M. Kdider, J.-F. Capon, F. Gloaguen, F. Y. Petillon, P. Schollhammer and J. Talarmin, *Inorganic Chemistry*, 2010, **49**, 2496–2501.

[11] T. B. Liu, M. Wang, Z. Shi, H. G. Cui, W. B. Dong, J. S. Chen, B. Akermark and L. C. Sun, *Chemistry-a European Journal*, 2004, **10**, 4474–4479.

[12] L. Schwartz, P. S. Singh, L. Eriksson, R. Lomoth and S. Ott, *Comptes Rendus Chimie*, 2008, **11**, 875–889.

[13] L. Schwartz, L. Eriksson, R. Lomoth, F. Teixidor, C. Vinas and S. Ott, *Dalton Transactions*, 2008, 2379–2381.

[14] J. L. Stanley, Z. M. Heiden, T. B. Rauchfuss, S. R. Wilson, L. De Gioia and G. Zampella, *Organometallics*, 2008, **27**, 119–125.

[15] G. Eilers, L. Schwartz, M. Stein, G. Zampella, L. de Gioia, S. Ott and R. Lomoth, *Chemistry-a European Journal*, 2007, **13**, 7075–7084.

[16] S. J. Borg, J. W. Tye, M. B. Hall and S. P. Best, *Inorganic Chemistry*, 2007, **46**, 384–394.

[17] G. A. N. Felton, B. J. Petro, R. S. Glass, D. L. Lichtenberger and D. H. Evans, *Journal of the American Chemical Society*, 2009, **131**, 11290–11292.

[18] A. Le Cloirec, S. P. Best, S. Borg, S. C. Davies, D. J. Evans, D. L. Hughes and C. J. Pickett, *Chemical Communications*, 1999, 2285–2286.

[19] E. J. Lyon, I. P. Georgakaki, J. H. Reibenspies and M. Y. Darensbourg, *Angewandte Chemie-International Edition*, 1999, **38**, 3178–3180.

[20] M. Schmidt, S. M. Contakes and T. B. Rauchfuss, *Journal of the American Chemical Society*, 1999, **121**, 9736–9737.

[21] G. A. N. Felton, C. A. Mebi, B. J. Petro, A. K. Vannucci, D. H. Evans, R. S. Glass and D. L. Lichtenberger, *Journal of Organometallic Chemistry*, 2009, **694**, 2681–2699.

[22] J. W. Tye, M. Y. Darensbourg and M. B. Hall, *Inorganic Chemistry*, 2006, **45**, 1552–1559.

[23] P. Li, M. Wang, C. J. He, G. H. Li, X. Y. Liu, C. N. Chen, B. Akermark and L. C. Sun, *European Journal of Inorganic Chemistry*, 2005, 2506–2513.

[24] S. Ezzaher, J.-F. Capon, F. Gloaguen, F. Y. Petillon, P. Schollhammer and J. Talarmin, *Inorganic Chemistry*, 2007, **46**, 3426–3428.

[25] D. Morvan, J.-F. Capon, F. Gloaguen, A. Le Goff, M. Marchivie, F. Michaud, P. Schollhammer, J. Talarmin, J.-J. Yaouanc, R. Pichon and N. Kervarec, *Organometallics*, 2007, **26**, 2042–2052.

[26] P.-Y. Orain, J.-F. Capon, N. Kervarec, F. Gloaguen, F. Petillon, R. Pichon, P. Schollhammer and J. Talarmin, *Dalton Transactions*, 2007, 3754–3756.

[27] S. Ezzaher, J.-F. Capon, F. Gloaguen, N. Kervarec, F. Y. Petillon, R. Pichon, P. Schollhammer and J. Talarmin, *Comptes Rendus Chimie*, 2008, **11**, 906–914.

[28] B. E. Barton and T. B. Rauchfuss, *Inorganic Chemistry*, 2008, **47**, 2261–2263.

[29] F. I. Adam, G. Hogarth, S. E. Kabir and D. Richards, *Comptes Rendus Chimie*, 2008, **11**, 890–905.

[30] T. Liu and M. Y. Darensbourg, *Journal of the American Chemical Society*, 2007, **129**, 7008–7009.

[31] A. K. Justice, T. B. Rauchfuss and S. R. Wilson, *Angewandte Chemie-International Edition*, 2007, **46**, 6152–6154.

[32] C. Tard, X. M. Liu, S. K. Ibrahim, M. Bruschi, L. De Gioia, S. C. Davies, X. Yang, L. S. Wang, G. Sawers and C. J. Pickett, *Nature*, 2005, **433**, 610–613.

[33] C. Tard, X. M. Liu, D. L. Hughes and C. J. Pickett, *Chemical Communications*, 2005, 133–135.

[34] P. Surawatanawong and M. B. Hall, *Inorganic Chemistry*, 2010, **49**, 5737–5747.

[35] G. Hogarth and I. Richards, *Inorganic Chemistry Communications*, 2007, **10**, 66–70.

[36] A. Winter, L. Zsolnai and G. Huttner, *Zeitschrift Fur Naturforschung Section B-a Journal of Chemical Sciences*, 1982, **37**, 1430–1436.

[37] S. Ezzaher, J.-F. Capon, F. Gloaguen, F. Y. Petillon, P. Schollhammer and J. Talarmin, *Inorganic Chemistry*, 2007, **46**, 9863–9872.

[38] J.-F. Capon, F. Gloaguen, P. Schollhammer and J. Talarmin, *Journal of Electroanalytical Chemistry*, 2006, **595**, 47–52.

[39] Z. Yu, M. Wang, P. Li, W. Dong, F. Wang and L. Sun, *Dalton Transactions*, 2008, 2400–2406.

[40] R. Adams and J. Yamamoto, *Journal of Cluster Science*, 1996, **7**, 643–654.

[41] F. I. Adam, G. Hogarth and I. Richards, *Journal of Organometallic Chemistry*, 2007, **692**, 3957–3968.

[42] F. I. Adam, G. Hogarth, I. Richards and B. E. Sanchez, *Dalton Transactions*, 2007, 2495–2498.

[43] S. P. J. Albracht, W. Roseboom and E. C. Hatchikian, *Journal of Biological Inorganic Chemistry*, 2006, **11**, 88–101.

[44] M. S. Arabi, R. Mathieu and R. Poilblanc, *Journal of Organometallic Chemistry*, 1979, **177**, 199–209.

[45] F. A. Armstrong, *Current Opinion in Chemical Biology*, 2004, **8**, 133–140.

[46] V. Artero and M. Fontecave, *Coordination Chemistry Reviews*, 2005, **249**, 1518–1535.

[47] A. J. Bard and L. R. Faulkner, *Electrochemical methods: fundamentals and applications (second edition)*, John Wiley and Sons, United States of America, 2001.

[48] B. E. Barton, M. T. Olsen and T. B. Rauchfuss, *Journal of the American Chemical Society*, 2008, **130**, 16834–16834.

[49] B. E. Barton, M. T. Olsen and T. B. Rauchfuss, *Current Opinion in Biotechnology*, 2010, **21**, 292–297.

[50] B. Bennett, B. J. Lemon and J. W. Peters, *Biochemistry*, 2000, **39**, 7455–7460.

[51] S. P. Best, *Coordination Chemistry Reviews*, 2005, **249**, 1536–1554.

[52] S. P. Best, S. J. Borg, J. M. White, M. Razavet and C. J. Pickett, *Chemical Communications*, 2007, 4348–4350.

[53] M. I. Bondin, S. J. Borg, M.-H. Cheah and S. P. Best, *Radiation Physics and Chemistry*, 2006, **75**, 1878–1883.

[54] G. M. Bonner, A. R. Ridley, S. K. Ibrahim, C. J. Pickett and N. T. Hunt, *Faraday Discussions*, 2010, **145**, 429–442.

[55] S. J. Borg, S. K. Ibrahim, C. J. Pickett and S. P. Best, *Comptes Rendus Chimie*, 2008, **11**, 852–860.

[56] C. A. Boyke, T. B. Rauchfuss, S. R. Wilson, M. M. Rohmer and M. Benard, *Journal of the American Chemical Society*, 2004, **126**, 15151–15160.

[57] C. A. Boyke, J. I. van der Vlugt, T. B. Rauchfuss, S. R. Wilson, G. Zampella and L. De Gioia, *Journal of the American Chemical Society*, 2005, **127**, 11010–11018.

[58] M. Bruschi, P. Fantucci and L. De Gioia, *Inorganic Chemistry*, 2002, **41**, 1421–1429.

[59] M. Bruschi, P. Fantucci and L. De Gioia, *Inorganic Chemistry*, 2003, **42**, 4773–4781.

[60] M. Bruschi, P. Fantucci and L. De Gioia, *Inorganic Chemistry*, 2004, **43**, 3733–3741.

[61] M. Bruschi, C. Greco, P. Fantucci and L. De Gioia, *Inorganic Chemistry*, 2008, **47**, 6056–6071.

[62] M. Bruschi, C. Greco, G. Zampella, U. Ryde, C. J. Pickett and L. De Gioia, *Comptes Rendus Chimie*, 2008, **11**, 834–841.

[63] M. Bruschi, G. Zampella, P. Fantucci and L. De Gioia, *Coordination Chemistry Reviews*, 2005, **249**, 1620–1640.

[64] J. M. Camara and T. B. Rauchfuss, *Nature chemistry*, 2011, **4**, 26–30.

[65] Z. X. Cao and M. B. Hall, *Journal of the American Chemical Society*, 2001, **123**, 3734–3742.

[66] J. F. Capon, S. El Hassnaoui, F. Gloaguen, P. Schollhammer and J. Talarmin, *Organometallics*, 2005, **24**, 2020–2022.

[67] J. F. Capon, F. Gloaguen, P. Schollhammer and J. Talarmin, *Coordination Chemistry Reviews*, 2005, **249**, 1664–1676.

[68] J.-F. Capon, S. Ezzaher, F. Gloaguen, F. Y. Petillon, P. Schollhammer and J. Talarmin, *Chemistry-a European Journal*, 2008, **14**, 1954–1964.

[69] J.-F. Capon, S. Ezzaher, F. Gloaguen, F. Y. Petillon, P. Schollhammer, J. Talarmin, T. J. Davin, J. E. McGrady and K. W. Muir, *New Journal of Chemistry*, 2007, **31**, 2052–2064.

[70] J.-F. Capon, F. Gloaguen, F. Y. Petillon, P. Schollhammer and J. Talarmin, *European Journal of Inorganic Chemistry*, 2008, 4671–4681.

[71] J.-F. Capon, F. Gloaguen, F. Y. Petillon, P. Schollhammer and J. Talarmin, *Coordination Chemistry Reviews*, 2009, **253**, 1476–1494.

[72] J.-F. Capon, F. Gloaguen, F. Y. Petillon, P. Schollhammer and J. Talarmin, *Comptes Rendus Chimie*, 2008, **11**, 842–851.

[73] K. Charreteur, J.-F. Capon, F. Gloaguen, F. Y. Petillon, P. Schollhammer and J. Talarmin, *European Journal of Inorganic Chemistry*, 2011, 1038–1042.

[74] M. H. Cheah, S. J. Borg, M. I. Bondin and S. P. Best, *Inorganic Chemistry*, 2004, **43**, 5635–5644.

[75] M. H. Cheah, S. J. Borg and S. P. Best, *Inorganic Chemistry*, 2007, **46**, 1741–1750.

[76] M. H. Cheah, C. Tard, S. J. Borg, X. Liu, S. K. Ibrahim, C. J. Pickett and S. P. Best, *Journal of the American Chemical Society*, 2007, **129**, 11085–11092.

[77] M.-H. Chiang, Y.-C. Liu, S.-T. Yang and G.-H. Lee, *Inorganic Chemistry*, 2009, **48**, 7604–7612.

[78] D. Chouffai, G. Zampella, J.-F. Capon, L. De Gioia, F. Gloaguen, F. Y. Petillon, P. Schollhammer and J. Talarmin, *Inorganic Chemistry*, 2011, **50**, 12575–12585.

[79] E. C. Constable, C. E. Housecroft, S. L. Kokatam, E. A. Medlycott and J. A. Zampese, *Inorganic Chemistry Communications*, 2010, **13**, 457–460.

[80] S. M. Contakes, S. C. N. Hsu, T. B. Rauchfuss and S. R. Wilson, *Inorganic Chemistry*, 2002, **41**, 1670–1678.

[81] H. Cui, M. Wang, L. Duan and L. Sun, *Journal of Coordination Chemistry*, 2008, **61**, 1856–1861.

[82] M. Y. Darensbourg, E. J. Lyon and J. J. Smee, *Coordination Chemistry Reviews*, 2000, **206**, 533–561.

[83] M. Y. Darensbourg, E. J. Lyon, X. Zhao and I. P. Georgakaki, *Proceedings of the National Academy of Sciences of the United States of America*, 2003, **100**, 3683–3688.

[84] P. Das, J. F. Capon, F. Gloaguen, F. Y. Petillon, P. Schollhammer, J. Talarmin and K. W. Muir, *Inorganic Chemistry*, 2004, **43**, 8203–8205.

[85] I. A. de Carcer, A. DiPasquale, A. L. Rheingold and D. M. Heinekey, *Inorganic Chemistry*, 2006, **45**, 8000–8002.

[86] A. L. De Lacey, V. M. Fernandez, M. Rousset and R. Cammack, *Chemical Reviews*, 2007, **107**, 4304–4330.

[87] L. L. Duan, M. Wang, P. Li, Y. Na, N. Wang and L. C. Sun, *Dalton Transactions*, 2007, 1277–1283.

[88] M. R. DuBois and D. L. DuBois, *Comptes Rendus Chimie*, 2008, **11**, 805–817.

[89] D. J. Evans and C. J. Pickett, *Chemical Society Reviews*, 2003, **32**, 268–275.

[90] S. Ezzaher, J.-F. Capon, N. Dumontet, F. Gloaguen, F. Y. Petillon, P. Schollhammer and J. Talarmin, *Journal of Electroanalytical Chemistry*, 2009, **626**, 161–170.

[91] S. Ezzaher, J.-F. Capon, F. Gloaguen, F. Y. Petillon, P. Schollhammer, J. Talarmin and N. Kervarec, *Inorganic Chemistry*, 2009, **48**, 2–4.

[92] S. Ezzaher, A. Gogoll, C. Bruhn and S. Ott, *Chemical Communications*, 2010, **46**, 5775–5777.

[93] S. Ezzaher, P.-Y. Orain, J.-F. Capon, F. Gloaguen, F. Y. Petillon, T. Roisnel, P. Schollhammer and J. Talarmin, *Chemical Communications*, 2008, 2547–2549.

[94] H. J. Fan and M. B. Hall, *Journal of the American Chemical Society*, 2001, **123**, 3828–3829.

[95] K. Fauvel, R. Mathieu and R. Poilblanc, *Inorganic Chemistry*, 1976, **15**, 976–978.

[96] G. A. N. Felton, R. S. Glass, D. L. Lichtenberger and D. H. Evans, *Inorganic Chemistry*, 2006, **45**, 9181–9184.

[97] G. A. N. Felton, A. K. Vannucci, J. Chen, L. T. Lockett, N. Okumura, B. J. Petro, U. I. Zakai, D. H. Evans, R. S. Glass and D. L. Lichtenberger, *Journal of the American Chemical Society*, 2007, **129**, 12521–12530.

[98] J. C. Fontecilla-Camps, A. Volbeda, C. Cavazza and Y. Nicolet, *Chemical Reviews*, 2007, **107**, 4273–4303.

[99] S. Gao, J. Fan, S. Sun, X. Peng, X. Zhao and J. Hou, *Dalton Transactions*, 2008, 2128–2135.

[100] W. M. Gao, J. H. Liu, C. B. Ma, L. H. Weng, K. Jin, C. N. Chen, B. Akermark and L. C. Sun, *Inorganica Chimica Acta*, 2006, **359**, 1071–1080.

[101] W. Gao, J. Ekstrom, J. Liu, C. Chen, L. Eriksson, L. Weng, B. Akermark and L. Sun, *Inorganic Chemistry*, 2007, **46**, 1981–1991.

[102] W. Gao, J. Liu, W. Jiang, M. Wang, L. Weng, B. Akermark and L. Sun, *Comptes Rendus Chimie*, 2008, **11**, 915–921.

[103] W. Gao, J. Sun, M. Li, T. Akermark, K. Romare, L. Sun and B. Akermark, *European Journal of Inorganic Chemistry*, 2011, 1100–1105.

[104] I. P. Georgakaki, L. M. Thomson, E. J. Lyon, M. B. Hall and M. Y. Darensbourg, *Coordination Chemistry Reviews*, 2003, **238**, 255–266.

[105] S. J. George, Z. Cui, M. Razavet and C. J. Pickett, *Chemistry-a European Journal*, 2002, **8**, 4037–4046.

[106] F. Gloaguen, J. D. Lawrence and T. B. Rauchfuss, *Journal of the American Chemical Society*, 2001, **123**, 9476–9477.

[107] F. Gloaguen, J. D. Lawrence, T. B. Rauchfuss, M. Benard and M. M. Rohmer, *Inorganic Chemistry*, 2002, **41**, 6573–6582.

[108] F. Gloaguen, J. D. Lawrence, M. Schmidt, S. R. Wilson and T. B. Rauchfuss, *Journal of the American Chemical Society*, 2001, **123**, 12518–12527.

[109] F. Gloaguen, D. Morvan, J.-F. Capon, P. Schollhammer and J. Talarmin, *Journal of Electroanalytical Chemistry*, 2007, **603**, 15–20.

[110] F. Gloaguen and T. B. Rauchfuss, *Chemical Society Reviews*, 2009, **38**, 100–108.

[111] C. Greco, G. Zampella, L. Bertini, M. Bruschi, P. Fantucci and L. De Gioia, *Inorganic Chemistry*, 2007, **46**, 108–116.

[112] C. Greco, M. Bruschi, J. Heimdal, P. Fantucci, L. De Gioia and U. Ryde, *Inorganic Chemistry*, 2007, **46**, 7256–7258.

[113] C. Greco, P. Fantucci, L. De Gioia, R. Suarez-Bertoa, M. Bruschi, J. Talarmin and P. Schollhammer, *Dalton Transactions*, 2010, **39**, 7320–7329.

[114] K. N. Green, J. L. Hess, C. M. Thomas and M. Y. Darensbourg, *Dalton Transactions*, 2009, 4344–4350.

[115] M. K. Harb, U.-P. Apfel, J. Kuebel, H. Goerls, G. A. N. Felton, T. Sakamoto, D. H. Evans, R. S. Glass, D. L. Lichtenberger, M. El-Khateeb and W. Weigand, *Organometallics*, 2009, **28**, 6666–6675.

[116] M. K. Harb, T. Niksch, J. Windhager, H. Goerls, R. Holze, L. T. Lockett, N. Okumura, D. H. Evans, R. S. Glass, D. L. Lichtenberger, M. El-khateeb and W. Weigand, *Organometallics*, 2009, **28**, 1039–1048.

[117] M. K. Harb, J. Windhager, A. Daraosheh, H. Goerls, L. T. Lockett, N. Okumura, D. H. Evans, R. S. Glass, D. L. Lichtenberger, M. El-Khateeb and W. Weigand, *European Journal of Inorganic Chemistry*, 2009, 3414–3420.

[118] Z. M. Heiden and T. B. Rauchfuss, *Journal of the American Chemical Society*, 2007, **129**, 14303–14310.

[119] G. Hogarth, M. O'Brien and D. A. Tocher, *Journal of Organometallic Chemistry*, 2003, **672**, 29–33.

[120] G. Hogarth, S. E. Kabir and I. Richards, *Organometallics*, 2010, **29**, 6559–6568.

[121] G. Hogarth, I. Richards and E. Subasi, *Transition Metal Chemistry*, 2008, **33**, 729–732.

[122] J. Hou, X. Peng, J. Liu, Y. Gao, X. Zhao, S. Gao and K. Han, *European Journal of Inorganic Chemistry*, 2006, 4679–4686.

[123] J. Hou, X. Peng, Z. Zhou, S. Sun, X. Zhao and S. Gao, *Journal of Organometallic Chemistry*, 2006, **691**, 4633–4640.

[124] C. E. Housecroft and A. G. Sharpe, *Inorganic Chemistry (third edition)*, Pearson Education Limited, Essex, England, 2008.

[125] M. Q. Hu, C. B. Ma, Y. T. Si, C. N. Chen and Q. T. Liu, *Journal of Inorganic Biochemistry*, 2007, **101**, 1370–1375.

[126] M. Q. Hu, C. B. Ma, X. F. Zhang, F. Chen, C. N. Chen and Q. T. Liu, *Chemistry Letters*, 2006, **35**, 840–841.

[127] S. K. Ibrahim, X. Liu, C. Tard and C. J. Pickett, *Chemical Communications*, 2007, 1535–1537.

[128] S. Ibrahim, P. M. Woi, Y. Alias and C. J. Pickett, *Chemical Communications*, 2010, **46**, 8189–8191.

[129] A. Jablonskyte, J. A. Wright, S. A. Fairhurst, J. N. T. Peck, S. K. Ibrahim, V. S. Oganesyan and C. J. Pickett, *Journal of the American Chemical Society*, 2011, **133**, 18606–18609.

[130] A. Jablonskyte, J. A. Wright and C. J. Pickett, *Dalton Transactions*, 2010, **39**, 3026–3034.

[131] A. Jablonskyte, J. A. Wright and C. J. Pickett, *European Journal of Inorganic Chemistry*, 2011, 1033–1037.

[132] S. Jiang, J. H. Liu and L. C. Sun, *Inorganic Chemistry Communications*, 2006, **9**, 290–292.

[133] S. Jiang, J. Liu, Y. Shi, Z. Wang, B. Akermark and L. Sun, *Dalton Transactions*, 2007, 896–902.

[134] S. Jiang, J. Liu, Y. Shi, Z. Wang, B. Akermark and L. Sun, *Polyhedron*, 2007, **26**, 1499–1504.

[135] A. K. Justice, L. De Gioia, M. J. Nilges, T. B. Rauchfuss, S. R. Wilson and G. Zampella, *Inorganic Chemistry*, 2008, **47**, 7405–7414.

[136] A. K. Justice, R. C. Linck and T. B. Rauchfuss, *Inorganic Chemistry*, 2006, **45**, 2406–2412.

[137] A. K. Justice, R. C. Linck, T. B. Rauchfuss and S. R. Wilson, *Journal of the American Chemical Society*, 2004, **126**, 13214–13215.

[138] A. K. Justice, M. J. Nilges, T. B. Rauchfuss, S. R. Wilson, L. De Gioia and G. Zampella, *Journal of the American Chemical Society*, 2008, **130**, 5293–5301.

[139] A. K. Justice, G. Zampella, L. De Gioia and T. B. Rauchfuss, *Chemical Communications*, 2007, 2019–2021.

[140] A. K. Justice, G. Zampella, L. De Gioia, T. B. Rauchfuss, J. I. van der Vlugt and S. R. Wilson, *Inorganic Chemistry*, 2007, **46**, 1655–1664.

[141] A. Kayal and T. B. Rauchfuss, *Inorganic Chemistry*, 2003, **42**, 5046–5048.

[142] S. Kaziannis, S. Santabarbara, J. A. Wright, G. M. Greetham, M. Towrie, A. W. Parker, C. J. Pickett and N. T. Hunt, *Journal of Physical Chemistry B*, 2010, **114**, 15370–15379.

[143] S. Kaziannis, J. A. Wright, M. Candelaresi, R. Kania, G. M. Greetham, A. W. Parker, C. J. Pickett and N. T. Hunt, *Physical Chemistry Chemical Physics*, 2011, **13**, 10295–10305.

[144] G. J. Kubas, *Chemical Reviews*, 2007, **107**, 4152–4205.

[145] J. D. Lawrence, H. X. Li and T. B. Rauchfuss, *Chemical Communications*, 2001, 1482–1483.

[146] J. D. Lawrence, H. X. Li, T. B. Rauchfuss, M. Benard and M. M. Rohmer, *Angewandte Chemie-International Edition*, 2001, **40**, 1768–1771.

[147] J. D. Lawrence, T. B. Rauchfuss and S. R. Wilson, *Inorganic Chemistry*, 2002, **41**, 6193–6195.

[148] A. Le Goff, V. Artero, B. Jousselme, P. D. Tran, N. Guillet, R. Metaye, A. Fihri, S. Palacin and M. Fontecave, *Science*, 2009, **326**, 1384–1387.

[149] B. Li, T. Liu, C. V. Popescu, A. Bilko and M. Y. Darensbourg, *Inorganic Chemistry*, 2009, **48**, 11283–11289.

[150] B. Li, T. Liu, M. L. Singleton and M. Y. Darensbourg, *Inorganic Chemistry*, 2009, **48**, 8393–8403.

[151] H. X. Li and T. B. Rauchfuss, *Journal of the American Chemical Society*, 2002, **124**, 726–727.

[152] P. Li, M. Wang, C. He, X. Liu, K. Jin and L. Sun, *European Journal of Inorganic Chemistry*, 3718–3727.

[153] P. Li, M. Wang, J. Pan, L. Chen, N. Wang and L. Sun, *Journal of Inorganic Biochemistry*, 2008, **102**, 952–959.

[154] C. Liu, J. N. T. Peck, J. A. Wright, C. J. Pickett and M. B. Hall, *European Journal of Inorganic Chemistry*, 2011, 1080–1093.

[155] T. Liu, B. Li, M. L. Singleton, M. B. Hall and M. Y. Darensbourg, *Journal of the American Chemical Society*, 2009, **131**, 8296–8307.

[156] X. M. Liu, S. K. Ibrahim, C. Tard and C. J. Pickett, *Coordination Chemistry Reviews*, 2005, **249**, 1641–1652.

[157] Z. P. Liu and P. Hu, *Journal of the American Chemical Society*, 2002, **124**, 5175–5182.

[158] R. Lomoth and S. Ott, *Dalton Transactions*, 2009, 9952–9959.

[159] S. Lounissi, J.-F. Capon, F. Gloaguen, F. Matoussi, F. Y. Petillon, P. Schollhammer and J. Talarmin, *Organometallics*, 2010, **29**, 1296–1301.

[160] S. Lounissi, J.-F. Capon, F. Gloaguen, F. Matoussi, F. Y. Petillon, P. Schollhammer and J. Talarmin, *Chemical Communications*, 2011, **47**, 878–880.

[161] R. Mathieu, R. Poilblanc, P. Lemoine and M. Gross, *Journal of Organometallic Chemistry*, 1979, **165**, 243–252.

[162] C. Mealli and T. B. Rauchfuss, *Angewandte Chemie-International Edition*, 2007, **46**, 8942–8944.

[163] R. Mejia-Rodriguez, D. S. Chong, J. H. Reibenspies, M. P. Soriaga and M. Y. Darensbourg, *Journal of the American Chemical Society*, 2004, **126**, 12004–12014.

[164] P. M. Monk, *Fundamentals of Electroanalytical Chemistry*, John Wiley and Sons, Chichester, England, 2001.

[165] D. Morvan, J.-F. Capon, F. Gloaguen, F. Y. Petillon, P. Schollhammer, J. Talarmin, J.-J. Yaouanc, F. Michaud and N. Kervarec, *Journal of Organometallic Chemistry*, **694**, 2801–2807.

[166] Y. Na, M. Wang, J. Pan, P. Zhang, B. Akermark and L. Sun, *Inorganic Chemistry*, 2008, **47**, 2805–2810.

[167] Y. Nicolet, C. Cavazza and J. C. Fontecilla-Camps, *Journal of Inorganic Biochemistry*, 2002, **91**, 1–8.

[168] Y. Nicolet, A. L. de Lacey, X. Vernede, V. M. Fernandez, E. C. Hatchikian and J. C. Fontecilla-Camps, *Journal of the American Chemical Society*, 2001, **123**, 1596–1601.

[169] M. T. Olsen, B. E. Barton and T. B. Rauchfuss, *Inorganic Chemistry*, 2009, **48**, 7507–7509.

[170] P.-Y. Orain, J.-F. Capon, F. Gloaguen, F. Y. Petillon, P. Schollhammer, J. Talarmin, G. Zampella, L. De Gioia and T. Roisnel, *Inorganic Chemistry*, 2010, **49**, 5003–5008.

[171] P.-Y. Orain, J.-F. Capon, F. Gloaguen, P. Schollhammer and J. Talarmin, *International Journal of Hydrogen Energy*, 2010, **35**, 10797–10802.

[172] S. Ott, M. Borgstrom, M. Kritikos, R. Lomoth, J. Bergquist, B. Akermark, L. Hammarstrom and L. C. Sun, *Inorganic Chemistry*, 2004, **43**, 4683–4692.

[173] S. Ott, M. Kritikos, B. Akermark and L. C. Sun, *Angewandte Chemie-International Edition*, 2003, **42**, 3285–3288.

[174] S. Ott, M. Kritikos, B. Akermark, L. C. Sun and R. Lomoth, *Angewandte Chemie-International Edition*, 2004, **43**, 1006–1009.

[175] A. Parkin, C. Cavazza, J. C. Fontecilla-Camps and F. A. Armstrong, *Journal of the American Chemical Society*, 2006, **128**, 16808–16815.

[176] F. Y. Petillon, F. Robin-Le Guen, R. Rumin, P. Schollhammer, J. Talarmin and K. W. Muir, *Journal of Organometallic Chemistry*, 2006, **691**, 2853–2858.

[177] C. J. Pickett and S. P. Best, *Coordination Chemistry Reviews*, 2005, **249**, 1517–1517.

[178] T. B. Rauchfuss, S. M. Contakes, S. C. N. Hsu, M. A. Reynolds and S. R. Wilson, *Journal of the American Chemical Society*, 2001, **123**, 6933–6934.

[179] M. Razavet, S. J. Borg, S. J. George, S. P. Best, S. A. Fairhurst and C. J. Pickett, *Chemical Communications*.

[180] M. Razavet, S. C. Davies, D. L. Hughes, J. E. Barclay, D. J. Evans, S. A. Fairhurst, X. M. Liu and C. J. Pickett, *Dalton Transactions*, 2003, 586–595.

[181] M. Razavet, S. C. Davies, D. L. Hughes and C. J. Pickett, *Chemical Communications*, 2001, 847–848.

[182] M. A. Reynolds, T. B. Rauchfuss and S. R. Wilson, *Organometallics*, 2003, **22**, 1619–1625.

[183] A. R. Ridley, A. I. Stewart, K. Adamczyk, H. N. Ghosh, B. Kerkeni, Z. X. Guo, E. T. J. Nibbering, C. J. Pickett and N. T. Hunt, *Inorganic Chemistry*, 2008, **47**, 7453–7455.

[184] M. Rospenk, J. Fritsch and G. Zundel, *Journal of Physical Chemistry*, 1984, **88**, 321–323.

[185] A. M. Royer, T. B. Rauchfuss and D. L. Gray, *Organometallics*, 2009, **28**, 3618–3620.

[186] D. E. Schwab, C. Tard, E. Brecht, J. W. Peters, C. J. Pickett and R. K. Szilagyi, *Chemical Communications*, 2006, 3696–3698.

[187] L. Schwartz, G. Eilers, L. Eriksson, A. Gogoll, R. Lomoth and S. Ott, *Chemical Communications*, 2006, 520–522.

[188] L. Schwartz, J. Ekstrom, R. Lomoth and S. Ott, *Chemical Communications*, 2006, 4206–4208.

[189] G. Si, W.-G. Wang, H.-Y. Wang, C.-H. Tung and L.-Z. Wu, *Inorganic Chemistry*, 2008, **47**, 8101–8111.

[190] G. Si, L.-Z. Wu, W.-G. Wang, J. Ding, X.-F. Shan, Y.-P. Zhao, C.-H. Tung and M. Xu, *Tetrahedron Letters*, 2007, **48**, 4775–4779.

[191] Y. Si, K. Charreteur, J.-F. Capon, F. Gloaguen, F. Y. Petillon, P. Schollhammer and J. Talarmin, *Journal of Inorganic Biochemistry*, 2010, **104**, 1038–1042.

[192] Y. Si, C. Ma, M. Hu, H. Chen, C. Chen and Q. Liu, *New Journal of Chemistry*, 2007, **31**, 1448–1454.

[193] P. E. M. Siegbahn, J. W. Tye and M. B. Hall, *Chemical Reviews*, 2007, **107**, 4414–4435.

[194] P. S. Singh, H. C. Rudbeck, P. Huang, S. Ezzaher, L. Eriksson, M. Stein, S. Ott and R. Lomoth, *Inorganic Chemistry*, 2009, **48**, 10883–10885.

[195] M. L. Singleton, N. Bhuvanesh, J. H. Reibenspies and M. Y. Darensbourg, *Angewandte Chemie-International Edition*, 2008, **47**, 9492–9495.

[196] M. L. Singleton, R. M. Jenkins, C. L. Klernashevich and M. Y. Darensbourg, *Comptes Rendus Chimie*, 2008, **11**, 861–874.

[197] L. C. Song, *Accounts of Chemical Research*, 2005, **38**, 21–28.

[198] L. C. Song, F. H. Gong, T. Meng, J. H. Ge, L. N. Cui and Q. M. Hu, *Organometallics*, 2004, **23**, 823–831.

[199] L. C. Song, Z. Y. Yang, H. Z. Bian and Q. M. Hu, *Organometallics*, 2004, **23**, 3082–3084.

[200] L. C. Song, Z. Y. Yang, H. Z. Bian, Y. Liu, H. T. Wang, X. F. Liu and Q. M. Hu, *Organometallics*, 2005, **24**, 6126–6135.

[201] L.-C. Song, W. Gao, C.-P. Feng, D.-F. Wang and Q.-M. Hu, *Organometallics*, 2009, **28**, 6121–6130.

[202] L.-C. Song, J.-H. Ge, X.-F. Liu, L.-Q. Zhao and Q.-M. Hu, *Journal of Organometallic Chemistry*, 2006, **691**, 5701–5709.

[203] L.-C. Song, J.-H. Ge, J. Yan, H.-T. Wang, X. Luo and Q.-M. Hu, *European Journal of Inorganic Chemistry*, 2008, 164–171.

[204] L.-C. Song, J.-H. Ge, X.-G. Zhang, Y. Liu and Q.-M. Hu, *European Journal of Inorganic Chemistry*, 2006, 3204–3210.

[205] L.-C. Song, C.-G. Li, J.-H. Ge, Z.-Y. Yang, H.-T. Wang, J. Zhang and Q.-M. Hu, *Journal of Inorganic Biochemistry*, 2008, **102**, 1973–1979.

[206] L.-C. Song, Q.-S. Li, Z.-Y. Yang, Y.-J. Hua, H.-Z. Bian and Q.-M. Hu, *European Journal of Inorganic Chemistry*, 2010, 1119–1128.

[207] L.-C. Song, H.-T. Wang, J.-H. Ge, S.-Z. Mei, J. Gao, L.-X. Wang, B. Gai, L.-Q. Zhao, J. Yan and Y.-Z. Wang, *Organometallics*, 2008, **27**, 1409–1416.

[208] L.-C. Song, L.-X. Wang, B.-S. Yin, Y.-L. Li, X.-G. Zhang, Y.-W. Zhang, X. Luo and Q.-M. Hu, *European Journal of Inorganic Chemistry*, 291–297.

[209] L.-C. Song, B.-S. Yin, Y.-L. Li, L.-Q. Zhao, J.-H. Ge, Z.-Y. Yang and Q.-M. Hu, *Organometallics*, 2007, **26**, 4921–4929.

[210] J. L. Stanley, T. B. Rauchfuss and S. R. Wilson, *Organometallics*, 2007, **26**, 1907–1911.

[211] A. I. Stewart, I. P. Clark, M. Towrie, S. K. Ibrahim, A. W. Parker, C. J. Pickett and N. T. Hunt, *Journal of Physical Chemistry B*, 2008, **112**, 10023–10032.

[212] A. I. Stewart, J. A. Wright, G. M. Greetham, S. Kaziannis, S. Santabarbara, M. Towrie, A. W. Parker, C. J. Pickett and N. T. Hunt, *Inorganic Chemistry*, 2010, **49**, 9563–9573.

[213] D. Streich, Y. Astuti, M. Orlandi, L. Schwartz, R. Lomoth, L. Hammarstrom and S. Ott, *Chemistry-a European Journal*, 2010, **16**, 60–63.

[214] L. C. Sun, B. Akermark and S. Ott, *Coordination Chemistry Reviews*, 2005, **249**, 1653–1663.

[215] C. Tard and C. J. Pickett, *Chemical Reviews*, 2009, **109**, 2245–2274.

[216] C. M. Thomas, M. Y. Darensbourg and M. B. Hall, *Journal of Inorganic Biochemistry*, 2007, **101**, 1752–1757.

[217] C. M. Thomas, T. Liu, M. B. Hall and M. Y. Darensbourg, *Inorganic Chemistry*, 2008, **47**, 7009–7024.

[218] C. M. Thomas, O. Ruediger, T. Liu, C. E. Carson, M. B. Hall and M. Y. Darensbourg, *Organometallics*, 2007, **26**, 3976–3984.

[219] J. W. Tye, M. B. Hall and M. Y. Darensbourg, *Proceedings of the National Academy of Sciences of the United States of America*, 2005, **102**, 16911–16912.

[220] J. W. Tye, J. Lee, H. W. Wang, R. Mejia-Rodriguez, J. H. Reibenspies, M. B. Hall and M. Y. Darensbourg, *Inorganic Chemistry*, 2005, **44**, 5550–5552.

[221] J. W. Tye, M. Y. Darensbourg and M. B. Hall, *Journal of Molecular Structure-Theochem*, 2006, **771**, 123–128.

[222] J. W. Tye, M. Y. Darensbourg and M. B. Hall, *Inorganic Chemistry*, 2008, **47**, 2380–2388.

[223] J. I. van der Vlugt, T. B. Rauchfuss, C. M. Whaley and S. R. Wilson, *Journal of the American Chemical Society*, 2005, **127**, 16012–16013.

[224] P. M. Vignais, *Coordination Chemistry Reviews*, 2005, **249**, 1677–1690.

[225] V. Vijaikanth, J. F. Capon, F. Gloaguen, P. Schollhammer and J. Talarmin, *Electrochemistry Communications*, 2005, **7**, 427–430.

[226] V. Vijaikanth, J.-F. Capon, F. Gloaguen, F. Y. Petillon, P. Schollhammer and J. Talarmin, *Journal of Organometallic Chemistry*, 2007, **692**, 4177–4181.

[227] P. I. Volkers, T. B. Rauchfuss and S. R. Wilson, *European Journal of Inorganic Chemistry*, 2006, 4793–4799.

[228] P. Volkers and T. B. Rauchfuss, *Journal of Inorganic Biochemistry*, 2007, **101**, 1748–1751.

[229] F. J. Wang, M. Wang, X. Y. Liu, K. Jin, W. B. Dong, G. H. Li, B. Akermark and L. C. Sun, *Chemical Communications*, 2005, 3221–3223.

[230] F. Wang, M. Wang, X. Liu, K. Jin, W. Donga and L. Sun, *Dalton Transactions*, 2007, 3812–3819.

[231] M. Wang, Y. Na, M. Gorlov and L. Sun, *Dalton Transactions*, 2009, 6458–6467.

[232] N. Wang, M. Wang, T. B. Liu, P. Li, T. T. Zhang, M. Y. Darensbourg and L. C. Sun, *Inorganic Chemistry*, 2008, **47**, 6948–6955.

[233] N. Wang, M. Wang, T. Zhang, P. Li, J. Liu and L. Sun, *Chemical Communications*, 2008, 5800–5802.

[234] W.-G. Wang, H.-Y. Wang, G. Si, C.-H. Tung and L.-Z. Wu, *Dalton Transactions*, 2009, 2712–2720.

[235] X. B. Wang, S. Q. Niu, X. Yang, S. K. Ibrahim, C. J. Pickett, T. Ichiye and L. S. Wang, *Journal of the American Chemical Society*, 2003, **125**, 14072–14081.

[236] X. Wang, Z. Li, X. Zeng, Q. Luo, D. J. Evans, C. J. Pickett and X. Liu, *Chemical Communications*, 2008, 3555–3557.

[237] Z. Wang, W. F. Jiang, J. H. Liu, W. I. Jiang, Y. Wang, B. Akermark and L. C. Sun, *Journal of Organometallic Chemistry*, 2008, **693**, 2828–2834.

[238] Z. Wang, J.-H. Liu, C.-J. He, S. Jiang, B. Akermark and L.-C. Sun, *Journal of Organometallic Chemistry*, 2007, **692**, 5501–5507.

[239] Z. Wang, J. Liu, C. He, S. Jiang, B. Akermark and L. Sun, *Inorganica Chimica Acta*, 2007, **360**, 2411–2419.

[240] J. A. Wright and C. J. Pickett, *Chemical Communications*, 2009, 5719–5721.

[241] J. A. Wright, L. Webster, A. Jablonskyte, P. M. Woi, S. K. Ibrahim and C. J. Pickett, *Faraday Discussions*, 2011, **148**, 359–371.

[242] F. Xu, C. Tard, X. Wang, S. K. Ibrahim, D. L. Hughes, W. Zhong, X. Zeng, Q. Luo, X. Liu and C. J. Pickett, *Chemical Communications*, 2008, 606–608.

[243] X. Yang, M. Razavet, X. B. Wang, C. J. Pickett and L. S. Wang, *Journal of Physical Chemistry A*, 2003, **107**, 4612–4618.

[244] G. Zampella, M. Bruschi, P. Fantucci, M. Razavet, C. J. Pickett and L. De Gioia, *Chemistry-a European Journal*, 2005, **11**, 509–520.

[245] Y. Zhang, M.-Q. Hu, H.-M. Wen, Y.-T. Si, C.-B. Ma, C.-N. Chen and Q.-T. Liu, *Journal of Organometallic Chemistry*, 2009, **694**, 2576–2580.

[246] X. Zhao, I. P. Georgakaki, M. L. Miller, R. Mejia-Rodriguez, C. Y. Chiang and M. Y. Darensbourg, *Inorganic Chemistry*, 2002, **41**, 3917–3928.

[247] X. Zhao, I. P. Georgakaki, M. L. Miller, J. C. Yarbrough and M. Y. Darensbourg, *Journal of the American Chemical Society*, 2001, **123**, 9710–9711.